Workshop Report

Baltic HIRLAM Workshop
St.Petersburg, 17-20 November, 2003

Participants of the Workshop photographed at the Sanatorium “Dunes” before leaving.

HIRLAM-6 Project, c/o Per Undén, SMHI, S-601 76 Norrköping, SWEDEN

Introduction

The Baltic HIRLAM Workshop was arranged at the Sanatorium “Dunes” in Sestroretsk, near St. Petersburg, in November, 17-20, 2003. The aim of the workhop was to bring together the project participants, to discuss four main items: (1) the finest scale atmospheric modelling based on nonhydrostatic HIRLAM, (2) modelling of stable boundary layer and surface-related processes, (3) dispersion and air quality studies using meteorological model data as input and (4) education of numerical modelling.

The workshop programme consisted of general and working sessions (see the attached programme). Approximately 45 participants from 11 countries and 13 institutes attended the workshop. On behalf of the host institute, the rector of Russian State Hydrometeorological University Lev Karlin opened the workshop.

The general and working sessions were arranged according to six topics:

1. Boundary layer modelling and parametrizations 2. Fine scale (nonhydrostatic model) dynamics and physics 3. Surface layer modelling and parametrizations 4. Air quality applications 5. Numerical modelling in education 6. Model systems, cooperation, other. In the present report, the extended abstracts follow the order of the workshop programme.

A summary of discussions in working sessions

Chairmen of the working sessions 1-5 made a short report of discussions and possible suggestions. These are summarized below:

Boundary layer modelling and parametrizations

Suggestions of this working session include:
• HIRLAM should take part in GEWEX Atmospheric Boundary Layer Study (GABLS), to test the vertical diffusion parametrizations.
• The use of Sodankylä mast, sounding and surface observation data is recommended for operational on-line verifications. The possible use of other mast data, e.g. the nuclear power plant masts could be studied.
• Data from NE Finland (Kuusamo) could be used for comparisons with HIRLAM during a period of snow melt.
• Both one- and three-dimensional comparisons between HIRLAM and Arpège would be useful in cases where comparisons can be done with observations.

Chairman: Stefan Gollvik

Fine scale (nonhydrostatic model) dynamics and physics

First the question how to verify high at high resolution was discussed. Conventional methods and conventional observations are not suitable and do not provide information about the value of high resolution simulation (rather the contrary due to the double penalty effect of higher amplitudes in combination with a phase error). Still radiosondes could be used, but one needs to know if it is before or after convection has occurred, e.g.

Indirect methods can be used, as e.g. air pollution measurements as the are plentiful. The most obvious method is the radar and the RSM. Precipitation can also be verified against high resolution automatic networks.

A probablistic approach must be taken towards verification at high resolution as a deterministic forecast of convection has so much of random elements in it. For the vertical structure mast data should be used and they exist in a number of locations.

The issue of climate generation is pressing when at high resolution and in Hirlam. At the time there are missing values when trying at 2.5 km, but this will be corrected. A more general issue is that high resolution input data to climate generation must be provided. ECOCLIMAP is a good example which is at 1 km.

Some discussion then ensued about the exact configuration of Hirlam at high resolution. So far OI and NMI have been used and not 3D-VAR and incremental DFI, which are believed to be more optimal.

The parameterisation at high resolution does probably not need a convection parameterisation but it needs a good micro-physics and turbulence scheme. The turbulence will need to be 3D prognostic and include non-local effects.

Chairman: Per Undén

Surface layer modelling and parametrizations

During the discussion several suggestions were made:

• When using the meteorological tower data for validation of numerical forecasts it could be important to consider the heterogeneous area seen by the tower instruments during different conditions (wind speed and direction, stability). Foot-print studies could be used for studying the origin of surface fluxes measured by instruments in towers.

• There seems to be an urgent need to modify how surface roughness and subgrid-scale orography features are treated in HIRLAM.

• When discussing the sloping surface radiation it was noted that it is complicated to account for sub-areas with different slope angles in a grid square since that should also be coordinated with vegetation fractions. However, an average slope for a grid square is much more simple to introduce.

• It was suggested to introduce to HIRLAM the lake model presented during the session by Dmitri Mironov.

Chairman: Patrick Samuelsson

Air quality applications

The papers presented at the section meeting were discussed in details by participants. An additional discussion was focused on the topic of interaction and more intensive cooperation between communities working on development and implementation of NWP models, especially HIRLAM, and on development and implementation of dispersion models. It was stressed out that the performance of dispersion models critically depends on the performance of their meteorological drivers - that is why dispersion modelers could benefit from improvements to be introduced in HIRLAM. From another point of view, dispersion modeling is not only a substantial end-user of the HIRLAM output. There is a lot of data of atmospheric tracer experiments that actually can be used to validate NWP models. Moreover, being highly irregular in space and time, measured concentration fields are very sensitive to variations in the wind and turbulence fields and, in a sense, are suited better to validation of the performance of meteorological models than even the meteorological fields.

Chairman: Yevgeny Genikhovich

Numerical modelling in education

In this session an active exchange of experiences took part. Several problems were raised for discussion, not so many firm conclusions drawn. One open question is the motivation of students. In the numerical modelling very big background is needed, so there may be problems with motivation.

The curricula in this topic are different. Some participants suggested that the results would benefit from unification, but not everybody agreed. Exchange of education materials in NWP was considered necessary, also the Baltic HIRLAM project web page could be used for that. RSHU representatives expressed an interest for cooperation to adapt to RSHU the course of data assimilation given in the University of Helsinki.

An initiative of Meteo France to form an European cooperative programme in education of numerical modelling, based on the experience of the Aladin training network (ALATNET) was supported by the participants.

Chairman: Katherina Kourzeneva

Baltic HIRLAM Cooperation

Baltic HIRLAM is a cooperation project between seven meteorological institutes around the Baltic Sea: Finnish Meteorological Institute, Division of Atmospheric Sciences at the University of Helsinki, Russian Hydrometeorological University, Estonian Meteorological and Hydrological Institute, Department of Environmental Physics at the University of Tartu, Lithuanian Hydrometeorological Service, Department of Earth Sciences at the University of Uppsala, Swedish Meteorological and Hydrological Institute.

"The aim of the cooperation is to coordinate research and education in order to develope and apply in the participating institutes a fine scale numerical weather prediction and atmospheric research model. The research and development will lead to an improvement of the quality of weather forecasts, including the forecast of natural disasters and atmospheric pollution events, and to better understanding of the underlying atmospheric processes. Creation of a Baltic academic network will allow a higher level of education in the area of atmospheric modelling in the participating countries." (from the project plan)

Baltic HIRLAM cooperation is closely linked to the International HIRLAM project. During the academic year 2003 - 2004 the Baltic cooperation is supported by the Nordic Council of Ministers.

Acknowledgements

The host institute RSHU arranged an excellent venue and environment for the fruitful work during the workshop. The support of Nordic Council covered travel expenses of most of the workshop participants. The international HIRLAM project included the present report into the series of HIRLAM workshop publications.

Helsinki 9.2.2004
Laura Rontu

Programme of the workshop

Monday, 17.11.2003

Opening of the workshop	Lev Karlin - rector of RSHU

General session

Current activities and the planned developments in the HIRLAM-6 Project	Per Undén (HIRLAM/SMHI)
The finest scale HIRLAM - the Tartu model	Rein Rõõm (UT)
Current problems of stable boundary layer modelling	Sergei Zilitinkevich (UU)
Experimental very high resolution forecasting at EMHI	Aarne Männik and Ivar Ansper (EMHI)
On the parametrization of precipitation in warm clouds	Priit Tisler (UH)

Working sessions (parallel)

1. Boundary layer modelling and parametrizations

The effects of small-scale inhomogeneity in the surface layer	Kirill Yegorov (RSHU)
Sodankylä mast data for model comparison studies	Markku Kangas (FMI)
One-dimensional model studies in stable boundary layer	Eric Bazile (Meteo France)
Discussion on model intercomparison studies for stable boundary layer	

2. Fine scale (nonhydrostatic) dynamics and physics

Convection in hydrostatic and nonhydrostatic HIRLAM	Sami Niemelä (UH)
High resolution NWP at the Met Office	Luke Jones (UKMO)
Modelling a heavy rain case in North-East Estonia in August 2003. Preliminary results.	Andres Luhamaa (UT)
Plans and first experiences of the use of fine-scale MM5 model over Baltic Sea and coastal areas	Erik Gregow and Jari Mustonen (FMI)
Discussion on the finest scale modelling development	

Tuesday, 18.11.2003

General session

Problems of surface layer modelling at Northern latitudes	Stefan Gollvik (SMHI)
Bridges between meteorological and dispersion models at different scales	Yevgeny Genihovich (MGO) and Mihail Sofiev (FMI)
Numerical model for fine structure planetary boundary layer prediction as applied to atmospheric pollution	Alexander Gavrilov et.al. (RSHU)

Working sessions (parallel)

3. Surface layer modelling and parametrizations

Modeling of neutrally stratified airflow over inhomogeneous vegetation	Andrey Sogachev (UH)
Some methods to consider soil freezing effect in land surface block of atmospheric models	Katherina Kourzeneva and Dina Kozlova (RSHU)
Orography-related problems in HIRLAM	Laura Rontu (FMI)
A study of radiation parametrizations for sloping surfaces	Anastasya Senkova (RSHU)
Parameterization of Lakes in NWP: Description of a lake model and single-column tests	Dmitrii Mironov (DWD)
Discussion on surface layer modelling and parametrizations	

4. Air quality applications

Effects of boundary-layer thermal stratification and underlying surface roughness to the deposition of coarse solid particles	Marko Kaasik (UT)
Some lessons from the SILAM model application to the European Tracer Experiment ETEX	Mihail Sofiev and Pilvi Siljamo (FMI)
Comparison of air quality forecasts based on different meteorological data as input	Marke Hongisto (FMI)
Modelling dispersion of birch pollen	Pilvi Siljamo (FMI) et al.
Discussion on air quality applications	

Wednesday, 19.11.2003

General session

Numerical modelling in education: The MISU experience	Nils Gustafsson et al.(SMHI/MISU)
MGO Regional Climate Model: present-day climate simulations	Igor Shkolnik et al. (MGO)
HIRLAM at Mars	Janne Kauhanen (UH)

Working sessions (parallel)

5. Numerical modelling in education

Atmospheric Modelling Training in RSHU	Katherina Kourzeneva et al.
Point of view of the international HIRLAM project on training in numerical modelling	Per Undén (SMHI/HIRLAM)
Curriculum of numerical meteorology at Tartu University	Rein Rõõm (UT)
Numerical methods and modelling at the division of Atmospheric Sciences at Helsinki University	Sami Niemelä (UH)
Discussion on education	

6. Model systems, cooperation, other

The planetary boundary layer parameterization scheme for the global and regional circulation and climate modeling with emphasis to the high latitude features including the highly stable stratification and baroclinity	Vladimir Romanov (AARI)
Assessing the role of observational errors in data assimilation: experiments with a global data assimilation system	Mihail Tsyroulnikov et al.
Variable resolution model of Russian Hydrometeorological Research Centre	Mihail Tolstyh (RHRC)
Regular Cycle Run of HIRLAM (RCR)	Kalle Eerola and Carl Fortelius (FMI)
Experiences of FMI pre-RCR runs	Simo Järvenoja (FMI)

Reports of the parallel sessions

General discussion and closure of the workshop

Abbreviations of the institutes

AARI - Arctic and Antarctic Research Institute, St.Petersburg
DWD - Deutscher Wetterdienst, Offenbach am Main
EMHI - Estonian meteorological and hydrological institute, Tallin
FMI - Finnish meteorological institute, Helsinki
LHMS - Lithuanian hydrometeorological service, Vilnius
MGO - Main geophysical observatory, St.Petersburg
MISU - University of Stockholm
RHRC - Russian Hydrometeorological Research Centre, Moscow
RSHU - Russian state hydrometeorological institute, St.Petersburg
SMHI - Swedish meteorological and hydrological institute, Norrköping
UH - University of Helsinki
UKMO - UK Met Office, Bracknell/Exeter
UT - University of Tartu
UU - University of Uppsala

List of participants

Ivar Ansper	EMHI	ivar.ansper@emhi.ee
Eric Bazile	Meteo France	eric.bazile@meteo.fr
Carl Fortelius	FMI	carl.fortelius@fmi.fi
Marke Hongisto	FMI	marke.hongisto@fmi.fi
Alexander Gavrilov	RSHU	gavr@mcep.rshmi.spb.ru
Jevgeni Genihovitsh	MGO	ego@city.com.ru
Stefan Gollvik	SMHI	stefan.gollvik@smhi.se
Eric Gregow	FMI	erik.gregow@fmi.fi
Luke Jones	UKMO	luke.jones@metoffice.com
Simo Järvenoja	FMI	simo.jarvenoja@fmi.fi
Marko Kaasik	UT	mkaasik@physic.ut.ee
Markku Kangas	FMI	markku.kangas@fmi.fi
Janne Kauhanen	UH	janne.kauhanen@helsinki.fi
Katherina Kourzeneva	RSHU	kourzeneva@rshu.ru
Andres Luhamaa	UT	bronto@ut.ee
Dmitri Mironov	DWD	dmitrii.mironov@dwd.de
Jari Mustonen	FMI	jari.mustonen@fmi.fi
Aarne Männik	UT	aarne.mannik@ut.ee
Sami Niemelä	UH	sami.niemela@helsinki.fi
Jurgita Ovadnevaite	LHMS	ovadnevaite@delfi.lt
Vladimir Romanov	AARI	romanov@aari.nw.ru
Laura Rontu	FMI	laura.rontu@fmi.fi
Rein Rõõm	UT	rein.room@ut.ee
Patrick Samuelsson	SMHI	patrick.samuelsson@smhi.se
Priit Tisler	UH/FMI	priit.tisler@fmi.fi
Anastasia Senkova	RSHU	nastya.senkova@rambler.ru
Igor Shkolnik	MGO	igor@main.mgo.rssi.ru
Pilvi Siljamo	FMI	pilvi.siljamo@fmi.fi
Mihail Sofiev	FMI	mikhail.sofiev@fmi.fi
Andrei Sogachev	UH	andrei.sogachev@helsinki.fi
Gennady Tarakanov	RSHU	
Mihail Tolstyh	RHRC	tolstykh@inm.ras.ru
Per Unden	SMHI	per.unden@smhi.se
Kirill Yegorov	RSHU	egorov@rshu.ru
Radomir Zaripov	RHRC	zaripov@rhmc.mecom.ru
Sergei Zilitinkevitsh	UU	sergej.zilitinkevich@geo.uu.se
Anna Orlova	RSHU	orlova@rshu.ru
Viktor Arkhangelsky	RSHU	viktor@rshu.ru
Jevgeny Atlaskin	RSHU	ea-mail1@rambler.ru
Anna Kanouhina	RSHU	anakan@rambler.ru
Rami Altalouli	RSHU	rtalouli@mail.ru
Ladislaus Changa	RSHU	changa60@hotmail.com
Hamza Kabelwa	RSHU	hkabelwa@hotmail.com
Aaed Mohanna	RSHU	aaedmohanna@hotmail.com
Roman Vasiljev	RSHU	
Aleksei Gorshkov	RSHU	

HIRLAM-6 Project, progress and status 2003.

Per Undén
Project Leader, HIRLAM-6, SMHI, S-60176 Norrköping, SWEDEN.

1 Introduction

The HIRLAM-5 Project finished at the end of 2002 and much of the work and tasks are continuing in the HIRLAM-6 Project. A comprehensive review of the member's views and demands was made during 2002 and a new Memorandum of Understanding was compiled and agreed. (The members are the National Meteorological Services in Denmark, Finland, Iceland, Ireland, Netherlands, Norway, Spain and Sweden. There is a research cooperation with Météo-France.)

The scientific strategy involves both optimising the performance of the synoptic scale modelling whilst gradually transferring resources to meso-γ scale modelling. Hirlam needs a non-hydrostatic model at the convective resolving scales of a few km. An an-elastic version has been developed by the Tartu group and experience is being gained from this, whilst the Project is aiming for a version using the full compressible set of equations. This means more intense collaboration with Météo-France to use the dynamics of ALADIN in one way or another.

The physical parameterisation is being improved for the synoptic scale model while also developing useable schemes for the meso-scale as a first stage, to gain experience in high resolution.

Data assimilation has evolved a lot in the 4D-VAR area to the stage of an efficient scheme for high resolution (20 to 10 km at this stage). For the meso-scale, there are varying views about the applicability of 4D-VAR due to both economics and non-linearities and time scales. We do however argue that a 4D-VAR (or ensemble Kalman filter) scheme is necessary to use high resolution moisture related data since the multi-variate relationships at the km resolution are not known explicitly.

The Regular Cycle with the Reference system (RCR) of analyses and forecasts is still a very important activity and is initially continuing at ECMWF, but will become the role of one member's operational system (Finland). When the RCR has become the operational system of a member institute (FMI), the requirements for testing each major release will be even higher. This work will be carried out at ECMWF by various members. Furthermore results from the runs and probably also of the RCR will be made available to the Hirlam members through the HEX NET server at KNMI.

2 Scientific Progress

2.1 Data Assimilation

3D-VAR has been introduced as the Reference at ECMWF and has been used by several members operationally for several years and only two are still using OI. The FGAT option (First Guess at Appropriate Time) has been implemented and also a seasonal variation of background errors. A new version management system (CVS) is being employed for the code.

Learning and development of the ensemble assimilation technique has been started. A 10-member ensemble assimilation has been carried out for a 10-day period with observation perturbations. The NMC-software for computing analysis structure functions has been modified to work on the ensemble assimilation output.

An effort to generate 3D-VAR background error statistics for the 40 level model version at 30 km horizontal resolution has been done by collecting a 4 month data set from the SMHI pre-operational forecast system. Applying the NMC-software on this data set and the analysis of the results remains to be done.

The feasibility study together with a fairly extensive testing of 4D-VAR have been carried out and written up in a submitted Technical Report. Positive impact of 4D-VAR was shown for the December 1999 period with the intensive storms, although the impact was neutral for the following February period (2002). Tangent linear and adjoint code of the semi-Lagrangian scheme of the spectral model for 4D-VAR has been written and tested. This will make the execution of 4D-VAR much more economical. Also the multi-incremental formulation has been implemented, and this again opens for further economy for the minimisation. A proposal paper discussing the prospects for Hirlam 4D-VAR has been written.

In the surface analysis, the SHIP observation weights have been tuned and BUOY data are not used anymore (for the SST). The scientific documentation of the surface analysis together with the new surface parameterisation have been produced.

The sea surface temperature (SST) OI analysis has been developed, in anticipation of the SST products from the Ocean Sea Ice SAF. The ice fraction product is available and work has started to process that for the surface analysis.

A new snow analysis using OI has been written and found to be better than the existing scheme. Tuning of T2m and RH background error statistics has been done based on long assimilations.

Extensive impact studies with QuikScat have been run and show slightly positive results or neutral, depending on period. A few important events dominate the impact.

A lot of results have been documented in the recent ATOVS technical report. Use of ATOVS data over ice has been prepared. The EUMETSAT re-transmission service is working with data from three stations, Tromsø, Las Palomas and Søndre Strømfjord. The 3 others will come later. A licence agreement between the Hirlam Project and the NWP SAF has been signed in order to use the radiative transfer software, RTTOV7, used in 3D-VAR. Reception equipment for the EUMETSAT ATOVS re-transmission service has been installed in several places and work on using the data in that way is underway. Positive impact of the AMSU-A data was shown at DMI and the data are now used operationally there.

Assimilation of humidities from (more) GPS stations has continued and data collection ensured. Further work has been done on understanding the bias problems. MODIS satellite retrieved humidities have been assimilated.

Observation operator work for radar doppler winds has continued, mainly to address biases in the data. An impact study of the European wind profilers has been carried out and has been written up. There is a marginal positive impact.

SSSM/I 1D-Var code developed in NWP SAF has been implemented in HIRVDA. Integrated Water Vapour and wind speed can be retrieved and the data has been assimilated.

2.2 Forecast model

The increasing negative bias of surface pressure as a function of forecast time has been shown to be strongly correlated with cyclones and their too slow filling. The CBR turbulence scheme has been further developed to use a Richardson number dependency for the length scale in stable conditions and with a Blackadar surface layer matching. Based on arguments of existence of sub-grid scale variations in shear and stability and effect of averaging stability is not the same as the stability of the average, an additional term has been added. For momentum the shear may be due to gravity waves and is applied in the troposphere, whereas for temperature it is in the boundary layer. Furthermore, there is both experimental and theoretical evidence for that the turbulence continues further than the current cut-off, and an extra term has been added for this and the mixing is not allowed to go to exactly zero. Also this term is applied in the boundary layer only. After a number of trials and tuning, the effect is quite remarkable for curing the pressure (and geopotential) problem without affecting the other parameters to any significant degree.

Full assimilation-forecast experiments covering all seasons show the same large improvement in rms msl pressure and in precipitation scores. The modified scheme has been tested extensively both at KNMI and at DMI. The positive effects for most parameters were counteracted by the higher positive wind speed bias (even though standard deviations were not affected). A more realistic tuning of roughness length has been done (to take into account actual landscape features). This in combination with a somewhat reduced stable mixing (enhancement) seems to retain most of the large scale pressure benefits and give almost unbiased near-surface winds.

There is also a moist version of the CBR schemes developed and it has been tried in a 1D-context and shown to be beneficial, particularly at very high vertical resolution.

The new surface package (ISBA tiled scheme + analysis of surface variables) has been studied in a 1 year assimilation run to check the seasonal evolution of soil water content and screen variables errors.

Pre-operational testing in Sweden revealed a problem that frozen ground had too much resistance certain days in the transition season. A revision to have a much smaller barrier effect has been developed. The Météo-France soil freezing and thawing approach based on the introduction of two additional variables (surface and total frozen soil water) was coded in the frame of the tiled surface scheme and compared against the current method based on the "barrier effect" for the thermal constant. The results show that the Météo-France method is better and this has been implemented.

As a consequence of the tiling, there are alternative ways of computing the grid average postprocessed 2m temperatures and humidities. Averaging over the land tiles gives consistently better observation verification, but may not be what all users want. Therefore the normal 2m values are reverted to be averaged over all tiles and a new parameter used for the land averaged ones.

The new snow tile scheme with heat conduction has been interfaced with data assimilation. It performs well but will be tested more extensively. In the Swedish operational model, time step diagnostics are stored for three sites in order to verify against flux measurements.

The Reference snow scheme has been investigated intensively since there were pronounced positive temperature biases in the very cold winter periods experienced in the Nordic countries. In fact the ISBA implementation used the old snow scheme, with heat conduction from climate, for the snow treatment as it is known that the ISBA snow scheme is not very realistic. A partial solution to address the problem was found, in terms of using saturation pressure over ice instead of over water and ice combined. This reduces the error by about 1 degree or a bit more.

Further updates to the STRACO convection/condensation scheme reducing the lateral entrainment formulation and adjusting the parameter which determines the fraction of moisture convergence available for convection have been proposed and tested. This set of updates cures the extreme and unrealistic precipitation episodes taking place under very warm and humid conditions with strong convergences and the release of small precipitation amounts from too warm and shallow model clouds. It is additional to the ones described before (cloud parcel ascent, shallow convection parameterisation, microphysics thresholds, cloud cover changes). Extended tests have been done and show a clear improvement in precipitation contingency tables but with quite a large reduction of cloud cover and increased winter negative 2m temperature bias.

The convection sub-project has continued and completed the concerted testing effort (at met.no, KNMI, INM and SMHI) of comparing Kain-Fritsch (KF) with STRACO, and the material has been published in Newsletter No 42. The scores are very similar for most parameters, except for the vertical profile of humidity where KF is consistently better, indicating that the clouds or cloud cover is better (it is better in standard deviation but has a negative bias). It has been agreed that a KF version will be installed as an option with the Reference and be maintained that way. The computing efficiency has been of some concern, but it is not excessively expensive on most computers including the CRAY SV1, but it is still on the NEC. The Bechtold version (Météo-France) has been shown to be efficient (on Fujitsu) and this is a likely code to be used in the future.

An extensive report documenting the Sub Grid-Scale Orography (SSO or "Gravity Wave Drag") scheme and all the experimentation has been published. The impact of the SSO scheme has been compared with Météo-France and verified to be very similar in behaviour. The overall effect in HIRLAM is neutral, although the effects of the scheme can clearly be seen. The SSO scheme introduces extra drag but this retards the surface winds and the turbulence scheme becomes less active in a corresponding way. The way of doing it through the SSO parameterisation is however deemed to be more physically correct than to have increased turbulence (and enhanced roughness length).

The radiation scheme has been reviewed in some aspects. New and clean interface routines to the tiled ISBA scheme have been written and are tested together with a correction of an older modification concerning the condensation nuclei plus a long wave modification described written and documented early in the Project. Testing of the radiation scheme updates and new interface have continued and show slightly positive impacts.

The ECMWF physics interface to HIRLAM has been updated to HIRLAM version 5.0.6. Meteorological assessment was done for one December month and one May month. Results showed better scores of screen variables for the ECMWF physics than with the old Hirlam physics, and particularly for one of the periods. The advantage of ECMWF physics was mainly gone after the implementation of the new surface treatment in HIRLAM (ISBA) including analysis of surface variables.

Work on physics-dynamics coupling has proceeded following two approaches of averaging physical tendencies. Results give small improvements of forecasts and better stability (for longer time steps). Radiation, convection and lately also vertical diffusion have been treated in the improved coupling.

The modifications of the semi-Lagrangian scheme for the noise problems at 10 km have been tested and will be implemented, following some more tests. An alternative method to compute vertical velocities with a finite volume approach has also been tried, but does not solve the problem.

The work on transparent Lateral Boundary Conditions (LBC) continued with inclusion of orography in the real-data demonstration. The transparent LBC have been tested for the non-linear shallow water equations in a nested environment with real data. Work on a number of proposals for well posed LBC, e.g., opaque, characteristic, first order transparent, "semi-Lagrangian", has proceeded and compared with HIRLAM's. Results, particularly wind forecast, are slightly better than the current Davies scheme when characteristic boundary conditions are applied.

The work has continued with waves whose advection speed are higher than the gravity waves and b.c. have successfully been implemented in the shallow water context. Another step which has been planned for a long time is the proper boundary condition for the semi-implicit Helmholtz solver, instead of having a zero b.c. for the second derivative of divergence, specify geopotential. This has been tested in 3D and had a large impact (for this one case).

Work on transparent Lateral Boundary Conditions (LBC) based on a mixed finite elements formulation of the shallow water equations has been conducted at met.no and the 3D formulation is being worked out.

Work has been done to evaluate boundary errors in a double nested HIRLAM set up. Varying the spatial resolution between the outer and inner area, show that the errors due to the Davies boundary formulation are smaller than the errors obtained from using coarser boundary fields.

Following the Dublin Workshop the boundary relaxation from the MC2 model, updating before physics (and then relaxing the physics tendencies towards zero), was shown to cure completely a problem with blow ups in the boundary zone in the new Finnish area. It has also been tested for an extended period.

It gives more realistic precipitation patterns near the boundaries and prevents code crashes experienced at FMI which manifested as grid point storms near the boundaries.

The nonhydrostatic, two-time level, semi-Lagrangian, semi-implicit Hirlam model has been developed and implemented for a parallel-computing Beowulf-cluster environment. The semi-Lagrangian version has some noise due to interpolation which is being sorted out.

A model comparison study (including the following models: Nonhydrostatic Aladin, Meso-NH and NH HIRLAM) has been carried out at Météo-France. Two ideal cases of dry flow over mountains have been selected for the comparison exercise. Hirlam showed to be more dissipative than the others.

The model has been further tested in 2.5, 5 and 10 km resolution, and the NH effects (differences) are mainly seen at 2.5 km. The SI version has been observed to overdevelop some cyclones in recent tests.

Testing was conducted at KNMI to study the possible effect of Digital Filtering Initialisation (DFI) on the damping of initial developments. The backward adiabatic step creates imbalance due to lack of boundary layer friction and the forecast after TDFI starts with pressure perturbations and with lowered values of some physical parameters. A solution is to do forward launching (at +1 hour) instead and has been developed. Still the incremental DFI is slightly better and does not have the problem of not producing initialised fields (at 0h).

Encouraging results and plans were shown at the INM/SRNWP European LAM EPS Workshop, where several interesting and very positive results were shown, by using ECMWF perturbations (met.no, DNMI and COSMO/Bologna.) and at NCEP (with bred perturbations) where very significant improvements in verification scores were seen. These effects are of course due to filtering effects. Some were showing multi-model results and improvements from this whereas other evidence from the Met Office showed that it was not necessarily adding much (if the 12h time handicap is removed). Singular vectors are inherently superior for finding the real analysis uncertainties whereas breeding is almost for free and shown to work in LAM, provided also globally bred vectors are supplied at the boundaries.

Plans for LAM EPS have been set up at INM, following last October's Workshop, and initial experiments have been done. The spread is difficult to reach in the short range.

The LAM EPS work with Hirlam has continued at met.no. Evolved Singular Vectors from ECMWF seem to give better results than non evolved ones.

3 System developments

The 3D-VAR analysis has now been introduced in the Reference system, following quite a bit of technical work at ECMWF. Tests were made for correctness of implementation. The general quality of the system is in no doubt as e.g. shown by the 5 members who have implemented it operationally. The upper air scores were very much in favour of the new release due to 3D-VAR.

Many members are testing with increased vertical resolution and the polynomial representation of levels has been enhanced and used to derive the definition of 40 (and 50 and 60) levels consistent with the current height of the lowest level at about 30 m.

The HIRVDA system at ECMWF was upgraded to its latest version, and scripts were updated accordingly. HIRVDA is being integrated with the rest of the reference and some aspects remain.

At the end of 2002, actions to move the system at ECMWF from Fujitsu to IBM were initiated and accelerated in March. The Hirlam Reference system was provided on the IBM from the beginning of April. Verification tests were carried out to validate its equivalence with earlier results run on the Fujitsu.

A "unified" version of asynchronous I/O (called Hirlam Gribfile Server, HGS) was introduced as an option in Hirlam version 5.2.2. There are two underlying implementations, called the IPC and MPI versions of

HGS. The IPC version is based on the code developed by Jan Boerhout (Hirlam Newsletter 39). The MPI version is based on code developed in Finland at CSC/FMI, but is modified to provide the same functionality as the IPC version. The unified version is described in Hirlam Newsletter 41.

The climate system has undergone extensions and corrections. The filtering of orography and all the new codes and fields for the SSO scheme are also being implemented. New data for the ISBA scheme have been added and this will be implemented. Several improvements and extensions to the climate generation system were implemented. There are now global coverages and orography and roughness length computation following Kai Sattler have been prepared. The filtering of orography has also been prepared and is being tested.

The DMR runs have continued but still remain to be brought under the control of mini-SMS. A new version of the Delayed Mode Runs based on Hirlam 5.2.3 was developed and implemented. This version uses mini-SMS, a 0.2° model grid, 40 vertical levels, "frame" boundaries from the ECMWF LBC project, and 3D-VAR for data assimilation. This version has been implemented on the hpc IBM at ECMWF.

A proposal has been made from FMI to host and run a DMR centre (or Regular Run of the Reference system, RCR), where the FMI would actually run the Reference system as its operational run. An agreement was made and it was approved by the Hirlam Council. Operational attention to the runs and real time monitoring are some of the advantages. Near real time data will be made available to members. Extensive experimentation and parallel runs as well as a lot of diagnostics would be carried out by Hirlam and FMI staff. New Reference system releases will be much more scrutinised and acceptance agreed between the Hirlam and FMI management. Having the Reference system run operationally will raise its status significantly.

The Project Leader has continued the discussion with ECMWF about the Optional Project short cut-off data assimilation and forecasts. ECMWF has investigated how verification of the other (than 00) cycles can be done and how the data can be stored (or short time archived; archiving was not part of the agreement). This has now been implemented by ECMWF.

The HeXnet has been maintained. Many documents were added. A new hosting machine at KNMI, outside its inner firewall, has been installed and is available. Security issues have been studied and a proposal for a safe access from the Hirlam members has been formulated. A new HeXnet system is being implemented on that machine, with both the remote access, for outside users to add contents, and with a modern overall design.

4 Meetings

- 1st European workshop on short range LAM EPS, 3-4 October 2002, INM, Madrid.
- EWGLAM/SRNWP meeting, 7-10 October, KNMI, De Bilt.
- Hirlam workshop on Meso-scale modelling, 14-16 October 2002, Dublin.

5 Publications

HIRLAM Newsletter No. 41, June 2002.

SRNWP Mesoscale Verification Workshop (23-24 April 2001) , September 2002.

HIRLAM Newsletter No. 42, November 2002.

HIRLAM-5 Scientific Documentation, December 2002.

HIRLAM workshop on Meso-scale modelling, 14-16 October 2002, Dublin. Workshop Report, January 2003.

HIRLAM Newsletter No. 43, June 2003.

HIRLAM-5 Final Report, September 2003.

The Technical Reports are available on the open HIRLAM NET, http://hirlam.knmi.nl/ During the period, the following ones have appeared:

56. Parametrization of subgrid-scale orography effects in HIRLAM Laura Rontu, Kai Sattler and Robert Sigg. Norrköping, October, 2002.

57. Four-dimensional variational data assimilation for a limited area model. Xiang-Yu Huang, Xiaohua Yang, Nils Gustafsson, Kristian Mogensen and Magnus Lindskog. Norrköping, December, 2002.

58. Analysis of surface variables and parameterization of surface processes in HIRLAM. Part I: Approach and verification by parallel runs. Ernesto Rodríguez, Beatriz Navascués, Juan José Ayusoand Simo Järvenoja. Norrköping, January, 2003.

59. Analysis of surface variables and parameterization of surface processes in HIRLAM. Part II: Seasonal assimilation experiment. Beatriz Navascués, Ernesto Rodríguez, Juan José Ayuso and Simo Järvenoja, January, 2003.

60. Assimilation of ATOVS data in the HIRLAM 3D-VAR System. Harald Schyberg, Tomas Landelius, Sigurdur Thorsteinsson, Frank Thomas Tveter, Ole Vignes, Bjarne Amstrup, Nils Gustafsson, Heikki Järvinen and Magnus Lindskog. Norrköping, April, 2003.

61. A Feasibility Study of Assimilating European Wind Profiler Data Using the HIRLAM 3D-VAR System. Xiang-Yu Huang and Magnus Lindskog. Norrköping, August, 2003.

The Finest Scale HIRLAM - the Tartu Model

R. Rõõm, Tartu University

1 Introduction

Low resolution ($\Delta x > 10$ km) numerical models, including HIRLAM, are hydrostatic. When moving to resolutions $\Delta x < 10$ km, this assumption becomes incorrect. There exists two choices: either to initiate a new numerical model which treats NH forces properly (the DWD *Local Modell* case) or to modify the existing HS model (this case). The task we raised was to develop a NH extension to the exiting numerical model HIRLAM without abandonment of existing numerical framework and with hybrid-coordinate maintenance. This task concerned adiabatic dynamics and did not affect various physical parameterizations.

2 General and Approximate Equations

The main problem consisted in introduction of NH forces into pressure-coordinate-based primitive-equation formalism. We started from the general NH equations (GE) in isobaric coordinates, proposed in (Rõõm, 1990) and comprehensively discussed in (Rõõm, 2001).

In GE dynamics, the main NH characteristic of motion is the non-dimensional density of matter in pressure coordinates, n. This field departures a little from unity at all scales: $|n - 1| \sim 10^{-5}$ - 10^{-6} for synoptic and planetary scale, $|n - 1| \sim 10^{-3}$ - 10^{-4} for HS meso-scale, $|n - 1| \sim 10^{-2}$ for shorter NH scale, yet substantial it becomes in the last case. Various approximations of different complexity, which can be deduced from GE, using the smallness of n, *Elastic acoustically relaxed model,Miller-Pearce semi-anelastic p-coordinate model, Anelastic p-coordinate model Hydrostatic primitive-equation model.*

The domains of application of these models are described in (Rõõm & Männik, 1999), and are as presented in Fig. 1.

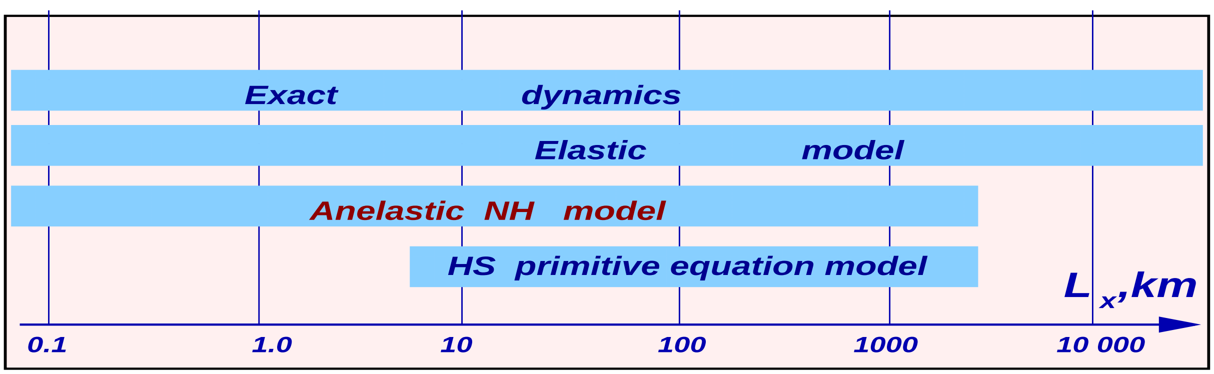

Fig. 1. Domains of applicability of different pressure-coordinate models.
L_x - *horizontal scale of the process.*

The choice was made in favor of the ANELASTIC P-COORDINATE APPROXIMATION, which coincides with HS model in the long-wave part and catches all NH effects of shorter scales. In addition, this model filters external acoustic (Lamb) waves, treating the surface pressure as the adjusted one and providing the most detailed presentation of small-scale surface pressure pattern.

3 Numerical Implementation of NH HIRLAM

Coordinate frame is the terrain following hybrid coordinate system of ECMWF origin. Spherical geometry is applied in horizontal dimensions, and the rotated spherical coordinates are used, like in the HS HIRLAM. The grid is the Staggered Arakawa C-grid.

Time integration scheme supported are the explicit leapfrog (Eulerian three-time-level scheme, *Expl. Euler*), semi-implicit leapfrog (Semi-implicit Eulerian three-time-level scheme, *SI Euler*), and semi-implicit, semi-Lagrangian two-time-level scheme (*SISL*).

Spectral smoothing is the horizontal implicit 4th order scheme and (optional) vertical explicit 4th order scheme.

Boundary conditions are the Davies' boundary relaxation scheme on lateral boundaries, surface pressure relaxation scheme on the lower boundary, and the sponge layer at the top.

Elliptic solver (ϕ-equation) to find the baric (complementary to ordinary hydrostatic) makes use of 3D orthogonal basis with boundary conditions treated as the singular boundary sources.

Physical parameterizations are the same as in hydrostatic HIRLAM (The physical tuning and updating was considered as a separate task for future, as it does not affect directly the NH updating of adiabatic dynamics).

The parallel computing environment is organized to be consistent with the Reference HS HIRLAM code.

4 Computational Efficiency

The time-consumption rate is approximately two times the HS scheme time-consumption rate.

Maximum time-step (in seconds):

Δx, km	U, m/s	$\Delta x/U$	Expl. Euler	SI Euler	SISL
11	60	183	60	150	250
2.0	20	100	40	80	200
0.5	30	18.3	16	18	55

5 Testing

Extensive testing with model flow regimes was carried out. Some examples of modeling of stationary flow regimes over circular hill are presented in Figures 2 and 3.

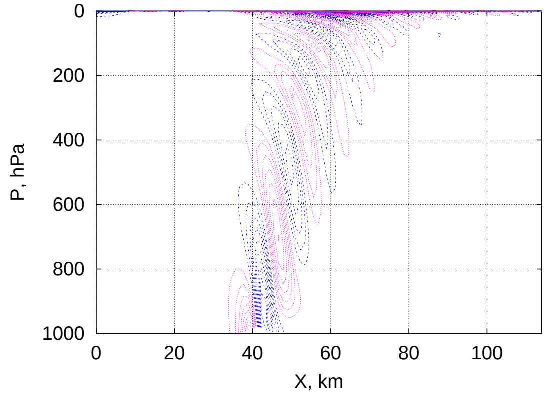

Fig. 2. Flow over circular hill. Vertical velocity distribution, contour interval 0.1 m/s. $\Delta x = \Delta y = 1$km; Vertical resolution: 60 level ECMWF grid.
$a = 3$ km, $h = 200$ m, $N = 0.015$ 1/s, $U = 20$ m/s.
(Männik & Rõõm, 2001).

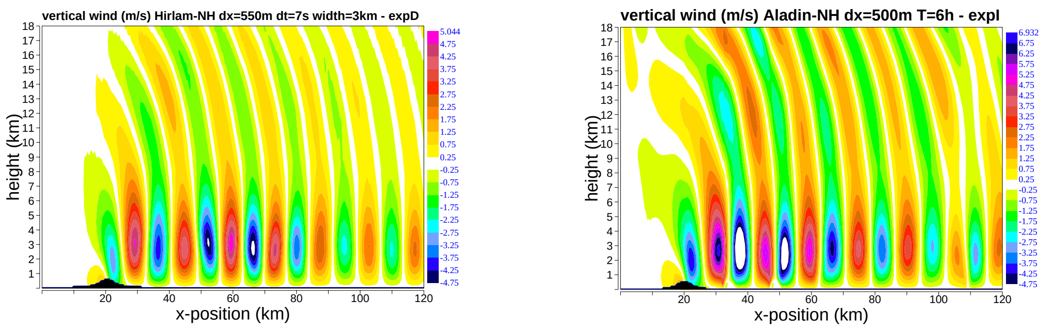

Fig. 2. Non-hydrostatic flow regimes over isolated mountain according to NH HIRLAM (left) and Aladin-NH of Meteo France (right). *$a = 3$ km, $h = 600$ m.* (Männik 2003).

Real-condition tests at 10 km resolution are presented in Figures 4 an 5.

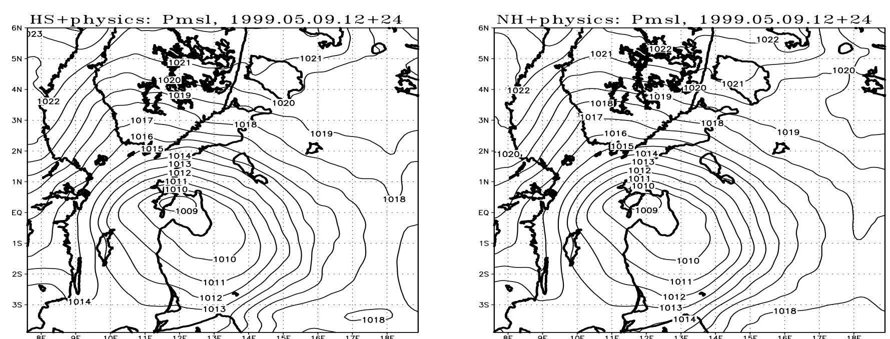

HS model *NH model*

Fig. 4. Forecast of the cyclone evolution with HS SI and NH SI Eulerian schemes. *0.1 deg (11 km) resolution, 31 levels.*

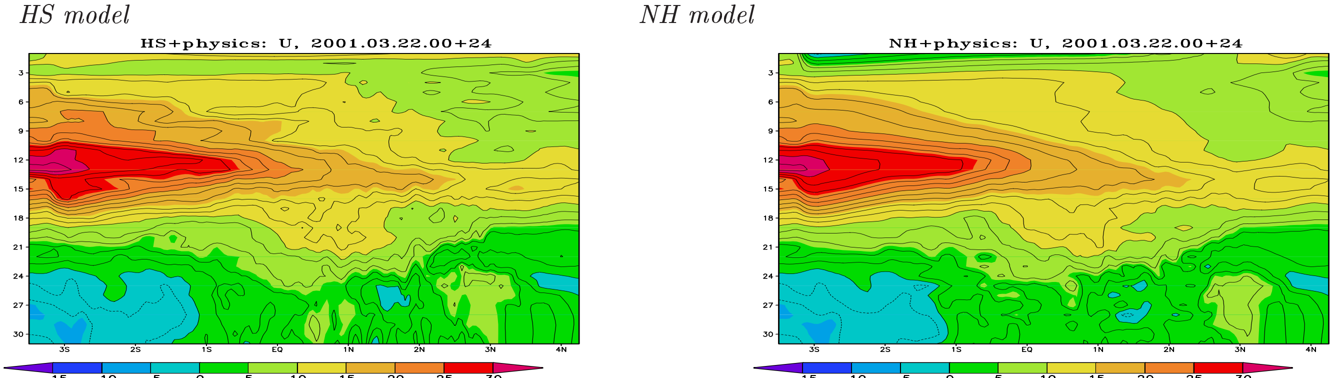

Fig. 5. Cross-section ($\lambda = 10E$) of the U-component of wind for 2001.03.22.00+24. over Norway. HS SI (left) and NH SI Eulerian schemes (right panel). *0.05 deg (5.5 km) resolution, 31 levels.*

6 Forecast Statistics

Up to date (late autumn 2003), statistics with 0.1 deg (11 km) resolution model are carried out (Männik, 2003). Results of these statistical experiments are presented in Fig. 6 for sea-level pressure, geopotential, and temperature.

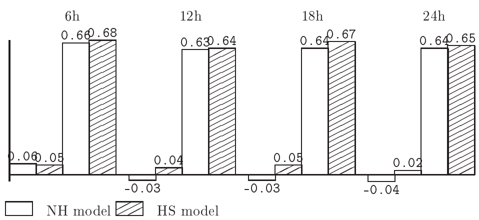

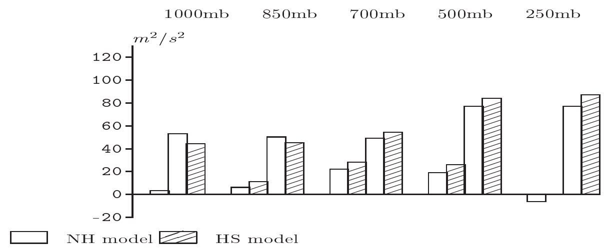

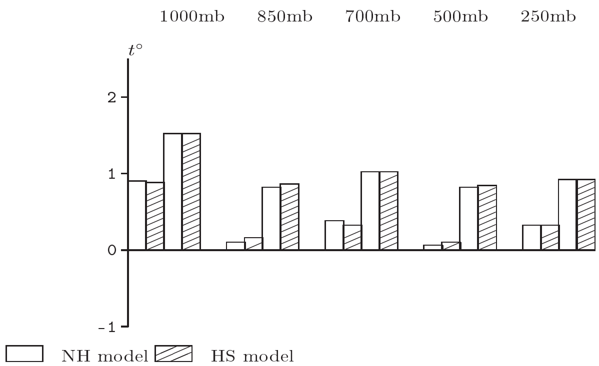

Fig. 6. Forecast statistics.
Grid 206×206*, 31 levels, 0.1 deg resolution.*
Period: 1999.08.24 - 09.04

At the 5 km resolution, the model accuracy looks quite similar. As these experiments demonstrate, the accuracy of NH model is comparable to the hydrostatic parent model at HS mesoscale resolutions.

So far we lack statistics at 1 - 3 km resolutions. Due to very small modeling domains, the standard HIRLAM verification procedures are not applicable in these cases, and new statistical testing tools must be developed which HIRLAM lacks so far.

7 Preoperational application

Currently (November 2003), with joint efforts by Finnish Meteorological Institute (FMI), Estonian Meteorological and Hydrological Institute (EMHI), and Insitute of Environmental Physics of Tartu University (TU), a preoperational NH HIRLAM is in the stage of implementation at EMHI. Model has two resolutions and two forecast areas, as shown in Fig. 7. The coarser model, named ETA, has 0.1 deg (11 km) resolution and 40 levels in vertical. It downscales initial and boundary data from 33 km resolution FMI HIRLAM. The finer one, ETB, has resolution 3.3 km and takes its initial and boundary data from ETA model.

8 Nonhydrostatic effects

Question, at which resolution the NH effects become considerable, is relevant for NH modeling. At orographically forced flows this scale is approximately $\Delta x \sim 5$ km (as the scale of the minimal resolved orography $a \sim 2\Delta x \approx 10$ km). Orographic effects emerge in down-stream tilting of orographic waves as demonstrate Figs. 2 and 3. For flat terrain with no mountain wave excitation, the NH effects should appear in deep convection events, like the thunderstorms, if the resolution is fine enought to resolve individual convective cells.

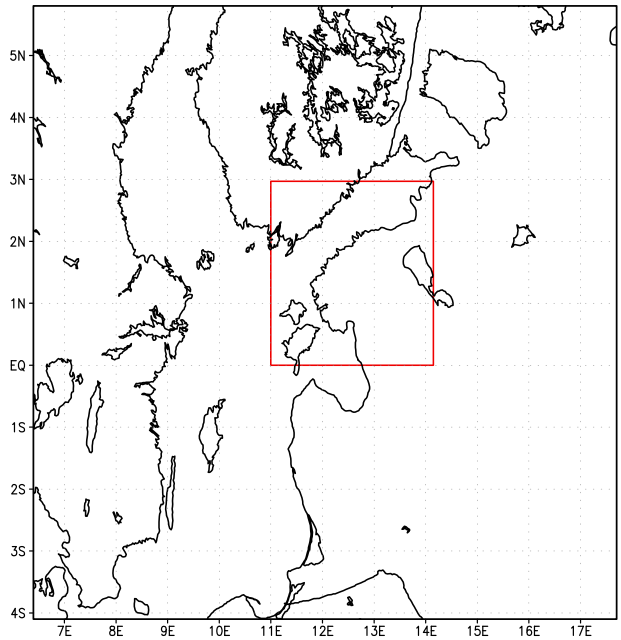

Fig 7. Forecast domains in ETA (large grid) and ETB (small box).

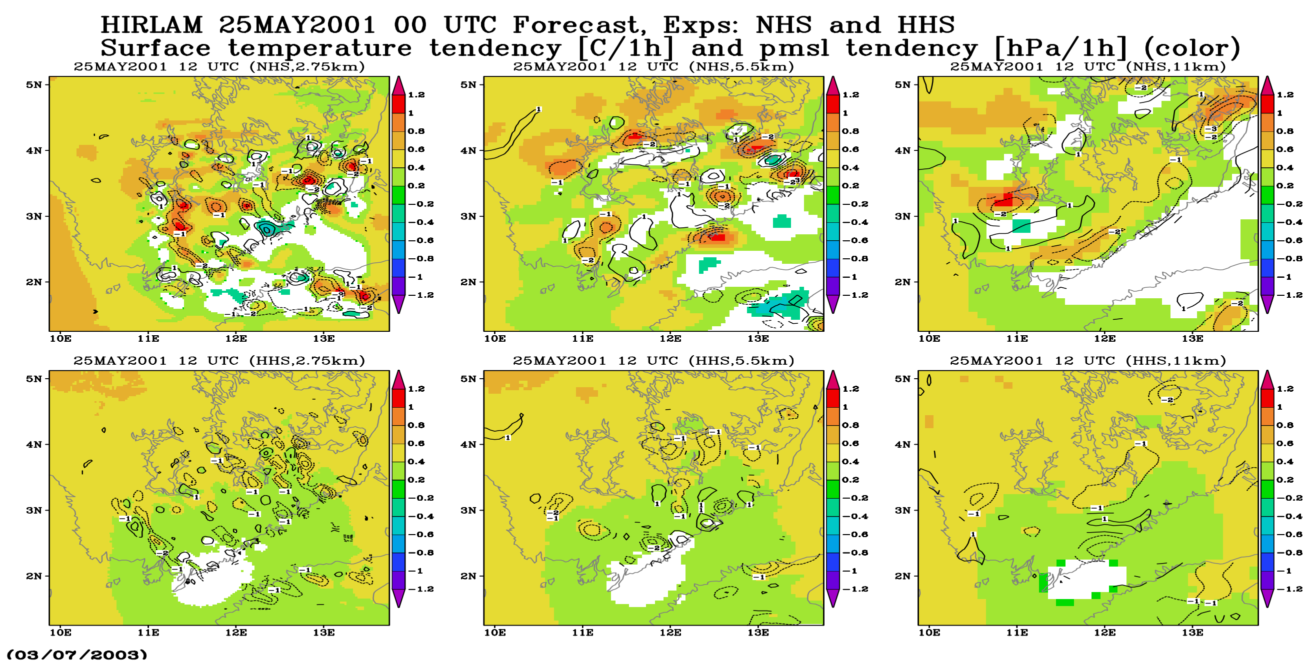

Fig. 8. Surface temperature and pressure fluctuation pattern, modeled with NH (top panels) and HS HIRLAM (bottom) for 2.75 (left), 5.5 (centre), and 11 km (right) resolution cases. *(With due reference to Sami Niemela)*

The oserved short-scale surface temperature and pressure fluctuations are

$$T_s' \sim 3 \text{ K}, \quad p_s' \sim 0.1 - 0.3 \text{ hPa}.$$

Convection modeling with both HS and NH HIRLAM at 2.75, 5.5 and 11 km resolution was lately carried out by Sami Niemela, Helsinki University (personal communication). As these experiments demonstrate (Fig. 8), both the HS and NH models get the near–surface temperature fluctuations properly, but only the NH model can catch the associated surface pressure fluctuations with correct amplitudes at 2.75 km resolution, and with somewhat reduced amplitudes at 5.5 km resolution. These examples demonstrate that the resolving power (resolution of relevant physical effects) of the NH HIRLAM with respect to the presentation of fine-scale surface pressure fluctuations is high.

9 References

Rõõm, 1990: General equations of atmospheric dynamics in isobaric coordinates, Izvestia, Atmospheric and Oceanic Physics, 26,1: 9 - 14.

Rõõm, R., 2001: Nonhydrostatic adiabatic kernel for HIRLAM. Part I: Fundamentals of nonhydrostatic dynamics in pressure-related coordinates. Hirlam Technical Report No 48, 25 p.

Männik, A., Rõõm, R., 2001: Nonhydrostatic adiabatic kernel for HIRLAM. Part II: Anelastic, hybrid-coordinate, explicit-Eulerian model. Hirlam Technical Report No 49, 53 p.

Rõõm, R., Männik, A., 2002: Nonhydrostatic adiabatic kernel for HIRLAM. Part III: Semi-implicit Eulerian scheme. Hirlam Technical Report No 55, 29 p.

Rõõm R., A. Männik , 1999: Responses of different nonhydrostatic, pressure-coordinate models to orographic forcing. J. Atm. Sci., v. 56, No 15, 2553 - 2570.

Männik, A., 2003: Implementation and validation of the nonhydrostatic adiabatic core of the numerical weather prediction model HIRLAM, Dissertationes Geophysicales Universitatis Tartuensis, Tartu Ülikool, TÜ Kirjastus, 2003.

Current Problems of Stable Boundary Layer Modelling

Sergej S. Zilitinkevich
Department of Earth Sciences, Uppsala University, Sweden

Turbulent boundary layers control the exchange processes between the atmosphere and the ocean/ice/land. The key problem of boundary-layer physics is to determine the momentum, energy and matter fluxes in a wide range of boundary-layer regimes from stable and neutral to convective. This paper presents the state of the art and modern developments in stable boundary-layer physics with focus on the recently recognised non-local mechanisms overlooked in the traditional theories. New developments are compared with experimental and large-eddy simulation (LES) data. They are motivated by urgent necessity to improve boundary-layer parameterisations in very high resolution environmental models, particularly, in the coupled atmosphere-ocean models.

It is common knowledge that basic features of SBLs exhibit a noticeable dependence on the free-flow static stability and baroclinicity. However, the concern of the traditional boundary-layer meteorology was almost without exception the barotropic nocturnal SBL, which develops at mid latitudes on the background of a neutral or slightly stable residual layer. The latter separates the SBL from the free atmosphere. It is not surprising that the nature of turbulence in the nocturnal SBLs is basically local, and their integral features do not depend on the properties of the free flow. The near-surface and the inner portions of these layers are well described by the Monin-Obukhov and the Nieuwstadt similarity theories, respectively. The nocturnal SBLs are sufficiently accurately modelled using traditional, comparatively simple local closure schemes.

An alternative type of the SBL frequently observed in Polar and coastal regions is the long-lived SBL, i.e. the layer in which the stable stratification is maintained day and night. Then no residual layer is observed, so that the SBL is placed immediately below the stably stratified free flow. Under these conditions, the turbulent transports of momentum and scalars even in the surface layer - far away from the SBL outer boundary - depend on the free-flow Brunt-Visl frequency, N. Furthermore, integral measures of the long-lived SBLs (their depths and the resistance law functions) depend on N and also on the baroclinic shear, S. In the traditional SBL models both non-local parameters N and S were overlooked. The key mechanism responsible for non-local features of the long-lived SBLs is the radiation of internal gravity waves (IGW) from the SBL upper boundary to the free atmosphere and the IGW-induced transport of the squared fluctuations of velocity and potential temperature.

The above reasoning obviously calls for a comprehensive revision of the traditional theory. In a series of papers (quoted below in References) an advanced theory has been proposed. It includes the following developments:

- Generalised scaling for the surface layer turbulence accounting for the distant effect of the free-flow stability. In the nocturnal SBL, it reduces to the classical Monin-Obukhov theory.
- SBL depth formulation accounting for the free-flow stability, baroclinicity and non-steady processes. It covers a wide range of regimes overlooked in earlier works and shows quite narrow limits of applicability of the widely used bulk Richardson number approach. For the truly neutral planetary boundary layer it yields the Rossby-Montgomery depth-scale and for the nocturnal SBL, the Zilitinkevich depth-scale.
- Generalised SBL bulk resistance and heat/mass transfer laws accounting for the effects of the free-flow stability and baroclinicity on the A, B, C and D-stability functions. The inclusion of the dependence on N and S resulted in essential collapse of LES data on these functions. In other words, the above laws are rehabilitated as a practical tool the SBL parameterisation. This approach has no alternative in very shallow SBLs, where traditional surface-later flux-profile relationships become inapplicable.

The above theoretical results are verified against LES and atmospheric data. The new theory answers a number of questions, which looked puzzling until present, in particular, how well-developed turbulence is maintained in the stable surface layer at much larger Richardson numbers than the classical theory permits. It affords development of principally improved SBL parameterisations for use in a range of applied environmental models.

The physical nature of the stably stratified turbulent layers in the ocean is principally the same as in the long-lived atmospheric SBL. In both cases large eddies in the boundary layer generate IGW in the adjacent stably stratified free flow (the thermocline in the ocean or lakes), which results in the IGW-induced third-order fluxes. Thus the above new developments could be reformulated in oceanographic term and after appropriate modification (in particular including the Langmuir circulations) and validation employed in ocean modelling.

References

Zilitinkevich, S., and Mironov, D.V., 1996: A multi-limit formulation for the equilibrium depth of a stably stratified boundary layer. Boundary-Layer Meteorol., 81, 325-351.

Zilitinkevich, S., Johansson, P.-E., Mironov, D.V., and Baklanov, A., 1998: A similarity-theory model for wind profile and resistance law in stably stratified planetary boundary layers. Journal of Wind Engineering and Industrial Aerodynamics 74-76, 209-218.

Zilitinkevich, S., and Calanca, P., 2000: An extended similarity-theory for the stably stratified atmospheric surface layer. Quart. J. Roy. Meteorol. Soc., 126, 1913-1923.

Perov, V., and S. Zilitinkevich, 2000: Application of an extended similarity theory for the stably stratified atmospheric surface layer to the HIRLAM, HIRLAM Newsletter No. 35, 137-142.

Perov, V., S. Zilitinkevich and K.-I. Ivarsson, 2001: Implementation of new parameterisation of the surface turbulent fluxes for stable stratification in the 3-D HIRLAM. HIRLAM Newsletter, No. 37, 60-66.

Zilitinkevich, S., Baklanov, A., Rost, J., Smedman, A.-S., Lykosov, V., and Calanca, P., 2002: Diagnostic and prognostic equations for the depth of the stably stratified Ekman boundary layer. Quart, J. Roy. Met. Soc., 128, 25-46.

Zilitinkevich, S., 2002: Third-order transport due to internal waves and non-local turbulence in the stably stratified surface layer. Quart, J. Roy. Met. Soc. 128, 913-925.

Soomere T., and Zilitinkevich, S.S., 2002: Supplement to "Third-order transport due to internal waves and non-local turbulence in the stably stratified surface layer". Quart, J. Roy. Met. Soc. 128, 1029-1031.

Zilitinkevich, S.S., Perov, V.L., and King, J.C., 2002: Near-surface turbulent fluxes in stable stratification: calculation techniques for use in general circulation models. Quart, J. Roy. Met. Soc. 128, 1571-1587.

Zilitinkevich, S.S., and Baklanov, A., 2002: Calculation of the height of stable boundary layers in practical applications. Boundary-Layer Meteorol. 105, 389-409.

Zilitinkevich S. S., and Esau, I. N., 2002: On integral measures of the neutral, barotropic planetary boundary layers. Boundary-Layer Meteorol. 104, 371-379.

Zilitinkevich S. S., and Esau, I. N., 2003: The effect of baroclinicity on the depth of neutral and stable planetary boundary layers. Quart, J. Roy. Met. Soc. 129, 3339-3356.

Maderich V., Nesterov O. and Zilitinkevich, S., 2004: "The influence of different parameterisations of meteorological forcing and turbulence schemes on modelling of eutrophication processes in a 3-D model of estuary. Submitted to Ocean Dynamics.

Zilitinkevich S. S., and Esau, I. N., 2004: Bulk resistance and heat transfer laws for geophysical stable boundary layers. Submitted to Quart, J. Roy. Met. Soc.1. Kalnay E. et al. The NCEP/NCAR 40 year reanalysis project. Bull. Am. Meteor. Soc.,Vol. 77, 1996.

Experimental very high resolution forecasting at EMHI

Aarne Männik, University of Tartu
Ivar Ansper, EMHI

1 Cooperation

In 2002 was made an agreement between Estonian Meteorological and Hydrological Institute (EMHI), Finnish Meteorological Institute (FMI), and University of Tartu (UT) to develop a very high resolution numerical weather prediction environment at EMHI by implementing experimentally the non-hydrostatic extension of HIRLAM developed by UT in the quasi-operational regime. The main goals of the agreement were:

- to develop an expert group and initiate numerical weather modeling at EMHI;
- to demonstrate the numerical weather prediction potential of very high resolution NH HIRLAM in near-operational conditions;
- to promote meteorological education at UT with emphasis on numerical modeling of atmospheric dynamics and weather prediction;
- to generate very high resolution numerical forecasts for the mutual use by EMHI and FMI.

2 Computing system

The computing system used to run HIRLAM at EMHI is a Linux cluster. The cluster consists of 12 computing nodes. Each node has 1GB RAM and the processor is 1.6 GHz Pentium IV. The nodes are connected together with Gigabit Ethernet cards. The operating system on each node is RedHat Linux 7.3. The LAM MPI software is used to arrange parallel computations on the cluster and the Intel Fortran (Fortran 95) and gcc are the compilers on the system.

3 Forecast model and integration areas

The environment is based on HIRLAM version 6.1.0 with the local fixes. The main features of HIRLAM which are employed in the numerical weather prediction environment are as follows:

- optimum interpolation for data analysis,
- implicit normal mode initialization as initialization scheme,
- semi-implicit semi-Lagrangian scheme for hydrostatic model,
- ISBA scheme for surface parameterization,
- the STRACO scheme for large scale and convective condensation,
- Savijärvi radiation scheme,
- CBR-turbulence scheme.

Two integration areas are defined in the forecasting environment at EMHI. The first area called ETA has $114 \times 100 \times 40$ grid with 11.1 km horizontal resolution. The model uses hydrostatic semi-implicit semi-Lagrangian integration scheme with 180 s time step. The 36h forecasts are produced continuously twice a day starting at 00 and 06 GMT. The boundary fields to the ETA area are provided by FMI from their operational model.

The second area called ETB has $106 \times 100 \times 40$ grid with 3.3 km horizontal resolution. During the workshop this area was reported to be hydrostatic semi-implicit semi-Lagrangian model with 60 s time step which is not running in continuous mode. During the writing of the extended abstract the area produces 36h forecast starting at 00 GMT every day. The nonhydrostatic model with semi-implicit Eulerian time-integration scheme with 30 s time step is employed. The boundary fields are taken from forecasts of ETA area. Both areas can be seen on the Figure 1

4 Problems and future developments

The installation and the short period of operations has revealed several shortcomings in the forecasting environment. The quality of climatology fields in standard HIRLAM has appeared to be poor for 3.3 km resolution. This is the main reason why ETB area is not working in continuous mode and the nonhydrostatic model has not been applied yet. Another problem is that the environment needs a strategy for verification of forecasts. The quality of forecasts has been estimated only subjectively so far. In the beginning standard verification procedures of HIRLAM should be applied. Based on subjective estimations, the model tends to over-predict the cloud fields. However, better verification statistics should be used to draw the conclusions.

In regard of future developments the problems mentioned before have to be addressed in the first place. Climate files have to be corrected and basic verification scores have to be introduced. The nonhydrostatic HIRLAM in 3.3 km resolution area has to be applied as soon as climate files are corrected. In fact during the time between the workshop and writing of the extended abstract the problems with high resolution climate fields have been corrected with the help from HIRLAM community and the nonhydrostatic model is running in continuous mode now. An important goal is that the semi-Lagrangian semi-implicit version of nonhydrostatic HIRLAM should be employed in the ETB area if ready. Also the physical package of HIRLAM needs critical revision at 3.3 km resolution. The interaction with nonhydrostatic adiabatic core should be investigated as well.

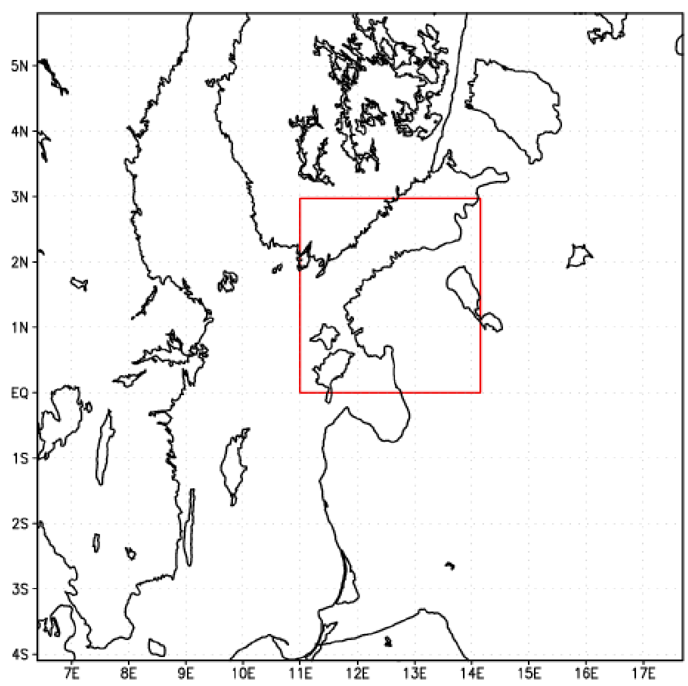

Figure 1: ETA and ETB forecasting areas at EMHI

On the parameterization of precipitation in warm clouds

Priit Tisler [1,2], Hannu Savijärvi[1]
[1]Division of Atmospheric Sciences, Department of Physical Sciences,
University of Helsinki, P.O. Box 64, FIN-00014 Helsinki, Finland
[2]Finnish Meteorological Institute,
P.O. Box 503, FIN-00101 Helsinki, Finland

It is well-known that "warm rain", i.e. rain from low warm clouds, is caused by coalescence and collection processes between different-sized cloud and rain drops, as these fall at their different terminal velocities within the cloud. This autoconversion leads into a bimodal droplet spectrum, the growth of which is reasonably well mimicked by the so-called stochastic coalescence models (Berry and Reinhard, 1974). However, such spectral representations are much too slow and cumbersome to be used in numerical weather prediction (NWP) models. Therefore, simpler bulk rain parameterizations are much-needed and much-used both in NWP and in climate (GCM) modelling. The accuracy and realism of such rain parameterizations is thus quite important, even more so as precipitation is one of the most important forecast products for weather and climate alike.

Sundqvist (1988) suggested a now widely adopted fast NWP cloud scheme, in which the amount of cloud water (cloud liquid water mixing ratio m) is predicted in each grid point. Precipitation (the amount of rain water) is not predicted in this scheme directly. Instead, it is parameterized (diagnosed) as the function of m, in a fairly simple but ingenious fashion. This "rain" parameterization has been adopted in many operational NWP models (e.g., HIRLAM), and even in some, which do not use the original Sundqvist cloud scheme itself (e.g., the ECMWF model, Tiedtke, 1993).

The amount of small drop cloud water, obtained from m, is important input for the radiation schemes of the models. Also the big drop contribution, i.e. the within-cloud rain water, obtained directly from the Sundqvist parameterization, might occasionally be important for solar radiation (Savijärvi et al., 1997). It is not yet included in most radiation schemes although Savijärvi (1997) shows a simple way to do that, provided that the within-cloud rain rates are available as input.

The aim of the present study is

- to test the Sundqvist rain parameterization scheme by defining a realistic liquid water profile of a warm low model cloud as input and compare with some remote sensing observations of rain rates
- to test the Sundqvist scheme sensitivity on the vertical profiling of the LWC, on the vertical resolution of the host model, on the coalescence parameterization
- to study the spectral compatibility of the Sundqvist bulk rain parameterization
- to study some auxiliary functions by direct numerical integration over the droplet spectrum (forced by the bulk Sundqvist rain rates), such as the mean terminal velocity and effective radius.

We assume here for our warm low cloud calculations a model, where cloud is assumed to be horizontally and vertically uniform plane-parallel layer inside gridbox. Adiabatic vertical stratification of liquid water content (LWC) as a basic profile is considered. However, in calculations vertical profiling is realized in two possible ways: firstly, as a variable LWC in each layer and secondly, as vertically uniform distribution, i.e. LWC equal to the vertical average of the above adiabatic values in each resolution. The latest mimics the representation in low resolution GCM model layers. Bergeron-Findeisen mechanism is not included, the cloud produces warm homogeneous rain by autoconversion only.

In Sundqvist (1988) cloud scheme the rate of release of precipitation $G_p(s^{-1})$ is parameterized by

$$G_p = C_o m\Big[1 - exp\Big(-\frac{m^2}{m_r^2}\Big)\Big]$$

where m is the cloud water mixing ratio (nondimensional, predicted by host model), $1/C_o$ gives a characteristic time for conversion of cloud droplets into precipitating drops and m_r is the typical cloud water content at which the release of precipitation begins to be efficient (in stratiform case $m_r = 3\times10^{-4}$ and $C_o = 10^{-4}s^{-1}$ are used). To simulate the collection of droplets by rain falling from above, an additional factor F_{co} is introduced,

$$F_{co} = 1 + C_1\sqrt{P},$$

which multiplies C_o and divides m_r. C_1 is an additional tunable constant, and P is the local precipitation flux, that is the vertically integrated G_p from the cloud top to the level of interest.

$$P = \int_{htop}^{h} \rho G_p dz.$$

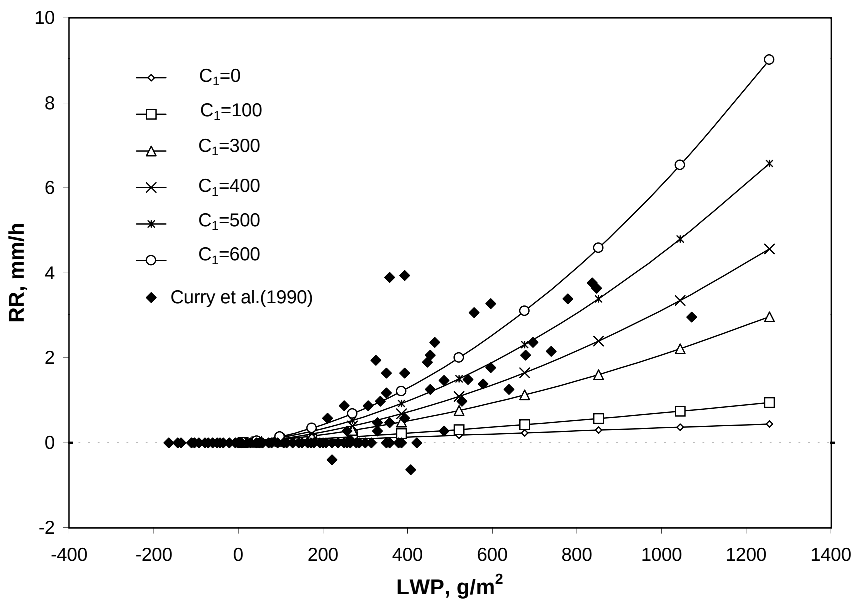

Figure 1: Plot of rain rate RR versus liquid water path LWP with different values for collection constant C_1. Curry et al.(1990) data from satellite microwave observations are shown as reference.

The results of our tests confirm that the Sundqvist parameterization of rain is acceptable, given its simplicity. It is somewhat sensitive to the vertical resolution, such that improving the vertical resolution of the host NWP or climate model may artificially reduce the rain rates, unless this is compensated for. It is sensitive to the typical vertical increase of m inside a cloud layer (constant value is typically assumed in NWP applications), but this is only a weak effect, if the vertical resolution is reasonable.

It is sensitive to its constant of collection efficiency C_1; we find that a value of 400-500, instead of the original 100 (Sundqvist, 1988) or the 300 (Sundqvist et al., 1989) SI units for C_1, gives a better fit with recent satellite microwave estimates of warm rain over the ocean.

We also did experimentation with cloud drop spectra, defining a typical gamma distribution (Miles et al., 2000, Wyser, 1989) for a marine Sc cloud, and a typical lognormal distribution for rain droplets

(Feingold and Levin, 1986), with the Sundqvist scheme providing the overall (bulk) rain rate. The evolution of the spectra, as the cloud gets thicker and starts to produce drizzle and then rain, looks reasonable. In the $100m$ thick low Sc, cloud drops are quite small in size with mode radius being about $6\mu m$. The very weak rain is drizzle, if any, the rain drop mode radius being around $60\mu m$. In the thicker clouds the distributions drift toward larger drops. For the $1.5km$ thick heavily precipitating cloud the vertically averaged cloud drop mode radius is about $14\mu m$ and the rain drop mode radius is up to $500\mu m$. These values look realistic although it should be added that in-situ widebrand raindrop size distribution observations within heavily precipitating clouds are not common.

Moreover, one can then calculate e.g. the effective drop radii and average terminal velocity of the falling drops, by numerical integration over the spectrum. These auxiliary values, as well as drizzling, agree reasonably well with various observational flight and satellite measurements.

Detailed description of the test and the results is given in Tisler and Savijärvi (2002).

References

Berry, E.X. and Reinhard, R.L., 1974. An analysis of cloud drop growth by collection. J. Atmos. Sci., 31, 1814-1831.

Curry, J.A., Ardeel, C.D. and Tian, L., 1990. Liquid Water Content and Precipitation Characteristics of Stratiform Clouds as Inferred from Satellite Microwave Measurements. J. Geophys. Res. 95 (D10), 16659-16671.

Feingold, G. and Levin, Z., 1986. The Lognormal Fit to Raindrop Spectra from Convective Clouds in Israel. J. Clim. Appl. Meteorol. 25, 1346-1363.

Miles, N.L., Verlinde, J. and Clothiaux, E.E., 2000. Cloud droplet size distributions in low-level stratiform clouds. J. Atmos. Sci. 57, 295-311.

Savijärvi, H., 1997. Short-wave optical properties of rain. Tellus 49A, 177-181.

Savijärvi, H., Arola, A. and Räisänen, P., 1997. Short-wave optical properties of precipitating water clouds. Q. J. R. Meteorol. Soc. 123, 883-899.

Sundqvist, H., 1988. Parameterization of condensation and associated clouds in models for weather prediction and general circulation simulation. Physically-Based Modelling and Simulation of Climate and Climatic Change, M.E.Schlesinger (Editor), Kluwer Academic Publisher, 433-461.

Sundqvist, H., Berge, E. and Kristjánsson, J.E., 1989. Condensation and Cloud Parameterization Studies with a Mesoscale Numerical Weather Prediction Model. Mon. Wea. Rev. 117, 1641-1657.

Tiedtke, M., 1993. Representation of Clouds in Large-Scale Models. Mon. Wea. Rev. 121, 3040-3061.

Tisler, P., Savijärvi, H., 2002. On the parameterization of precipitation in warm clouds. Atmos. Res. 63, 163-176.

Wyser, K., 1998. The effective radius in large-scale models: impact of aerosols and coalescence. Atmos. Res. 49, 213-234.

THE EFFECTS OF SMALL-SCALE INHOMOGENEITY IN THE SURFACE LAYER

K.L.Yegorov
The Russian State Hydrometeorological University
St.Petersburg, Russia

The investigation concern the problem of computing of area-averaged values of the fluxes of momentum, heat and vapor from the sea or ground surface in the presence of small-scale temperature and moisture heterogeneity. To compute the average fluxes it is necessary firstly to decide the problem of mathematical description of horizontal and vertical structure of the wind speed and temperature in the surface layer of the atmosphere over the small-scale heterogeneous of sea or land surface. In the study we consider the effects of temperature and humidity. The analytical solution of the problem is presented when surface temperature is a periodical function in horizontally and there are some others simplifications. The analyses of computing wind and temperature structure and the relationships between average fluxes and the surface parameters are represented.

INTRODUCTION

The investigations of the large-scale or meso-scale processes in the atmosphere by numerical hydrodynamic methods suppose to use the averaged fields of different meteorological parameters over horizontal space with some length scale $L_{\tilde{M}}$ >10km. Sometimes it is much more than dimensions of small heterogeneity of the physical parameters (roughness, temperature, moisture) of the underlayer surface (ground or sea) whose length scales L is less then 1km. As an example we can consider the sea surface covered by small-scale ice floes (Gust and Davidson, 1987, 1991, Hanssen-Bauer and Gjessing, 1988), or the ground surface with complex landscape and covered by different types of canopy. Such heterogeneity can influence additional effects, which have to be included in the models with large-scale or meso-scale space averaging.

It is possible to note few factors that bear the responsibility for these additional effects. One of them is the averaging of usual turbulence which has a different intensity in the areas with different surface roughness length and different temperature stratification that was demonstrated and analyzed by Maykut (1982), Overland (1985), Glendening, JW (1994), Gust P.S et al.(1995), Nadjojina.E.D., and Sternzat (1999). The turbulent fluxes of momentum, heat and water vapor have nonlinear dependence from the different meteorological parameters and so the result of space averaging of varying fluxes fields is not equal to the average fluxes computed with use of space averaged values of meteorological parameters. But horizontal heterogeneity of dynamical and thermal properties of the surface changes not only turbulent mixing in the atmosphere surface layer but it influences directly on the mean flow. Firstly it creates a horizontal divergence of wind velocity which is formed due to distinction of the wind profiles over different peaces of the surface, and as a result the fluctuations of vertical wind component w is appeared in the surface layer (Scanlon T. M. et al., 2001). And at last the space structure of atmosphere in the surface layer will contain a field of vertical convective plumes, which are forced by the horizontal small-scale temperature heterogeneity (Yegorov K.L., 1999, Lunn Barry M. et al., 2001) .

One of the possible ways for including the effects noted above in the large- or meso-scales hydrodynamic atmosphere models is presented in the paper.

BASIC EQUATIONS, SCALE ANALYSES AND EFFECTS OF AREA-AVERAGING

The model is based on a hydrodynamic equations for conservation of mass, momentum and enthalpy within the boundary layer of atmosphere ; it is simplified by the use of incompressible, and Bussinesk approximation. But we do not use hydrostatic approximation, because namely vertical accelerations influenced by small-scale surface sources of buoyancy, create a heterogeneous field of vertical motion. That is an important distinctionof the model that is used here from the models used in others investigations of air-flow properties and meso-scale processes over the heterogeneous surface (Kantha and Mellor,1989, Glendening, 1994, Gust et al, 1995, Nadiojina E.1999).

In common case we can use three-dimensional unsteady equations with vertical and horizontal turbulent exchange for description of the boundary layer over the surface with meso- and small-scale inhomogeneity.

Then, let's represent every meteorological parameter $f_i(x,y,z)=\{u,v,w,T,E\}$ as a sum:

$$f(x,y,z)=<f>+f'(x,y,z) \tag{1}$$

Here $<f_i>$ is an area average value of any parameter

$$<f_i>=\frac{1}{S}\int\limits_{(S)} f_i(x,y,z)dxdy\,, \tag{2}$$

$f'(x,y,z)-$ "non-turbulent" fluctuations of the parameter *f*, so that $<f'>=0$, S is area of averaging, which is much more than scale of horizontal heterogeneity *L,* but it is much less than meso-scale L_M. Value of $<f_i>$ is a function not only of *z,* but it depends on *x* and *y* due to a horizontal meso-scale inhomogeneity. So, we will use further following marks for averaged functions $<f_i>=\bar{f}_i(x,y,z)$.

After including of area-average values $\bar{u}$, $\bar{w}$, $\bar{\rho}$, $\bar{\theta}$, $\bar{q}$ and their fluctuations $u', w', \rho', \theta', q'$ we obtain two set of equations. For simplicity we suppose steady-state conditions and horizontal inhomogeneity along *x*-direction only. The set of equations for average values contain the ordinary equations of meso-scale problem for horizontal inhomogeneous boundary layer (Nadiojina E.,1999) with additional sources of momentum J_U, J_W heat J_T and moisture J_q :

$$J_f=-\frac{\partial}{\partial z}<\Pi_f>=-\frac{\partial}{\partial z}(<f_i'w'>-<\alpha_i k'\frac{\partial \bar{f}_i}{\partial z}>),\quad f_i=\{u,\theta,q\},\ \alpha_i=\frac{k_{ix}}{k_x}=\frac{k_{iz}}{k_z} \tag{3}$$

Here k_z, k_T, k_q- eddy viscosity for momentum, heat and moisture accordingly. We assumed that it is possible to use Bussinesk simplifications $\rho=const$ for averaging of momentum and so $<\rho f w>=\rho<fw>$ The fluctuations of meteorological parameters, which is necessary to know to compute the additional sources J_f, are found using another set of equations for fields of small-scale 'non-turbulent' fluctuations, which can be separate from full nonaveraged equations by well known method. The scale analyzes with L <300m, u≈5-10m/c and $\Delta\theta_0=5^oC$ allows to use following simplifications: the thickness *h* of the layer with small-scale fluctuations is not more than 50m, so we can neglect the Coriolis force and the term with pressure fluctuations in the equation for vertical momentum in compare with the buoyancy term. Using these simplifications and well-known relationship

$$g\frac{\rho'}{\bar{\rho}}=-\frac{g}{\bar{T}}\left(\theta'+0.608\bar{T}q'\right),\qquad \beta=g/\bar{T}\ , \tag{4}$$

we can write the equations for small-scale fluctuations in following form:

$$\bar{u}\frac{\partial u'}{\partial x}+w'\frac{\partial \bar{u}}{\partial z}=-\frac{1}{\bar{\rho}}\frac{\partial p'}{\partial x}+\frac{\partial}{\partial x}k_x\frac{\partial u'}{\partial x}+\frac{\partial}{\partial z}k_z\frac{\partial u'}{\partial z} \tag{5}$$

$$\bar{u}\frac{\partial w'}{\partial x}-\beta(\theta'+0.608\bar{T}q')=\frac{\partial}{\partial x}k_x\frac{\partial w'}{\partial x}+\frac{\partial}{\partial z}k_z\frac{\partial w'}{\partial z}; \tag{6}$$

$$\frac{\partial u'}{\partial x}+\frac{\partial w'}{\partial z}=0 \tag{7}$$

$$\bar{u}\frac{\partial \theta'}{\partial x}+w'\frac{\partial \bar{\theta}}{\partial z}=\frac{\partial}{\partial x}k_x\frac{\partial \theta'}{\partial x}+\frac{\partial}{\partial z}k_z\frac{\partial \theta'}{\partial z}; \tag{8}$$

$$\bar{u}\frac{\partial q'}{\partial x}+w'\frac{\partial \bar{q}}{\partial z}=\frac{\partial}{\partial x}k_x\frac{\partial q'}{\partial x}+\frac{\partial}{\partial z}k_z\frac{\partial q'}{\partial z}. \tag{9}$$

The equations (5)-(9) are solved with use the boundary conditions:

$$z=0:\quad w=0,\ \theta'=\theta_0(x),\ q'=q_0(x) \tag{10}$$

$$z\to\infty:\quad w=0,\ \theta'=0,\ q'=0. \tag{11}$$

ESTIMATION OF THE EFFECT OF AVERAGING

First of all we will consider that average values do not vary in horizontally. It means that <w>=0. Within of the atmosphere surface layer we can write the conservation laws for average fluxes in well-known form:

$$\frac{\partial}{\partial z}<\tilde{\tau}_i>=0,\ \frac{\partial}{\partial z}<\tilde{P}>=0,\ \frac{\partial}{\partial z}<\tilde{E}>=0. \tag{12}$$

It means that average values of full fluxes of momentum flux $<\tau>$, heat $<P>$ and moisture $<E>$ do not vary in vertical direction

$$\bar{k}_f\frac{\partial \bar{f}}{\partial z}+<\Pi_f>=<k_f\frac{\partial f}{\partial z}>\big|_{z=0}=\mathrm{H}_{0f}=const, \tag{13}$$

$\mathrm{H}_0=v_*^{\,2}$, if f=u; $\mathrm{H}_0=-\tilde{P}_0$, if f=θ; $\mathrm{H}_0=-\tilde{E}_0$, if f=q.

where $\bar{k}=<k>,\ \bar{u}=<u>,\ \bar{\theta}=<\theta>,\ \bar{q}=<q>$ - are area-average values of eddy viscosity, temperature, and humidity. If $\bar{k}(z),\ \bar{u}(z),\ \bar{\theta}(z),\ \bar{q}(z),\ <\Pi_f>$ are known as function of z it is easy to integrate the equations (13) on z from z=z_0 till the level z=h where small-scale fluctuations can be neglected and to get following results:

$$\mathrm{H}_0=\hat{\mathrm{H}}_0+\alpha_i\frac{\delta\tilde{f}}{\varphi(h)},\quad \delta\tilde{f}=\int_{z_0}^{h}\frac{<\Pi_f>}{k}dz\quad, \tag{14}$$

where $\varphi(h)=\int_{z_0}^{h}\frac{dz}{k}$. For $k=\chi v_* z$ we obtain that $\varphi(h)=\frac{1}{\chi v_*}\ln\frac{h}{z_0}$.

The values $\hat{\mathrm{H}}_0\equiv\{\hat{\tau}_0,\hat{P}_0,\hat{E}_0\}$ are the parts of turbulent fluxes which can be computed by usual gradient method:

$$\hat{\mathrm{H}}_0=\frac{\Delta f}{\varphi(h)};\ \hat{\tau}_0=\frac{\bar{u}(z)}{\varphi(h)};\ \hat{P}_0=-\alpha_t\frac{\Delta\bar{\theta}}{\varphi(h)};\ \hat{E}_0=-\alpha_q\frac{\Delta\bar{q}}{\varphi(h)} \tag{15}$$

Here $\Delta\bar{\theta}=-(\theta_0-\bar{\theta}(z)),\ \Delta\bar{q}=-(\bar{q}_0-\bar{q}(z))$. The second terms in the relationships (14), are additional values of fluxes that are connected with the effects of horizontally heterogeneous conditions on the surface. Hence $\delta\tilde{u}$, $\delta\tilde{\theta}$ and $\delta\tilde{q}$ are corrections, that is necessary to subtract from values $\bar{u}$, $\bar{\theta}$, $\bar{q}$ measured on the level h if we wish to compute the full fluxes v_*^2, $\tilde{P}_0$, $\tilde{E}_0$

by usual gradient formulas (15). In other words $\delta\tilde{u}, \delta\tilde{\theta}$ and $\delta\tilde{q}$ represent deformations of the logarithmical profiles of wind speed, temperature and humidity due to small-scale horizontal heterogeneity of the surface properties.

To estimate the additional sources and fluxes we will use a few simplifications. First of all we suggest that

$$\frac{\partial\overline{\theta}}{\partial z} = \Gamma_\theta = \text{const}, \quad \frac{\partial\overline{q}}{\partial z} = \Gamma_q = \text{const}, \quad \Gamma_v = \frac{\partial\overline{\theta}_v}{\partial z} = \text{const}. \tag{16}$$

Further we introduce three new functions:

$$U = w + i\sqrt{\beta/\Gamma_v}\,\theta_v, \quad F(x,z) = \frac{\theta'_v}{\Gamma_v} - \frac{\theta'}{\Gamma_\theta}, \quad \psi(x,z) = \frac{\theta'_v}{\Gamma_v} - \frac{q'}{\Gamma_q}. \tag{17}$$

Here $\overline{\theta}_v = \overline{\theta} + 0.608\overline{T}\overline{q}$, $\theta'_v = \theta' + 0.608\overline{T}q'$.

In this case the equations (6), (8), (9) can be transformed to three others equations

$$\overline{u}\frac{\partial U}{\partial x} + i\sqrt{\beta\Gamma_v}U = \frac{\partial}{\partial x}k_x\frac{\partial U}{\partial x} + \frac{\partial}{\partial z}k_z\frac{\partial U}{\partial z} \tag{18}$$

$$\overline{u}\frac{\partial F}{\partial x} = \frac{\partial}{\partial x}k_x\frac{\partial F}{\partial x} + \frac{\partial}{\partial z}k_z\frac{\partial F}{\partial z}, \tag{19}$$

$$\overline{u}\frac{\partial \psi}{\partial x} = \frac{\partial}{\partial x}k_x\frac{\partial \psi}{\partial x} + \frac{\partial}{\partial z}k_z\frac{\partial \psi}{\partial z}, \tag{20}$$

which can be solved independently every one from others to find the functions $U(x, z)$, $F(x, z)$ and $\psi(x, z)$. The small scale perturbations we find using that functions. Namely,

$$w'(x,z) = \operatorname{Re}U(x,z); \tag{21}$$

$$\theta'_v(x,z) = \sqrt{\frac{\Gamma_v}{\beta}}\operatorname{Im}U(x,z); \tag{22}$$

$$\theta'(x,z) = \theta'_v(x,z)\frac{\Gamma_\theta}{\Gamma_v} - \Gamma_\theta F(x,z) = \Gamma_\theta\left(\frac{1}{\sqrt{\beta\Gamma_v}}\operatorname{Im}U(x,z) - F(x,z)\right); \tag{23}$$

$$q'(x,z) = \theta'_v(x,z)\frac{\Gamma_q}{\Gamma_v} - \Gamma_q\psi(x,z) = \Gamma_q\left(\frac{1}{\sqrt{\beta\Gamma_v}}\operatorname{Im}U(x,z) - \psi(x,z)\right). \tag{24}$$

If we suggest that

$k(z)=k_1(z/z_1)^m$, $u(z)= u_1(z/z_1)^n$, and $\theta'(x)|_{z=0} =\Delta\theta_0 \, Sin\, nx$, $n =2\pi/L$

the dimension analyzes allows to get the expression for additional fluxes from the surface in the following form

$$P' = \frac{g}{T}\Delta\theta_0^2\left(\frac{L}{u_1}\right)^\alpha\left(\frac{z_1^2}{k_1}\right)^\gamma\Phi(v_n, z_n) \tag{25}$$

Here $v_n = L\sqrt{\beta\Gamma}/2\pi u_1$ -nondimensional Vaisal-Brent frequency; $z_n=z/L$- nondimensional height; α=(2-m)/(2+n-m), γ =n/(2+n-m). If m=1, n=1 →α =½, γ =½.

If the values of Γ_{qn} and $\Gamma_{\theta n}$ are given → $\Phi(\Gamma_{qn}, \Gamma_{\theta n})= constant$. We can estimate the order of this constant value using a simple model.

SOME RESULTS FROM SIMPLIFIDE MODEL

To estimate the effect of temperature heterogeneity on the heat fluxes we assume that q=0, the eddy viscosity $k_x, k_z,$ wind velocity $\bar{u}$, $\frac{\partial\bar{\theta}}{\partial z} \equiv \Gamma_T$ are constant values; the surface temperature is a periodical function of X: $z = 0$: $w' = 0,\ \theta' = \Delta\theta_0 \cdot \sin nx,\ \Delta\theta_0 > 0$, and $\alpha_T = 1$. The solution for fluctuations w and θ with these simplifications is presented by Yegorov, K.L. and N. Sherbo (1999) and allows writing the average correlation heat flux <w'θ'> , deformation of the temperature profile δθ(z) and additional sources J(z) in following form

$$< \theta' w' >= \frac{\Delta\theta_0^2}{4}\sqrt{\frac{\beta}{\Gamma}} \cdot \exp(-qz) \cdot \sin pz \tag{26}$$

$$\delta\tilde{\theta}(z) = \frac{\Delta\theta_0^2}{4k}\sqrt{\frac{\beta}{\Gamma}} \cdot \frac{p}{q^2 + p^2} \cdot \Psi(z,\Gamma), \tag{27}$$

$$J_\theta = -\frac{\partial}{\partial z} < w'\theta' >= -\frac{\Delta\theta_0^2}{4}\sqrt{\frac{\beta}{\Gamma}} \cdot \exp(-qz)(p \cdot \cos pz - q \cdot \sin pz). \tag{28}$$

Here : $\Psi = 1 - exp(-qz)(cospz + \frac{q}{p}\sin pz)$, $\quad p = \frac{b_1}{M_1} - \frac{b_2}{M_2}$; $\ q = b_1 M_1 + b_2 M_2$.

$$b_{1,2} = b_0\sqrt{1 \pm v_n}\ ,\quad n = \frac{2\pi}{L},\ M_1 = (\sqrt{1 + m_1^2} + m_1)^{1/2},\ M_2 = (\sqrt{1 + m_2^2} + m_2)^{1/2},$$

$$m_1 = \frac{k_x}{k_z}\frac{2\pi^2}{L^2}\frac{1}{b_1^2},\ m_2 = \frac{k_x}{k_z}\frac{2\pi^2}{L^2}\frac{1}{b_2^2},\ \sigma = \frac{2\pi u}{L},\ b_0 = \sqrt{\frac{\pi u}{Lk_z}}.$$

From (26), (27) is following a conclusion that the dynamical factors u and k lead to veakenary of the effects of surface temperature heterogeneity. And the more the length scale L of heterogeneous, the more heat flux $\overline{P}_W$. The height, h of the influence of surface heterogeneous can be estimated from condition $b_0 h = \pi$. It gives: $h = \sqrt{\frac{\pi L k_z}{u}}$. So we obtain that h≤8m, if L≤100m, $u = 7m/c,\ k \le 1m^2/c$. A numerical value of additional heat flux $\overline{\Pi}_W = \rho c_P \overline{P}_W$ in this example for $\Delta\theta_0 = 5^o C$ is about 30 Wt/m^2, which is corresponded to order of normal values of mean turbulent heat fluxes above the surface.

Using the continuity equation (7) solution for w' we can get the solution for u'

$$u' = C_1(z) + \frac{\Delta\theta_0}{4\ \pi}\sqrt{\frac{\beta}{\Gamma}} \cdot L\{\exp(-b_1 M_1 z)[b_1 M_1 \sin\varphi_1 + \\ + \frac{b_1}{M_1}\cos\varphi_1] - \exp(-b_2 M_2 z)[b_2 M_2 \sin\varphi_2 + \frac{b_2}{M_2}\cos\varphi_2]\} \tag{29}$$

and expression for the additional value of the momentum flux at the surface:

$$\tau_{0w} = \left[\frac{\Delta\theta_0 \beta}{8\pi}\right]^2 \sqrt{\frac{L^5}{\pi u^3 k}} \tag{30}$$

The estimation of τ'_w for the same values of parameters $\Delta\theta_0, L, u, k$ gives value 0.16m^2/c^2, that is similar to normal mean values of momentum fluxes over the sea surface covered by ice floes, with drag coefficient $C_D = 2.58 \cdot 10^{-3}$ presented by Overland (1985), Gust, Glendening and Davidson (1995).

CONCLUSIONS

The conclusions which follow from analytical solution are:

-the dynamical factors u and k lead to weakening of the effects of surface temperature heterogeneity;

-the more the length scale L of heterogeneity, the more heat flux; but in common case,when $\Gamma \neq 0$, there is a resonance frequency in space heterogeneity which gives the equality $\frac{L}{u} = 2\pi / \sqrt{\beta \Gamma}$. In this case the additional fluxes have a maximum value, that is connected with the value of flux for neutral conditions ($\Gamma=0$) as $\langle w'\theta' \rangle|_{REZ} = \sqrt{2} \langle w'\theta' \rangle|_{\Gamma=0}$;

-the height h of the influence of surface temperature heterogeneity can be estimated from the following condition: $b_0 h = \pi$. It gives

$h=(Lk_z \pi/u)^{1/2}$; If u=5m/c, k=1m^2/c, L=100m $\rightarrow h \approx 8$m.

-a numerical value of additional heat flux in this example, at $\Delta\theta_0 = 5^{o}$C is about $\delta P_0 \approx$ 30 Wt/m^2, which corresponds to the order of normal values of mean turbulent heat fluxes above the surface;

-the effect of horizontal turbulence becomes appreciable only for a small values of length scale L<50m.

-additional heat flux by evaporating from the surface with horizontal humidity contrast Δq_0 =8‰ has the same value as a sensible heat flux due to the temperature contrast of $\Delta\theta_0 = 5^{o}$ C.

Thus we have demonstrated the effects of space averaging of the momentum and heat fluxes over the sea surface with a small-scale heterogeneous in temperature and moisture. The resulting equations constructed for description of fields of the small-scale fluctuations of temperature and vertical wind component are differed from form of equations using in the models for mesa-scale convection and transformation. We have proposed that small-scale buoyancy force is a dominant one which induces the vertical convective plumes.

We used a rather simple model for vertical profiles of mean wind velocity and eddy viscosity to get analytical solution and visual dependence of the fluxes from the physical parameters of the process.

The numerical estimations to be obtained gives a ground to make a conclusion that the investigated effect is a value of the same order of magnitude as a usual turbulent heat and momentum fluxes. We have shown that the effect of buoyancy on the additional surface stress is much more than the effect of horizontal divergence due to the surface roughness variations.

We suppose that the results gives a ground for using our main assumptions about role of small-scale buoyancy in the further modeling of this effect with a more correct models for the vertical profiles of wind and eddy viscosity.

REFERENCES

Glendening, J.W., Dependence of Boundary Layer Structure near an Ice-Age Coastal Front upon Geostrophic Wind Direction, *J. Geophis. Res,* Vol 99, No D3, 1994.

Guest, P.S. and K.L.Davidson, The Effect of Observed Ice Condition on the Drag Coefficient in the Summer East Grenland Sea Marginal Ice Zone, *J. Geophys. Res,* Vol 92, 1987

Guest, P.S. and K.L.Davidson, The Aerodynamic Roughness of Different Types of Sea Ice, *J. Geophys. Res,* Vol 96, No C3, 1991.

Guest, P.S., Glendening, J.W.,and K.L.Davidson, An Observational and Numerical Study of Wind Stress Variations Within Marginal Ice Zones, *J. Geophys. Res,* Vol 100, No C6, 1995.

Hanssen-Bauer, I. and Y.T.Gjessing, Observations and Model Colculations of Aerodynamic Drag on Sea Ice in the Fram Strait, *Tellus,* Vol 40A, 1988.

Kantha, L.H., and G.L.Mellor, A Numerical Model of the Atmospheric Boundary Layer Over Marginal Ice Zone, *J. Geophys. Res,* Vol 94, No C4, 1989.

Lunn Barry M, Tao Wei-Kuo and A.Frank, 2001: A parameterization for the triggering of landscape-generated moist convection. Part 1. Analysis of high-resolution model results, *Journ. Atmos. Seince*, v.58, 6, p.575-592.

Maykut, G.A., Large-Scale Heat Exchange and Ice Production in the Central Arctic, *J. Geophys. Res,* Vol 87, 1984.

Nadiojina, E. and Sternzat, 1999: Computing results from two- and three-dimension models of heat exchange between the ocean and atmosphere near the Polar regions, *Meteorology and hydrology,* No10**,** p. 53-62.

Overland, J.E., Atmospheric Boundary Layer Structure and Drag Coefficients Over Sea Ice, *J. Geophys Res*, Vol 90, 1985.

Scanlon Todd M. et al., 2001: Scale effects in estipating large eddy-driven sensible heat fluxes over heterogeneous terrain*, IAHS Publ.*, No 287, p.175-180.

Yegorov, K.L., and N. Sherbo, 1999: Modeling of heat exchange in the atmosphere above the surface with temperature in homogeneity. *Mat. Modeling and Numeric. Methods*, 5, St. Petersburg.

Sodankylä mast data for model comparison studies

Markku Kangas
Finnish Meteorological Institute

1 Introduction

Sodankylä mast is located at the Arctic Research Centre of the Finnish Meteorological Institute (FMI), or FMI-ARC for short, about 100 km north of Arctic Circle. The mast is situated on a sandy soil in a scots pine forest with tree height of about 20 meters. The forest is not very thick, and to the west there is also a river (Kitinen) running close to the site. The mast itself is 48 meters high, so about half of the mast is within and another half above the tree-tops.

FMI-ARC is also an official SYNOP measurement site run by the Finnish Meteorological Institute. In addition to synoptic measurements, also balloon soundings are made. The mast is located about 500 meters south-east of the main observatory site. The exact location of the observatory is 67.3679 ^{o}N 26.6328 ^{o}E, 179 m above the mean sea level.

Sodankylä mast belongs to an international measurement network project CEOP (Coordinated Enhanced Observing Period).

2 Measurement mast

Fig.1 shows a diagram of the mast. As one can see, it is quite heavily instrumented, a lot of different sensors are located at different levels. The diagram shows the situation in August 2003.

The table below shows the measured parameters. Some parameters are measured at different levels, enabling the determination of vertical profiles. The flux measurements shown in the table are not included in Fig.1.

Parameter	*Measurement height (metres)*
Wind speed	*48, 47, 38, 30, 25, 23, 18, 8 m*
Wind direction	*48, 47, 23, 8 m*
Air temperature	*48, 32, 18, 8 m*
- ventilated	*47, 38, 32, 25, 18, 8, 3 m*
Relative humidity	*48, 32, 25, 18, 8, 3 m*
LW radiation up	*45 m*
Global radiation	*45 m*
Reflected radiation	*45 m*
Turbulent fluxes	*23 m*
- sensible & latent heat	
- momentum	
- carbon dioxide	
Surface temperature	*45 m*
- infrared sensor	

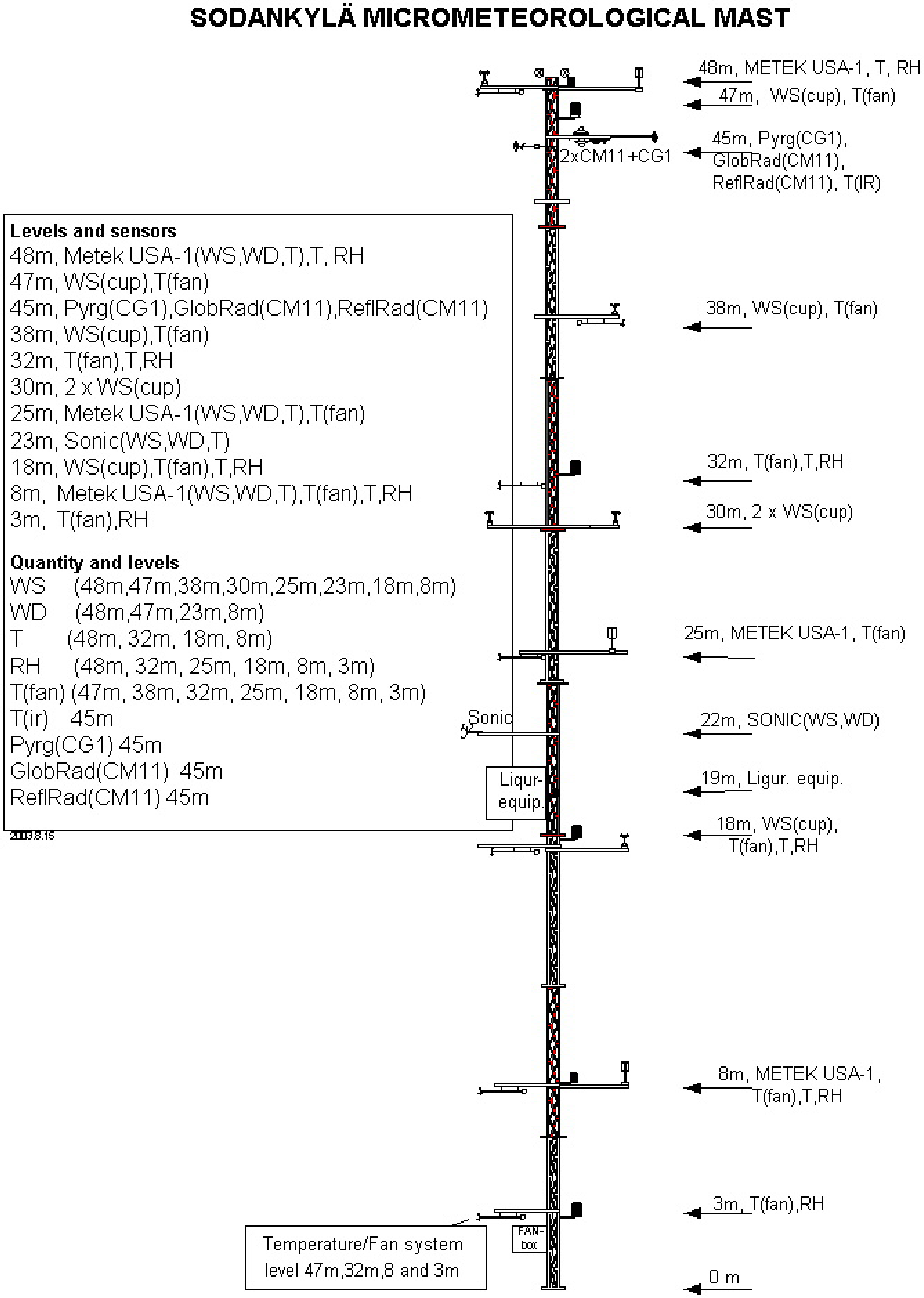

Figure 1 : Mast diagram (August 2003).

2 Measurement data sets

In order to enable a more efficient use of the measurements in model development, data sets covering specific periods are being collected. The idea is to choose some interesting periods and collect all available data. In case of Sodankylä, this means SYNOP and balloon sounding in addition to mast measurements.

So far two periods of data for Sodankylä have been collected and made available on-line in the internet. This data covers two cold and calm periods in December 2002 and January/February 2003. The data consists of five sets:

- mast measurements : "basic" data (temperature, radiation, wind)
- mast measurements : turbulent fluxes
- mast measurements : soil and snow properties
- balloon soundings
- SYNOP measurements

More data periods and probably also other measurement sites will be added in the future.

3 Hirlam monitoring

As an application of the utilization of mast measurements, at FMI we have also set up a system for monitoring of HIRLAM forecasts. This system plots operatively some parameters from both HIRLAM forecasts and measurements, thus enabling not only monitoring of forecasting process but also on-line comparison of forecasts and measurements.

In addition to Sodankylä mast, three other masts are included in the suite. The additional masts are TV broadcast masts of the National Television Corporation (YLE) and not so well instrumented as the Sodankylä mast. They do, however, provide better vertical coverage (up to 300 meters height), and also improve the spatial coverage of the monitoring.

At present (January 2004), the system is run every two hours. Two Hirlam versions are included, the main operational Hirlam 5 system of FMI as well as an older Hirlam 4 system with finer resolution.

The parameters included in the plot are :

2 x Temperature (T2m , T1ModLevel)	Surface LW radiation (LWrad)*
Temp.difference (T2m - T1ModLevel)	Sensible heat flux (w'T')*
Relative humidity (Rh2m)	Latent heat flux (w'q')*
Wind speed (v10m)	Evaporation (Evap)*
Global radiation (SWrad)*	Momentum flux (u'v')*

*) *available for Sodankylä only*

As one can see, three temperature values are plotted. First, we have to temperature values, the surface temperature and first model level temperature. The third plot shows the difference of these two, giving thus an indication of the amount of temperature inversion.

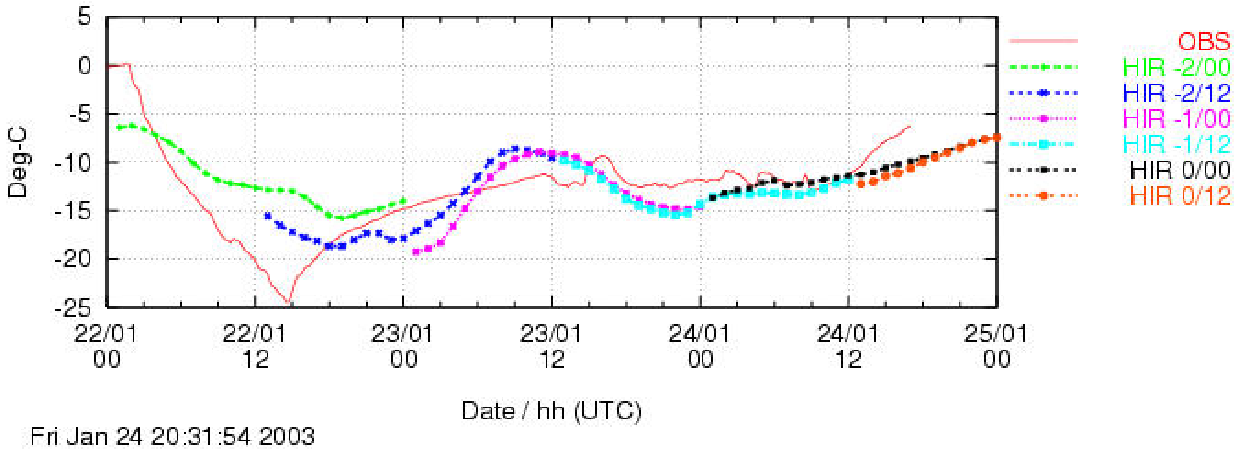

Figure 2 : Verification plot.

The plots for various parameters are as shown in Figure 2. The plot is drawn starting from two days backward in time up to present, as far as data is available. The red line denotes the measurements and the dotted lines various forecasts for 00 and 12. For each available forecast except the last one (present day 12UTC forecast), the first 24 hours are plotted.

The plot shows then the fit of measurements against forecasts, but because they overlap in time, we also get an indication how consistent the consecutive forecasts are and what is the effect of analysis.

4 Conclusions and future

Sodankylä mast measurements with two applications have been briefly described. The measurements are part of an international CEOP programme.

In the future, more data sets will be included in the mast data sets. The possibility of adding other masts will also be studied.

As to the on-line monitoring and verification plotting, the system has been built on the present operative forecast system of FMI. It can, however, quite easily be changed for the new RCR forecast system that will adopted in FMI in the near future. The adding of other models as well as measurements in the verification suite is also possible and will be considered in the future.

1D model studies in stable boundary layer

Eric Bazile[1]
Météo-France/CNRM

1. INTRODUCTION

The study of the stable atmospheric boundary layer (SBL) with a 1D model is very useful for the understanding and the representation of the PBL in numerical weather prediction model. The GABLS (GEWEX Atmospheric Boundary Layer Study) project (Holtslag, 2003) provides a clear framework for 1D and LES simulation and intercomparison, the case is based on the results presented in a study by Kosovic and Curry (2000) . Furthermore, the Sodankylä site observation, situated at 67.3°N and 26.4°E , provides an extensive routine measurements. The modification deduced from the GABLS experiment could be validate on a long period during the winter time with the Sodankylä data.

2. THE GABLS CASE

This project is not only a 1D model intercomparison (contact person: Joan Cuxart Rodamilans) but also an intercomparison for LES (contact person: Malcom Mac Vean), that will provide exchange and interaction between the two groups. The single-column artic case is driven by an imposed geostrophic wind, with a specified surface cooling rate. The roughness length is specified, the radiation scheme is switched off and therefore only the vertical diffusion is active. The boundary layer height is between 150m and 250m (Fig: 1). From the GABLS case, we already learn for ARPEGE/ALADIN that we have a too strong mixing on the wind. The model is not able to reproduce correctly the Ekman spiral and the height of the low level jet is too high. The excessive mixing is also probably true for the temperature but with a wrong wind profile it is difficult to be confident on the exchange coefficient computed from the Richardson number. Nevertheless, the surface heat flux ($\overline{w'\theta'}$) and the friction velocity (u^*) are in good agreement with the LES results.

The computation of the PBL height has been modified in order to take into account of the surface flux and the vertical stability (Troen and Mahrt, 1986). The wind and the temperature profile are slightly improved (Fig: 2). But, some works are still needed to obtain a correct wind profile and thus, improve the exchange coefficient for heat.

However, we need to keep in mind that the NWP models have to represent turbulence in grid-squares with heterogeneity. The Sodankylä data should be an additional validation for the study of the SBL and would provide a nice framework to define the "minimum residual mixing".

3. THE SODANKYLÄ DATA

The Sodankylä data contains measurement instrumentation along a mast, in the soil and in the snow pack (for more detail see the M. Kangas extended abstract). Long time series are

[1] *Corresponding author address*: E. Bazile Météo-France, CNRM/GMAP 42 Av. Coriolis, 31057 Toulouse Cédex, France tel : (33) (0)5 61 07 84 68 - fax : (33) (0)5 61 07 84 53 email: eric.bazile@meteo.fr

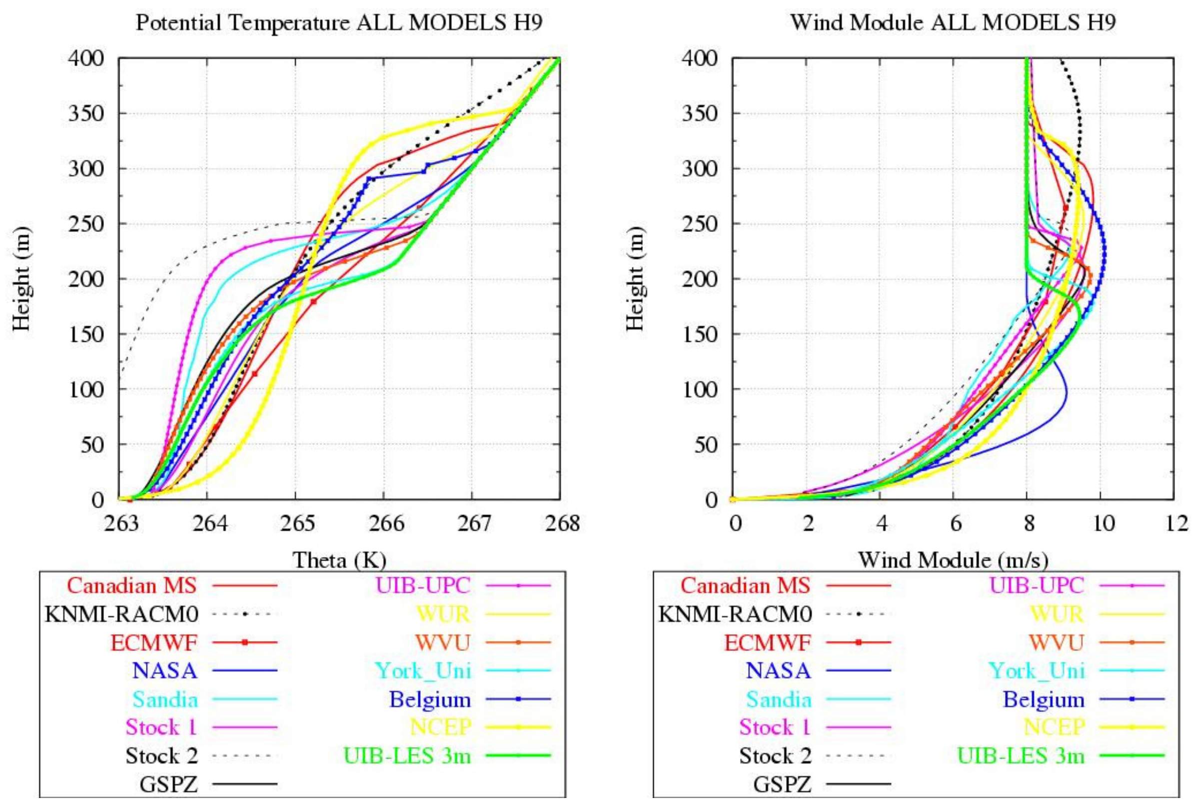

Figure 1: Vertical profile for the potential temperature and the wind speed after 9 hours of simulation. Thanks to Joan Cuxart for providing the pictures. (www.uib.es/depart/dfs/meteorologia/webgabls.htm)

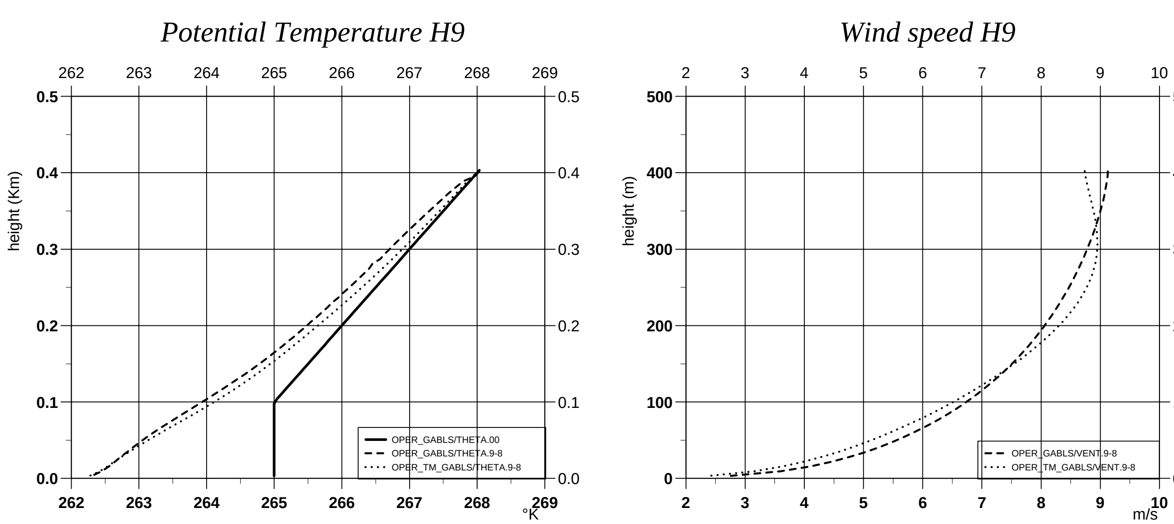

Figure 2: Vertical profile for the potential temperature and the wind speed after 9 hours of simulation. Dotted line: Troen and Mahrt. Dashed line: Standart version. Full line: intitial profile for the potential temperature.

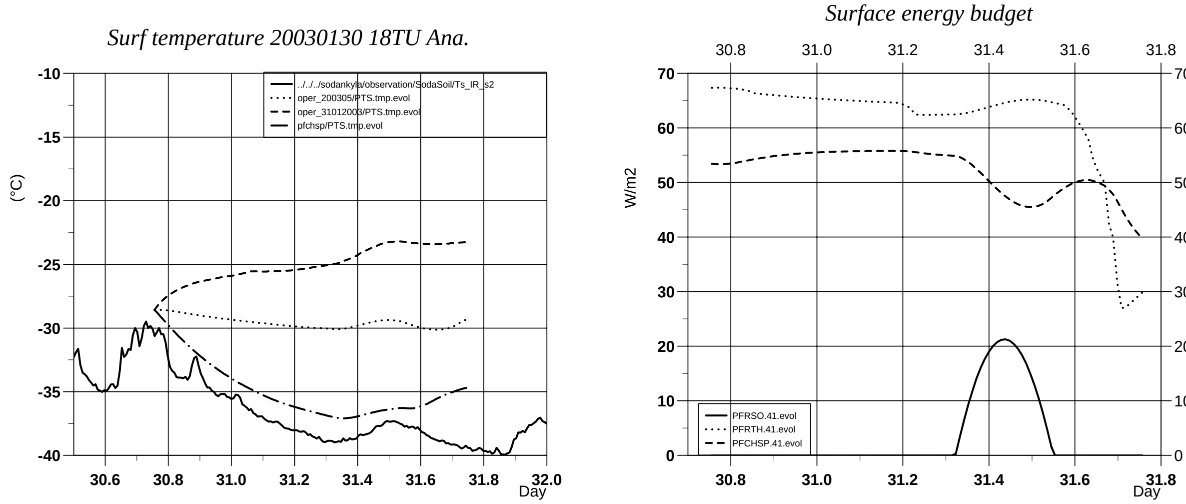

Figure 3: 1D 24h forecast. Left: Surface temperature. Full line: observed infrared temperature. Dashed line: old operational version. Dotted line: modified residual mixing. Dashed-dotted line: modified the soil heat transfer computation. Right: Surface energy budget. Full line: net solar radiation. Dotted line: net longwave radiation. Dashed line: soil heat flux.

available and systematic comparison could be very useful. During the last week of January 2003, between the 30th at 18TU and the 31th 18TU a clear day with a strong net radiative cooling occured. The snow surface temperature fell to $-40°$C, the 2m temperature to $-39°$C and the 48m temperature to $-34°$C. The 24h operational ARPEGE forecast was too warm, by 15°C for the surface temperature and by 11°C at 48m. Several reason can explain this underprediction: clouds, vertical diffusion, snow properties.

Savijärvi and Kauhanen (2001) showed that the same surface temperature can be obtained with a modification of the residual mixing or changing the heat capacity of snow. It shows clearly the danger to generate a compensating error using only one data for the validation.

No clouds were reported at Sodankylä and either in the model. Some experiments have been done with the 1D model, starting from the analysis field, to understand this sizeable underprediction. First of all, with no large-scale advection and no vertical forcing the 1D model reproduce correctly the warm bais seen in the 3D. With the Troen and Mahrt height of PBL tested on the GABLS case and a modification of the critical Richardson number (Ri_c) to reduce the "residual" vertical mixing in stable condition, the warm bais is diminished (Fig: 3 left dotted line compared to the dashed line). Nevertheless, the bais remains and the reason is that the soil heat flux compensates the net radiative cooling (Fig: 3 right). Its computation does not take the insulating properties of the snow into account. Introducing a function of the quantity of snow in the soil heat flux computation, we improve significantly the surface temperature forecast (Fig: 3). However, it is a preliminary result obtained in 1D. A assimilation cycle is really needed to be sure that the modification does not generate a drift on the deep soil temperature.

4. CONCLUSION

The study of the stable boundary condition on the GABLS case shows an excess of mixing for the wind and the temperature. Consequently, the low level jet is under estimated and too high. The modification of the PBL height computation does not solve the problem.

The Sodankylä data are very interesting to study on a more complex area the SBL. A problem on the soil heat flux computation has been identified (thanks to the Sodankylä data for the soil) and probably solved.

A clear cold day was found with a stable boundary layer. The next step will be to use the observation to initialize the 1D model and to force the upper air by the sounding data to try to provide a "nice" real case for the SBL study.

I wish to thank Markkus Kangas and Carl Fortelius for providing all the Sodankylä data and Joan Cuxart for the GABLS case.

References

Holtslag, A. A. (2003). GABLS initiates intercomparison for stable boundary layer case. *GEWEX News*, 13:7–8.

Kosovic, B. and Curry, J. (2000). A large eddy simulation study of a quasi-steady, stably stratified atmospheric boundary layer. *J. Atmos. Sci.*, 57:1052–1068.

Savijärvi, H. and Kauhanen, J. (2001). High resolution numerical simulations of temporal and vertical variability in the stable wintertime boreal boundary layer: a case study. *The. and. Appl. Climatology,*, 70:97–103.

Troen, I. and Mahrt, L. (1986). A simple model of the atmosphere boundary layer; sensitivity to surface evaporation. *Bound.-Layer Meteor.*, 37:129–148.

Convection in hydrostatic and non-hydrostatic HIRLAM

Sami Niemelä
Division of Atmospheric Sciences
Department of Physical Sciences
University of Helsinki

Carl Fortelius
Finnish Meteorological Institute

1 Introduction

The HIRLAM community is all the time aiming to better horizontal resolutions. The largest operational resolutions currently used in HIRLAM are between 10 and 20 km. The next natural step is to decrease the grid size below 10 km. The resolution range from about 3–10 km is a very difficult region especially for treatment of convective processes (Molinari and Dudek, 1992). Weisman et al. (1997) proposed that with better resolutions than 1–4 km the convection could be resolved explicitly. However, explicit methods need very sophisticated microphysical package in order to make successful simulations. The grid lengths below 10 km requires also non-hydrostatic dynamics.

The motivation of the study was to evaluate how the default convection and condensation scheme (STRACO; Undén et al., 2002) of HIRLAM behaves with better resolution than 11 km. The secondary objective was to study the performance of the experimental non-hydrostatic HIRLAM (Rõõm, 2001; Männik and Rõõm, 2001) in convective situation. We concentrated to seek how and in which horizontal resolution the results of hydrostatic and non-hydrostatic models start to differ. The evaluations were mainly made by comparing the model-calculated radar reflectivities to observations from Finnish radar network. The simulated reflectivities were produced by Radar Simulation Model (Haase and Crewell, 2000).

2 Experiments

The model experiments were based on HIRLAM 5.0.0 with the non-hydrostatic extension and updated STRACO-scheme (Jan-2002). The STRACO-scheme is based on moisture convergence closure like well known Kuo (1974) scheme. The microphysics and precipitation release (diagnostic) follows the work of Sundqvist et al. (1989). The convection parameterization is resolution dependent both horizontally and vertically. As a consequence of that, the satisfying of convective triggerning conditions gets more difficult when grid length decreases or if convective cloud is shallow.

The calculation area was 156×156 grid-points with three different grid lengths: 2.75, 5.5 and 11 km. The largest domain covered the Scandinavian area whereas the smallest one covered only Southern Finland and Gulf of Finland. The results from each experiment were studied only in the smallest area. 40 vertical levels were used. Two different simulations were made in each area: hydrostatic (HYD) and non-hydrostatic (NH). Lateral boundaries were taken from the operational HIRLAM analyses (22 km resolution). Optimal interpolation was used as data-assimilation system.

Only one convective case was studied. Almost the whole Southern Finland was covered by convective precipitation cells on 25th of May 2001. However, lightning activity was not observed. Even if this case is not severe convective event, it is also important to evaluate models in conditions, which are very typical for the regions under examination. The model runs were launched at 25th of May 00 UTC and the length of simulations was 21 hours.

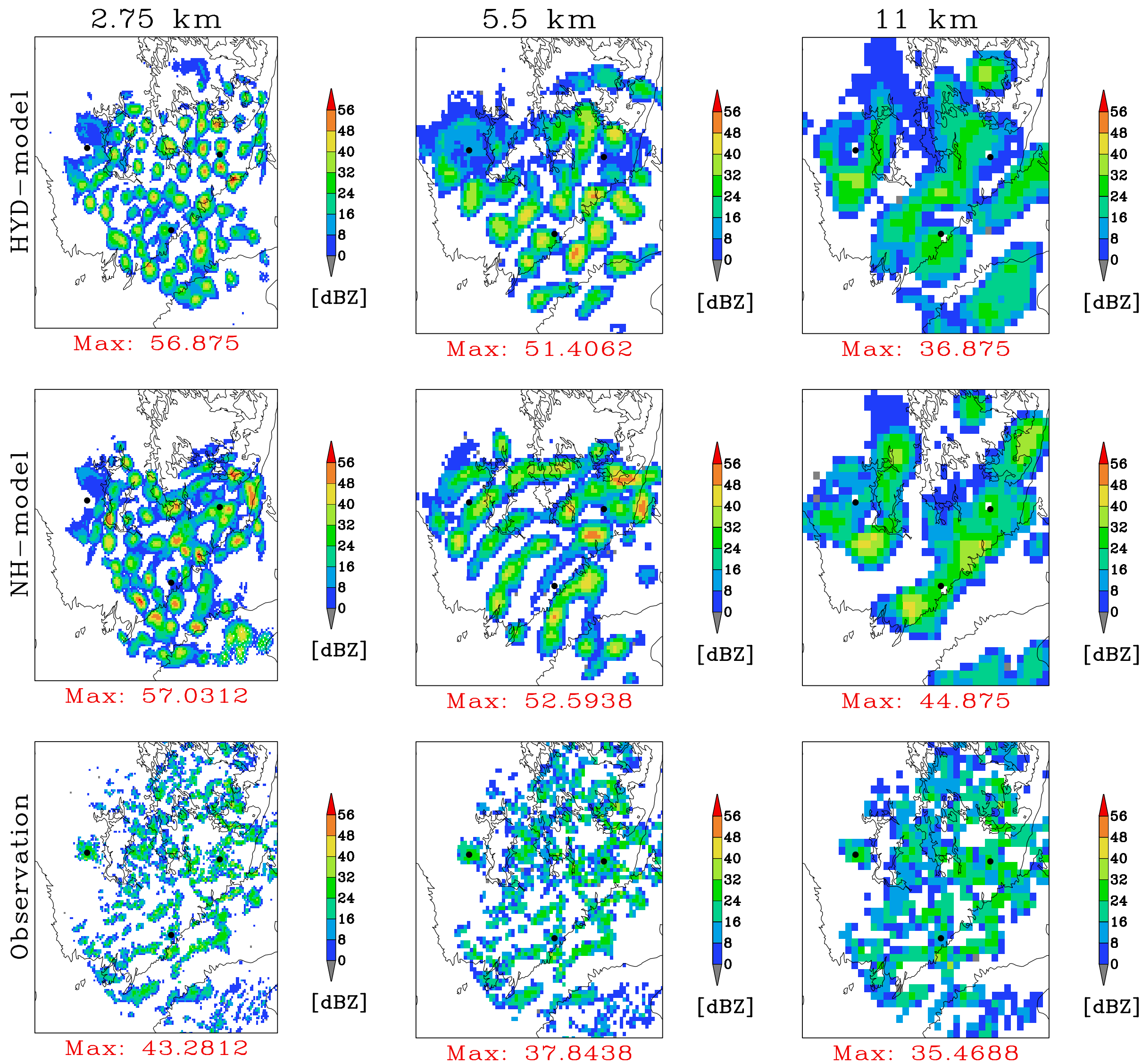

Figure 1: Comparison of radar reflectivity fields (dBZ) on 25th of May 2001 (+12h simulation). The rows show the results from HYD-model, NH-model and radar observations (radars are marked with black dots), respectively. The columns represent different horizontal resolutions: 2.75, 5.5 and 11 km. The elevation angle of the radar antenna is 0.4 °.

3 Results

The results section contains two aspects. Firstly, the evaluation of the performance of the STRACO-scheme in convective situation. Secondly, the comparison between non-hydostatic and hydrostatic model. This comparison concentrates to find a horizontal resolution, in which the results starts to differ. Furthermore, the study also aims to investigate if the results of experimental NH-model are physically reasonable.

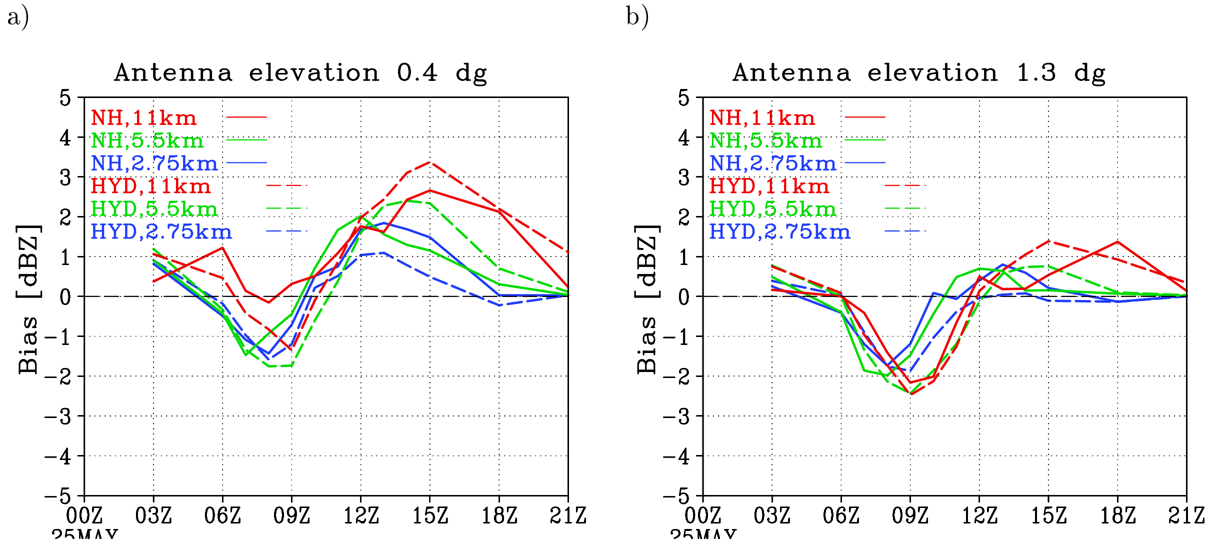

Figure 2: Time series of the areal averaged reflectivity bias. a) Antenna elevation angle 0.4 °. b) Antenna elevation angle 1.3 °. Solid lines are from NH-model and dashed from HYD–model. Red–11 km, green–5.5 km and blue–2.75 km.

3.1 The performance of STRACO

Fig. 1 shows the modelled and observed radar reflectivity fields (expotentially proportional to rain intensity) with different resolutions. The modelled fields are the result of 12 hour simulation (valid at 12 UTC).

It is evident that STRACO is able to form similar cellular precipitation patterns as observed, when the grid size gets smaller. However, the intensity and lateral extent are far too large compared to observations. The reason for too large precipitation areas is understandable, because the size of the observed convective cells are less than $5\Delta x$ (if $\Delta x = 2.75$ km). Typically numerical models cannot solve phenomena smaller than about $8\Delta x$.

Another feature in Fig. 1 is that maximum modelled dBZ-value increase more than observed, when resolution improves from 11 to 2.75 km. Too strong precipitation maximas mainly follow from the large vertical velocities (2–3 m/s) in both models (not shown).

Fig. 2 shows the time evolution of the areal averaged reflectivity bias with two antenna elevation angles. The figure with 0.4° angle represents the precipitiation closest the surface, whereas the figure with 1.3° angle represents rain higher above the ground. However, it should be remembered that the radar beam bends upward further away from the radar. Consequently, the reflectivity value only near the radar truely represent the rain intensity close the surface.

All experiments with 0.4° elevation angle, produce too much precipitation and it occurs 3–5 hours too late. In the morning the mean dBZ-value is underestimated whereas in the afternoon it is overestimated. Overestimation of precipitation mainly comes from too intense precipitating cells (Fig. 1).

Fig. 3 illustrates the areal averaged 12-hour precipitation amount as a function of grid length. The precipitation amount is divided to large scale and convective parts. The role of convection scheme is slowly diminishing as resolution improves, as it should do. Still, approximately 2/3 of the rain comes from the convective part of STRACO.

3.2 Comparison between hydrostatic and non-hydrostatic models

The precipitation amounts of NH- and HYD-models start to differ at 5.5 km resolution (Fig. 3). The difference comes mainly from the convective part of the model, which indicates that the convection scheme

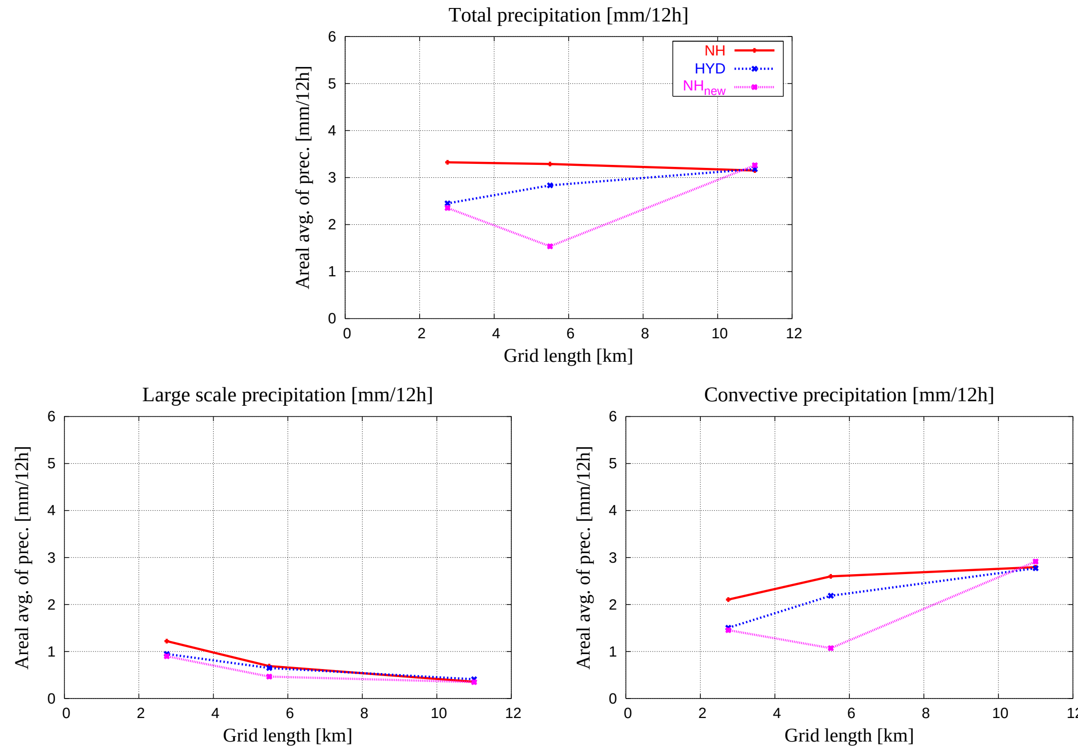

Figure 3: Areal averaged 12-hour accumulated precipitation amounts as a function of the grid length. Red lines are from NH-model, blue lines are from HYD-model and purple lines are from modified NH-model.

receives different forcing from dynamics part of the model. However, NH-model slightly increases the total precipitation amount as the resolution improves, whereas HYD-model decreases it. Also the maximum dBZ-values (Fig. 1) are a bit larger in NH-model than in HYD-model. This difference follows from that NH-model produces stronger updrafts than HYD-model (not shown). This behaviour is undesirable, because in principle, non-hydrostatic dynamics should prevent the formation of too strong updrafts (e.g. Weisman et al., 1997; Kato and Saito, 1995).

For this reason, the non-hydrostatic part of the model was slightly modified (made by Aarne Männik). In the original model, the calculation of non-hydrostatic updates to tendencies were made after physics. In new version updates were performed before physics, as it is done in most of the NH-models. Now the precipitation amount (Fig. 3: $\mathrm{NH_{new}}$) is reduced significantly. Also the updrafts are not as strong as in HYD-model (not shown). On the other hand, this modification caused some undesirable features in surface pressure field. Therefore the behaviour of the non-hydrostatic HIRLAM in convective conditions needs more investigation.

With high resolution, the NH-model tends to diminish the delay of onset of convection compared to HYD-model (Fig. 2). Main reason for this is that most probably larger updrafts in NH-model compared to HYD-model.

4 Conclusions

The goal of this study was to evaluate the performance of STRACO scheme in convective situation with a better resolution than 11 km. The second objective was to investigate the behaviour of the experimental non-hydrostatic version of HIRLAM. Overall 9 different model experiments were made in order to simulate one convective event over Southern Finland.

The STRACO-scheme was able to produce similar type of cellular precipitation structures as observed. However, the model overestimated the rain intensity and delayed the onset of convection. The underestimation of the precipitation at the beginning of the simulation originates from that the convective scheme does not trigger the convection widely enough during the first hours. Consequently, this lead to increasingly unstable temperature profiles (not shown), which furthermore are the main reason for strong updrafts and precipitation. However, it is unfair to blame only convection scheme, because other physical processes and interaction with dynamics will certainly have some effect. Therefore this issue needs more detailed study.

The precipitation amounts from NH- and HYD-models start to differ at 5.5 km resolution. Overall NH-model produced more precipitation than HYD-model. This feature was due to stronger vertical velocities in NH-model than in HYD-model. This result was in conflict with other studies and our expectations. The modification was performed in the non-hydrostatic code and precipitation amount and the magnitude of updrafts were more realistic. However, some pressure related problems were present in the new code. Therefore, more investigation is needed to understand how NH-HIRLAM should work in convective conditions.

A limitation of this study is the limited number of cases. More cases with different type of convective events should be studied in order to get the thorough understanding of the model. It would be also interesting to see how the implementation of more sophisticated microphysics affect to the results, especially to precipitation amount and vertical velocity.

Acknowledgements

Aarne Männik and Rein Rõõm for technical support advices with NH-model.

References

Haase, G. and S. Crewell, 2000: Simulation of radar reflectivities using a mesoscale weather forecast model. *Water Resour. Res.*, **36**, 2221–2231.

Kato, T. and K. Saito, 1995: Hydrostatic and non-hydrostatic simulations of moist convection: applicability of the hydrostatic approximation to a high-resolution model. *J. Meteor. Soc. Japan*, **73**, 59–77.

Kuo, H. L., 1974: Further studies of parameterization of the influence of cumulus convection on large-scale flow. *J. Atmos. Sci.*, **31**, 1232–1240.

Männik, A. and R. Rõõm, 2001: Nonhydrostatic adiabatic kernel for HIRLAM. Part II: Anelastic, hybrid-coordinate, explicit-Eulerian model. Tech. Rep. 49, SMHI, Norrköping, Sweden. Hirlam-5 Project.

Molinari, J. and M. Dudek, 1992: Parameterization of convective precipitation in mesoscale models: A critical review. *Mon. Wea. Rev.*, **120**, 326–344.

Rõõm, R., 2001: Nonhydrostatic adiabatic kernel for HIRLAM. Part I: Fundamentals of nonhydrostatic dynamics in pressure-related coordinates. Tech. Rep. 48, SMHI, Norrköping, Sweden. Hirlam-5 Project.

Sundqvist, H., E. Berge and J. E. Kristjánsson, 1989: Condensation and cloud parameterization studies with a mesoscale numerical weather prediction model. *Mon. Wea. Rev.*, **117**, 1641–1657.

Undén, P., L. Rontu, H. Järvinen and et al., 2002: *HIRLAM-5 Scientific Documentation.* HIRLAM-5 project, c/o Per Undén SMHI, S-601 76 Norrköping, Sweden.

Weisman, M. L., W. C. Skamarock and J. B. Klemp, 1997: The resolution dependence of explicitly modeled convective systems. *Mon. Wea. Rev.*, **125**, 527–548.

Modeling heavy rain case in North-East Estonia in August 2003. Preliminary results.

Andres Luhamaa, MSc
University of Tartu, Estonia

1 Overview

In this modeling experiment a heavy rainfall case in North-East Estonia during August 6 - 8, 2003 was studied. It was a very rear situation for particular area - in 24 hours there was about 1.5 times more precipitation than monthly mean, 117mm. Unexpected amount of water caused small scale local economic disaster, including overfloods in cellers, stopping several factories for days and destroing some roads. Heavy precipitation was measured only in town Jõhvi (figure 1), all other nearby stations around it had about three or four times less rain. Estonian Meteorological and Hydrological Institute (EMHI) gave general storm warnings for Estonia, but nothing specific for North-East part of it. The goal of experiment is to find out wether and how well, numerical weather prediction model HIRLAM could have predicted this rainfall.

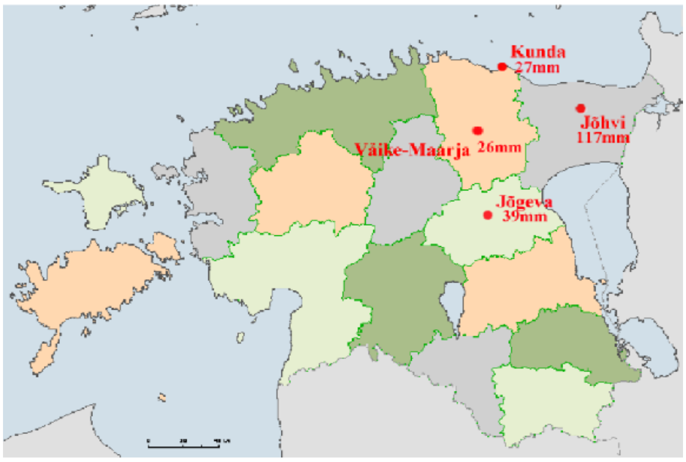

Figure 1: Precipitation at August 5, 00.00 to August 6, 12.00 as measured in stations

2 Modeling

Three versions of hydrostatic HIRLAM were used trying to predict this event in 36h forecasts. First the operational FMI 33km resolution and then 11km resolution HIRLAM 6.1.0 model with two different versions of STRACO scheme. The latter is being used experimentally in EMHI, but only since autumn 2003 and was not available in August 2003.

The FMI model gave no information about heavy rainfalls in Estonia for those days, most probably due to the low resolution.

First 11km model with older STRACO scheme shows quite a good results, shown in figure 2. We can already see strong precipitation in one certain point. Still, the maximum amount of precipitation in the forecast is about 70mm against 117mm in real situation. The point of maximum precipitation is also about 50km west from the real one. But overall, this model could have improved the quality of forecast a lot, if it where available at the right time.

The 11km model with a newer STRACO scheme, wich was introduced to the reference HIRLAM in version 6.1.2, has a totally different results, shown in figure 3. The maximum amount of precipitation is much closer to the real one, but this appears in Finland, where no heavy rainfall took place. Compared to the older scheme it shows even less realistic and reliable results.

3 Conclusions

Current 11km model at EMHI uses older version of STRACO. This seems to be already quite good in providing forecasters with information and gives significant improvement over the FMI operational model. The newer STRACO scheme does not seem to be reliable enough and needs more testing, before can be taken into use. This weather situation itself can be used for further studies and model evaluation.

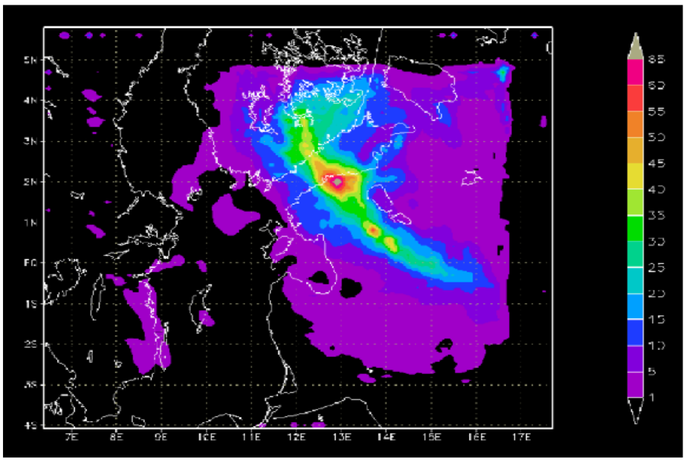

Figure 2: 36h forecast precipitation with older STRACO.

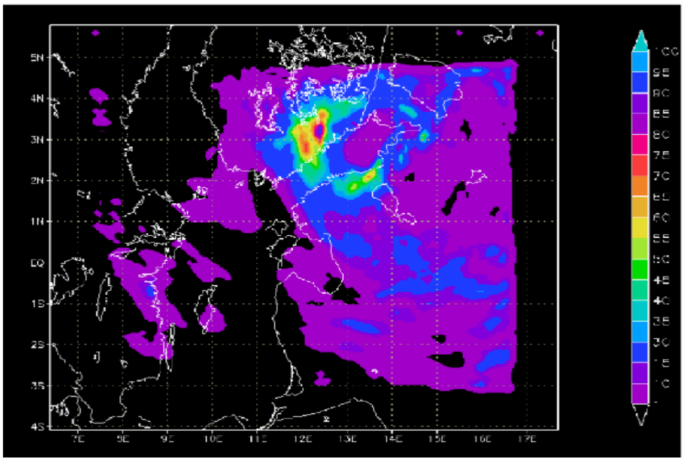

Figure 3: 36h forecast precipitation with new STRACO.

MM5-model: first experience and results

Erik Gregow and Jari Mustonen
Finnish Meteorological Institute

1 Introduction

FMI has produced the Finnish Wind Atlas in 1991, using the WASP-methodology. However, as most of the regions for potential wind power plants are located in complex terrain, there is a need for high-resolutions models when predicting and simulating winds in those difficult areas; topographical/mountainous-, coastal- and offshore areas. Therefore, the MM5-model has been chosen in the purpose of getting better wind estimation and consequently better approximation of the wind power output.

2 Methodology and goals

The model has been downloaded from the internet, it is free and the set-up time was about 4 month. This also included a test run with detailed instructions how to run the model. There are many technical difficulties in setting up a model and it is very time demanding for the computer system. Furthermore our department has access to a super-computer at CSC (Finnish IT-center for science) and this gives the advantages of much shorter modeling time.

One needs to have a very good insight in how the models physical parameterization is handled, in order to get correct results. For this reason it takes a lot of time to make the right settings and use the right meteorological schemes.

Included in this work is also the set up and learning of different programs, especially graphical programs. Also a good knowledge of the programming language Fortran, is required.

2.1 Erik's goal

To start with I'm going to compare the MM5-model results with meteorological observations for two different locations; Kopparns (a complex terrain and semi off-shore area in southern Finland) and Sodankylä (a topographic inland and forest area in northern Finland). In the beginning I will use NCEP-analyzes as input data to MM5 and as the next step I will implement Hirlam-analyzes to the model. Before we can use the Hirlam-data one of the program in MM5 has to be modified, that is REGRID. This work has been done by Jari and the new program has to be tested and verified before it can be taken into use. When we are sure that it works, I will start to make forecasts (6-48 hour) and wind simulations for longer periods than one day and validate the results with meteorological observations.

Further on I will compare the results with another meso-scale model called MIUU, this model is invented at Uppsala University in Sweden and it has for as an example been used to make the Swedish Wind Atlas. The MM5-model will be used when producing the new Finnish Wind Atlas 2.

More about the network that I am working within and my results can be found on the homepage of this EU-project site:

http://www.windeng.net

2.2 Jari's goal

The model is going to be used for simulating air pollution drift and fallout, especially in coastal areas along the Finnish bay. The other research purpose for the model is simulations on impact of industrial water vapor emissions.

3 Model description

The MM5-model is build up by 7 different programs. Each program handles one of the modeling processes and the programming code is FORTRAN. One has to run the programs after each other and in the right order. More detailed information are found at; http://www.mmm.ucar.edu/mm5/mm5-home.html Here is a short description of every program;

TERRAIN - sets the mesoscale domains (small scale area) and horizontally interpolates the latitude and longitude.

REGRID - set of programs which reads meteorological analysis on pressure levels and interpolates the analysis to the grid and map projection specified with TERRAIN.

RAWINS (or little_r) - performs an objective analysis of surface and upper-air observation data to improve meteorological analysis from REGRID.

INTERPF - interpolates the pressure level meteorological fields to the models sigma levels.

MM5 - Performs the numerical modeling (with the specified physics).

NESTDOWN - Makes input files to MM5-program with higher resolution. The advantage is that one doesn't have to run every program one more time.

INTERPB - Changes the SIGMA-coordinates back to pressure levels.

There are several different graphical programs that can be used together with this model. The three most commonly used are; GRAPH, RIP and GrADS. Each one of those have there own advantages and are different to handle. An example of wind speed simulation done with RIP can be seen in Figure 1.

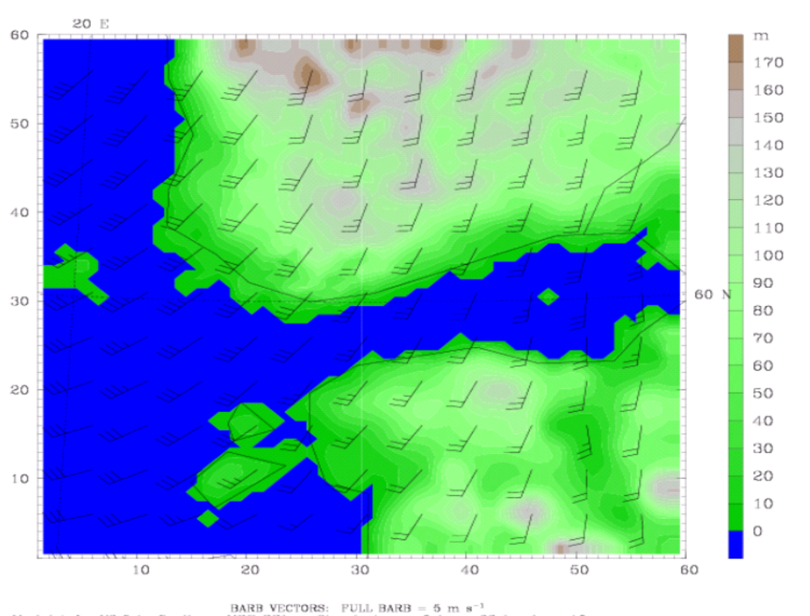

Figure 1: Wind speed over the Finnish Bay, presented by program RIP.

Surface Modelling in Northern Europe

Stefan Gollvik, SMHI, Sweden

Abstract

This is a short description and discussion about surface models. An overview about the development of surface models, for applications in NWP and climate models is described. Different formulation of the uppermost soil layer, and the use uf tiled schemes is also discussed. A particular formulation of a snow scheme, is also included.

1 Introduction to surface modelling

1.1 What is a surface model supposed to do?

Most of the energy, unevenly distributed by the solar radiation is reaching the ground, which is then transferred to the atmosphere via the planetary boundary layer. For a detailed description of the atmospheric flow, the fluxes of heat, moisture and momentum from the boundary layer, is crucial. These processes strongly depend on the surface conditions, and include both physical and biological processes. Moreover, the local conditions in the boundary layer, strongly dependent on the surface conditions, is important information itself. Also secondary information about the soil conditions, runoff, frost, etc. is an important outcome of the surface model.

1.2 Surface energy balance

The surface scheme must solve the *surface energy balance*:

$$R_n = H + \lambda E + G(+F)$$

here R_n is the net radiation balance for the surface:

$$R_n = S(1-\alpha) + \epsilon(L_w - \sigma {T_s}^4)$$

and S is the incoming solar radiation, $(1-\alpha)$ of which is absorbed at the ground, and L_w is the incoming longwave radiation. H and λE are the sensible and latent heat fluxes between the surface and the atmosphere and G is the heat flux that goes to the ground via heat conduction. The term F is the chemical energy stored during the photosynthesis and is usually omitted (< 1 % of Rn, but might be important in climate models). The sensible and latent heat fluxes are often described as:

$$H = \frac{T_s - T_a}{r_a}\rho c_p \quad \text{and} \quad \lambda E = \frac{q_{sat}(T_s) - q_a}{r_a + r_s}\rho\lambda$$

here r_a and r_s are the atmospheric resistance and surface resistance respectively. The partioning of the energy into heat and moisture fluxes, as well as the heat conduction into the ground, can be crucial, and there is a risk that compensating errors evolve, between the surface scheme, the vertical diffusion formulation, and the radion scheme.

1.3 Surface water balance

One of the most important things in surface modelling is the water cycle, i.e., from the atmosperic point of view, to model the surface resistance r_s in the energy equation, which is a function of how the evapotranspiration is treated in the surface scheme. A lot of water processes are connected with the surface. The precipitation of rain and snow, are intercepted on the vegetation, and, at that stage, subject to direct evaporation to the atmosphere, on a short time scale. The rest of the water, percolates into the soil, sometimes stored as snow on the surface for a long time. In the soil, the water is entering the biological cycle of photosynthesis, by supplying water to the plants, and trees, in the root zone. The fluxes of water from the root zone to the leaves is regulated by the stomata in the leaves, and the photosynthesis is dependent on external conditions, like PAR (Photosynthetically Active Radiation), temperature, carbon dioxide concentration etc.

The water in the snow can melt and refreeze, several times, and thus delaying the excess runoff during the spring. Besides that, the snow is important also due to the good insulation to the ground, which implies a low heat capacity, and thus rapid surface temperature changes.

2 Overview of evolution of surface models, focused mainly on evaporation

2.1 First generation

The first surface model, used in a climate model was made by Manabe (1969). It was not designed to describe the seasonal and diurnal cycles, and did not contain any heat conduction. This means that the surface temperature was calculated diagnostically at each time by using the energy balance with zero heat capacity for the surface.

Only one single layer of soil moisture, and excessive water became runoff after the "bucket" was filled. The evapotranspiration process was not explicitely adressed, and instead the formula for the latent heat flux was written:

$$\lambda E = \beta \frac{(q_{sat}(T_s) - q_a)}{r_a} \rho \lambda \ , \quad 0 \leq \beta \leq 1$$

i.e. the reduction from potential evaporation was modelled with a single parameter β which was a simple function of the soil moisture w.
A simple relation could be linearily varying between 0 and 1 for w varying from 0 (or w_{wilt}) to w_{max}.

2.2 Second generation

A big step was taken when the effect of vegetation was introduced. The modelling of evaporation on two different timescales, became possible. The very rapid timescale where the intercepted water evaporates, and the slower evapotranspiration, where the photosynthesis is parameterized.

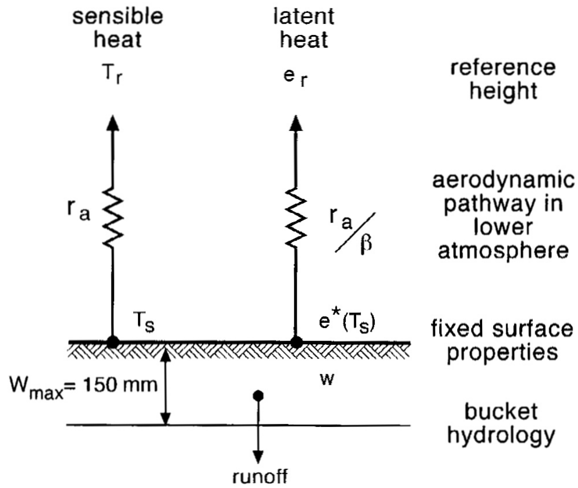

Figure 1: Figure after Pitman(2003)

Also the introduction of the so called *force-restore* formulation where the upper layer temperature forced by the surface energy balance is modified by a "deep" temperature (e.g.Deardorff, 1978, Noilhan and Planton, 1989):

$$\frac{\partial T_s}{\partial t} = C_T G - \frac{2\pi}{\tau}(T_s - T_2)$$

$$\frac{\partial T_2}{\partial t} = \frac{1}{\tau}(T_s - T_2)$$

Here T_s could be interpreted as the temperature of both the canopy and the uppermost soil layer, dependent on how much of the ground that is covered by vegetation (parameter $veg, 0 \leq veg \leq 1$). τ is one day.

In ISBA (Noilhan and Planton,1989) the water in the soil for a surface layer (w_g), and a total layer (including the root zone) (w_2) is given by:

$$\frac{\partial w_g}{\partial t} = \frac{C_1}{\rho_w d_1}(P_g - E_g) - \frac{C_2}{\tau}(w_g - w_{geq}) \ , \quad 0 \leq w_g \leq w_{sat}$$

$$\frac{\partial w_2}{\partial t} = \frac{1}{\rho_w d_2}(P_g - E_g - E_{tr}) \ , \quad 0 \leq w_2 \leq w_{sat}$$

Here C_1 and C_2 are functions of the soil type and have been calibrated using a multilayer model. w_{geq} is the moisture where gravity is balancing the capillary forces (field capacity).

The modelling of the evapotranspiration E_{tr} is important, and the stomata of the leaves regulate the evaporation, and could be modelled by the stomatal resistance r_{st} (Jarvis, 1976):

$$r_{st}^{-1} = g_{st} = g_{st}(PAR)[f(\delta e)f(T)f(w)]$$

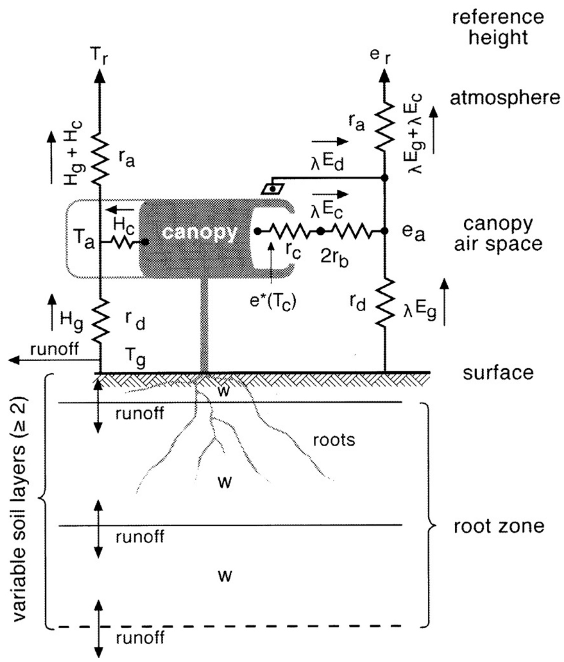

Figure 2: Figure after Pitman(2003)

Here PAR is the photosynthetically active radiation, δe is the vapour difference between the plant and the surrounding air, T the air temperature and f is a function of the water amount in the root zone (water stress).

Also the introduction of more layers in the soil, both for temperature and moisture can be regarded as belonging to this generation of surface models. The introduction of a separate temperature of the canopy is a further refinement.

2.3 Third generation

The photosynthesis is a biological process, where the plants import carbon dioxide, and while this is done, the stomata are open and the evapotranspiration takes place. In the third generation these chemical/biological processes are modelled more accurately. This is important for climate simulations, where the amount of CO_2 is increasing, and also the feedback on the vegetation growth can be taken into account. In the second generation models, the photosynthesis is tuned for the present climate, by a simpler paramemerization.

3 Skin temperature and heat conduction

3.1 Zero heat capacity

To describe the diurnal cycle in temperature one must be able to treat the short time scales of the soil and/or the vegetation. One method is to use the so called *skin temperature* which can be derived diagnostically by solving the energy balance and assuming zero heat capacity, i.e.:

$S(1-\alpha) + \epsilon(L_w - \sigma {T_{sk}}^4) - H - \lambda E = G$

G is describing the flux into the soil from the zero heat capacity skin layer and can be described as:

$G = \Lambda_{sk}(T_{sk} - T_1) \qquad \Lambda_{sk}\ [Wm^{-2}K^{-1}]$ is the skin conductivity.

This formulation is used e.g. at ECMWF (except for a small portion of shortwave radiation that goes directly to the uppermost soil layer). For the tile "high vegetation", the different fluxes in stable and unstable conditions, between the trees and the ground is parameterized by using different values of Λ_{sk}. The use of skin temperature makes it possible to tune the temperature evolution.

3.2 Non-zero heat capacity

Another way to describe the ground temperature, is to choose the uppermost layer of soil thin enough (1 cm), and write the time evolution in the same way as the force restore formulation, where now we are dealing with soil with a “ given” heat capacity:

$$\rho c \Delta z_1 \frac{\partial T_1}{\partial t} = S(1-\alpha) + \epsilon(L_w - \sigma {T_1}^4) - H - \lambda E - \frac{\lambda}{\Delta z}(T_1 - T_2)$$

This in turn requires, in cases of high vegetation, that the flow between the canopy and the ground below is described in a realistic way, e.g. as a function of the canopy temperature, which now should be modelled as a prognostic variable. The above equation, can cause numerical problems if not treated implicitely.

4 The formulation of tiled schemes

The gridsquare is generally heterogeneous, and this must be taken into account. From the atmospheric point of view, we are interested of grid average values of sensible and latent heat fluxes and the momentum flux. There are in principle two ways to treat inhomogenities, either to estimate mean values over the gridsquare of $z0$, albedo etc. and compute only one energy balance (parameter aggregation), or to use separate energy balances for different fractions of the gridsquare (tiling).

There is also a possibility to use a mix of these methods, which is often the case. Parameter aggregation is simple, but less physical than tiling, since the fluxes are very nonlinear. Most modern schemes use tiling, but parameter aggregation is robust and safe, and are used in earlier schemes.

4.1 Tiling in the soil

Some schemes keep the same profile in the soil for all tiles, e.g. ECMWF, where the tiling is only confined to the skin layer (the net energy flux into the soil is given by a weighted average over the tiles), while a pure tiled scheme, like Hirlam-ISBA is storing the soil variables separately for each tile. The latter is more physical and should be important for e.g. soil under or outide the snow cover.

5 Northern Europe problems, lakes and snow

5.1 Lakes

Generally there is a large inhomogenity in Northern Europe, due to the big number of lakes (in Sweden about 95000 lakes > 100m x 100m, the total volume is about 588 km^3). Both Finland and Sweden has roughly 10 % of the area coverd by lakes. Probably the most important thing is to keep track of wether the lakes are frozen or not. In the beginning of the winter and in spring, there are big differences in this respect between different lakes.

Lake models exist, like PROBE (Ljungemyr et.al., 1996), where the lakes are treated as one-dimensional thermodynamic boxes, covering a part of the gridsquare. A simple parameterization, of wether the lake is frozen or not, is to relate this to a deep temperature in the soil, which has a timescale near that of lakes.

5.2 Snow

When modelling snow one of the biggest problems is the estimation of the snowcover. In surface schemes, which are non-tiled, a parameter aggregation of snow/no snow makes the schemes robust. In a tiled scheme, whith a separate temperature for the snow tile, things become more sensitive, since the snow coverage is directly related to the snow depth, and thus the temperature evolution.

As an example of a snow scheme, we take the snow scheme of RCA3 (from the Swedish climate centre, Rossby Centre), developed by P. Samuelsson and S. Gollvik. A common way to estimate the fraction of snow is by:

$frsn = sn/sncrit$ where $sncrit$ is a parameter (≈ 0.015 m watereq.)

There are indications that this relation is not very good. It has been shown by Lindström et.al. 2000, that there is an hysteresis effect in the snow coverage, such that there is less coverage during the melting phase, for the same snow amount. The following algorithm is adopded for the coverage in RCA3:

We use a simple formula for the growth of snow cover (for numerical reasons)

$frsn = frsnlim * tanh(100 * sn)$, $(frsnlim{=}0.95)$

We also define an extra variable $snmax$ which initially is zero, and is put to sn when we reach full coverage. Then for the melting phase, we don't decrease the snow cover until we reach a factor $sndist$ (≈ 0.6) of $snmax$:

$frsn = sn/(snmax * sfdist)$, $frsn \leq frsnlim$

We then let $snmax$ gradually decrease, during the melting period (B. Bringfelt):

$snmax(\tau + 1) = snmax(\tau) - (zk1 * snmax - sn(\tau + 1) * (1 - zk)/zk1$

$zk1 = 0.2$ and $zk = \exp(10^6 * \Delta t)$, used if $sn(\tau + 1) < zk1 * snmax$

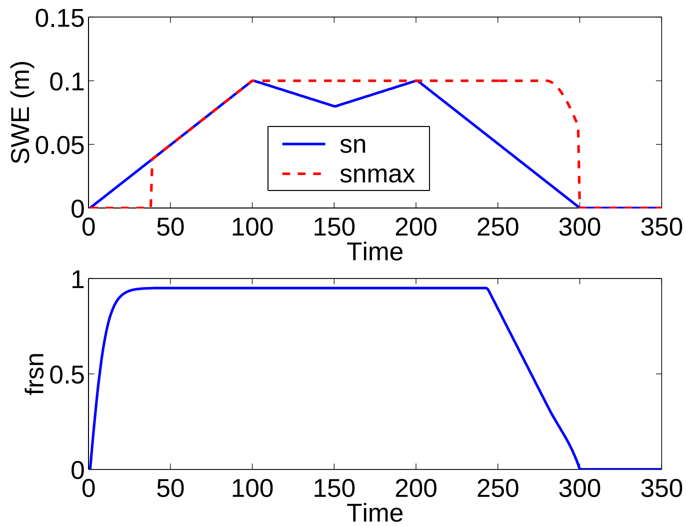

5.2.1 Heat conduction

Here we use only one layer of snow, the depth of which is Z_{snow} [m snow]. Only the upper part is thermally active in cases of deep snow:

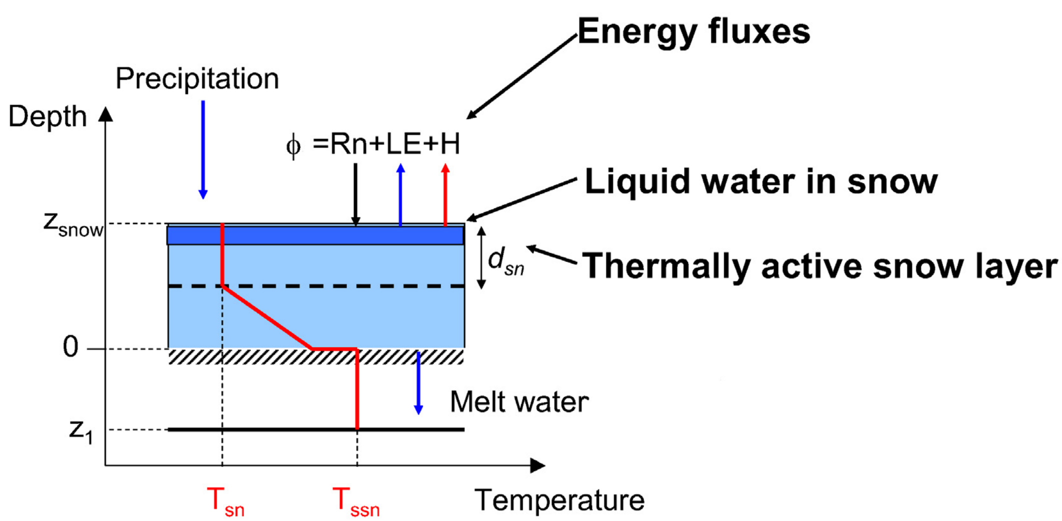

The time evolution of the snow temperature is given by:

$$\frac{dT_{sn}}{dt} = \frac{1}{c_{snow} * MIN(Z_{snow}, d_{sn})}[\Phi - \alpha_{snow}(T_{sn} - T_{ssn})]$$

$c_{snow} = vhice * \rho_{sn}/\rho_{ice}$

Here the coefficient α_{snow} (formulation from ERA 40) is parameterizing a "fictive" profile through the snow, since the isolation is a function of the snowdepth:

$$\alpha_{snow}^{-1} = 0.5\frac{Z_{snow}}{\lambda_{sn}} + 0.5\frac{Z_1}{\lambda_{soil}} \ ; \quad \lambda_{sn} = \lambda_{ice}\left(\frac{\rho_{sn}}{\rho_{ice}}\right)^{1.88}$$

5.2.2 Melting/freezing

The melting is straight forward and is invoked if the total flux into the snow pack is large enough to reach the melting point. The melted water is kept in the snow, until it reaches 10 % of the total snow water equivalent, the excess is going to the soil. The temperature T_{sn} is kept at 0° C. Freezing of the water in the snow, is less straight forward, since the negative energy flux must be partitioned between freezing and coling of the snow. We parameterize this fraction, *freezefrac*, as a function of snow depth, and water in the snow. Technically the melting/frezing is done by partitioning the timestep into temperature changes and phase shift.

5.2.3 Density and albedo changes

Here we use a simple method from Douville et.al. 1995, where the snow density is increasing with time, (e-folding time $\approx$ 4 days), and modified with new snow with less density. Then a weighteing between "dry" snow and the water in the snow is done. Also the albedo is following Douville et.al., and varies between 0.5 for old and wet snow, and 0.85 for fresh new fallen snow

6 Something about Hirlam-ISBA surface analysis

The analysis of soil temperatures is difficult, due to lack of observations. Instead the screen level temperature, T_{2m}, is analysed by optimal interpolation. The analysis increments is added to each tile (only tiles 3-5):

$\Delta T_{si} = \Delta T_{2m}$, i = 3,4,5

Then for the restore temperatures T_{2i} :

$\Delta T_{2i} = \Delta T_{si}/2\pi$

This is of course only one assumption of many! In the version of the analysis coupled to the new snow scheme, where we solve a heat conduction problem, we calculate the values in the soil by using analysed values of the uppermost layers

7 Complexity versus tiling problems

When developing surface models, it is possible to do more and more refined physical formulation, of the relevant processes. However, one must always bare in mind, the limitation that comes from the uncertainties in the horizontal representations. In the case of tiles, usually the fractions of different properties are given. In reality also the statistical distribution of these fractions are important, and also subgrid scale flow patterns, can significantly change the grid average fluxes. In other words, if half the gridsquare is forest and the other half is sea, the real fluxes differ if the air is advected from the sea or from the forest. Moreover if the water is more patchy (archipellago), even more complex fluxes can appear. A pure tiled scheme implies that there exists a local turbulent equilibrium for each tile, and that parameters like screen level temperatures are meaningful to estimate. This means that the only communication between the tiles goes via the lowest model layer, which then in turn should be high enough over the ground, to be described by one single value, i.e. the lowest model layer should be above blending height (the height at which the individual inhomogenities of the ground are not felt).

It is often stated that these problems dissapear when the horizontal resolution is increased, so that non-tiled schemes can be used. If there are large horizontal differences in the surface characteristics, there might be numerical problems, caused by these inhomogenities.

8 References

Deardorff, J.W., 1978: Efficient prediction of ground-surface temperature and moisture with inclusion of a layer of vegetation. Journal of Geophysical Research 83: pp 1889-1903

Douville, H., Royer, J.-F., Mahfouf, J.-F., 1995: A new snow parameterization for the Météo-France climate model. Climate Dynamics, 12: pp 21-35

Jarvis, P.G., 1976: The interpretation of variations in leaf water potential and stomatal cunductance found in canopies in the field. Phil. Transactions of the Roy. Soc. of London, Series B 273: pp 593-610

Lindström, G., Gardelin, M., Bringfelt, B., Gollvik, S.,2000: Integration of hydrological modelling routines in a regional climate model. XXI Nordic Hydrological Conference, Uppsala, Sweden 26-30 June 2000, NHP Report No. 46.

Ljungemyr, P., Gustafsson, N., Omstedt, A., 1996: Parameterization of lake thermodynamics in a high resolution weather forecasting model. Tellus 48A, pp 608-621

Mason, P.J., 1988: The formation of areally-averaged roughness lengths. Quart. Journ. Roy. Met. Soc., 114: pp 399-420

Manabe, S., 1969: Climate and the ocean circulation: 1, the atmospheric circulation and the hydrology of the Earth's surface. Mont. Wea. rev. 97, pp 739-805

Noilhan, J., Planton, S., 1989: A simple parameterization of land surface processes for meteorological models. Mon. Wea. Rev. 117: pp 536-549

Pitman, A.J.,2003: The Evolution of, and Revolution in, Land Surface Schemes Designed for Climate Models. Int. Journal of Climatology, 5, Vol 23, pp 479-510.

Viterbo,P., Beljaars A.C.M, 1995: An improved land surface parameterization scheme in the ECMWF model and its validation. Journal of Climate 8: pp 2716-2748

Bridges between meteorological and dispersion models at different scales

Genikhovich[1] E., Sofiev[2] M.

[1] Main Geophysical Observatory
[2] Finnish Meteorological Institute

The general methodology of dispersion modelling is based on linking of meteorological and dispersion models. A general understanding of the corresponding interface is that the dispersion models should assimilate the information coming from meteorological ones with minor internal processing, mainly oriented at computation of some surrogate indices like stability parameters or mixing layer height. However, the situation is rarely that simple. The dispersion model (DM) as a client of the meteorological model (MM) requires variable spatial resolution because fields of concentration of atmospheric pollutants on the scales ranging from local to regional ones are usually much more irregular than those of meteorological variables. Consequently, the spatial resolution of DM should be significantly higher than those used when computing the fields of meteorological variables. Thus, procedures of downscaling of meteorological fields are an important component of the dispersion modelling. Special restrictions applied to these procedures are discussed in this paper, in particular, those eliminating the non-conservation of mass.

We discuss here the following types of errors of dispersion simulations: (i) resulting from predictions of atmospheric processes of stochastic nature using deterministic models; (ii) induced by errors in input data transferred from the NWP driver. Some of these errors are objective and cannot be reduced below certain level. The others reflect quality of specific models and their compatibility. There are several key areas for harmonization of meteorological and dispersion models: (i) effects of natural variability and scales of processes should be adequately represented, (ii) extra variables required by dispersion models should be derived from the input, (iii) representations of various processes in NWP and dispersion models have to be made coherent (iv) technical problems and associated losses in accuracy during transfer of large amounts of data should be taken into account, (v) when a feedback from the dispersion model is important for the NWP model, an appropriate 2-way interface should be set.

A stochastic nature of atmospheric motions results in widely recognized limitations on the accuracy of deterministic models. This phenomenon inevitably affects the dispersion fields, but much stronger than meteorological ones, because of sharp gradients of pollutant concentrations, which makes the observed fields highly vulnerable to any fluctuations of meteorological variables (Gifford, 1958). In the case of centreline concentrations from the single point source, for example, corresponding errors cannot be reduced less than approximately 100% (see Genikhovich, 2003). In addition, computed fields of concentrations of pollutants are "contaminated" with the noise due to uncertainties in governing parameters generated by the NWP model. The last ones result from (i) limitations on the spectral band of atmospheric motions that could be reproduced by the NWP model (especially, on the scales not resolved by the NWP models); (ii) deficiencies in parameterizations of physical and chemical processes in the atmosphere; (iii) numerical errors; and (iv) reduced number of digits used when transferring the date from NWP to dispersion model (for example, when using the Gridded Binary Data Format). The resulting errors could be estimated on the basis of sensitivity studies (e.g. Kiselev, Gorelova, 1979). It should be noted here that the variability of fields of meteorological parameters and concentrations is quite noticeable, especially in urban conditions.

Corresponding quantitative estimates are published by Lokhard & Irvin (1980), Genikhovich et al. (2003), Nappo and other authors.

Significant errors in dispersion calculations could appear as a result of downscaling, if the self-consistency of the both coarse and fine grids, as well as their mutual coherence (transparent boundary conditions) are not ensured. It is easy to show that interpolation of the fields near the boundary between the outer coarse and inner fine grids do not provide the self-consistency to either of them. In application to the transport equation, this results in violation of the mass consistency because the interpolated fields do not conform to the continuity equation. As shown above, natural variability of the meteorological and pollution fields depend on spatial resolution, so the downscaled parameters should, in principle, resolve the corresponding variability, which is inside the internal uncertainty of the coarse fields. Taken together with probable non-linearity of the involved processes, this again poses the problem of consistency and mutual agreement of the coarse and fine grids. A potential cost of disagreements at this stage is illustrated by Cameron-Smith & Connell (2003). The problem of coherent representation of natural variability and scales of the processes leads to significant challenges. However, there is one more dimension for harmonization: chemical and physical processes, including advection and diffusion. As shown by Gong (2003) and Cameron-Smith (2003), violation of continuity equation can result in dramatic consequences, such as 100% error in total mass in air of some chemical or two orders of magnitude local peaks of concentrations, appearing and disappearing in chaotic manner. They can show up if the downscaled wind fields are not solenoidal, *i.e.*, do not satisfy the continuity equation to ensure the local mass conservation. In such a case, fictitious sources and/or sinks of pollutants distributed over the computational domain are introduced in the model.

The above effects can originate either from non-conservative advection (as often happens in meteorological models), from an inconsistency between the schemes in meteorological and dispersion models, from limited accuracy of the data transfer or from grid interpolation and transformation. One of efficient, though expensive, recipes here is to explicitly restate the continuity equation in the meteorological fields inside the dispersion model right before using the fields. Residuals should be distributed in the horizontal wind components as they are less sensitive to such a disturbance. Problems of harmonization of other physical and chemical processes can be illustrated by the following example. Let at some time an air volume limited by the grid cell borders contains a certain amount of liquid cloud water, with some species dissolved in it. Let at the next time step the liquid water content becomes zero due to cloud microphysical processes, which are computed in meteorological model. What should then be done with the dissolved species? It is easy to show that virtually all ways of handling such situations lead to errors, which significance depend on mutual relation of timescales – chemical and microphysical.

One of the most important extra variables used by the dispersion models are the scaling parameters for the similarity theory applications to the atmospheric boundary layer. These variables, like Monin-Obukhov length L, friction velocity $u*$, temperature scale $T*$ and convection velocity scale $w*$, can be obtained from vertical profiles of wind and temperature, or from the sensible heat flux H, which, however, is not always in a standard output of the NWP models. A well-known iteration approach for computing L, $u*$, $T*$ does not always provide good estimates due problems with convergence (especially in stable conditions) and necessity to perform numerical differentiations of slowly varying parameters. The scope of corresponding problems is illustrated on Fig. 1 that reproduced the fields of friction velocity computed with HIRLAM (right-hand panel) and estimated with a "standard" M-O similarity approach. A one-step approach introduced by Genikhovich & Osipova (1984) and Groisman & Genikhovich (1997) can be used to provide robust estimates of parameters listed above. The method is based on the following formulation for eddy diffusivity:

$$K_z = \{0.5\kappa \int_0^z \frac{[(dU/dz)^2 - \sigma\beta d\theta/dz]^{5/4}}{(dU/dz)^2 - 0.5\sigma\beta d\theta/dz} dz\}^2$$

Here *z~1m* is a characteristic height, $\sigma =$ *10* is a dimensionless constant, $\beta = g/T_0$ is a buoyancy parameter and *g=9.81* m s^{-2}. From that equation, it is straightforward to get the required scaling variables:

$$u^* = \sqrt{K_z(z_K)\frac{\partial U}{\partial z}(z_K)}\,, \qquad H = -\frac{c_p\rho}{\Pr} K_z(z_K)\frac{\partial T}{\partial z}(z_K)\,,$$

$$T^* = -\frac{H}{c_p\rho\, u^*}\,, \qquad L = -\frac{(u^*)^3 c_p\rho}{\kappa\beta H}\,, \qquad w^* = u^*\left(\frac{h_{ABL}}{-\kappa L}\right)^{1/3}$$

Its performance is demonstrated on Fig. 2 by comparison of the sensible surface heat fluxes computed with HIRLAM (right-hand panel) and estimated a robust parameterization scheme (left-hand panel).

Meteorological models produce a vast amount of information describing a large variety of processes and phenomena. Therefore a task of coding / decoding, storing and transferring the data becomes far from trivial. More than that, a selection of particular tools and methods becomes a matter of optimization largely depended on further use of data. As a result, the data perfect for one application, such as a weather forecast, may appear problematic for another one such as dispersion modelling.

An example of the Gridded Binary data format, which is one of the most widely used de-facto standards for meteorological data, illustrates possible obstacles. A basis for GRIB compressing is a principle of “reasonable accuracy”, which states that the number of digits to store should not exceed a reasonable precision achievable in and needed for practical applications (for meteorological models it is, evidently, weather forecast). In practice, HIRLAM fields for temperature have an accuracy $5*10^{-3}$ – $2*10^{-2}$ degrees, horizontal wind components – 10^{-2}m s^{-1}, ECMWF fields have $5*10^{-3}$ – 10^{-2} for both of them, etc. These precisions are fully sufficient for describing the weather situations, but they create major problems if a dispersion model has to find a temperature or wind speed gradients because it involves numerical differentiation and subtraction of very close values. Sometimes the signal-to-noise ratio may become equal or less than 1.

The most straightforward approach to cope at least some of the above difficulties is "integrated" one when transport and transformation equations are integrated simultaneously with the NWP model. It requires, however, significant computational resources and a higher resolution that it not always possible to achieve. In addition, this method does not solve problems of methodological compatibility of the models. Therefore, in many cases the "interfaced" approach is used when results of the NWP modelling are transferred to dispersion model with downscaling, if necessary. In this case, however, the downscaling procedures could introduce additional errors in computed concentration fields. If one write the dynamic system of equation in the Vorticity-Stream Function form, it becomes obvious that these procedures should properly account for the effects of baroclinicity in the outer flow as well as for correct description of distribution of the second derivatives of the wind velocity field. That is why the Hermite polynomials seem to be more appropriate for interpolation of the outer fields in the computational domain than the Lagrange ones.

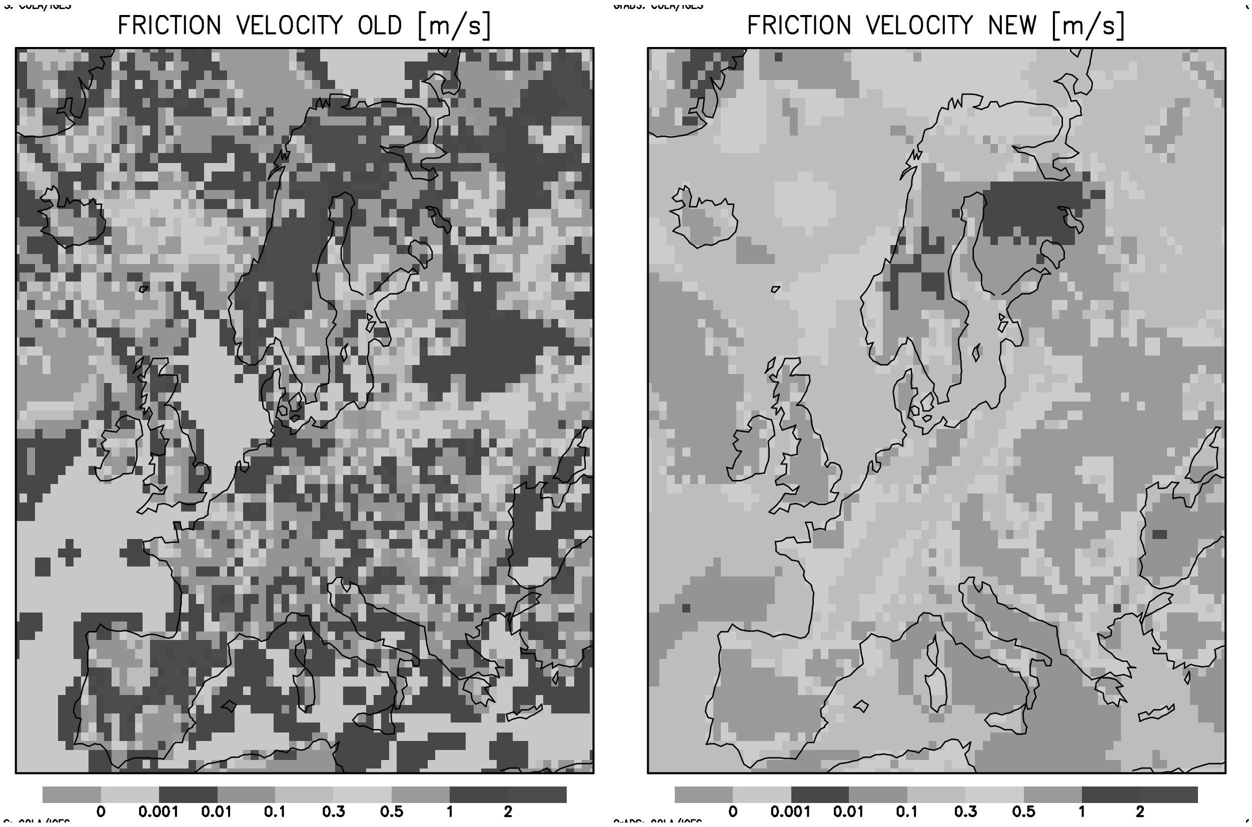

Fig. 1. Friction velocity computed with HIRLAM (right-hand panel) and estimated with a "standard" M-O similarity approach.

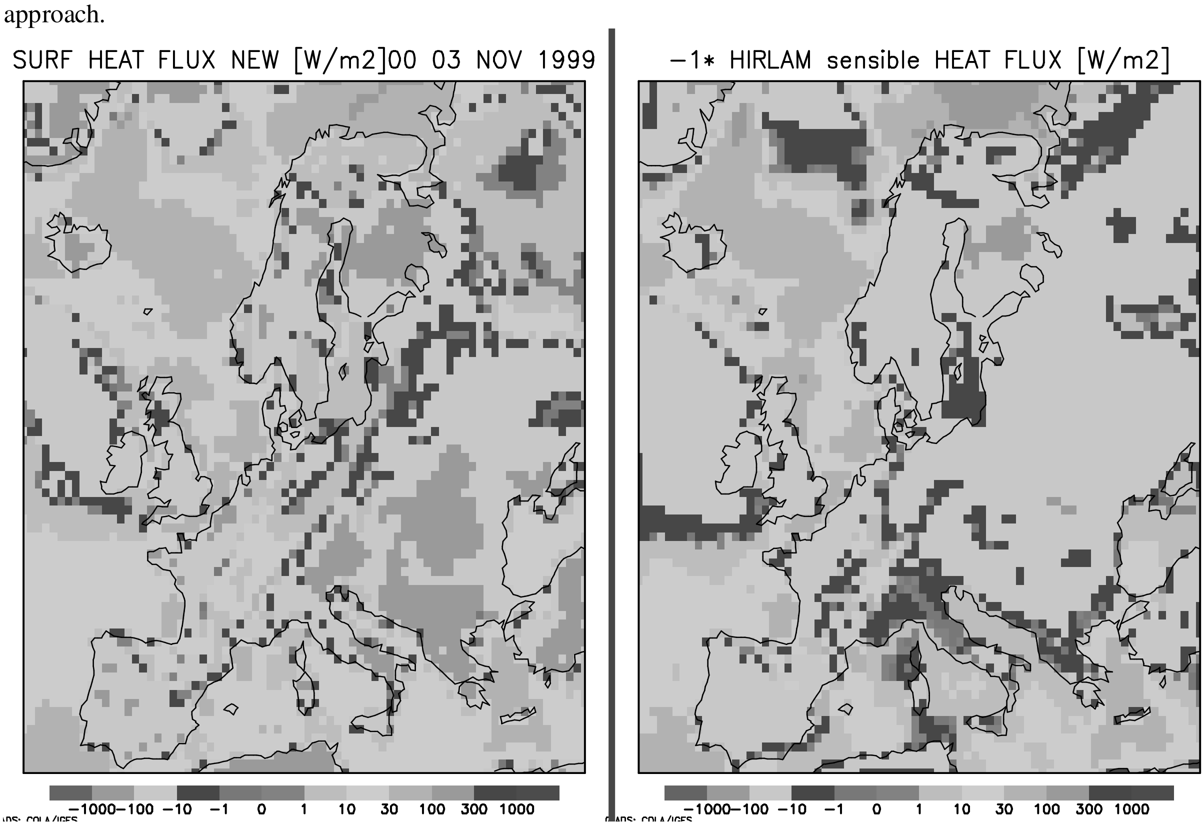

Fig. 2. Sensible surface heat flux computed with HIRLAM (right-hand panel) and estimated with the robust parameterization scheme (left-hand panel).

References

Gong, W., Makar, P.A., Moran, M.D. (2003) Mass-conservation issues in modelling regional aerosols. *In pre-prints of 26thNATO/CCMS International Technical Meeting on Air Pollution Modelling and its Application,* Instanbul, May 2003, pp. 317-325.

Cameron-Smith, P., Connell, P. (2003) Pressure fixers: conserving mass in chemical transport models by adjusting the winds. Internet publication, http://asd.llnl.gov/pfix/.

Genikhovich E.L. (2003) Indicators of performance of dispersion models and their reference values. *International Journalof Environment and Pollution* (in press)

Genikhovich E., Ziv, A., Iakovleva, E., Palmgren, F., Berkowicz, R. (2003) Joint analysis of air pollution in street canyons in St. Petersburg and Copenhagen (submitted for publication in *Atmospheric Environment*)

Genikhovich, E.L., Osipova, G.I. (1984) On determination of the turbulent eddy diffusivity from standard meteorological observation data. *Trudy GGO (Proc. Main Geoph. Observatory*), iss. 479, pp. 62 – 69 (in Russian)

Gifford (1958) Statistical plume model, in: Frenkiel, F.N., and Sheppard, P.A. (Eds.): Atmospheric Diffusion and Air Pollution, Acad. Press, NY, pp. 143 - 164

Groisman, P., Genikhovich, E. (1997) Assessing surface-atmosphere interaction using former Soviet Union standard meteorological network data. Part 1: Method, *Journal of Climate*, v. 10, No 9, pp. 2154 – 2183

Kiselev, V.B., Gorelova, V.V. (1979) The study of the atmospheric diffusion equation by means of perturbation theory for functionals. *Trudy GGO (Proc. Main Geoph. Observatory*), iss. 436, pp. 37 – 42 (in Russian)

Modeling of airflow over inhomogeneous vegetation at microscale

Andrey Sogachev*and Oleg Panferov†

1 Introduction

Experiments with both general circulation models and regional mesoscale models have shown a significant sensitivity of modeled circulation patterns to the variations in land surface caused by different reasons, e.g. climate or land-use changes. It was becoming clear that the use of simple bucket models in which the land surface is represented as a bucket with a finite water-holding capacity was not adequate. This led to the development of several land-surface parameterizations, which recognized several vegetation types, and to models describing the interaction of the vegetated land surface with the atmosphere in a more realistic manner. Nevertheless most of the models describe the interaction between land surface and the atmosphere in a simplified one-dimensional sense and assume homogeneous surface cover. However the real Earth's surface is always heterogeneous in some degree (especially when covered with different vegetation types) and thus, all models have to take this heterogeneity into account.

Due to the surface inhomogeneity the relationships between the land-surface characteristics and energy and matter fluxes from surface to the atmosphere are non-linear. This non-linearity implies that simple averaging of parameter values over the model's grid cell does not necessary yield the correct values of fluxes in this cell (Dolman, 1992). To investigate the aggregation of land-surface parameters and to define effective parameters, two- and three-dimensional modeling approaches are used at a range of spatial scales. The complexity of such models depends on typical large-scale model horizontal grid size and increases with decreasing of the latter. The dimension of model's grid cell tends to decrease as far as the growing computer possibilities allow.

The aim of the present study is to overview briefly the approaches to model an air motion over the vegetation (as mostly heterogeneous surface type) at microscale which could be used for the aggregation procedure. Short introduction of SCADIS model as one of the most promising for aggregation procedure is also given.

2 Air motion features in plant canopies

The literature is rich on the subject of air motion in vegetation. In a recent article Finnigan (2000) reviewed the current state of knowledge about air flow mainly for idealized conditions: neutral to slightly unstable atmospheric stratification, homogeneous and extensive canopy, flat terrain. He demonstrated that canopy air motion is far from random, with major contributions to turbulent motions arising from coherent eddies. Some particular features of canopy flow are:

1. The single-point statistics of turbulence differ significantly from those in the surface layer: a) velocity profile is inflected; b) second and higher moments are strongly inhomogeneous with height.
2. Large coherent structures (ejections and sweeps) control turbulence dynamics.
3. Aerodynamic drag on the foliage causes the unstable inflected velocity profile and removes energy from large eddies. Total dissipation rates are very large.

*Division of Atmospheric Sciences, Department of Physical Sciences, University of Helsinki, POBox 64, FIN-00014, Helsinki, Finland (e-mail: Andrei.Sogachev@helsinki.fi)

†Institute of Bioclimatology, University Gttingen, Bsgenweg 2, D-37077, Gttingen, Germany (e-mail: opanfyo@gwdg.de)

The review paper of Lee (2000) summarized the studies of the flow in non-ideal situations: non-neutral stratification, heterogeneous vegetation, topography variations.

3 Modelling approaches

Turbulent motions are stochastic and difficult to predict on the basis of first principles. However, over the last thirty years a succession of modelling approaches of increasing complexity has been applied to the horizontally homogeneous case and these form a point of departure for study of more complex flows. Certain statistical properties and their vertical dependence on canopy structure can be predicted by multiple-layer approach assuming that the canopy is composed of several vertical layers, each of which is modeled separately.

Turbulent transport between the successive layers of multiple-layer models is mainly simulated using an Eulerian framework. Such modeling studies of canopy flow face two fundamental issues: 1) how to quantify the drag and heat exchange of individual plant elements and 2) how to treat the closure problem. Theories addressing the first issue are well established now (Thom, 1975; Wilson and Shaw, 1977; Raupach and Shaw, 1982; Finnigan, 1985). The closure problem remains an active area of research. The problem exists because there are more unknowns than the equations that can be derived from first principles. Methods of handling the problem are called closure schemes, which add to the model a few more (empirical) parameterization equations so that the number of model equations equals the number of unknowns (Stull, 1988).

Ayotte et al. (1999) came to conclusion that the minimum level of complexity that is capable of simulating turbulence fluxes within canopy is second-order closure because a simple first-order closure based on eddy diffusivities in plant canopy airflows is failed. In extreme cases counter-gradient fluxes of momentum and scalars are observed (Shaw, 1977; Denmead and Bradley, 1985). Raupach (1987) showed that this phenomenon was caused by the large scale of the dominant canopy turbulent eddies relative to the scale of distribution of sources and sinks in the vegetation. Nevertheless, Gross (1993) pointed out that these authors came to this conclusion by comparing their observations with the results of one-dimensional model calculations. One-dimensional in this context implies that any advection, which may also be directed against the gradient of the mean quantity, is not taken into account. Gross (1993) argued that the application of the flux-gradient approach by 2D- and 3D-modelling is admissible, in particular, in simulations for which advective processes are of greater importance than diffusive processes. Such situations are typical for inhomogeneous vegetation. Flux-gradient approach has also an advantage of being less time-consuming.

An alternative Lagrangian formulation was developed by Raupach (1987) to describe scalar transport in canopies. This approach, however, is not obviously applicable to momentum transfer. Furthermore, the Lagrangian approach requires knowledge of Eulerian velocity statistics and Lagrangian length scales so the interest in producing robust models of canopy turbulent flow fields has continued (Ayotte et al., 1999).

Another alternative is the Large Eddy Simulation (LES) method. Although it has made great strides over the last few years the merit of such models for disturbed flows very much remains to be demonstrated, and there is a profound difficulty in how to parameterize the increasingly dominant subgrid turbulence, very near ground (Wilson and Yee, 2003). So it is likely that the ensemble models will remain the optimal choice for complex flow description for at least the next few decades (Launder, 1990)

4 Flow models

In spite of certain theoretical developments described above there are few models taking into account the heterogeneity of underlying surface. Lee (2000) gives a short review of existent models for air motion over inhomogeneous landscapes like by forest edge transitions, forest clearings, and patchy canopies. According to Lee all modeling studies of the disturbed flow with only one exception (Patton et al., 1998) rely on ensemble models. Two of the simplest ones are: a similarity solution with a modified wall-jet approach (Shinn, 1971) and a phenomenological analytical description (Albini, 1981) for the edge flow.

Subsequent models can be sorted into groups based on their closure schemes (up to 1.5 order). Second-order schemes have been used for windbreak flow (Wang and Takle, 1997), however, they are too computer time consuming to be used effectively for larger scales. For similar reasons higher order schemes are used in one-dimensional calculations only.

The models were sorted by Lee (2000) into groups regarding to closure hierarchy: first-order closure models (K-l) (Li et al., 1990; Miller et al., 1991), and first-and-a-half order closure models of two types: E-l (Schilling, 1991; Wilson et al., 1998; Wilson and Flesch, 1999) and E-ϵ (Green, 1992, Liu et al., 1996). Here K - the eddy diffusivity, l is mixing length, E and ϵ are turbulent kinetic energy (TKE) and its dissipation rate respectively.

First type of model (K-l) often draws criticism because model parameters are tuned to match observations. Another limitation is that higher-order statistics useful for wind load studies, such as TKE and velocity variances are not computed. Central failure of second type of model (E-l) is the need of length scale formulation accounting for the presence of distributed canopy. E-ϵ model has the advantage of simulating the mean velocity field without a predetermined mixing length and, therefore, reduces unwanted subjective errors in the modeled results.

5 Model SCADIS

Model SCADIS was developed accounting for above statements. That is a simple three-dimensional atmospheric boundary layer (ABL) model for a limited area which takes into account the leaf energy balance, water vapour and CO2 exchange, and scalar transport within vegetation. The model SCADIS initially based on E-l closure scheme was described in (Sogachev et al., 2002). It was further enhanced for the conditions of variable relief using the E-ϵ closure (Sogachev et al., 2003). Figure 1 shows the general structure of the model, illustrating the main boundary condition variables and representative vertical profiles of the wind velocity components, air temperature, specific humidity and CO2 concentration typically obtained from the model calculations. Using the data on the turbulence coefficient profile obtained during calculations, it is possible to deduce the fluxes of all necessary variables. The relationships between separate processes described in each grid cell and characteristic horizontal grid cell size are also shown.

Despite the simplifications used to describe the natural processes, the model has demonstrated a reasonable agreement between modeled and observed data under different environmental conditions. The model has shown the ability to simulate correctly the diurnal course of ABL dynamics in presence of vegetation without significant computational expenses. Thus, it can be applied as a practical tool for many scientific tasks. A number of applications concerning mainly environmental studies (e.g. diurnal and spatial dynamics of carbon dioxide in ABL, footprint estimations, etc) have been already demonstrated (Sogachev et al., 2002, Sogachev and Lloyd, 2003). Due to high vertical (from 0.1 m near ground till 200 m near the upper border) and horizontal resolutions (up to 10 m) the model has also a great potential for implementation in large-scale modeling, namely for investigations of the spatial aggregation of energy fluxes across a heterogeneous landscape (the up-scaling problem).

6 Summary

At sufficiently large modeling scale it has become standard to form weighted averages of local values of different parameters to obtain values representative of a large heterogeneous area. This approach assumes that local values of those parameters are available and meaningful. Estimations of these parameters is one of the motivations for 3-D airflow modeling above and within the vegetation canopies (as mostly heterogeneous surface type) where flow conditions are evolving spatially. The turbulent structure of canopy flows is complicated. However, gaining a good knowledge of air motion in forest vegetation is a necessary step towards a better understanding of energy and matter exchanges between underlying surface and atmosphere above. The numerical simulations based on theoretical and experimental results provide additional information about exchange processes in complex conditions. Due to its features the E-ϵ based model is at present the best instrument to study of air motion within and above forest vegetation

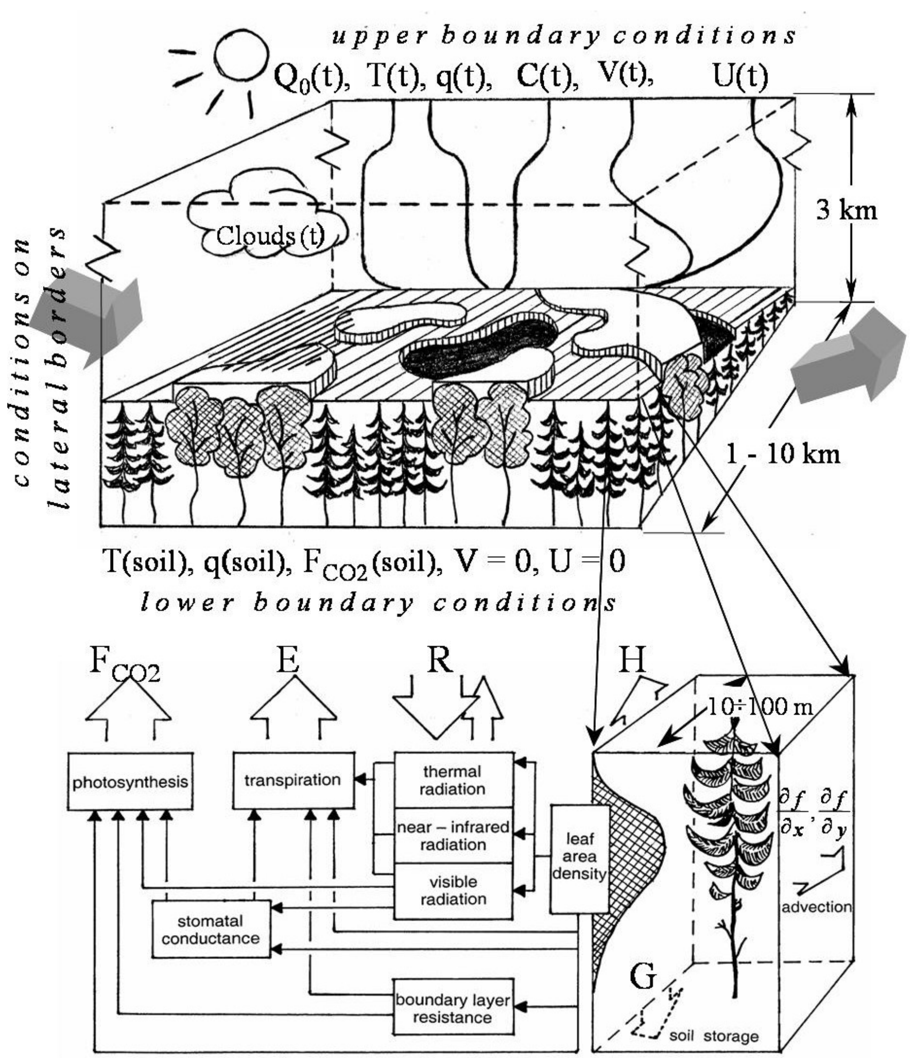

Figure 1: The schematic representation of the model domain and boundary conditions as well as the relationships between separate processes within a grid cell of the model.

in non-ideal conditions since it is the optimal compromise between the accuracy of higher order closure models and computational expenses. There are few models based on such closure that is capable to simulate an air motion over complex terrain. The model SCADIS presented here has the potential to be used for further investigations of land-surface parameters aggregation and to define effective parameters for HIRLAM's gridcells.

References

Albini, F.A.: 1981, 'A phenomenological model for wind speed and shear stress profiles in vegetation cover layers', J. Appl. Meteorol. 20, 1325-1335.

Ayotte, K.,W., Finnigan, J.J. and Raupach, M.,R.: 1999,'A second-order closure for neutral stratified vegetative canopy flows', Boundary-Layer Meteorol. 90: 189-216.

Denmead, O.T., Bradley, E.F.: 1985, 'Flux-gradient relationships in a forest canopy'. In: Hutchinson, B.A., Hicks, B.B. (Eds.), The Forest-Atmosphere Interactions. De. Reidel Publishing Co., 421-442.

Dolman, A.J.: 1992, 'A note on areally-averaged evaporation and the value of the effective surface conductance', J. Hydrol., 138, 583-589.
Finnigan, J.J.: 1985, 'Turbulent transport in flexible plant canopies' In: Hutchinson, B.A., Hicks, B.B. (Eds.), The Forest-Atmosphere Interactions. De. Reidel Publishing Co., 443-480.
Finnigan, J.J.: 2000, 'Turbulence in plant canopies', Annu. Rev. Fluid Mech. 32, 519-571.
Green, S.R.: 1992, 'Modelling turbulent airflow in a stand of widely-spaced trees'. PHOENICS J. Comp. Fluid Dyn. Applic. 5, 294-312.
Gross, G.: 1993, Numerical simulation of canopy flows, Springer Verlag, Berlin, 168 pp.
Launder, B. E.: 1990, 'Phenomenological Modelling: Present and Future?' In J. L. Lumley (ed.), Lecture Notes in Physics No. 357, Springer-Verlag, 439-485.
Lee, X.: 2000, 'Air motion within and above forest vegetation in non-ideal conditions', For. Ecol. Manage. 135, 3-18.
Li, Z., Lin, J.D. and Miller, D.R.: 1990, 'Air flow over and through a forest edge: a steady state numerical simulation', Bound.-Layer Meteorol. 51, 179-197.
Liu, J., Chen, J.M., Black, T.A. and Novak, M.D.: 1996, 'E - modelling of turbulent air flow downwind of a model forest edge', Bound.-Layer Meteorol. 77, 21-44.
Miller, D.R., Lin, J.D. and Lu, Z.N.: 1991, 'Air flow across an alpine forest clearing: a model and field measurements', Agric. For. Meteorol. 56, 209-225.
Patton, E.G., Shaw, R.H., Judd, M.J. and Raupach, M.R.: 1998, 'Large-eddy simulation of windbreak flow', Bound.-Layer Meteorol. 87, 275-306.
Raupach, M. R.: 1987, 'A Lagrangian Analysis of Scalar Transfer in Vegetation Canopies', Quart. J. Roy. Meteorol. Soc. 113, 107-120.
Raupach, M.R. and Shaw, R.H.: 1982, 'Averaging procedures for flow within vegetation canopies', Bound.-Layer Meteorol. 22, 79-90.
Schilling, V.K.: 1991, 'A parameterization for modelling the meteorological effects of tall forests - a case study of a large clearing', Bound.-Layer Meteorol. 55, 283-304.
Shaw, R.H., 1977. Secondary wind speed maxima inside plant canopies. J. Appl. Meteorol. 16, 514-523.
Shinn, J.H., 1971. Steady-state two-dimensional air flow in forests and the disturbance of surface layer flow by a forest wall. Technical Report ECOM-5383, Atmospheric Sciences laboratory, White Sands Missile Range, New Mexico, USA, 60pp.
Sogachev A, Rannik U, and Vesala T.: 2003, 'On flux footprints over the complex terrain covered by a heterogeneous forest', Agric. For. Meteorol, accepted.
Sogachev, A. and Lloyd, J.: 2003, 'Using a one-and-a-half order closure model of the atmospheric boundary layer for surface flux footprint estimation', Bound.-Layer Meteorol., accepted.
Sogachev, A., Menzhulin, G., Heimann, M., and Lloyd, J.: 2002, 'A Simple Three Dimensional Canopy - Planetary Boundary Layer Simulation Model for Scalar Concentrations and Fluxes', Tellus 54B, 784-819.
Stull, R.B.: 1988, 'An Introduction to Boundary Layer Meteorology', Kluwer Academic Publishers, The Netherlands, 666pp.
Thom, A.S.: 1975, 'Momentum, mass and heat exchange of plant communities'. In: Monteith, J.L. (Ed.), Vegetation and The Atmosphere, Academic Press, Vol. 1, 57-110.
Wang, H. and Takle, E.S.: 1997, 'Momentum budget and shelter mechanism of boundary-layer flow near a shelterbelt', Bound.-Layer Meteorol. 82, 417-435.
Wilson, J.D. and Flesch, T.K.: 1999, 'Wind and remnant tree sway in forest openings III. A windflow model to diagnose spatial variation', Agric. For. Meteorol. 93, 259-282.
Wilson, J.D. and Yee Eugene: 2003, 'Calculation of winds disturbed by an array of fences', Agric. For. Meteorol. 115, 31-50.
Wilson, J.D., Finnigan, J.J. and Raupach, M.R.: 1998, 'A first-order closure for disturbed plant-canopy flows, and its application to winds in a canopy on a ridge', Quart. J. R. Meteorol. Soc. 124, 705-732.
Wilson, N.R. and Shaw, R.H.: 1977, 'A higher order closure model for canopy flow', J. Appl. Meteorol. 16, 1197-1205.

Some Methods to Consider Soil Freezing Effect in Land Surface Block of Atmospheric Models

Kourzeneva K., *Russian State Hydrodynamical University*
Kozlova D., *Russian State Hydrodynamical University*

1 Introduction

The importance of the exchange processes between the atmosphere and the underlying surface accurate description is well recognized. Surface temperature and humidity play a significant role to determine temperature conditions and motions in the atmospheric surface layer. Processes in the atmosphere-vegetation-land system are of different kinds and are very complicated. But it is known that sophisticated land surface models hardly outperform the relatively simple schemes and the desirable feature of such schemes is the minimum number of soil and vegetation parameters. It is important to use the fast scheme as well. The soil moisture freezing effects influence the soil and surface temperature greatly. Due to such effects the temperature oscillations smooth and their amplitude $1-2^o$C decreases. In mathematics the problem of heat transfer with the mobile boundary is known as Stephan problem. There are many methods to solve it, the analytical and numerical ones. There are numerical methods that are often used in land surface blocks of atmospheric models to consider the freezing-thawing effects. The so called "effective heat capacity" method is often implemented (e. g. Viterbo et al., 1999). The same results as "effective heat capacity" method can be obtained with "pseudo-delta-function" method (Tikhonov, Samarski, 1972). From one hand, this method is fast and we need not to set the new variables. From the other hand, the disadvantage of the method is the arbitrary choice of the approximating function and the approximating interval. The purpose of the research is to choose the optimum approximating interval. For this the more complicated "test" method - the Palagine method with converting of coordinate system and linearization in time - was instrumented.

2 Mathematical Description of Problem

When soil temperature falls below 0^oC, soil water freezes, and when temperature rises, soil ice thaws. So, it is the freezing-thawing mobile boundary (front) with the additional heat source, positive or negative. We don't know a priori the speed (and sometimes the direction) the front moves. So we write the heat transfer equation for frozen and unfrozen zones:

$$\rho c_1 \frac{\partial T}{\partial t} = \frac{\partial}{\partial z}\lambda_1 \frac{\partial T}{\partial z}, \qquad \rho c_2 \frac{\partial T}{\partial t} = \frac{\partial}{\partial z}\lambda_2 \frac{\partial T}{\partial z}. \tag{1}$$

Here $T(z,t)$ is the soil temperature; ρ , c , λ are soil density, specific heat capacity and heat conductivity respectively; the indexes 1 and 2 mark non-frozen and frozen zones. Upper boundary condition is set on the upper boundary of soil $z=0$, lower boundary condition - on the temperature oscillations damping level $z=H$. So the boundary conditions and initial condition are:

$$S\Big(T\Big|_{z=0}\Big) - \lambda\frac{\partial T}{\partial z} = 0, \qquad T\Big|_{z=H} = T_H, \qquad T\Big|_{t=0} = T^0(z), \tag{2}$$

where $S\Big(T\Big|_{z=0}\Big)$ is the sum of all the heat fluxes from the atmosphere, to be calculated from the atmospheric model and depends upon the surface soil temperature itself, so the upper boundary condition is non-linear. On the freezing-thawing front the boundary conditions are:

$$T\Big|_{z=h+0} = T\Big|_{z=h-0} = T^*, \tag{3}$$

$$\lambda_1 \frac{\partial T}{\partial z}\Big|_{z=h-0} - \lambda_2 \frac{\partial T}{\partial z}\Big|_{z=h+0} = \widetilde{L}\rho \Big[W\Big|_{z=h} = W_0\Big] \frac{dh}{dt}. \tag{4}$$

Here $T^* = 273,16K$; $\frac{dh}{dt}$ is the front speed; $\widetilde{L}$ is the ice thawing heat capacity; W is the soil volumetric wetness; W_0 is the amount of moisture unfrozen at negative temperature. The term $\Big[W\Big|_{z=h} = W_0\Big]$ is known from the soil moisture transport equation, which is to be solved together with the heat transport equation and is not displayed here to be brief.

3 Pseudo-delta-function or Effective Heat Capacity Method

(Tikhonov, Samarski, 1972, Viterbo et al., 1999).

We introduce Dirac delta-function $\delta\big(T - T^*\big)$, so the equations can be rewritten:

$$\Big(c\rho + \widetilde{L}\Big[W\Big|_{z=\xi} - W_0\Big]\delta\Big(T - T^*\Big)\Big)\frac{\partial T}{\partial t} = \frac{\partial}{\partial z}\lambda\frac{\partial T}{\partial z} \tag{5}$$

$$c = \begin{cases} c_1, & T < T^* \\ c_2, & T > T^* \end{cases}, \lambda = \begin{cases} \lambda_1, & T < T^* \\ \lambda_2, & T > T^* \end{cases}$$

and then we approximate the delta-function as pseudo-delta-function, we distribute it along the temperature interval.

$$\rho\widetilde{c}\frac{\partial T}{\partial t} = \frac{\partial}{\partial z}\widetilde{\lambda}\frac{\partial T}{\partial z}, \qquad \widetilde{c} = c + \frac{\widetilde{L}}{\rho}\Big[W\Big|_{z=\xi} - W_0\Big]\delta\Big(T - T^*, \triangle\Big) \tag{6}$$

$$\widetilde{\lambda} = \begin{cases} \lambda_1, & \text{when } T < T^* - \triangle \\ \lambda_2, & \text{when} T > T^* + \triangle \\ \frac{\lambda_1+\lambda_2}{2}, & \text{when } T \in \Big[T^* - \triangle; T^* + \triangle\Big] \end{cases},$$

$$\delta\Big(T - T^*, \triangle\Big) = \begin{cases} f(x), & \text{when } \Big|T - T^*\Big| \le \triangle \\ 0, & \text{when } \Big|T - T^*\Big| > \triangle \end{cases}.$$

Here $\triangle$ is the approximating interval, $f(x)$ is the approximating function. In Viterbo scheme the approximating $\triangle$ interval of 3K (de-centered) and trigonometric function were used. In our study the "step" approximating function $f(x) = \frac{1}{2\triangle}$ and different approximating intervals were used. We solve the heat transport equation numerically; the implicit scheme with the direct differences in time and centered differences in space, sweep method were implemented. We used 6 levels in soil.

The choice of temperature interval $\triangle$ problem was discussed in the mathematical literature (Samarski, Moiseenko, 1965). The conclusion about optimum of $\triangle = 0,15K$ was made. But the problem which was solved by the authors was abstracted from the physical sense, no concrete physical parameters and physical processes were considered. The verification results of Viterbo scheme are not very good (Rodrigues et al., 2003). So the additional research to (i) examine, if the value of parameter depends on concrete physical processes and (ii) to find it optimum value if possible was undertaken. We specified the $\triangle$ parameter comparing the temperature profiles, obtained by the pseudo-delta-function method with different $\triangle$ and the Palagine method (Palagine, 1981).

4 Palagine method

Palagine method contains (i) the conversion of variables which makes the front to be non-mobile and (ii) linearization which makes it possible to leave the heat transport equation in the same mathematical form. To be breaf only the formulas used in the study are displayed here. The case with only one frozen and one non-frozen layer was considered. New independent variables are ξ and τ , m is the number of the layer (frozen and non-frozen), h_m is the depth of the boundary. Linearization is on the time interval from t^{s+1} to t^s:

$$\xi = \frac{z - h_m(t)}{\triangle h_m(t)} + m, \qquad m-1 \leq \xi \leq m, \qquad (m = 1, 2) \tag{7}$$

$$\tau = \frac{t^s - t^{s-1}}{\triangle t} \frac{\triangle h_m^s}{\triangle h(t)}. \tag{8}$$

The new dependent variable is introduced as well, in the beginning of time interval and in the end of time interval it is marked as:

$$u(\xi, 0) = u^s(\xi), \qquad u(\xi, 1) = U^s(\xi). \tag{9}$$

This variable is connected with temperature as:

$$u_m^s(\xi_n) = \sqrt{\frac{\triangle h_m^{s-1}}{\triangle h_m^s}} exp\left\{\frac{d_1(\xi_n - m)^2 + 2d_2(\xi_n - m)}{4b_m \triangle h_m^s}\right\} T_m^s(\xi_n, 0), \tag{10}$$

$$U_m^s(\xi_n) = \sqrt{\frac{\triangle h_m^{s-1}}{\triangle h_m^s - d_1}} exp\left\{\frac{d_1(\xi_n - m)^2 + 2d_2(\xi_n - m) + \frac{d_2^2}{\triangle h_m^s}}{4b_m(\triangle h_m^s - d_1)}\right\} T_m^s(\xi_n, 1), \tag{11}$$

$$d_1 = \triangle h_m^s - \triangle h_m^{s-1}, \qquad d_2 = h_m^s - h_m^{s-1}, \qquad \varphi(\tau) = \triangle h_m^s - d_1 \tau. \tag{12}$$

So the heat transport equation can be rewritten (b_m - the thermal conductivity coefficient):

$$\frac{\partial u}{\partial \tau} = b(t) \frac{\partial^2 u}{\partial^2 \xi^2}, \qquad b_m = \frac{a_m \triangle t}{\triangle h_m^s \triangle h_m^{s-1}}. \tag{13}$$

The heat transport equation is solved numerically; the implicit scheme with the direct differences in time and centered differences in space, sweep method is used. We used 10 levels in non-frozen layer and 10 levels in frozen layer. The depth of the front is forecasted according to the formula:

$$h_1^s = h_1^{s-1} + \frac{\triangle t}{\widetilde{L}\gamma\Big(W_1^0(z_{11}) - W_0\Big)} \left[\lambda_1 \frac{T_1^s(z_{11}) - T_1^s(z_{10})}{z_{11} - z_{10}} - \lambda_2 \frac{T_2^s(z_2) - T_2^s(z_1)}{z_2 - z_1}\right]. \tag{14}$$

To calculate soil temperature from the newly introduced variable the following relationship is used:

$$T_m^s(\xi_n, 1) = \sqrt{\frac{\triangle h_m^{s-1}}{\triangle h_m^s - d_1}} exp\left\{-\frac{\Big(d_1(\xi_n - m)^2 + 2d_2(\xi_n - m) + \frac{d_2^2}{\triangle h_m^s}\Big)}{4b_m(\triangle h_m^s - d_1)}\right\} U_m^s(\xi_n). \tag{15}$$

5 Numerical experiments

The numerical experiments were carried out with the educational atmospheric model of RSHU. The 12 h forecasted soil temperature profiles were considered (time step is 10 min). The $\triangle$ parameter varied in the interval of $0,01-5K$. The least differences between temperature profiles was at $\triangle = 0,1K$, the maximal biases near the surface are $\approx 0,22K$ (see fig. 1). Fig. 2 displays the temperature profiles with $\triangle = 0,15K$ which was recommended in (Samarski, Moiseenko, 1965). To our processes this value appeared to be unacceptable. Besides, we tried to examine, if the "successfull" $\triangle$ value was dependent on the different forecast intervals. We compared the temperature profiles on different forecast intervals: T=10 min (one time step), T=3 h, T=12 h, T=24 h. On the first time step the "successful" value was $\triangle = 1,3K$, but then the following situation appeared. The bias between two temperature profiles at this value of $\triangle$ decreases up to 30^{th} time step, but then it increases. At the case with $\triangle = 0,1K$ the bias decreases fluently. This result may probably appear because of new non-frozen and frozen layers, so the medium became multilayered, and we did not considered it in our calculation. From the numerical experiments carried out by now we can made the conclusion that (i) the optimum value of interval depends upon the specific physical processes and (ii) the best value of for the problem considered is $\triangle = 0,1K$, but this result is preliminary. Experiments with different values of $\triangle$ interval could be undertaken within the frames of HIRLAM. "Reduced" Palagine method could be applied in the soil block of HIRLAM, but new variables appear in that case.

References

1. Rodriguez E., Navascues B., Ayuso J., Jarvenoja S., 2003. Analysis of Surface Variables and Parameterization of Surface Processes in HIRLAM. Part I. HIRLAM Technical Report, No. 58, Norrkoping, Sweden.

2. Viterbo P., Beljaars A., Mahfouf J. F., Teixeira J., 1999. The representation of soil moisture freezing and its impact on the stable boundary layer. Q. J. R. Meteorol. Soc., 125, pp. 2401-2426.

3. Palagin E. G. Mathemathical Modeling of Meteorologycal Conditions for agricultures in winter. Leningrad, Hydrometeoizdat, 1981, 190 p.

4. Tikhonov A.N., Samarski A.A., Equations of Mathematical Physics. Moskow, 'Nauka', 1972, 734 p. 1

5. Samarski A.A., Moiseenko B.D., Express Scheme for Multidimentional Stephan Task.

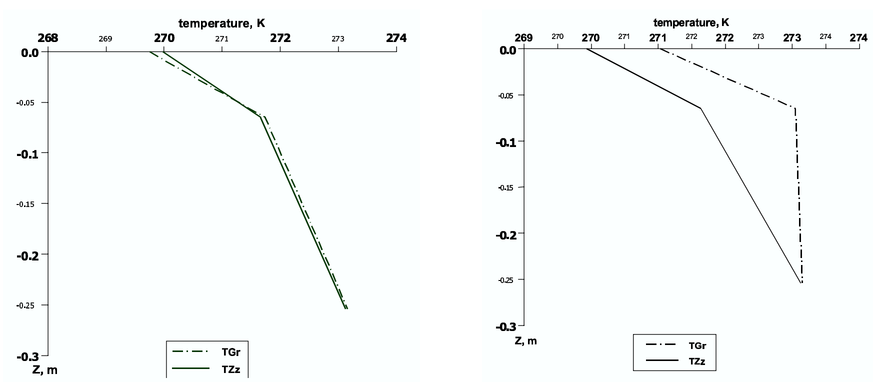

Figure 1: *Temperature profiles, 12-hour forecast, after pseudo-delta-function (TGr) an Palagine (TZz) methods. 1 -* $\triangle = 0,1K$*, 2 -* $\triangle = 0,15K$

Orography related problems in HIRLAM

Laura Rontu
Finnish Meteorological Institute

1 Introduction

In a present-day synoptic-scale NWP model with a typical horizontal resolution of 10-20 km many orography-related processes are resolved explicitly. The resolved wave processes include a significant part of vertically propagating inertio-gravity waves and hydrostatic gravity waves. Turbulent drag due to surface roughness and to unresolved small-scale orography, blocked flow drag due to mesoscale orography and drag due to breaking buoyancy waves still need parametrization at least partially. The parametrization schemes have been shown to interact with each other and with the resolved dynamics (Rontu et al., 2002; Rontu and Bazile, 2002). To avoid unphysical compensation between the different parametrization schemes scaling considerations require proper attention.

On the other hand, the present-day high-resolution elevation data bases provide better description of the orography. The scaling starts when defining the orography-dependent variables needed by the parametrization schemes and resolved-scale dynamics. In HIRLAM, variables derived from the terrain elevation of a digital map, are used for the definition of the mean surface height (geopotential) at every grid point. Parametrization of mesoscale orography effects and small scale orographic stress require information of subgrid-scale variations of the surface elevation.

In this study, some orography-related variables derived from a high-resolution data base are presented and the related problems discussed. More information about the methods used is available in (Rontu, 2003).

2 Parametrized drag due to orography

Table 1 lists the parametrization schemes related to the orography of a NWP model, e.g. in the near-future HIRLAM. (In the present HIRLAM only turbulent drag is taken into account as a surface forcing term by using the vegetation and orographic roughness (Undén et al., 2002).)

Table 2 lists parameters used by the schemes and their related horizontal scales. In this study, these variables were derived from a high-resolution elevation data base (Hydro1k, 2003). The Hydro1k data, prepared specially for the hydrological use, cover the whole globe excluding Greenland and Antarktis. The basic resolution of the data represented in an equal area azimuthal Lambert projection is 1 km x 1 km. The method of derivation is described in more detail by Rontu (2003).

Table 1: Parametrized drag due to orography

drag	related to	momentum sink
$\vec{\tau}_{ts}$	turbulent drag due to surface roughness	surface (2D)
$\vec{\tau}_o$	drag due to unresolved small-scale orography	internal (3D)
$\vec{\tau}_m$	blocked flow drag due to mesoscale orography	internal (3D)
$\vec{\tau}_w$	drag due to breaking buoyancy waves	internal (3D)

3 Examples of derived fields

Figs. 1 and 2 show transsections over Northern Iceland terrain with a highly variable surface elevation. The horizontal resolution of the derived fields is 0.025 deg in the rotated grid of HIRLAM, corresponding roughly the resolution of 2.8 km. In both figures, transsections are derived both from unfiltered and filtered fields. For the filtering a two-dimensional Fourier decomposition programme (Carl Fortelius, personal communication) was used with a cut-off frequency corresponding roughly three gridlengths.

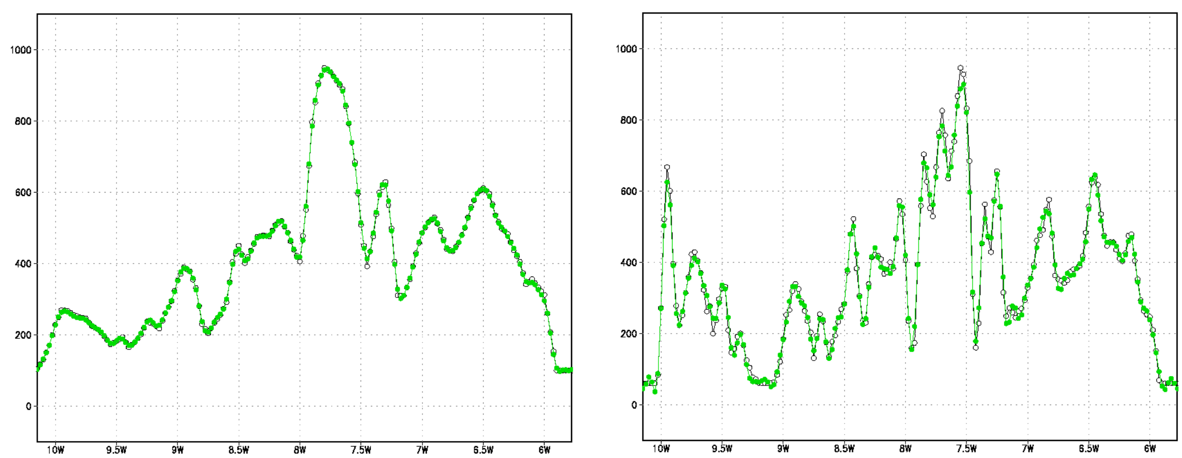

Figure 1: *Mean elevation (m) along rotated latitude 6.6N over Iceland: HIRLAM reference (left) and Hydro1K-based (right). Unfiltered values are shown by the (black) line with open circles, filtered values by the (green) line with filled cirles.*

Fig. 1 shows profiles of mean height from the reference HIRLAM 6.2.0 and from the newly calculated Hydro1k-based data. The maximum values of both profiles are close, but significantly more details can be seen in the Hydro1k-based profile. The effect of the Fourier smoothing is larger but still not very pronounced in the latter case. Note that the HIRLAM 6.2.0 reference elevation data is by definition filtered with a Raymond filter (Undén et al., 2002).

In Fig. 2 the profiles of mesoscale and small scale standard deviation, calculated from the Hydro1k data, are shown. Locally, both meso-scale and small-scale variability may be quite large compared to the resolved orography height. A significant effect of Fourier smoothing is

Table 2: Variables related to orography

variable	definition	scale of orography
	For resolved dynamics	
$H_{2\Delta x}$	mean height	$> 2\Delta$x
	For mesoscale orography parametrization	
σ_m	standard deviation of mesoscale orography	3 km - 2Δx
α	anisotropy of the mesoscale orography	3 km - 2Δx
θ	angle between mesoscale ridges and model's x-axis	3 km - 2Δx
	For small-scale orographic stress	
($z_{0,oro}$	orographic roughness	$<$ 3 km)
s_t	averaged maximum slope s_{max}	$<$ 3 km
σ_t	smallest scale standard deviation	$<$ 3 km
	For turbulence over flat rough surface	
z_0	roughness	$<<$ 1 km

seen in both profiles.

4 Items for further study

Until now, the basic orography-related parameters have been only derived but not applied to the model. Among the questions waiting answer are:

How does the model react on

- new surface elevation?
- changes in surface roughness?
- new parametrization of small-scale orographic stress?
- mesoscale orography parametrization?
- their interactions?

How should the derivation of parameters be improved?

- definitions

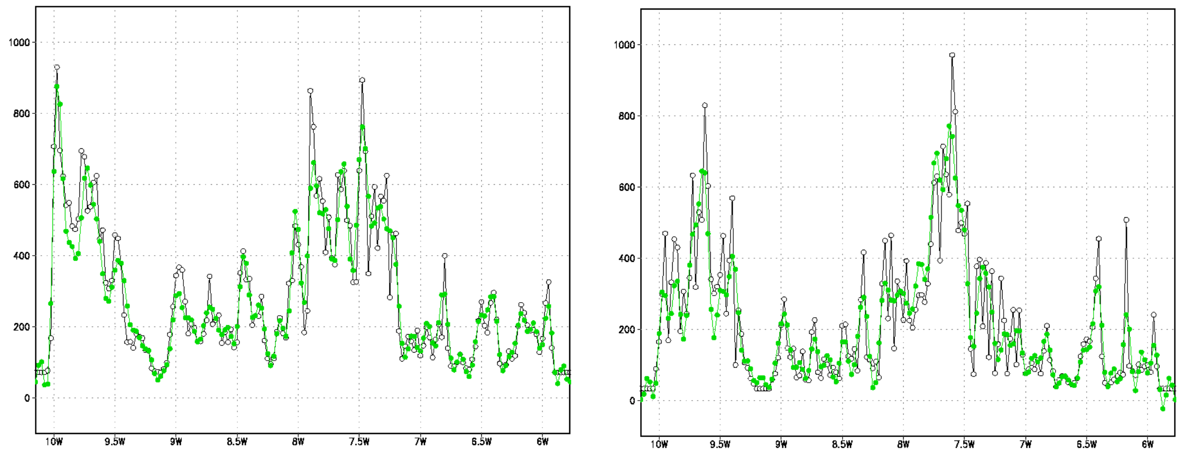

Figure 2: *As in. Fig. 1 but for standard deviations of mesoscale orography* σ_m *(left) and small-scale orography* σ_t *(right).*

- scales and filtering
- input data

How should the parametrizations be developed?

These questions will be sought answer for in a subsequent study to be reported later.

Acknowledgements

Thanks to Carl Fortelius, FMI, for the possibility to use the graphical two-dimensional Fourier decomposer programme.

References

Hydro1k Team, 2003. Web page of the Hydro1K elevation derivative database. Available at http://edcdaac.usgs.gov/gtopo30/hydro

Rontu L., 2003. Derivation of orography-related climate variables for a fine resolution HIRLAM. Hirlam Newsletter, 44, 83-96. Available at http://hirlam.knmi.nl

Rontu L., K. Sattler and R. Sigg, 2002. Parametrization of subgrid-scale orography effects in HIRLAM. HIRLAM Technical report N:o 56, 59 pp. Available at http://hirlam.knmi.nl

Rontu L. and E. Bazile, 2002. Problems of MSO parametrization: a case study with ARPEGE-HIRLAM comparison. In: Proceedings of HIRLAM Workshop on Mesoscale Modelling Dublin, 14 to 16 October 2002, 15-20. Available at http://hirlam.knmi.nl

Undén P. and coauthors, 2002. HIRLAM-5 scientific documentation. Available at http://hirlam.knmi.nl

A study of the radiation parameterization for sloping surfaces

Anastasia V. Senkova, *Russian State Hydrodynamical University*
Laura Rontu, *Finnish Meteorological Institute*

1 Introduction

Solar radiation is the energy source for atmospheric motions and physical processes. Accurate handing of radiation effects is important for weather prediction or climate modeling. The main purpose of the radiation scheme of an atmospheric model is to provide the air and surface temperature change resulting from heating due to radiation fluxes.

Continually growing computation power allows the use of models with increased horizontal and vertical resolution. Meso-scale and non-hydrostatic models are developed. The description of surface relief is more detailed in such models. It gives a possibility to consider the sloping surface particularities for calculating the radiation fluxes near the Earth surface. The surface radiation flux dependence on surface slopes is discarded in models with low resolution, but it can be important for fine scale models. The different sloping surfaces receive a very different amount of solar radiation during a solar day. It is necessary to take into account this effect of non-homogeneous surface radiation heating in meso-scale models (Savijärvi, 2003)..

In this study some basic concepts of the slope effects are presented and discussed. Methods of derivation of the surface elevation information for a radiation scheme are developed and compared.

2 Calculation of solar radiation flux on the sloping surface

The solar radiation flux on the upper boundary of the atmosphere is calculated in models by the formula:

$$S_{ub} = S_0 \cdot cos(\xi), \tag{1}$$

where S_0 is the solar constant,$S_0 = 1365 J/(m^2 s)$; ξ is the zenith angle. The zenith angle of The Sun is determined as:

$$cos(\xi) = cos(\varphi)cos(\delta)cos(t_0 + \lambda) + sin(\varphi)sin(\delta), \tag{2}$$

where φ and λ are the geographical latitude and longitude; δ is the declination of the Sun, which can be found from astronomical formulas; t_0 is the local hour angle of the Sun at the Greenwich.

Then, the solar radiation flux passes through the atmosphere where it can be absorbed, scattered and reflected by water vapor, atmospheric gases, aerosols and clouds. The Earth's surface receives some part of this flux, which arrives on the flat surface with an angle ξ.

The flux arriving to the sloping surface is described by formula (Kondratiev et al., 1978):

$$S_{surf} = S_{\perp} \cdot cos(i), \tag{3}$$

where $S_{\perp}$ is a flux on surface which is perpendicular to sun rays; i is the angle between solar rays direction and normal of given sloping surface. The angle i can be determined by using two sloping surface parameters: slope angle and slope direction (in the following called slope aspect)

$$cos(i) = cos(a_s)cos(\xi) + sin(a_s)sin(\xi)cos(\psi - \psi_s), \tag{4}$$

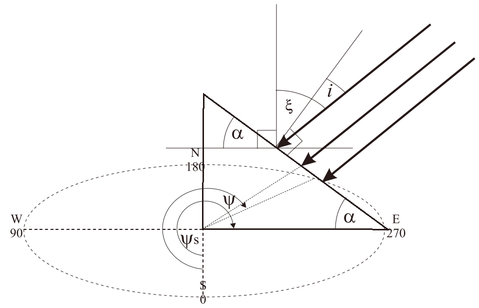

Figure 1: *The geometry of sloping surface and the direction of solar ray.*

where a_s is the slope angle of surface; ξ is the zenith angle; ψ is the azimuth of the Sun; ψ_s is the slope aspect (Fig. 1)

To define the azimuth of the Sun we use the astronomical expressions:

$$cos(\psi) = \frac{cos(\xi)sin(\varphi) - sin(\delta)}{sin(\xi)cos(\varphi)}, sin(\psi) = \frac{cos(\delta)sin(t_0 + \lambda)}{sin(\xi)} \tag{5}$$

3 Experiments and tests

Changes described above have been included in the HIRLAM radiation scheme to account for the sloping surface effects. One-dimensional tests have been made to calculate the surface solar flux with different surface slope angles and aspects. Examples of these calculations are shown in Figs. 2 and 3.

One can see that the amount of solar radiation received by Earth depends significantly on the angle and aspect of sloping surface. The varying of slope aspect and angle results in that the maximum of surface solar radiation flux occurs at different time and has different values.

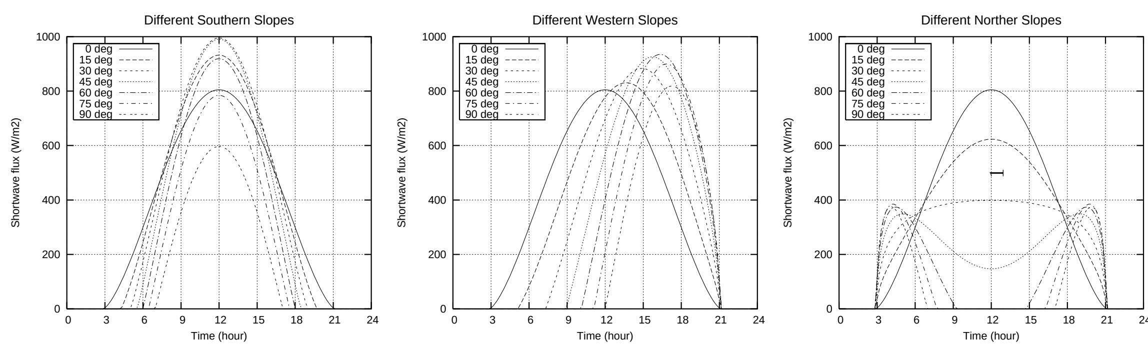

Figure 2: *The solar radiation fluxes during sunny clear day depending on surfaces slope angle and aspect. Summer, 21 June,* 60^0 *northern latitude at Greenwich*

To make a full three-dimensional experiment accounting sloping surface effects to radiation we need real information about surface slope and aspect in each grid cell of HIRLAM. We can use data about slope and aspect from the Hydro1k data base (web site http://edcdaac.usgs.gov/gtopo30/hydro/). This information is given with 1x1 km resolution. As an example, maps of slope angle and aspect of Iceland, based on the Hydro1k data, are shown in fig. 4. Usually there are not very large sloping angles in nature. The maximum of sloping is 15-20^o.

If we want to use the direct information about slope angle and aspect with resolution 1 km, we should convert the elevation data to the resolution of a HIRLAM experiment. There are two methods:

• Find average values of angle and aspect for each HIRLAM grid cell;
• Use fractional values, i.e. define the fractions of grid cell surface with different slope directions.

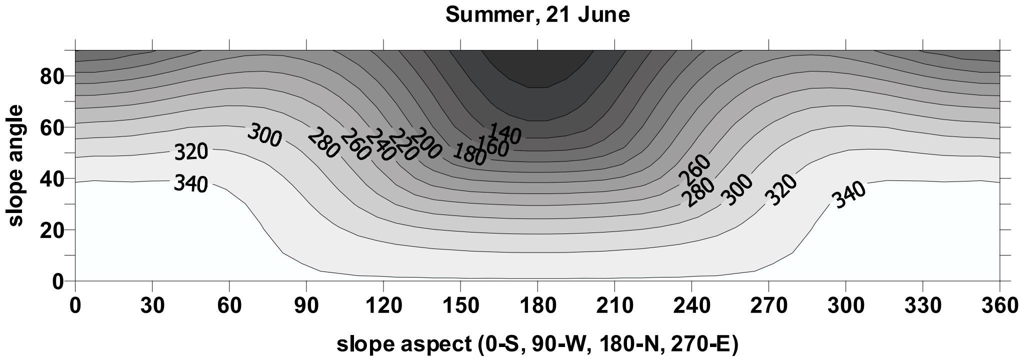

Figure 3: *Solar radiation fluxes on different slope angle and aspect of underling surface averaged over 24 hours. Summer, 21 June,* 60^0 *northern latitude at Greenwich*

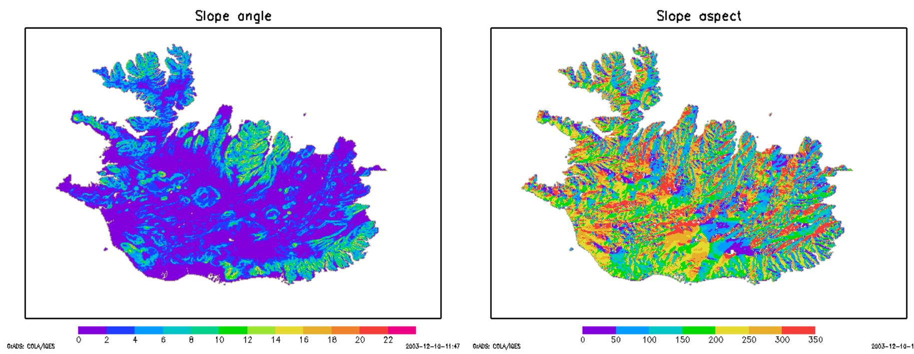

Figure 4: *The sloping surface angle (left) and aspect (right) of Iceland (both slope and direction in degrees).*

The methods were included into the radiation scheme and experiments comparing the two averaging methods were made.

We divided all Hydro1k points inside a HIRLAM cell to four types according their aspect: Northern, Eastern, Southern and Western. We calculated their fractions - the percentage of area having the Northern, Eastern, Southern and Western aspect related to the full cell area. Then we define the average slope angle for each surface type. Thus, for each mean direction (North, East, South and West) we have the slope angle and the fraction of the area with this direction within a HIRLAM grid cell. Next we define the solar radiation fluxes for each surface type and summarize fraction-weigted values thus we receiving the average flux for the grid cell.

Fig. 5 shows examples of calculations with different proportions of sloping surface in a grid cell. One can see that there is large difference between fluxes calculated by the two methods. Using averaged aspect and slope leads to large errors and shifts the maximum of radiation flux. This is natural, as the aspect accepts values between [0,360] - therefore e.g. the mean aspect for East and West angle is South, which is clearly unrealistic. Using directional describes the effects of relief variability more accurately.

4 Conclusions

The account of sloping surfaces for calculation of surface radiation flux was included in HIRLAM radiation scheme. Two methods to convert fine scale information into HIRLAM grid were applied and shown to lead different radiation fluxes. The fractional method (average of flux) is more accurate for areas with different sloping surfaces, but requires more calculations and variables.

We should not use the mean value of slope angle and aspect for grid cell with many sloping surfaces with different aspects because (i) the dependency of surface flux on surface aspect is non-linear, (ii)

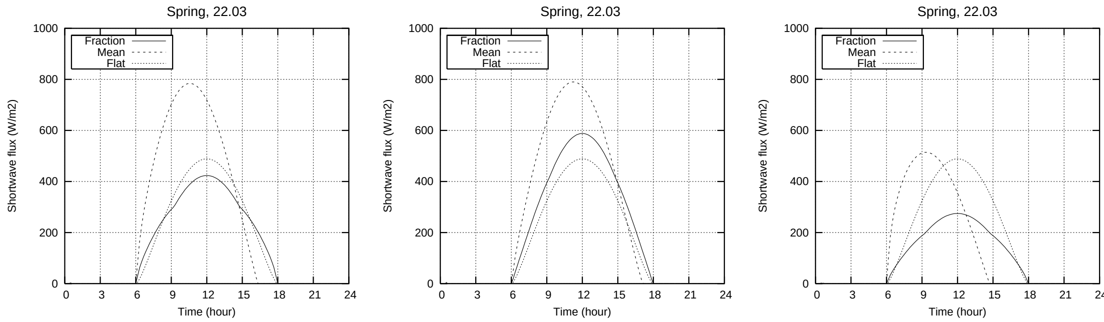

Figure 5: *The solar fluxes, calculated by different methods: a) all fractions (N,E,S,W) are equal to 0.25, mean slope=30^0, mean aspect=135^0. b) Southern fraction=0.5, other=0.125 (N,E,W and flat), mean slope=26.25^0, mean aspect=154^0. c) Northern fraction=0.5, other=0.125 (E,S,W and flat), mean slope=30^0, mean aspect=77^0.*

averaging the directions is meaningless and leads to unrealistic fluxes. Use of the mean slope angle and aspect derived from the mean surface elevation of HIRLAM could also be tried. With a high enough model resolution the methods should converge as each grid square will represent no more than one directional fraction.

In future we plan to compare 1D tests with radiation observations over mountainous terrain and make three-dimensional experiments, model comparison and verification. For an experiment we need a mountainous area, fine scale resolution and a sunny, clear sky period. Later, the effects of shadows from terrain features and clouds of neighbouring grid columns could be taken into account by introducing handling of diffuse radiation into the scheme.

Acknowledgements

Our thanks are due to Hannu Savijärvi for useful discussions and introduction to the methods of handling slope effects and diffuse radiation within the HIRLAM radiation scheme.

References

1. Hannu Savijärvi H., 2003: Radiation in high-resolution mesoscale models - what can be done? *HIRLAM Newsletter*, no. 43, 65-69.

2. Kondratiev K.Ja., Z.I. Pivovarova, M. P. Fedorova, 1978: The radiation regime of sloping surfaces. *L., Hydrometeoizdat*, 216 p.

3. Hydro1k data base
   Available at http://edcdaac.usgs.gov/gtopo30/hydro/.

A Two-Layer Lake Model for Use in Numerical Weather Prediction

Dmitrii Mironov[1], *Arkady Terzhevik*[2], *Frank Beyrich*[1], *Erdmann Heise*[1] *and Horst Lohse*[3]

[1] German Weather Service, Offenbach am Main, Germany[†]

[2] Northern Water Problems Institute, Russian Academy of Sciences, Petrozavodsk, Russia

[3] Institute for Coastal Research, GKSS Research Centre, Geesthacht, Germany

Lakes significantly affect the structure of the atmospheric surface layer and therefore the surface fluxes of heat, water vapour and momentum. In most numerical weather prediction (NWP) systems the effect of lakes is either entirely ignored or is parameterized very crudely. A physically sound model is required to predict the lake surface temperature and the effect of lakes on the structure and transport properties of the atmospheric surface layer. Apart from being physically sound, a lake model must meet stringent requirements of computational economy. The problem is twofold. For one thing, the interaction of the atmosphere with the underlying surface is strongly dependent on the surface temperature and its time-rate-of-change. It is common for NWP systems to assume that the water surface temperature can be kept constant over the forecast period. The assumption is to some extent justified for seas and deep lakes. It is doubtful for small-to-medium size relatively shallow lakes, where the short-term variations of the surface temperature (with a period of several hours to one day) reach several degrees. A large number of such lakes will become resolved scale features as the horizontal resolution is increased. Another important aspect of the problem is that lakes strongly modify the structure and the transport properties of the atmospheric surface layer. A major outstanding question is the parameterization of the roughness of the water surface with respect to wind and to scalar quantities, such as potential temperature and specific humidity.

A lake model intended for use in NWP systems (also in climate modelling and other numerical prediction systems for environmental applications) is developed (Mironov, 2003). The model is capable of predicting the surface temperature in lakes of various depth on time scales from a few hours to a year. It is based (i) on a two-layer parametric representation (assumed shape) of the temperature profile, where the structure of the stratified layer between the upper mixed layer and the basin bottom, the lake thermocline, is described using the concept of self-similarity of the evolving temperature profile (Kitaigorodskii and Miropolsky, 1970), and (ii) on the (integral) heat and kinetic energy budgets for the layers in question. The same concept is used to describe the interaction of the water column with bottom sediments and the evolution of the ice and snow cover. In this way, the problem of solving partial differential equations (in z, t) for the temperature and turbulence quantities is reduced to solving ordinary differential equations for the time-dependent parameters that specify the temperature profile. This approach, that is based on what could be called "verifiable empiricism" but still incorporates much of the essential physics, offers a very good compromise between physical realism and computational economy.

The proposed lake model incorporates a flexible parameterization of the temperature profile in the thermocline, an advanced formulation to compute the mixed-layer depth, including the equation of convective entrainment and a relaxation-type equation for the depth of a wind-mixed layer, both mixing regimes are treated with due regard for the volumetric character of the short-wave radiation heating, a module to describe the vertical temperature structure of the thermally active layer of bottom sediments and the interaction of the water column with bottom sediments, and an advanced snow-ice module. Empirical constants and parameters of the proposed model are estimated, using independent empirical and numerical data. They should not be re-evaluated when the model is applied to a particular lake (there are, of course, lake-specific external parameters, such as depth to the bottom and optical properties of water, but these are not part of the model physics). In this way, the model does not require re-tuning, a procedure that may improve an agreement with a limited amount of data but should generally be avoided as it greatly reduces the predictive capacity of a physical model (Randall and Wielicki, 1997).

In order to compute fluxes of momentum and of sensible and latent heat at the lake surface, a parameterization scheme is developed that accounts for specific features of the surface air layer over

[†]Corresponding author address: Deutscher Wetterdienst, AP2003, Frankfurter Str. 135, D-63067 Offenbach am Main, Germany. E-mail: Dmitrii.Mironov@dwd.de.

lakes. The scheme incorporates a fetch-dependent formulation for the aerodynamic roughness of the water surface, advanced formulations for the roughness lengths for potential temperature and specific humidity in terms of the roughness Reynolds number, and free-convection heat and mass transfer laws to compute fluxes of scalars in conditions of vanishing mean wind.

The new lake model and the new surface-layer parameterization scheme are tested against data through single-column numerical experiments. Figure 1 shows the water surface temperature θ_s as computed by the proposed lake model againsts data from measurements in Kossenblatter See, a shallow lake (mean depth is 2 m, maximum depth is 6 m, depth to the bottom at the point of measurements is 1.2 m) located in Land Brandenburg, Germany. The lake model is forced by the fluxes of momentum and heat at the air-water interface. The fluxes of momentum and of sensible and latent heat depend on the water surface temperature and are, therefore, part of the solution. They are computed with the proposed surface-layer scheme, using mean values of meteorological quantities measured in the vicinity of the air-water interface. The downward fluxes of short-wave radiation and of long-wave radiation are not part of the solution. These fluxes are taken from measurements (details of measurements are given in Beyrich (2000). In Fig. 2, fluxes of sensible Q_{se} and latent Q_{la} heat computed with the surface-layer scheme are compared with data from flux measurements in the atmospheric surface layer over the lake. As seen from Figs. 1 and 2, the model predictions show a good agreement with observations.

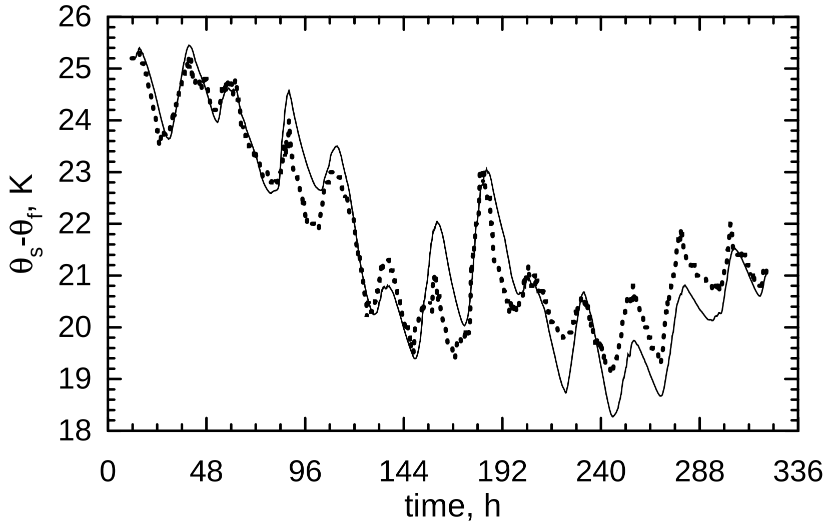

Figure 1: The water surface temperature ($\theta_f = 273.15$ K is the fresh-water freezing point) computed with the new lake model, solid curve, versus data from measurements in Kossenblatter See over the period from 8 to 21 June 1998, dotted curve.

One more example of the lake model performance is given in Fig. 3, showing a simulated perpetual-year temperature cycle in Lake Swente, a medium-depth lake (mean depth is 7.8 m, maximum depth is 35 m) located in Latvia. The model is driven by climatological-mean values of the surface-layer meteorological quantities. The year-long integration is repeated until a perpetual-year periodic solution is obtained. This solution is representative of the like climatologically-mean state. As different from Kossenblatter See, the downward fluxes of short-wave radiation and of long-wave radiation for Lake Swente are not known from measurements. These fluxes are computed using empirical recipes, possibly introducing large uncertainties into the solution. The model results are compared with four-year mean values of the water temperature measurements taken at a number of levels from the lake surface down to the bottom at 17.5 m. In spite of considerable uncertainties of the input data, results from the simulation show a satisfactory agreement with empirical data.

Work is underway at the German Weather Service to further test the new lake model against data from measurements in different lakes and to integrate it into the full three-dimensional NWP system environment.

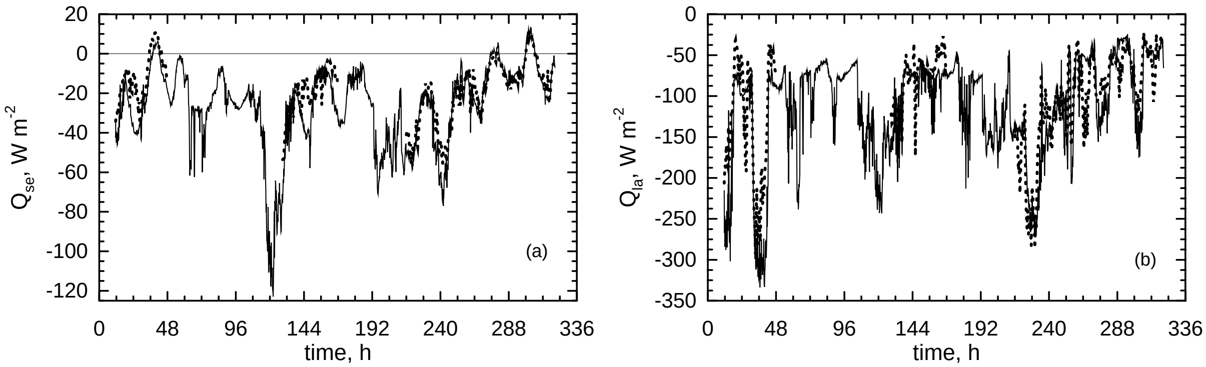

Figure 2: Computed with the surface-layer scheme, solid curves, and measured, dotted curves, fluxes of sensible heat (a) and of latent heat (b) over Kossenblatter See during the period from 8 to 21 June 1998.

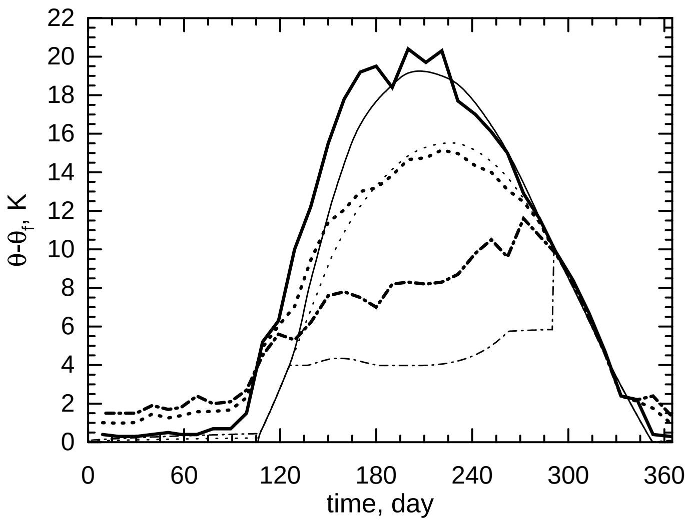

Figure 3: Perpetual-year temperature cycle in Lake Swente simulated with the lake model. Solid curves show the water surface temperature, dotted curves show the mean temperature of the water column, and dot-dashed curves show the bottom temperature. Thin curves are computed with the lake model, and heavy curves show data from measurements averaged over the period from 1961 to 1964.

Acknowledgements. The work was partially supported by the EU Commission through the project INTAS-01-2132.

References

Beyrich, F., (Ed.), 2000: *LITFASS-98 Experiment. 25.5.1998 – 30.6.1998. Experiment Report.* Arbeitsergebnisse Nr. 62, Deutscher Wetterdienst, Geschäftsbereich Forschung und Entwicklung, Offenbach am Main, Germany, 78 pp.

Kitaigorodskii, S. A., and Yu. Z. Miropolsky, 1970: On the theory of the open ocean active layer. *Izv. Akad. Nauk SSSR. Fizika Atmosfery i Okeana*, **6**, 178–188.

Mironov, D. V., 2003: Parameterization of lakes in numerical weather prediction. Part 1: Description of a lake model. In preparation.

Randall, D. A., and B. A. Wielicki, 1997: Measurements, models, and hypotheses in the atmospheric sciences. *Bull. Amer. Met. Soc.*, **78**, 399–406.

Effects of boundary-layer thermal stratification and underlying surface roughness to the deposition of coarse solid particles

Marko Kaasik*

1 Introduction

The underlying surface effects to the dry deposition of airborne ingredients are well known at least in qualitative sense: rougher surface initiates stronger wind-induced turbulence and therefore, as a rule, larger deposition velocities. This paper deals with the application of Monin-Obukhov surface layer theory to the airborne deposition fluxes. Recent updates for long-lasting inversion are taken into account. Theoretical results are compared with field studies in the north-eastern Estonia, the area which is found to be an appropriate test site due to relatively flat natural landscape and highly dominating well-identified point sources of particles.

Although these investigations have no direct connection with HIRLAM so far, there is expected two links in the close future: (1) application of HIRLAM output meteorological fields and (2) ideas for updating the parameterisation schemes of surface fluxes for meteorological models, including HIRLAM.

2 Methods

The study is based on two natural assumptions:

1. dry deposition depends on underlying surface roughness and surface-layer condition;
2. wet deposition is a funcion of precipitation amount and therefore does not substantially depend on the landscape.

Theoretical approach is based on the classical Monin-Obkhov formulation with recent updates for long-lasting inversion (Zilitinkevich et al., 1998, Zilitinkevich and Galanca, 2000). The deposition velocity is calculated as the reciprocal value of total resistance. The aerodynamic resistance is calculated in Businger-Dyer formulation, quasi-laminar sublayer resistance by means of Stokes and Schmidt numbers and finally, the gravitational settling velocity of particles from the Stokes law. Field data are based on sampling of atmospheric precipitation. Two measurement series series are applied. For wintertime series (December 2 - 14, 2002, 17 samples) snow was sampled from a well-identified snow layer on the natural surface. Summer series (August 2 - 12, 2002, 6 samples) was collected using slightly modified EMEP (EMEP, 1996) precipitation sampling method. In order to collect the dryly deposited matter into the water reservoir,

*Institute of Environmental Physics, University of Tartu, Tartu, Estonia, 50090;mkaasik@ut.ee

the plastic funnel of a sampler was washed with super-pure water at the end of sampling period. About a half of samples were collected from open areas (open bog or ice-covered lakes in wintertime) and half from forest.

The research area, north-eastern Estonia, is characterised as follows:

1. A few large regional pollution sources - oil-shale-fired thermal power plants, specific fly ash composition;

2. surroundings sparsely inhabited, relatively flat, open bog and forest patches. The diameter of fly ash particles was assumed 10 micrometers, resulting in settling velocity about 0.01 m/s (assuming density of particulate matter 2800 kg/m^3).

Typically the oil-shale fly ash contains about 22% Ca, nearly same fraction of sulphate, other alkaline oxides, heavy metals and specific spheroidal (chemically inert) ash particles.

The winter data set includes five samples from Background area (South-eastern Estonia, 140 km away, similar landscape) and summertime data set two such samples.

3 Results

For winter campaign the weather analysis data from from http://www.arl.noaa.gov/ready.html suggest a fine long-lasting thermal inversion: surface heat flux was negative, potential temperature gradient positive and surface air temperature well below zero during most of time.

When applying the Monin-Obukhov scaling (almost regardless of Zilitinkevich corrections) to these data, certain difficulties were met: often (at high reference wind speed and low surface roughness) there is no positive friction velocity. The conditions (wind speed, roughness) of friction velocity vanishing depend highly of reference height for wind speed. Probable explanation is that analysed (and possibly, forecasted as well) wind fields are inconsistent with surface-layer scaling. To avoid this inconsistency, it was supposed that all deposition resistance components except the gravitational settling vanish for coarse particles at mentioned conditions. Due to such an effect the average calculated total deposition velocity for the winter campaign does not significantly depend on on the underlying surface roughness (i.e. on forest/open land pattern in fact), especially for favourable wind directions (blowing from the Narva power plants): from north, northeast and east (Figure 1). The measured deposition fluxes of calcium and solid particles in forest and open land do not differ significantly, in agreement with theoretical calculations. The AEROPOL model (a Gaussian dispersion model, developed in Tartu Observatory, Estonia) run for winter campaign suggests deposition fluxes rather close to the measured ones (Figure 2). Roughness lengths for that model run were assumed as follows: open land 0.01 m, woodland 0.70 m.

The summer campaign shows definitely prevailing convective conditions and 2-4 times higher measured deposition fluxes of spheroidal particles in forest than over the open land. This is sound with theoretical calculations for convective conditions (due to wind-forced turbulence over canopies). The calcium flux study, however, does neither support nor deny this result. The deposition fluxes of Ca in summertime are uniformly high everywhere, even in background sites. It can be due to hot dry wether, soil erosion and several forest fires around. Spheroidal particles, in contrary, indicate the high-temperature (i.e. mainly industrial) combustion.

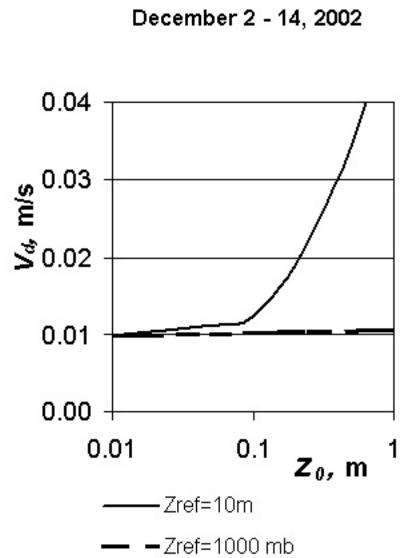

Figure 1: Average deposition velocities for winter campaign dependig on surface and reference height, surface-layer scaling by Zilitinkevich et al., 1998.

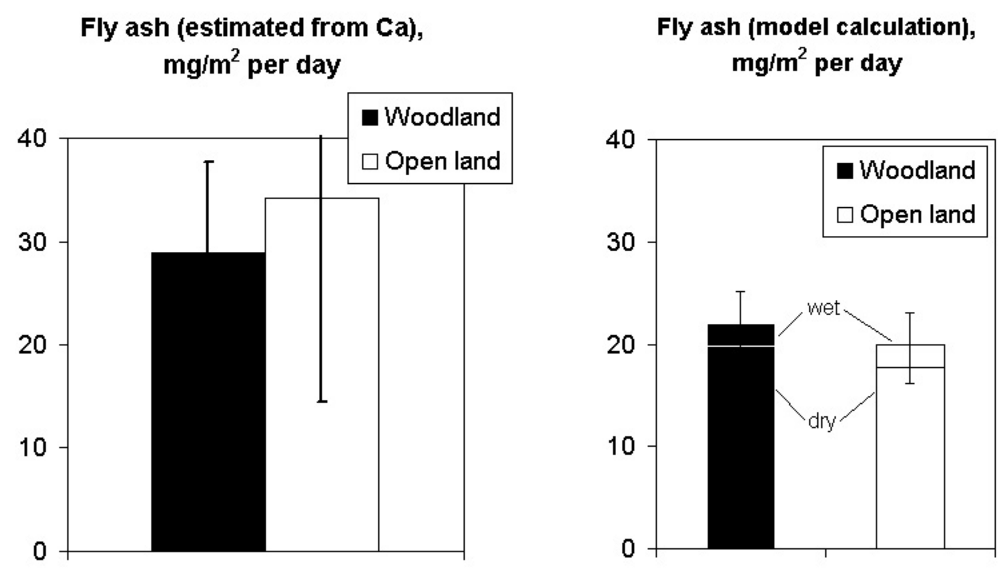

Figure 2: Modelled (AEROPOL model) and measured deposition fluxes during the winter campaign.

4 Conclusions

1. Deposition model is extremely sensitive to the meteorological input, surface-layer wind profile in particular.
2. Similar scaling is applied to all fluxes in the surface layer, therefore we need urgently more knowledge about the surface layer in order to perform adequate modelling.
3. AEROPOL model estimations for December 2002 campaign fit with field data within 1.5 times - not bad for first attempt!
4. More campaigns are needed, in warm (predominantly convective) season in particular.

Acknowledgements

Author would like to thank:

Estonian Science Foundation: Grant 5002, "The interaction of forest and atmospheric fly ash influx" - fieldwork and AEROPOL runs.

Baltic HIRLAM project - travel grant.

Mikhail Sofiev and Jaakko Kukkonen (FMI) - for help in Helsinki.

References

T. Alliksaar, P. Hörstedt, I. Renberg, Characteristic fly-ash particles from oil-shale combustion found in lake sediments, Water, Air, and Soil Pollution, 104, 149-160 (1998).

EMEP manual for sampling and chemical analysis. NILU, Kjeller, 97 (1996).

S. Zilitinkevich, P.-E. Johansson, D. V. Mironov, A. Baklanov, A similarity-theory model for wind profile and resistance law in stably stratified planetary boundary layers, J. of Wind Engineering and Industrial Aerodynamics, 74-77, 209-218 (1998).

S. Zilitinkevich, P. Galanca, An extended similarity theory for the stably stratified atmospheric surface layer, Q. J. R. Meteorol Soc., 126, 1913-1923 (2000).

Some lessons of SILAM model application to European Tracer Experiment

M. Sofiev and P. Siljamo
Finnish Meteorological Institute

1 Introduction

Current abstract presents an outline of verification of the Finnish Emergency dispersion model SILAM against the data of European Tracer Experiment ETEX; preliminary results of inverse model application to the experiment, and the model sensitivity studies, with a stress to features of the meteorological data influencing the model performance.

The European Tracer Experiment ETEX was conducted in October 1994 (Graziani et al., 1998), (ETEX, 1998). It consisted of a release of an inert non-depositing substance, which plume was followed by more than 160 monitoring stations in Europe, by aircraft measurements, and by 30 dispersion models. The experiment also included a model comparison with measured concentrations using some 20 statistical measures. Positions of the cloud after two days since the release are shown in the left panel of Fig.1.

A Finnish Emergency Modelling Framework SILAM v.3.0.1 (Sofiev et al., in prep.) used in the verification exercise includes Lagrangian particle dispersion model with a built-in random walk mechanism (developed in FMI), radio-active dose assessment unit (VTT Energy), meteorological pre-processor (FMI), and output post-processors and supplementary routines (FMI). It handles point and area emission sources, and has a simplified parameterization for nuclear explosion cloud. Currently, the framework has three main areas of applications: operational 48-hours forecast of areas of risk for the potentially dangerous installations near Finland; manual emergency and exercise simulations; and scientific researches of forward and inverse dispersion problems.

For the current verification, a set of statistical measures was taken to be similar to that of the ETEX experiment (Sofiev & Siljamo, in prep.). It includes time- and space-related characteristics with final aggregation into one general target quality function. Since none of the measures originally selected for ETEX is truly robust, a special attention was paid to the problem of statistical significance of the obtained results: every quantity was accompanied with its uncertainty estimate, usually expressed via standard deviation.

2 Verification scores of the operational SILAM configuration

The scores were computed for four different sub-sets of the ETEX data: (i),(ii) Arches 1 and 2 including four and seven stations covered with the plume by the end of the first and second days since the release, respectively, (iii) time-related analysis made for the whole set of ETEX stations with a completeness threshold of 5 valid observations within 60-hours period, (iv) space-related analysis made for the whole set of ETEX stations with the same completeness threshold. Qualitatively, an example of the patterns is shown in , where the left panel presents observations projected onto the map assuming 40km correlation radius, the right one is the computed field, while the central one is built from extracted data at the station locations with further projection of the values to the grid with the same 40km correlation radius. As a result, left and central panels are directly comparable, while the central and right panels are based on the same data.

Quantitative verification results are presented in Table 1. Compared to the scores of other models participated in ETEX, they look very good, positioning SILAM in the top part of the list. Probabilities

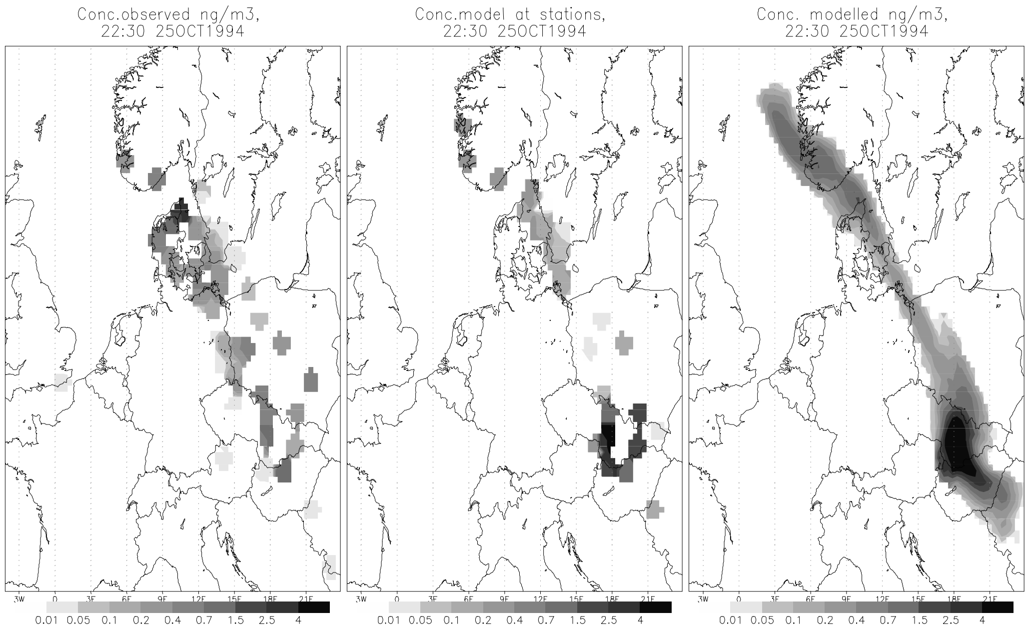

Figure 1: Position of the pollution cloud after 2 days since the release: observed (left panel), modelled (right panel), modelled data extracted at the station locations (central panel).

for correct and false alerts were 0.9 and 0.1 respectively. However, considerable over-estimation of the absolute concentrations raises certain questions on parameterization of the vertical and horizontal diffusion (despite such an over-estimation was shown by almost all other models as well).

3 Inverse studies of the ETEX case

An inverse study of the ETEX case considered a source apportionment problem in its classical formulation: to determine the source location and strength from available observations. Assumptions were: (i) the source was not moving during the release, (ii) horizontal source size is negligible, (iii) background concentration of the tracer is zero, (iv) detection limit of the monitoring devices is negligible in comparison with observed concentration levels.

For the problem solution, the technique of adjoint dispersion simulations was used to outline the

Table 1: Verification scores of the SILAM operational setup

Verification set	Corr. coeff.	FMT / FMS	Abs. dev., %	Rel. dev., %
ETEX Arch 1(t0+24hr)	0.75	0.15	138	-9
ETEX Arch 2 (t0+48hr)	0.77	0.36	85	-11
All stations, time-related	0.6	0.3	90	-10
All stations, space-related	0.51	0.92	160	9
Significance (std.dev range)	0.013	-	45	7

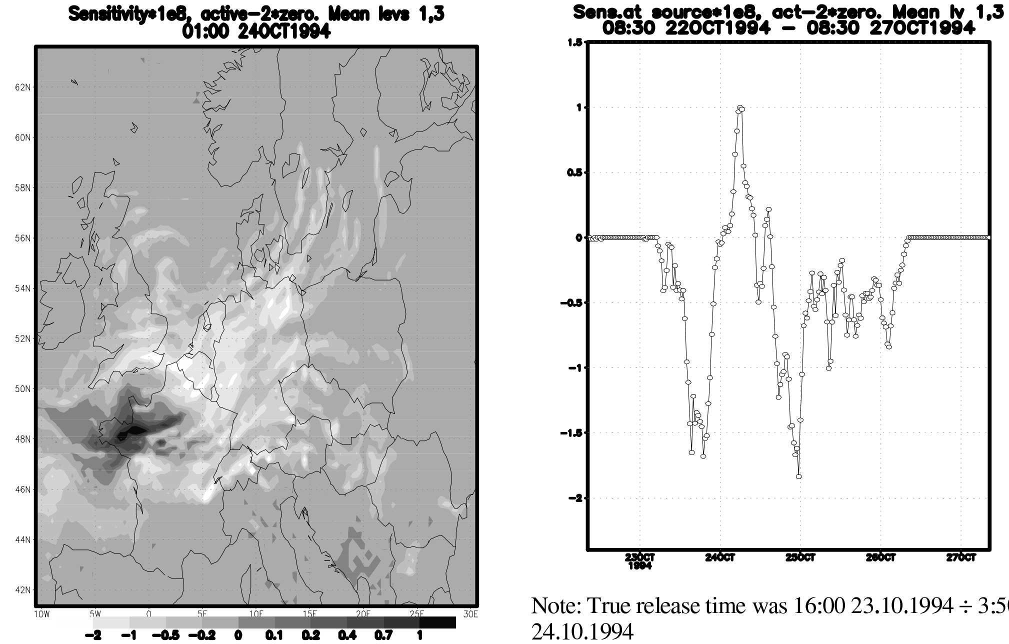

Figure 2: Position of sensitivity distribution by the mid-time of the true release (left panel), and its time variation at the true source location (right panel).

area where the source can be located. Under the above assumptions, one can distinguish between two sets of observations with zero and with positive reported concentrations. For the first set, the adjoint sensitivity function delineates the areas where the probability not to find the source is high, while the second set generates the sensitivity distribution highlighting the area with essentially positive probability to find the source. Their subtraction with scaling, being somewhat ad-hoc, leads to a sharpening of the image and more accurate source allocation. Formal procedure for the data processing is not yet ready, but preliminary results are encouraging (Fig.2). Final guess about the source location should follow the rules: (i) positive sensitivity means high probability to find the source at the location (dark grey area in Fig.2), (ii) negative sensitivity means high probability not to find the source there (white area); (iii) zeroes show the area where both probabilities are small (light grey area).

4 Sensitivity studies

In order to highlight the most important parameters of the input data and SILAM internal setup, a set of more than 100 sensitivity runs has been performed using 5 different data sets generated by HIRLAM 2, HIRLAM 5 and ECMWF T213 models, 5 methods for ABL height estimating, two model time steps and 2 types of the output processing (Sofiev & Siljamo, in prep.).

One of surprises of the study was a prevalence of the datasets from the old models HIRLAM 2 and EC T213 over those from the new model HIRLAM 5. None of the best 6 setups was based on the new dataset. Even twice better resolution appeared to have little, if any, advantages to old ECMWF and HIRLAM 2 fields. A possible explanation comes from an erroneous first-night development of the ABL height at the release point (Fig. 3).

High-resolution forecasts (1-hour) have significantly suffered from the HIRLAM spin-up. Therefore better dispersion results have been shown with the 3-hours or even 6-hours long forecasts.

One of the most important internal characteristics of the runs was an algorithm of ABL height estimation. It is shown that if this surrogate parameter is available directly from meteorological model,

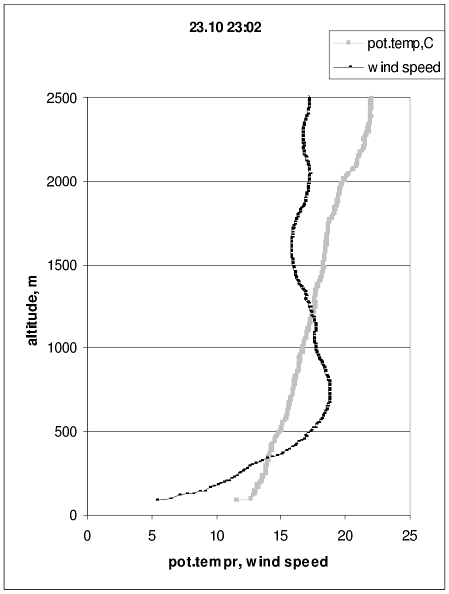

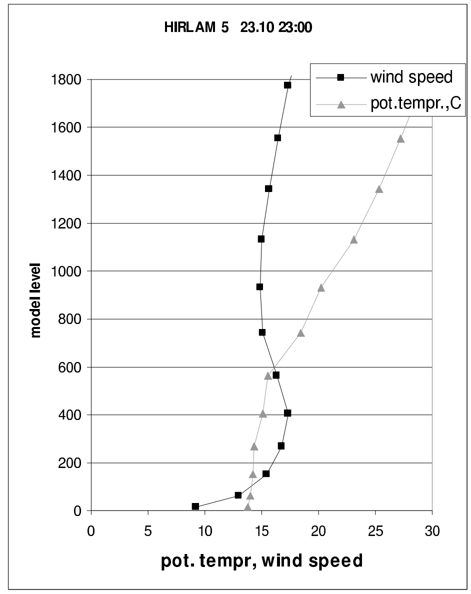

Figure 3: Measured (left) and computed by HIRLAM 5 (right) vertical profiles at the release point at 23:00 23.10.1994 (close to middle of the release period).

it is better to use it. Otherwise, the best results were shown by combination of the critical Richardson number and dry parcel methods. It is worth mentioning that Richardson number method alone has failed, while parcel approach was quite good also in a stand-alone mode.

References

ETEX (1998) A special issue of Atmosph. Environ. dedicated to the ETEX experiment. 32, Issue 24, pp.4089-4375.

Graziani, G., Klug, W., Mosca, S. (1998) Real-time long-range dispersion model evaluation of the ETEX first release. Office for official publications of the European Communities, L-2985, Luxembourg, 215 pp.

Sofiev, M., Siljamo, P. Finnish Emergency modelling frameworkj SILAM. Part 2. Model verification with European Tracer Experiment. (in preparation.)

Sofiev, M., Valkama, I., Ilvonen M., Siljamo, P. Finnish Emergency modelling frameworkj SILAM. Part 1. Model description. (in preparation.)

Modelling of chemical transport and transportation of air pollutants: uncertainties connected to the meteorological input

Marke Hongisto, Finnish Meteorological Institute

General uncertainties and effects of the accuracy of meteorological fields as external forcing factor to a chemistry-transport model are discussed. Of the most important parameters the mixing height derived from HIRLAM or Jokioinen sounding profiles, and some atmospheric boundary layer parameters derived from two different Hirlam versions are compared. The effects of the change of the Hirlam version to air pollution estimates are described.

1 Importance of meteorological parameters for the air pollution models

Chemistry-transport models (CTM:s) need meteorological forcing for calculating the transport and mixing of pollutants in the lower troposphere. The emissions are split partly in to the atmospheric boundary layer (ABL), partly in to the free atmosphere, depending e.g. on the heat content and exhaust velocity of the stack gases and thermal state of the atmosphere. While the wind direction does veer with the height, the effective height of the plume determines the initial transport direction and transport speed of the pollutants. Later, convection or vertical advection connected e.g. to the fronts, mix contaminants to the upper troposphere and to the surface. The strength of the dilution process is mainly controlled by the stability state and the height of the ABL.

For the sink terms, temperature and humidity determine the chemical conversion and the in-cloud-scavenging rates, while the below-cloud scavenging depends on the vertical distribution, intensity and type of the precipitation. Dry deposition is a rather complicated process, normally described by the resistance analogy: The dry deposition velocity v_d is defined by $v_d = (r_a + r_b + r_c)^{-1}$, where the aerodynamic resistance r_a, determining how fast the pollutants are transported down to the surface, is a function of stability state of the atmosphere, (surface roughness, friction velocity and Monin-Obukhov legth L being the controlling parameters). The r_b is the resistance to penetration across the atmospheric near-surface layer (where molecular transport dominates over turbulent transport) by convection, diffusion or inertial processes, and r_c, the resistance associated with pollutant-surface interaction, depends on the state and type of the surface, on solar radiation, surface temperature, relative humidity, amount of rain, dew or fog and pollutant exposure time.

The relative importance of various meteorological parameters to the transport distance of pollutants, their direct exposure to surfaces and deposition amounts, depends on the pollutant type, weather situation and on the type of the model used. In Eulerian 3D models, the horizontal resolution is the most critical factor, determining the initial dilution of the emissions. While the computational resource requirements state an upper limit to the horizontal grid dimensions, the mixing (the ABL) height becomes the next important parameter to the model performance. Most pollutant episodes occur or get their origin in stable conditions with a low mixing height, so the estimate of the inversion height, strength and dynamics have often been named to be the most important parameter for the air quality studies.

2 The Hilatar model

The model Hilatar (Hongisto 1998, 2003) was constructed for calculating and forecasting air quality situations at the background areas. Hilatar is of Eulerian type: a grid-point model in which the time change of concentrations in air are calculated by numerically solving the transport equation containing emission, advection, turbulent diffusion, chemical transformation and deposition terms. The vertical mixing is written using the gradient transport theory, already developed in the 1920's. The turbulent fluxes are assumed to be proportional to local mean concentration gradients and the proportionality factor, the eddy diffusivity, is analogical to molecular diffusion but 10^4-10^5 times stronger.

In Hilatar, the meteorological input parameters are taken from the 6-hour predictions of the HIRLAM (HIgh Resolution Limited Area Model) weather model. The boundary layer parameterization in the various HIRLAM versions used (1990-2002), has been the most importance factor to the success of the air quality simulations.

The Hilatar model has been applied in calculating in European scale the concentrations and depositions of nitrogen and sulphur compounds in background areas since 1995 June simulations over Scandinavia cover a longer period. It has been used e.g. in estimating the nutrient flux to the Baltic Sea, factors that affect it and gradients from coastal areas to the open sea, in analyzing some dust episodes and for simulating heavy metal transport over the Nordic countries.

The model has been verified by comparing the daily concentrations of SO2, NO2, NH3, SO42-, NO3-, NH4+, HNO3+, NO3- and NH3+NH4+ in air, and monthly mean wet depositions of SO4=, NO3- and NH4+, with EMEP measurements extracted from the EMEP/NILU database. Over the period June 1995 September 1999 around 90 European EMEP stations and over the years 1993 and 1996-1998 data from 29 Nordic EMEP stations were used. Additionally the model has been verified against national and field campaign measurements. For verification of the wet deposition, un-accuracy of the measured precipitation common at the EMEP-stations, has some effect to the results. Differences in the monthy precipitation collected by close to the each other situated meteorological and an air quality gauges at the same station can be 50 %. (Hongisto et al., 2003, Sofiev et al., 2001, Zlatev et al., 2001, Schulz et al., 1999)

3 Uncertainties in air quality model

An air quality model is a numerical simplification of a chain of dynamical processes, it contains accumulated errors both of the model structure and its input data. Pure numerical errors (e.g. the models capability to conserve mass and solve the theoretical advection or diffusion equations properly) are easy to test and correct; in all the individual algorithms, the maximum error can be limited to be less than 0.05-0.5 % of the total mass advected, diffused or converted. Much more serious deviations are connected to the emissions, their time variation and to the model structure: The splitting up method produces artificial diffusion during diagonal advection, only a limited number of chemical compounds can be simulated at the time, in low resolution models local effects (sea breeze, low-level jets) are ignored, theoretical parameterization does not always cover all phenomena and the limited time step (225 s) and the 6 h time interval of the input data also produce errors. The more detailed the parameterization is (e.g. dry deposition) the more inaccuracies it can contain. Additionally most fluxes, especially over water surfaces, are bi-directional, however the water concentrations are unknown, as well as natural emissions and response from the surface to the atmosphere in fast changing conditions (up-welling, swells). The Monin-Obukhov theory cannot always satisfactorily describe meteorological situations and grid averages are rather theoretical concepts (Hongisto 1998, 2003).

4 Comparison of the mixing height derived from HIRLAM or Jokioinen sounding profiles

Time series of the ABL height values derived from the Jokioinen soundings with 12 hour interval in 1996-1998 were compared with the HIRLAM ABL-height estimates of the respective grid, calculated with the same algorithm. The largest instant differences were hound in summer. HIRLAM hmix exceeded the measured one by around 2 km four times in 1996, and underestimated it by more than 1 km in 22 cases. As seen from Fig. 1, a negative anomaly was more frequent if the summer months are excluded. On average the deviation was below $\pm$ 400 m in summer and the positive bias was ¡ 150 m in winter and spring as a monthly average. There was no time bias in the instant differences as is demonstrated in Fig. 2. The nighttime difference was around $\pm$ 150 m throughout the year, In Fig. 3 the relative deviation in 1996 and 1997 is presented

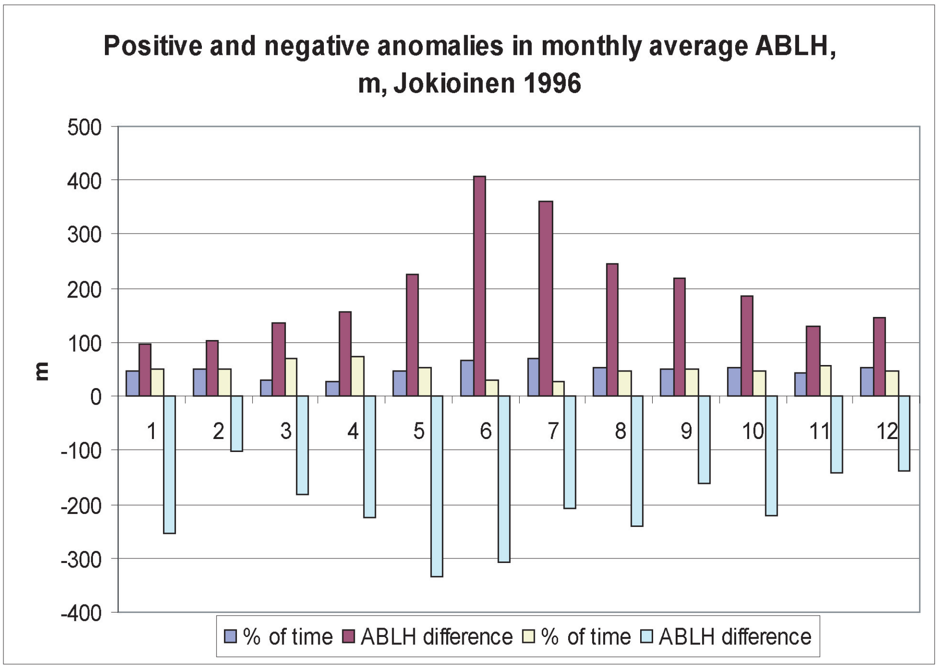

Figure 1: ABL height differences

The reasons for the differences cannot be in the method, while the same formula (see Hongisto 1998) has been applied to estimate the hmix from the both profiles. The internally in the Hirlam-model calculated hmix value was not available, thus a post-processing package for the ABL parameterization was used. The reasons for the discrepancy are hidden in the surface scale parameterization and heat balance of the lower ABL of HIRLAM. The vertical resolution (10 Hirlam levels below 3 km) does not make a big role, while instant differences extended over several vertical grids. While it is not possible to analyze the reasons from such a short inter-comparison study (detailed comparison of the differences in the surface layer energy budget parameterization is a subject of a new study), estimates of the general field differences discussed on the Hirlam group www-pages at the FMI are just recommended for introduction on the subject.

5 Comparison of ABL parameters estimated by HIRLAM 5 and earlier version

In order to see, what was the quantitative effect to the ABL parameter values from the change of the Hirlam version 4 to version 5 in 2003, differences in monthly averages of the ABL height, precipitation, 2-meter humidity q2, total cloudiness, wind velocity and direction, temperature scale, friction velocity and Monin-Obukhov length, of the both versions, were compared over one month, January 2003. Both data sets were linearly interpolated to the 0.1^o horizontal grid. The comparison was made as monthly averages over the Baltic Sea and the surrounding states. The differences are presented as the new ATC model (hirlam 5)-value the old, ATA (hirlam 4)-value. The slopes of the Köli mountains should be ignored, while the differences were generally larger and discontinuous, which might be due to interpolation of a marine and mountain grid fields over a complicated terrain.

Over land areas the ABL height was generally 0-250 m higher in the new HIRLAM, generally < 100 m, occasionally even < 250 m lower over the Baltic Sea. In southern Sweden, Denmark and Southern Baltic Proper, precipitation was even > 50 % lower, $\pm$ 10 % in Southern Finland but, however up to 50 % higher over the Atlantic, North Finland and Northern parts of the Russian Karelia. Differences in

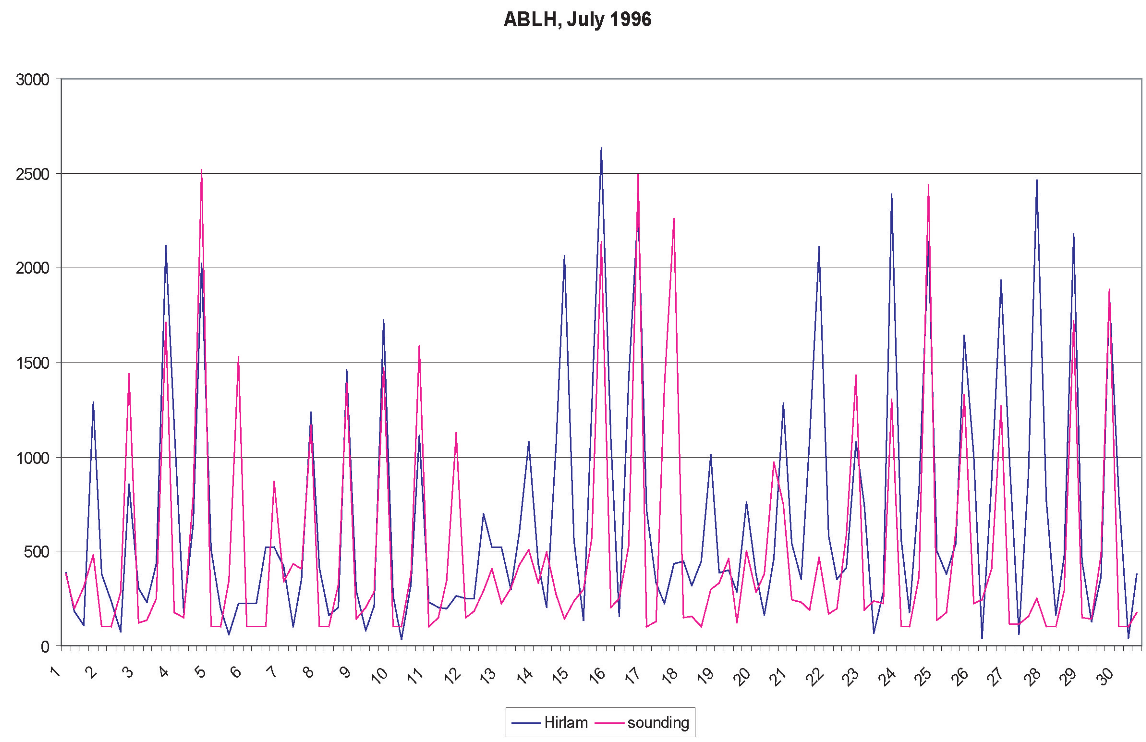

Figure 2: ABL height in June 1996, month of the largest bias.

the 2-m specific humidity and cloudiness have geographically the same characteristics. The 10 m wind velocity was up to 1-1.5 m/s higher over the Atlantic, $\pm$ 0.5 m/s elsewhere. Also the monthly mean flow direction was affected by the change of the model version, which is illustrated in Fig 4. The ABL stability parameters show, that the north-eastern or northern areas became slightly more unstable, while the southern and south-western areas are more labile in the new Hirlam 5.

6 Impact to the Hilatar model results

The new meteorological data set (ATC) with a 0.3^o grid resolution was used to re-estimate the long-range transport and deposition of nitrogen and sulphur compounds over Europe in January 2003, simulated with the old 0.4^o resolution ATA fields. While the emission inventory was updated for the new simulations, the generally declining emission trend produced slightly smaller depositions in ATC-runs. Increase in the model resolution also led to a finer scale structure in the deposition. As a results of the change of the forcing fields it was found, that in Scandinavia the increase of the ABL height by 50-250 m resulted to smaller surface concentrations in dry situations. The precipitation increase in Europe and in the North-Eastern Scandinavia (by up to 50 %) increased wet deposition over the respective areas. Decrease in friction velocity u* in Scandinavia yielded to lower dry deposition flux. Due to a local changes in temperature, moisture and wind parameters (q2, clf, uabs, udir) should have an effect to chemical transformation rates, however the differences are instant, and while the effects partly compensate each other, the comparison should be made by detailed process analysis. In general, the use of ATC-meteorology leads to shorter transport distances in Europe and higher depositions near the sources. In the target areas, e.g. in Finland, use of the new data will reduce calculated deposition estimates in winter.

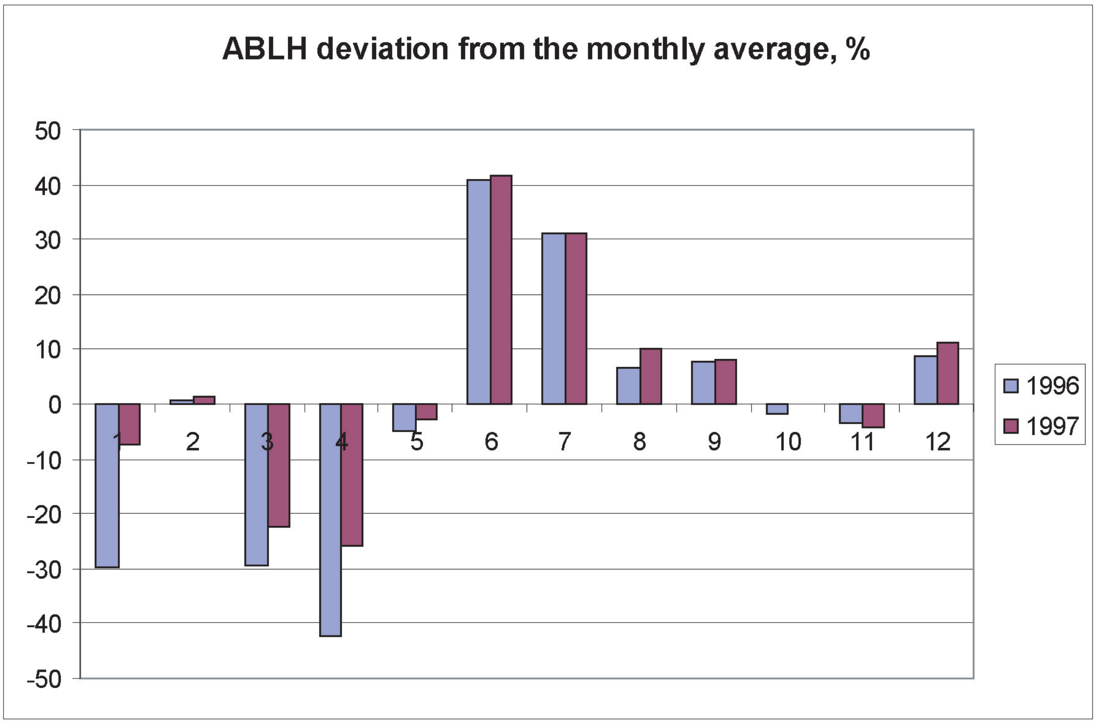

Figure 3: The bias from the average ABL height value in %, 1996, 1997.

7 Discussion

Some Hirlam parameters are verified on an operational basis. On the HIRLAM verification scores http://hebe.fmi.fi/ hirlam/wire/asm2000/node4.html it has been suggested that the diurnal cycle is strongly underestimated in the forecasts. During the daytime the temperatures are too low and in the night-time too warm. The same is also seen in the two meter humidity values. This feature is most prominent in winter and in spring. In winter especially strong inversions during nights are difficult to forecast. In spring the difficulties are often during the day, when the predicted temperature is too cold.

This result was nor fully confirmed by this short study, while the highest discrepancies in the ABL height were found in summer. Anyway, soundings are point measurements. Hirlam is a living model, the parameterization is constantly under development to reach more reliable forecasts. Also, although some earlier experiments with snow cover show, that the forecast is rather stable to changes in surface conditions, the changes in the latest Hirlam versions to the wintertime ABL parameters was percentually rather high.

References

HIRLAM, 1990. HIRLAM Forecast model level 1. On-line documentation manual. Per Kllberg, (ed.), SMHI S 60176, Norrkping, Sweden, June 1990.

HIRLAM 2002a. HIRLAM, a High Resolution Limited Area Model, International Project. In: HIRLAM 5 Scientific Documentation. Unden P. et al., December 2002, 144p.
Available at http://hirlam.knmi.nl/

Hongisto 2003. FMI Contributions No. 40, Helsinki 2003, 188 p.
http://lib.hut.fi/Diss/2003/isbn9512264811/index.html

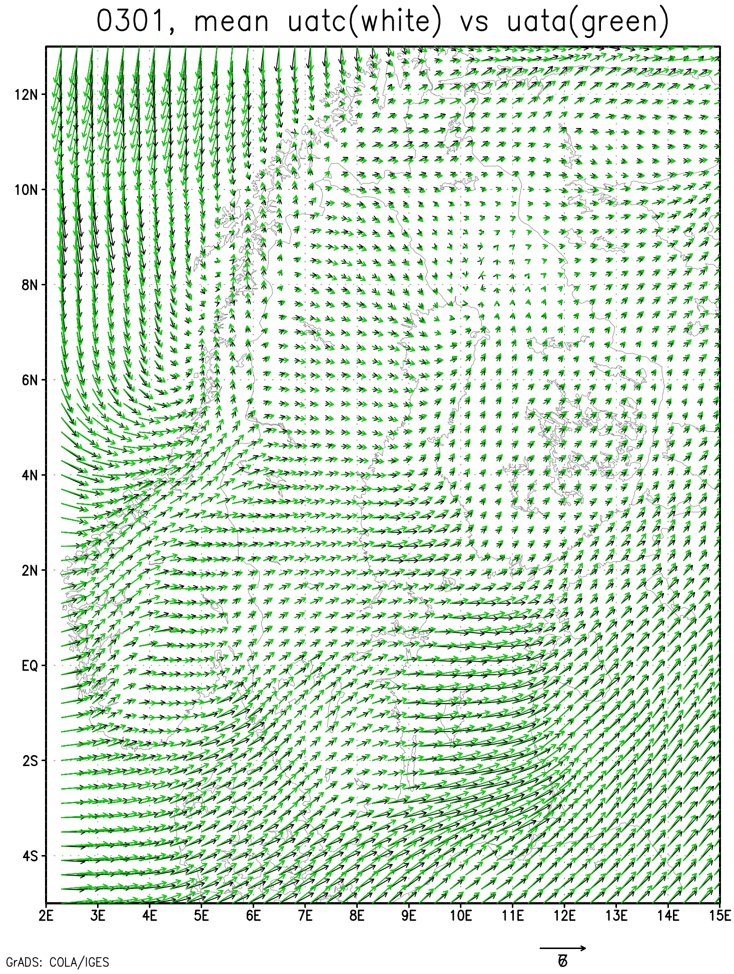

Figure 4: The difference in the monthly average flow direction, January 2003. ATC-ATA.

Hongisto 1998. FMI Contributions No, 21, Helsinki 1998, 152 p. http://www.fmi.fi/research_air/air_25.html

Hongisto et al., 2003, Atmosp. Environ. 37/11 pp. 1535-1547 and 1549-1560

Sofiev et al. (2001), Atmosp. Environ. 35 (2001) 1395-1409.

Zlatev et al. (2001). TemaNord 2001:569. Nordic Council of Ministers, Copenhagen 2001. 47 p.

Schulz et al. (1999) in Zuelicke C., (ed.) Proc. of the Third BASYS Annual Sci. Conf. http://www.io-warnemuende.de/Projects/Basys/bio/con3/con3top.htm#T2-2 p. 60-67.

Long range transport of birch pollen
A problem statement and feasibility studies

Pilvi Siljamo[1] Mikhail Sofiev[1] Hanna Ranta[2] Laimdota Kalnina[3] Agneta Ekebom[4]

1 Introduction

Natural pollen is a known source of allergy-related deceases, with a pronounced peak of concentrations in spring time during an intensive flowering. Therefore, several European countries perform permanent monitoring of pollen concentrations and provide short-term forecasts of concentration of allergens in atmosphere (e.g. Føsig and Rasmussen, 2003).

Due to climate specifics, a local flowering in northern countries starts a few weeks later than in Central Europe and Russia. However, a large-scale atmospheric transport can significantly distort the picture by bringing large amounts of pollen from the southern regions to the north. Such phenomena has an episodic character but its effect is significant and registered by aerobiological network in Finland and other Scandinavian countries (Corden et al., 2002; Małgorzata et al., 2002; Hjelmroos, 1992). Forecasting of such episodes requires a proper treatment of both meteorological and biological mechanisms and can only be addressed via combination of a phenological model of flowering and an atmospheric dispersion model.

A birch pollen is probably the most widely transported pollen species, which can find its way through thousands of kilometers. The birch tree is the most common broadleaf tree in Scandinavia, Baltic Countries and north-western part of Russia. It is also widespread in other parts of Europe with moderate climate conditions.

Current paper presents a problem statement and first results of a recently started joint project of Finnish Meteorological Institute and Aerobiological Group of Turku University aiming at creation of a model prototype, capable of operational forecasting of high pollen concentrations due to the long-range atmospheric transport. As a part of a feasibility study, two cases of early pollen presence registered in springs 2002 and 2003 were analyzed and potential source areas were delineated.

2 Phenological background

Typical diameter of a birch pollen grain is 20 μm. It is very light, almost round-shaped with slight distortions and capable of long-distance traveling with air masses. The main mechanism of the pollen removal from atmosphere is believed to be scavenging with precipitation. However, a role of dry deposition should not be under-estimated either.

There are two treelike birch species in Europe. Downy birch (*Betula pubescens*) is the most common in the northern part of Europe. Silver birch (*Betula pendula*) is also common, but more in the southern regions.

There are several empirical models of flowering. Out of this list, a few simple but widely used robust approaches were selected: degree day sum (DD in eq. 1), period units (PU in eq. 2), and calendar days (CD).

[1]Finnish Meteorological Institute
[2]University of Turku, Department of Biology
[3]University of Latvia, Faculty of Geography and Earth Sciences
[4]Swedish Museum of Natural History,Palynological Laboratory

$$DD = \sum_{\text{days}} (\bar{T} - A)\,1(\bar{T} - A), \tag{1}$$

$$PU = \sum_{\text{hours}} (T - B)\,1(T - B), \tag{2}$$

where $1(\chi) = \begin{cases} 0, & \chi < 0 \\ 1, & \chi > 0 \end{cases}$ is a Heaviside step function.

Here T is an hourly mean temperature, $\bar{T}$ is a daily mean temperature, and A and B are place-specific constants (Sarvas, 1972). In Finland, both A and B are usually assumed equal to 5^oC (Luomajoki, 1999). In all models, the flowering starts when the corresponding quantity (DD, PU, or CD) exceeds some place-dependent threshold level.

Luomajoki (1999) noticed that PU is usually the best quantity for describing the timing of pollination, but DD and CD are not too bad either. Calendar days approach was better for *B. pendula* in 25% cases, but for *B. pubescens* it usually performs worse than the other methods.

A more sophisticated promoter-inhibitor model of flowering used by Schaber and Badeck (2003) shows the way of accounting for both temperature and lightness.

While the heat sums are the most important factors for bud and leaf burst, geographical location (latitude, longitude, altitude), habitat and heredity have an effect, usually reflected in the corresponding threshold levels. In case of *B. pubescens*, the latitude determines an amount of heat to be accumulated before the flowering can start. In particular, an average heat sum allowing the bud burst ($A = 5^o$C in eq. 1) is 68 dd in the south of Finland, while in the northern part of the country it can be as small as 40 dd for some years averaging at 52 dd (Leppälä, 2003).

In the current project, a lack of quantitative information about geographical distribution of individual birch species does not allow to consider them separately neither in dispersion nor in biological parts of the integrated model. Therefore, the above species were mixed into a "general birch" pollen with appropriate averaging of their characteristics.

3 Case studies for spring 2002 and 2003

Both springs in 2002 and 2003 were characterized by high pollen concentrations recorded at Finnish aerobiological monitoring sites approximately one week before the local flowering started. Thus, in 2002 the flowering season started at the beginning of May, while the birch pollen was registered already on April 22. Late spring 2003 delayed the flowering in Europe and high concentrations were recorded by Finnish sites only on May 5-7, when the local flowering had not yet started. The most probable reason for such time shift was an atmospheric transport from Central Europe or Russia, where the leaf burst happened earlier in both cases.

Analysis of the cases included: (i) delineation of potential source areas using the FMI dispersion model SILAM in adjoint mode (Sofiev et al., submitted), (ii) comparison of the obtained sensitivity functions with observed pollen concentrations in the suspected source areas.

A setup of SILAM adjoint runs was based on data of Finnish stations Turku, Kangasala, Kuopio, Oulu and Kevo for 2002, and Turku, Kangasala, Joutseno, Vaasa and Oulu for 2003. Observed concentrations were approximated with step-wise functions and used as the source terms. Simulated periods covered $\sim$100 hours. For each case, the meteorological data were taken from operational FMI-HIRLAM model (HIRLAM 4 for 2002 and HIRLAM 5 for 2003) with 3 hour time step.

An example of the simulation results in fig. 1 shows that possible sources of pollen during April 2002 are located in Baltic countries, Russia and Belarus.

Another example in fig. 2 for May 2003 shows a different pattern pointing at the south-western sector as a potential source. Baltic countries are an important source areas again, but this time the grains could originate also from Sweden, Poland and Germany.

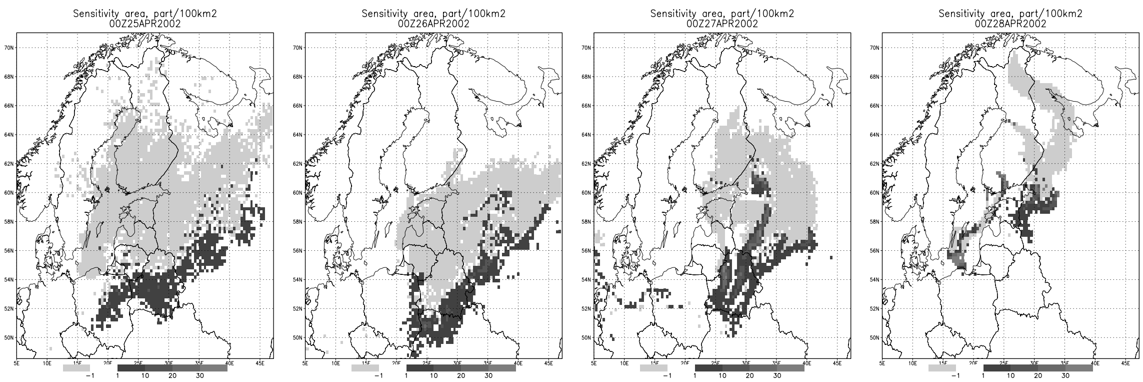

Figure 1: Possible source areas of long range tarnsported *Betula* pollen in Finland in 2002, 25th–28th of April. Light grey (negative values) indicates area, which could not supply the grains; the dark grey areas could serve as sources.

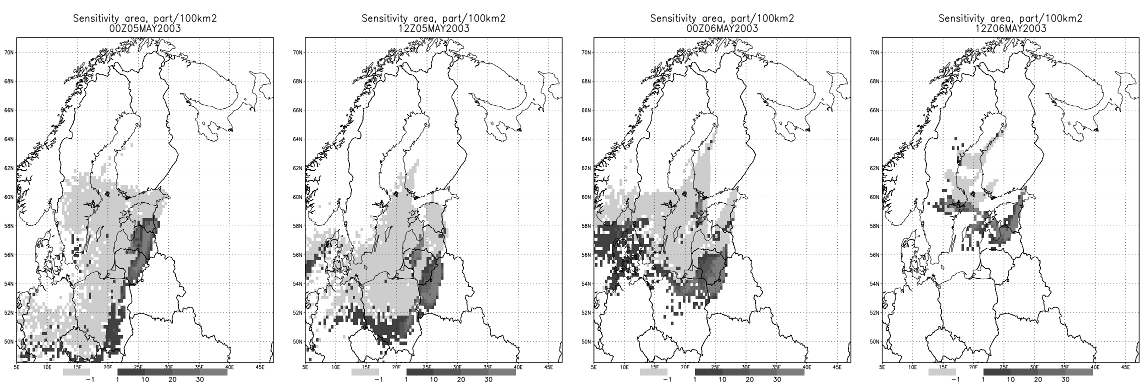

Figure 2: Possible source areas of long-range transported *Betula* pollen in Finland in 2003, 5th–6th of May. Light grey (negative values) indicates area, which could not supply the grains; the dark grey areas could serve as sources.

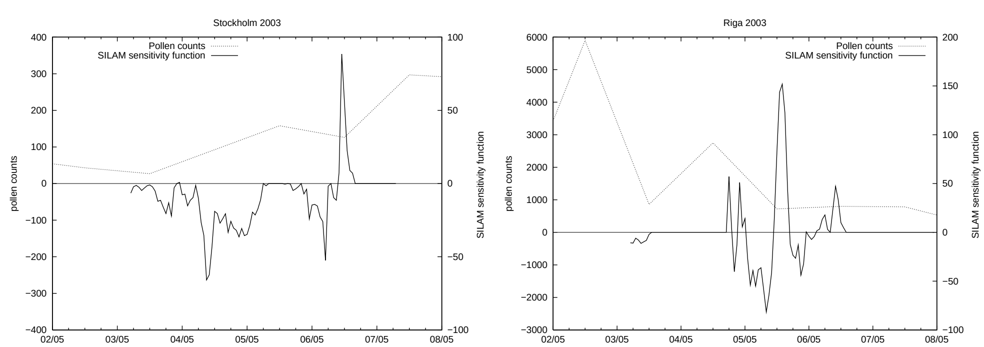

Figure 3: An example of observed pollen counts and SILAM sensitivity function for Stockholm and Riga in 2003

A total amount of pollen Fr that comes from a specific location is proportional to a product of the sensitivity function φ^* and the concentration C at the place:

$$Fr = \int_0^T \tilde{\varphi}^* C \, dt, \ \tilde{\varphi}^* = \begin{cases} \varphi^*; & \varphi^* > 0 \\ 0, & \varphi^* \le 0 \end{cases} \tag{3}$$

The integral in eq. 3 also highlights the time periods when the pollen from a particular region can reach the receptor sites in Finland (periods when φ^* is significantly positive over the region). Negative and zero values of φ^* show the periods when meteorological conditions were not favoring the transport to Finland from the region. This is illustrated by fig. 3 charts for Riga and Stockholm areas.

4 Conclusions

A long-range atmospheric transport of natural allergens is recognized as a potential source of difficult-to-forecast events of high concentrations of allergens in atmosphere of Nordic countries, which can happen weeks before the local flowering season. The most important species in this content is the birch pollen, which features favor a large-scale atmospheric transport of the grains.

The problem of short-term forecasting of early peaks of pollen concentration can be addressed via combination of atmospheric dispersion and biological models.

For the current study, a simple calendar-based table, two temperature sums (degree days and period units) and a more complicated promoter-inhibitor phenological model are selected for description of start time of flowering around Europe.

Two cases (in 2002 and 2003) were analyzed with the FMI dispersion model SILAM using the adjoint dispersion technique. The results show that source areas can significantly vary from year to year. However, in both cases the forests in Baltic countries were pointed as possible source areas. The other important regions were Russia, Poland, Germany and Southern Sweden, but their influence was much more dependent on meteorological situations.

References

Corden, J. M., A. Stach and W. Millington, 2002: A comparison of *Betula* pollen season at two European sites; Derby, United Kingdom and Poznan, Poland (1995-1999). *Aerobiologia*, **18**, 45–53.

Føsig, A. and A. Rasmussen, 2003: Pollen- & sporemålinger i Danmark. Sæsonen 2001. Technical report 03-10, Danish Meteorological Institute.

Hjelmroos, M., 1992: Long-distance transport of *Betula* pollen grains and allergic symptoms. *Aerobiologia*, **8**, 231–236.

Leppälä, M., 2003: *Hieskoivun (Betula pubescens Ehrh) fenologia Suomessa vuosina 1997-2002*. Master's thesis, University of Oulu.

Luomajoki, A., 1999: Differences in the climatic adaptation of silver birch (*Betula pendula*) and downy birch (*Betula pubescens*) in Finland based on male flowering phenology. Acta Forestalia Fennica 263, Finnish Society of Forest Science.

Małgorzata, L., M. Miętus and A. Uruska, 2002: Seasonal variations in the atmospheric *Betula* pollen count in Gdańsk (southern Baltic coast) in relation to meteorological parameters. *Aerobiologia*, **18**, 33–43.

Sarvas, R., 1972: Investigations of the annual cycle of development of forest trees. *Metsäntutkimuslaitoksen julkaisuja*, **76**(3).

Schaber, J. and F.-W. Badeck, 2003: Physiology-based phenology models for forest tree species in Germany. *Int J Biometeorol*, **47**, 193–201.

Sofiev, M., I. Valkama, M. Ilvonen and P. Siljamo, submitted: Finnish emergency modelling framework SILAM. Part. 1. Model description. *Submitted to Atmospheric Environment.*

MGO Regional Climate Model: present-day climate simulation

I.M. Shkolnik, V.P. Meleshko, V.M.Gavrilina
Voeikov Main Geophysical Observatory, St Petersburg

1 Introduction

It is well known the deficiencies of an RCM cannot be correctly determined using GCM simulated lateral boundary conditions (LBC) alone because GCM produced large scale fields have discrepancies with observation. The resulting errors (some of them are systematic) of the regional model appear to be a combination of internal and external errors. Thus, the validation of present-day regional climatology is usually carried out using quasi-observed boundary fields instead of or along with those simulated by GCM. The study is aimed at evaluation of the MGO RCM errors using different types of LBC: derived from the NCEP/NCAR reanalysis [1] and simulated by the MGO GCM.

2 Model and experimental design

The MGO RCM is based on primitive system of equations in hydrostatic approximation. The prognostic variables are the components of horizontal wind, air temperature, specific humidity, and surface pressure. In the vertical the model has 14 unequally spaced ?-layers. For solving the modeling equations in the horizontal a cartesian grid domain with 105?121 points is used (projection - Lambert conformal). The spatial step is 50 km. The model incorporates full physical package of the MGO GCM (AMIP II version). A slab ocean is used to compute the surface temperature of internal water bodies; horizontal diffusion - fourth order linear.The LBC data are assimilated using newtonian relaxation over 10 grid points adjacent to lateral boundaries; the inflow/outflow formulation for humidity is modeled. Detailed description of the model is given in [3].

The NCEP/NCAR reanalysis data has been retrieved spanning time slice from 1982 to 1987 (ftp://ftp.cdc.noaa.gov/Datasets/ncep.reanalysis/). The data is 2.5^o x 2.5^o and available at 17 pressure levels every 6 hours for wind, temperature, water vapor, and surface pressure. The horizontal resolution of reanalysis data has been reduced to spectral T42.

Same characteristics from the MGO GCM AMIP II climate simulation have been stored at 6-hour intervals covering years from 1982 to 1987 at spectral T42 resolution.

Two 6-year climate simulations with the RCM have been carried out driven first reanalysis and then GCM produced fields (further referred to as "RCM+REA" and "RCM+GCM", respectively). Both runs included the same observed SST and sea ice distributions. The first year of each run has been rejected from the analysis of results.

Particular interest has been focused on the computed surface air temperature, precipitation, and annual runoff over large terrestrial watersheds of the Baltic sea (BAL), several northern rivers (NRV), several southern rivers (SRV), and the Volga/Ural rivers (VUR). For comparison of the modeling estimates with observations the fairly good surface climatology dataset [2] has been used.

3 Results

In Fig.1 shown are the seasonal cycles of temperature computed in the experiments and that observed for the time slice 1983 to 1987. The seasonal cycles are generally in agreement with observations in both experiments reasonably well reproducing the phase and amplitude of seasonalities over all watersheds.

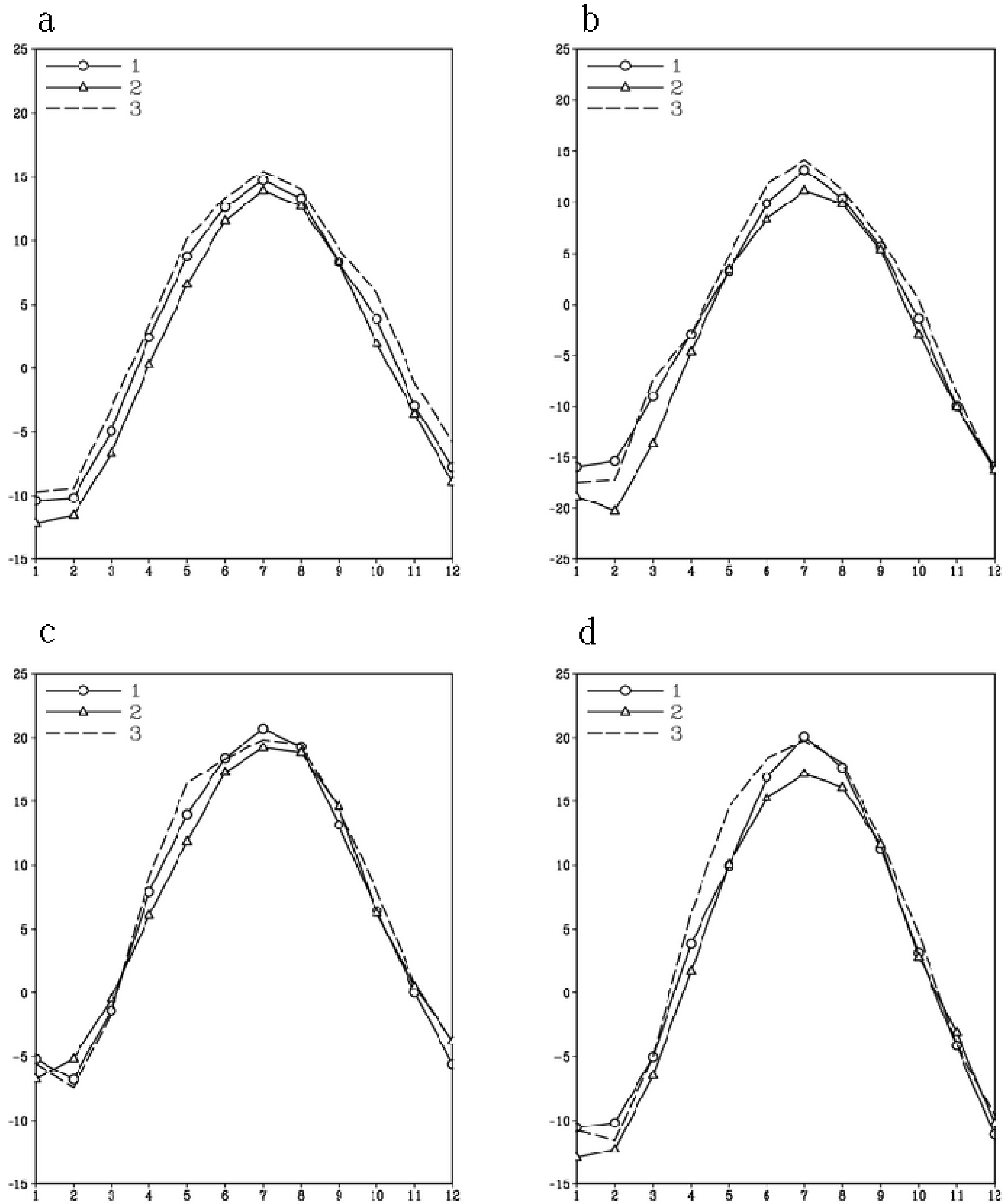

Figure 1: Simulated and observed seasonalities of surface air temperature (^oC) over BAL(a), NRV(b), SRV(c) and VUR(d). Curves 1, 2 and 3 denote RCM+REA, RCM+GCM and observation, respectively.

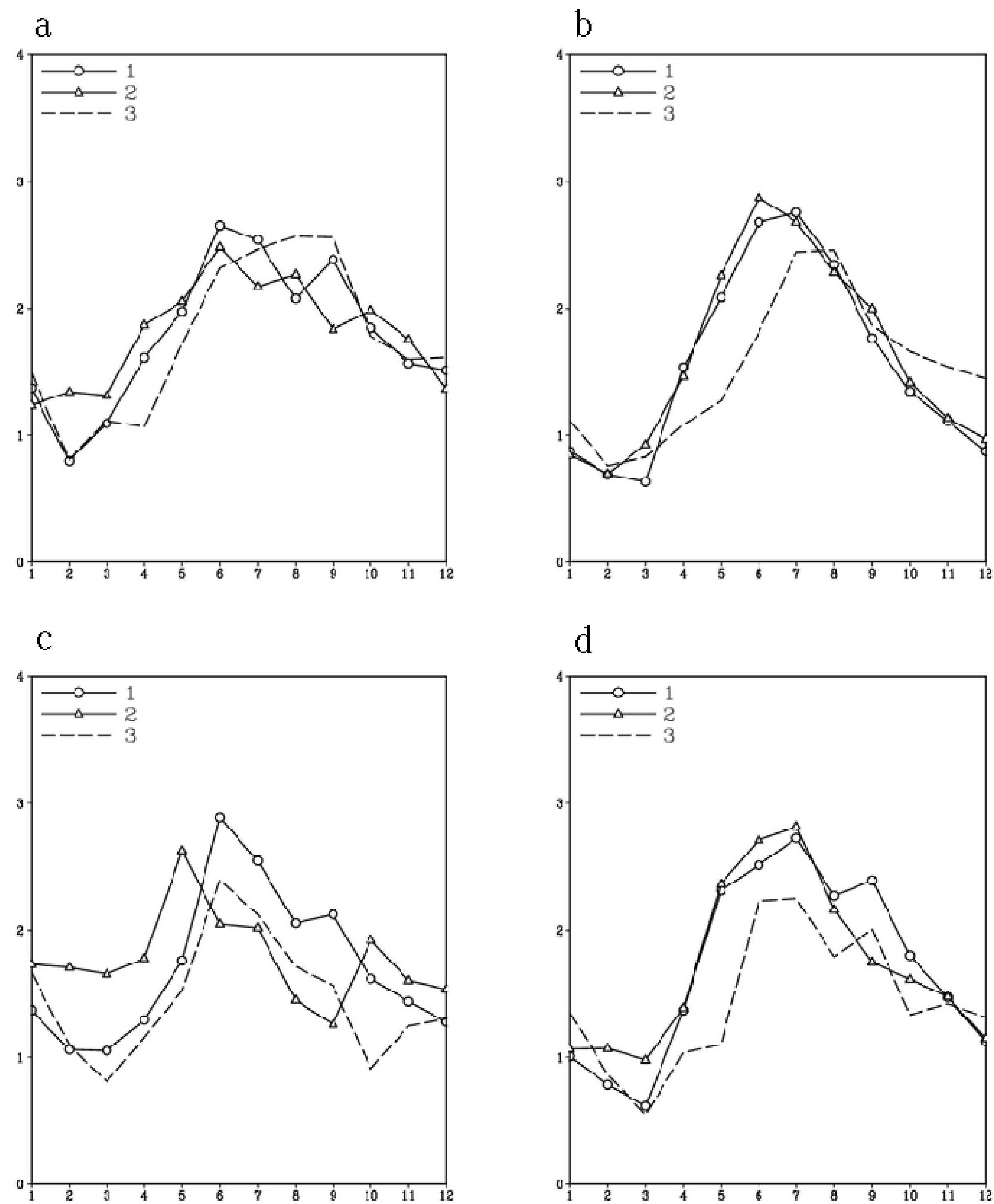

Figure 2: Same as in Fig.1 but for precipitation (mm/day).

Table 1: Simulated and observed annual runoff (km^3) over the watersheds.

	BAL	NRV	SRV	VUR
RCM+REA	228	209	77	190
RCM+GCM	285	250	96	244
OBS	483	382	98	314

Slight cooling is pronounced in RCM+REA throughout the year. However, the simulated LBC produce more remarkable cooling, notably over BAL and NRV. Both models tend to undersimulate temperature in spring over Volga and Ural rivers be probably due to deficiencies in snow cover evolution.

Fig 2 displays the seasonalities of precipitation over the watershed. The agreement between computed and observed precipitation is less pronounced as compared against that of temperature. The model tends to oversimulate precipitation over all the watersheds except BAL. The use of reanalysis data at the boundaries leads to considerable improvement when reproducing the phase of seasonal cycle. Both models tend to compute maxima of precipitation shifted to the beginning of the year. This feature is less expressed with quasi-observed LBC.

Tab.1 contains simulated in RCM+REA and RCM+GCM annual runoff compared to that derived from various observational databases. Both models undersimulate runoff by 10-50in RCM+REA. This descrepancy with observation may be related to enhanced warm season evaporation. However, the reliable observational estimates of evaporation are unavailable. There is an indication the short wave radiation balance in summer is slightly oversimulated in both models suggesting evaporation is also oversimulated.

4 Summary

Two 6-year regional climate simulations with the MGO RCM have been performed. Simulations included quasi-observed and GCM simulated lateral boundary conditions. As compared against GCM driven model, the observation driven model produces seasonalities of surface air temperature and precipitation closer to that observed over the watersheds. In both experiments precipitation and evaporation are likely to be oversimulated over the watersheds, while runoff is undersimulated.

References

1. Kalnay E. et al. The NCEP/NCAR 40 year reanalysis project. Bull. Am. Meteor. Soc.,Vol. 77, 1996.
2. New, M. M. Hulme and P.D. Jones. Representing twentieth century space-time climate variability. Part I: development of a 1961-1990 mean monthly terrestrial climatology. J. Climate, 12, pp. 829-856. 1999.
3. Shkolnik, I.M., V.P.Meleshko, T.V.Pavlova. Regional hydrodynamical model for climate studies over Russia. Meteorol. Hydrol. (Allerton press), 2000, 4 , pp.32-49.

MLAM,
Three dimensional limited area modelling of the Martian Atmosphere

Janne Kauhanen
Division of Atmospheric Sciences
Department of Physical Sciences
University of Helsinki

1 Introduction

Planet Mars is the fourth planet of our solar system. It has fascinated mankind hundreds of years. Modern day technology has made it possible to explore Mars in new ways and increase our knowledge of the solar system and of Mars. The increased amount and accuracy of observational data from Mars due to successfull missions has enhanced modelling of the Martian atmosphere. The global coverage of observational data from the Mars has made it possible to validate the general circulation. There are five different Mars general circulation models (MGCM) with advanced parameterization schemes at present.

Already a decade ago, among the very first, Savijärvi (1991a,b) (Savijärvi and Siili, 1993) used the University of Helsinki 1-D and 2-D mesoscale models to simulate locally Martian small scale weather phenomena. The 3-D mesoscale limited area models are a natural step forward to simulate local phenomena. There are three acknowledged mesoscale models for Mars presently, all already in an advanced stage. These are: 1) MRAMS (Rafkin et al., 2001), 2) OSU MMM5 (Tyler et al., 2002) and 3) The Cornell/CalTech Mars MM5 (Toigo and Richardson, 2002). A fourth model, MLAM - M(ars) (HIR)LAM - is developed in co-operation between Division of Atmospheric Sciences of University of Helsinki and the Finnish Meteorological Institute.

2 Modifications

HIRLAM 5.0.0 model version is the basis of the latest version of MLAM. The modifications have included e.g. a new radiation scheme based on that used in the UH/ATM 1-D Mars model and validated against line-by-line calculations by D. Crisp. Boundary and initial conditions have been derived from the Mars Climate Database (Lewis et al., 1999) (versions 2.3 and 3.0) and from the Oxford Mars GCM.

2.1 Changes in the model

Conversion for Mars requires, e.g., changing the Earth's constants to the Martian ones. These include: gas constant, gravity, radius of the planet, speed of rotation, soil properties, solar constant and reference pressure. These constant are in principle included in common blocks, but, unfortunately, some constants (gas constant, gravity and reference pressure) were hard-coded in several subroutines (list of these constants and subroutines will be available soon). The average surface pressure on Mars is 800 Pa and average surface temperature is lower than that of the Earth. The reference pressure and temperature for Mars were set to 450 Pa and 210 K, respectively.

The length of the Martian day is 24 h 40 min, which is close to the length of the Earth's day. Mainly for this reason the 'Earth's clock', i.e. time handling routines, is kept as such. Thus the naming of history files is kept unchanged as well.

The radiation routine (RADIA) was rewritten for Martian conditions. The routine takes into account the different day length of the Mars, dissimilar orbital parameters such as the declination angle as well as different composition of Martian atmosphere compared to the Earth's. The effects of dust are also included in the radiation parameterization.

The basics of the surface scheme (SURF) are kept unchanged, but an additional variable - thermal inertia - has been introduced. This spatially varying variable describing the thermal properties of the Mars' surface substance, regolith, has been added into the climate file.

The HIRLAM environment (and scripts) are retained in the MLAM system unchanged as much as possible. There are, however, two new 'home made' packages that are run outside HIRLAM system. These are the climate and boundary generations.

2.2 Climate and boundary generation

The climate files, including different surface fields for the Mars are constructed from several different datasets with different resolutions and data formats. Therefore the original HIRLAM climate generation was completely re-structured. The following surface fields are created from different Mars datasets: orography, surface temperatures, albedo and thermal inertia. Some variables are simply set to constant values. Fraction of land is set to 1, since there is not (much) water on the Mars. The snow cover is set to 0, in the first experiments at least, and the soil moisture is set to 0. Furthermore, the roughness lenght is set to 1 cm.

For boundary generation, a GRIB converter was written. It creates a HIRLAM standard type GRIB file needed for the HIRLAM system. At present, data from the Mars Climate Database (MCD) and Oxford Mars GCM are used for boundaries as well as initial conditions. They provide temperature and wind components on 25-σ levels and the surface pressure and temperature. These data sets do not include humidity, which is very small on the Mars anyway. Therefore the specific humidity is set to zero in the boundary files. The difference between these datasets are that the MGCM data is continuous and the MCD data is averaged. Thus, we are using more and more Oxford MGCM data.

3 Results

For the test runs, we chose the simulation area to cover VL1 and Pathfinder landing sites. Reason for this is that there have been made real observations and we have good data to compare our model with. Also we have the model results for previous 1-D and 2-D experiments to compare with. We have made simulations with different size areas consisting 66*50 to 194 * 140 gridpoints with 1° to 0.2° resolution (about 55 to 11 km). Time of the simulations was selected as Martian summer solstice (Ls=90) near the actual landing time of VL1 and Pathfinder. In vertical we have used 25 to 32 σ levels. Orography was taken from MCD 3.0 dataset with coarse 5.0° resolution, but we have also run the model with 1° topography from MGS's MOLA instrument data. Thermal inertia and albedo were taken from MGS's TES instrument with 2.0° * 2.0° resolution for coarse run and 0.5° * 0.5° resolution for nested runs. Initial and lateral boundary conditions were taken from MCD average data and Oxford Mars GCM continuous data with 5.0° resolution. We have got good results from our simulations. For example in figure 1 a) we see great surface temperature differences during the sunrise. That is very realistic behavior of regolith. The figure 1 b) presents diurnal cycle of boundary layer. Observed night time inversions were simulated fairly well.

a) b)

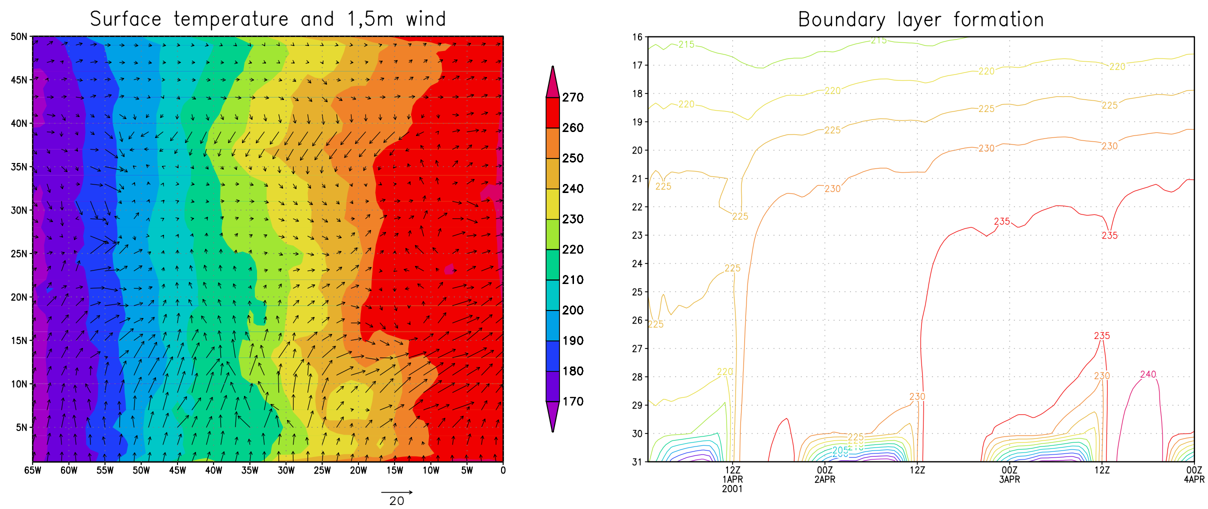

Figure 1: Some results from VL1/Pathfinder simulations. Time is given at 0 ° longitude. a) Surface temperature and lowest level (1.5m) winds at 12 o'clock. b) Diurnal cycle of boundary layer at Pathfinder landing site (19.3 °.N, 33.5 ° W). Top of the picture is about 2.3 km above the ground.

4 Conclusions

We have now the fourth working Mars 3D mesoscale model and the only European one. We have taken part in an intercomparison of all Mars 3D-models and our results have been presented in an international Mars modelling workshop in Granada in January 2003. We will continue MLAM's development. Near-future model developments include implementation of CO_2 and H_2O condensation/sublimation as well as dust and water transport processes. We will add the effects of variable topography to the radiation code. Due to new Mars missions (Mars Express/Beagle2, 2 NASA's MERs) in very near future we will have new data to compare with. Future regions of interest include Beagle 2 and other future mission sites, Hellas and Argyre basins, Valles Marineris and the polar regions. The figure 2 presents predicted diurnal surface pressure cycle at Beagle 2 landing site (10.6 °N, 90 °E).

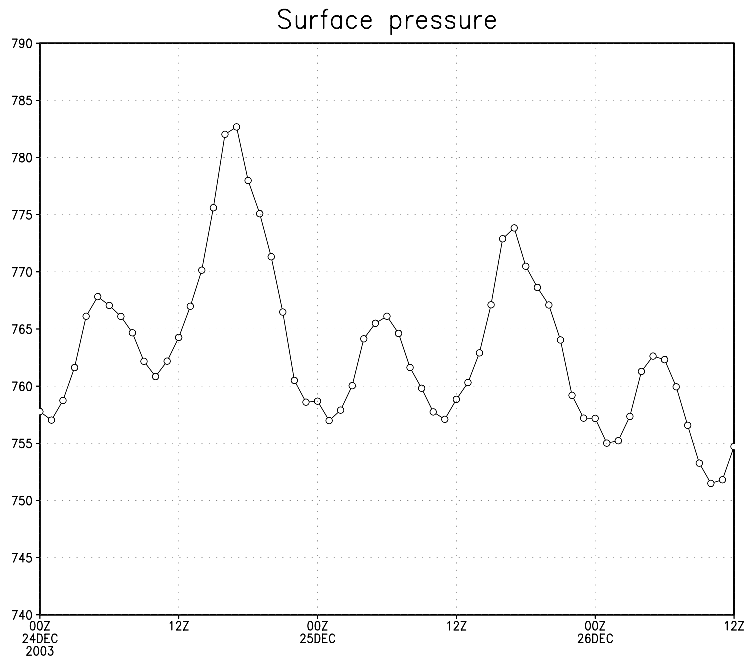

Figure 2: MLAM's predicted surface pressure cycle at Beagle 2 landing site (10,6 °N, 90 °E) Pressure in Pascals(Pa).

Acknowledgements

Hannu Savijärvi (UH), Tero Siili (FMI), Simo Järvenoja (FMI)

References

Lewis, S. R., M. Collins, P. L. Read, F. Forget, F. Hourdin, R. Fournier, C. Hourdin, O. Talagrand and J.-P. Huot, 1999: A climate database for Mars. *J. Geophys. Res.*, **104**(E10), 24177–14194.

Rafkin, S., R. Haberle and T. Michaels, 2001: The Mars regional atmospheric modelling system: Model description and selected simulations. *Icarus*, **151**(2), 228–256.

Savijärvi, H. and T. Siili, 1993: The Martian slope winds and the nocturnal PBL jet. *J. Atmos. Sci.*, **50**, 77–88.

Savijärvi, H., 1991a: A model study of the PBL structure on Mars and the Earth. *Beiträge zur Physik der Atmosphäre*, **64**(3), 219–229.

Savijärvi, H., 1991b: Radiative fluxes on a dustfree Mars. *Beiträge zur Physik der Atmosphäre*, **64**(2), 103–112.

Toigo, A. D. and M. I. Richardson, 2002: A mesoscale model for the Martian atmosphere. *J. Geophys. Res*, **107**(E7).

Tyler, D. J., J. R. Barnes and R. M. Haberle, 2002: Simulation of surface meteorology at Pathfinder and VL1 sites using a Mars mesoscale model. *J. Geophys. Res*, **107**(E4).

Atmospheric Modeling Training in RSHU

Kourzeneva K., Aniskina O., R. Repinskaya
Russian State Hydrometeorological University

1 Introduction

The atmospheric modeling course in RSHU is done for IV and V year students. The main purpose of the course is to give students the knowledge conserning atmospheric modeling mainly in the area of NWP. The background for the course are the courses in different brunches of mathematics, physics, dynamical meteorology, programming. So, this course should combine all this brunches of knowledge.

2 Contents of lecture course for year IV students

Grid method:

The theoretical aspects of numerical problems: order of approximation, stability, numerical mode, dispersion errors, aliasing errors. Those aspects are displayed on the base of linear and non-linear advection equations, adaptation equations for different grid schemes.

Different types of models and numerical methods for them:

Filtered models (vortex and divergence equations). Historically they were the first, on their base methods to convert the Laplasian are displayed.

Barotropic (shallow water) model. It is the basic educational model: staggered (in time and in space) grids, different numerical schemes on grids, splitting method, explicit - implicit - semi-implicit methods, box-method, semi-Lagrangian method, integral invariants, filters are displayed on the base of shallow water model equations.

Baroclinic models. Different coordinate systems in vertical - arbitrary, pressure, sigma, hybrid; in horizontal - Cartesian (on different map projections), spherical, rotated spherical; different types of lateral boundary conditions, the algorithms of system of equations integrating.

3 Contents of lecture course for year V students

Spectral method:
Base functions, used in atmospheric models, methods to obtain the determinative system of equations, pseudo-spectral method, methods to solve the non-linear equations: spectral, spectral-grid transformation.
Finite elements method.
Model physics (parameterizations)
(the basic approaches, some concrete algorithms):
Turbulence in free atmosphere and PBL;
Convection: convective adjustment, Kuo scheme
Land-surface block

Radiation
Non-convective condensation and precipitation.
Digital filter.
TVD-schemes.

4 Practical course

For those who do not specialize in modeling to write the program code for:
numerical solution of linear advection equation for different explicit schemes + theoretical analysis for the scheme;
Fourier transform.
For those who specialize in modeling to write the program code for numerical solution of:
linear advection equation for implicit schemes - the sweep method;
the barotropic vortex equation by iteration methods;
linear/nonlinear advection equation by various spectral methods;
the shallow water equations (the simplest methods).

5 Final works: Bachelor, Master, Speshialist's

Students get bachelor degree and perform their final bachelor work after 4 years of study, Master degree and final muster work after 6 years. "Speshialist" is the old, but at the same time very popular Russian standart, it is something average between Bachelor and Master. Students study for 5 years, and then perform their final work.
The problem for any final work desired to be dangling and the student should attain the concrete final result, much attention is paid to this issue.
Examples of final works:
To make the code and numerical experiments with shallow water model, use some complicated methods.
Different applications for shallow water model: for the sensitivity theory, TVD and monotone schemes, tropical cyclones.
There is the educational atmospheric model in the university: some parameterization blocks were made by our students during their final works, they make works to solve different numerical problems, make numerical experiments.
Since last year we use HIRLAM for the final works of the students, this activity is in progress.

6 Questions, Problems

At the moment we need to update the course of parameterizations, it is the large amount of methodical work. It is difficult to find the best way of presentation of parameterizatons algorithms for students, it should be concrete enough, but without unwanted details.
At the moment there is no course of data assimilation and analysis.
There is the psychological problem - the gap between basic course of numerical mathematics and modeling (but almost no gap between physics, dynamical meteorology and modeling). It is difficult for young person to go from abstract tasks to concrete ones.
Students have bad background in programming, the reasons are bad equipment and psychological problem.
We have great amount of students, so most of final works are training, not scientific, that is useful for students, but useless for supervisor's scientific work.

Numerical Methods and Modelling at the Division of Atmospheric Sciences at University of Helsinki

Sami Niemelä
Division of Atmospheric Sciences
Department of Physical Sciences
University of Helsinki

Hannu Savijärvi
Division of Atmospheric Sciences
Department of Physical Sciences
University of Helsinki

1 Introduction

There is only one university in Finland, University of Helsinki, which provides education and degrees in the field of meteorology. All courses are given by the Division of Atmospheric Sciences at Department of Physical Sciences. Our education covers widely different areas of meteorology: numerical models of the atmosphere, measurement techniques (e.g. in situ and remote sensing), climatology, micrometeorology and atmospheric chemistry among others. In this summary we will concentrate on education of numerical modelling.

2 Education of numerical methods

The practical numerical methods are mainly teached in three courses, Numerical meteorology I–II and Numerical laboratory, which basically is working course. Our students usually get the theoretical background of dynamics, thermodynamics and turbulent processes during their first three years of studies.

Numerical meteorology I is aimed for the 3rd year students. The course gives the basic knowledge about the different methods of the atmospheric models. First, there is a physics section, which covers the treatment of turbulence, condensation, convection and radiation. After that there is a dynamics part including basic numerical methods (e.g. finite differencing, time integration methods). This course has a few very simple numerical exercises of above topics.

Numerical meteorology II is a more advanced data assimilation course. It explains the principles of optimal interpolation, 3DVAR- and 4DVAR-methods. Also different initialization methods are studied. So far this course has not included practical numerical exercises. At the moment, theoretical exercises have got more emphasis.

Besides with courses above, occasionally some models are used also in other courses. For example, our division's 2-dimensional mesoscale model was used in mesometeorology-course. However, this additional use of models usually depends on the lecturer.

3 Numerical laboratory

The course, which involves the real practical work with numerical models, is the Numerical laboratory (Numlab). This course has been active from the mid 70's. The main idea of this course is that the group of 3-5 students solve different problems with a given model. Numlab is held every other year. The topics change from year to year (e.g. general circulation, NWP and atmospheric chemistry). The last three subjects were the stratospheric ozone model (1997), HIRLAM (1999) and lower tropospheric chemistry model (2001).

Hirlam was used first time in the Numlab-course in 1999 (Rontu and Ruosteenoja, 2000). The basic idea was that all groups concentrate in their own topic, which could be quite unconventional. This requires quite deep investigation of some specific model routines. In 1999 the Hirlam-course contained 5 themes: consequences of a large-scale forest fire, removing the Scandinavian mountains, the surface energy balance during an artificial ice age, the simulation of a solar eclipse and the influence of anomalies in the sea surface temperature on the cyclone development.

The feedback from the students usually indicate that the Numlab-course is very interesting and usefull, although quite laborious. The course is also advantageous for model developers, because the thorough studing of different methods very often reveal some unexpected problems and bugs from the code. Therefore, these courses also give some additional benefit as a form of a bug report.

References

Rontu, L. and K. Ruosteenoja, 2000: HIRLAM in the Numlab course at the University of Helsinki. *HIRLAM newsletter*, **35**, 20–22.

The planetary boundary layer parameterization for the climate modeling with emphasis to the high latitudes

Vladimir F. Romanov,

Arctic and Antarctic Research Institute, St.-Petersburg, RUSSIA.
e-mail: romanov@aari.nw.ru

Correct modeling the Arctic climate circulation structure (CCS) (that is bordered from the south by the climatic sub-polar frontal zone, for example, [*Glansdorff and Prigogine, 1971*, *Nicolis and Prigogine*, 1977, *Romanov et al.,* 1979, *Mokhov* and *Petukhov,* 1989], where the typical synoptic-scale circulation patterns accumulated during climatic periods and show the quasi-decadal oscillations in many parameters) represents very topical problem of the climate theory while most of the climate models do not reproduce these oscillations correctly. Meanwhile realistic reproduction of the planetary heat energy sink within the Arctic greatly defines realistic modeling the atmospheric baroclinity, sub-polar frontal zone and its stability, activity of the synoptic eddy meridional exchange and finally the global circulation and climate. In a high degree this modeling is through the sufficiently correct parameterization of the turbulence within the planetary boundary layer (PBL) that is responsible for the surface energy (mass) exchange, horizontal atmospheric baroclinity and energy redistribution in the Arctic/Antarctic atmosphere.

Present parameterization scheme (PS) of the atmospheric planetary boundary layer (APBL) is aimed at application to the global circulation and climate models (GCM) and in difference to other PS is focused at the main key points allowing the economical and correct modeling of the APBL, its interaction with different surfaces and including significant peculiarities of the high latitudes. Instead of the widely used PS in many GCM where parameterization is based on the Monin-Obukhov similarity [e.g., *Boer et al.*, 1984; *Schubert et. al.*, 1993; *Kiehl et. al.*, 1998] that is developed just for the surface layer (SL) and does not connect the GCM variables independent of the APBL turbulence with the APBL local variables driven by turbulence this scheme is based on the advanced similarity theory [*Romanov*, 1977] that connects the APBL boundary parameters (unaffected by turbulence) with the turbulent APBL variables. This scheme closure is through the surface energy and mass balance [*Romanov*, 1976c] and guarantees modeling of the important energy and mass sources/sinks and local conservations, the natural modeling of the typical Arctic/Antarctic winter temperature inversions as well as the convectively unstable stratification. The similarity connections of the GCM variables [the PBL external parameters (EP) with the near surface local turbulent parameters and profiles, the PBL internal parameters (IP)] are through the universal dimensionless functions (UDF) that depend only on two dimensionless numbers and easily approximated. These UDF are the universal solution of the APBL and the oceanic PBL (OPBL) nonlinear multilevel numerical models where formulation corresponds to present similarity. Effects of the baroclinity and mean vertical motions are described through additional UDFs that also depend on two numbers [*Romanov*, 1976b, 1977] and represent the dimensionless perturbations. Due splitting of to this UDF and account of the PS closure through the surface energy/mass balance, this PS describes the quasi-stationary variations in the boundary parameters. Scheme is accompanied with the advanced modeling of the energy conduction through the surface macro-scale quasi-laminar roughness sub-layer, of the radiation balance [*König-Langlo, Augstein*, 1994] and humidity stratification with respect to features of the high latitudes, etc. The OPBL modeling includes both temperature and salinity stratification. The latter is important account of the ice formation/melting. This PS has been applied to runs of the regional Arctic climate model and widely tested against different data showing good comparisons [for example, *Dethloff et al.*, 2000, *Makshtas et al.*, 2002]. While this PS produces realistic parameters, uses variables available as the current GCM output, or data and describes special Arctic features, it is rather economical and guarantees very good agreement with different data.

The APBL-OPBL IP connections with the EP (that are available as the current GCM output or data) are similar to the similarity [*Monin*, *Zilitinkevich*, 1967] for the stationary and horizontally homogeneous PBL, the Ekman PBL (EPBL). In present PS this theory has been improved describing the real, baroclinic and quasi-stationary PBL with respect to effect of the vertical mean circulation [Romanov, 1976b, 1977]. The APBL PS EP represent variables available from the bottom GCM level (for example the 850 mb level that is yet unaffected by turbulence), G_Z, wind, θ_Z, the potential temperature and the specific humidity h_Z. The surface is characterized by the macro-scale surface roughness length z_0 (available as a constant for different underlying surfaces [*Zilitinkevich*, 1970]). Additionally the known quasi-constant parameters are the EP of the APBL similarity, f, the Coriolis parameter and $\beta = g/T_0$, the buoyancy constant (with g, acceleration of gravity and T_0, the constant air temperature in Kelvins). The near surface ($z=z_0$) temperature θ_0 (is defined through the surface heat balance) and humidity h_0 (as the saturated humidity determined through the known surface pressure P_0 and temperature θ_0) determine the temperature and humidity jumps through the APBL thickness z=H, $\Delta\theta = \theta_H - \theta_0$, $\Delta h = h_H - h_0$. These EP determine the dimensionless numbers, $Ro = G/fz_0$, the Rossby number and $S = \beta\Delta\theta/fG$, $S_h = \kappa(g/\rho_0)\delta h\rho_0/Gf$, the integral temperature and humidity stratification numbers respectivelly where κ is the Von Carman constant and ρ_0 is the constant surface air density. Using these numbers the APBL similarity determines the APBL IP,

$$u_* = \kappa G\mathbf{X}(\mu, \lg Ro),\ \ \alpha = \mathrm{A}(\mu, \lg Ro),\ \ \mu = \Theta(\lg S, \lg Ro),\ \ H = L\gamma(\mu),\ \mu = L_0/L = -\kappa^2\beta q/c_p\rho_0 f V_*^2,$$
$$q = -\alpha_T c_p\rho_0 k(\partial T/\partial z + \gamma_e),\ \ \mu_h = \mathbf{\Theta_h}(\lg S_h, \lg Ro),\ \ q_h = -\rho_0\alpha_h k\, \partial h/\partial z, \qquad (1)$$

with u_* and α as the surface friction velocity and direction (reflecting the surface turbulent momentum flux), μ and μ_h are the local APBL temperature and humidity stratification parameters, $L_0 = \kappa u_*/f$, is the Monin-Kazansky (1960) EPBL scale, H is the APBL thickness, lg is the decimal logarithm, c_p is specific heat of air at constant pressure, γ_e [=0.006 °C/m] is the constant equilibrium vertical temperature gradient, α_T and α_h are the dimensionless ratios for heat and momentum (k) and for humidity and momentum diffusivities taken as 1 [*Monin and Yaglom*, 1971], **X, A, Θ,** γ and $\mathbf{\Theta_h}$ are the UDF as the universal solution of the PBL numerical model and verified against different data [*Romanov et al.*, 1979].

The surface heat balance equation at the surface roughness level z_0 closes this system (the surface humidity balance could be used instead of the assumed surface saturated humidity, if the precipitation rate is known from the GCM runs, or from data),

$$q_0 + Lq_h + q_S = R_0 + l\,\rho_{i,s}\, h^t_{i,s}\Theta(\theta_0), \qquad (2)$$

where q_0 is the surface turbulent sensible heat flux, Lq_h is the evaporation heat loss, L is the latent heat of vaporization/sublimation, q_S is the heat flux from the surface through the surface quasi-laminar sublayer $z\in[0,z_0]$, R_0 is the surface radiation balance and $l\rho_{i,s}h^t_A\Theta(\theta_0)$ is the energy loss to melting snow or ice, where l is the latent heat of fusion, $\rho_{i,s}$ is the mass density for ice or snow, respectively, $h^t_{i,s} = \partial h_{i,s}/\partial t$ is the rate of change of the thickness of the ice (snow) cover and $\Theta(\theta_0)$ is the Heaviside function: $\Theta(\theta_0) = 0$ for $\theta_0 < 0^oC$, and $\Theta(\theta_0) = 1$ for $\theta_0 \geq 0^oC$.

The heat flux q_S comes as a solution of the molecular heat conduction equation using the heat flux from the surface at level z=0. If the temperature contrast in sub-layer z_0 is too large (empirical known extreme), then the smallest turbulent mixing $k = \kappa u_* z_0$ is used instead of the molecular diffusivity and model the intermittent turbulence in the locally broken macro-scale roughness sub-layer. The surface radiation balance is defined through the known solar radiation and macro-scale surface albedo [*Kukla, Robinson*, 1994], but the infrared radiation is detfined through empirical scheme [*König-Langlo, Augstein*, 1994] respecting the cloudiness and specific high latitude constants. The heat flux at the z_0 bottom, or at the top of the surface comes as a solution of the heat conduction equation for the underlying land, ice and snow surfaces, but if the OPBL is below the drifting sea ice, or represents the ocean free surface, the PS includes modeling of the OPBL. The OPBL similarity is similar to the APBL similarity while instead of the humidity stratification the salinity stratification is described. The total temperature and salinity integral and local stratification parameters represent their sums following the nonlinear equation of the seawater state. The OPBL EP represent the nonlocal parameters, the surface flow (seaice drift) velocity known from the GCM, or from climate data), macro-scale ocean surface (ice bottom surface) roughness as well as the temperature and salinity below the OPBL (known from the ocean GCM, or from data). The OPBL PS is closed and connected with the APBL scheme through the surface (free ocean surface, or the seaice bottom surface) heat and salinity balances where the surface heat and salinity turbulent fluxes are balanced by the corresponding boundary fluxes known from connection of the OPBL and APBL problems. The rate of change of the ice/snow melting (APBL bottom) and of the ice melting/formation (OPBL top) follow as the balance residuals to satisfy this balance. All connections introduce into the interactive nonlinear APBL-OPBL system many feedbacks. Adjustment of the APBL-OPBL is through special approximations. For example, the first step gives the APBL and OPBL thickness where G_Z, θ_Z, h_Z and water temperature and salinity are extrapolated through usual linear profile. This evaluates horizontal distribution of θ_0, h_0, etc. in the GCM grid points and determines the baroclinity parameters and the UDF corrections describing the baroclinity effect. Distribution of the surface turbulent momentum flux determines the Ekman regular vertical velocity and the corresponding UDF corrections describing this effect. Local surface energy and mass imbalances and the integral PBL mass imbalance determine the rate of APBL/OPBL thickness changes to correct the Monin-Kazansky scale to the real APBL-OPBL thickness. Additional unit describes the typical elevated temperature inversions in vicinity of the APBL top as the joint solution of the coupled local APBL turbulent kinetic energy (TKE) balance and the large-scale heat balance equation above the APBL (information on the heat advection and diabatic sources comes from the GCM). Special UDF parameterize the vertical profiles of different turbulent variables.

The APBL and OPBL nonlinear multilevel numerical models [Romanov, 1976a, b] are used determining the UDF where closure is through the TKE balance, the Von Carman hypothesis (generalized for the stratified PBL) and flux of heat (moisture, salinity) comes as a solution of the differential heat (mass) balance equation. Vertical logarithmic resolution is very high. The advanced PBL models with very high resolution, modeling the nonstationary PBL and including the second order correlations like the TKE dissipation rate; the pressure-velocity correlations, etc. represent the excessively complex tools for the climate runs of the GCM. Moreover, these models often need too detailed information characterizing the surface, which is unavailable for the globe and for the climate periods. At the same time, these models often contain the insufficiently accurate modeling of the higher order correlations, many unknown coefficients, etc. At the same time the present APBL and OPBL models have produced the UDF, which are well compared to different data and show the sufficiently accurate tools in resolution of the GCM.

This PS has been widely tested in the Arctic regional climate model runs against different aerosounding data. Results have been compared to different Antarctic field experiments for very complicated conditions. For example, these results comparisons with the North Pole data including the elevated inversions show better agreements number than the NCEP data for the same samples (moments and point positions).

References

Boer, G. J., N. A. McFarline, and R. Laprise, The climatology of the Canadian Climate Centre general circulation model Jan Mayen location shows that this region as obtained from a five-year simulation, *Atmos.–Ocean, 22,* 430–473, 1984.

Dethloff, K., C. Abegg, A. Rinke, I. Heberstadt, V. F., Romanov, Sensitivity of Arctic climate simulation to different boundary layer parameterizations in a regional climate model. –Tellus. 2000, 53 A, pp. 634-659.

Glansdorff, P., I. Prigogin, Thermodynamic Theory of Structure, Stability and Fluctuations *(Wiley Interscience NY),* 1971.

Kiehl, J. T., J. J. Hack, G. B. Bonan, B. A. Boville, D. L. Williamson, and P. J. Rash, The National Center for Atmospheric Research Community Climate Model: GCM3, *J. Climate, 11*, 1131–1149, 1998.

König-Langlo, G., E. Augstein, Parameterization of the downward long-wave radiation at the Earth’s surface in polar regions, *Meteorol. Z. 3*, 1994, 343-347.

Kukla, G., D. Robinson, Annual cycle of surface albedo, *Mon. Wea. Rev., 108*, 56–68, 1980.

Makshtas, A. P., V. F. Romanov, S. V. Shoutilin, Sensitivity of modeled sea ice to external forcing and parameterizations of heat exchange processes, Ice in the Environment: Proceeding of 16th IAHR International Symposium on ice, Dunedin, New Zealand, 2-6 December 2002, 76-85.

Mokhov, I. I., V. K. Petukhov, Space-time climatic structures, Preprint, USSR Academy of Sciences, Institute of Atmospheric Physics, Moscow, p.1 and p 2, 99 p., 1989.

Monin, A. S., and S. S. Zilitinkevich, Planetary boundary layer and large-scale atmospheric dynamics, *Proc. GARP Study Conference,* WMO, Stockholm, 73–77, 1967.

Nicolis, G., I. Prigogine, Self-Organization in Nonequilibrium Systems: From Dissipative Structures to Order through Fluctuations *John Wiley & Sons NY,* 1977.

Romanov, V. F., Vertical motions and turbulence in the planetary boundary layer, *Izv. Acad. Sci. USSR Atmos. Oceanic Phys., 12*, 478–484, 1976a.

Romanov, V. F., Turbulence in the ocean boundary layer under the ice cover, *Oceanology, 16*, 32–40, 1976b.

Romanov, V. F., Parameterization of the nonlinear small-scale air-sea interaction with allowance for ice cover, *Meteorol. Hydrol., 12,* 39-56, 1976c.

Romanov, V. F., Similarity theory for baroclinic planetary boundary layer, *Izv. Acad. Sci. USSR Atmos. Oceanic Phys., 13*, 739–743, 1977.

Romanov, V. F., N. V. Ariskina, V. F. Vasiliev, V. E. Lagun, Energetics of the atmosphere in polar regions (in Russian), *Gidrometeoizdat*, Leningrad, 296 pp, 1987.

Schubert, S. D., R. B. Rood, and J. Pfaendtner, An assimilated data set for Earth science applications, *Bull. Amer. Meteorol. Soc., 74*, 2331-2342, 1993.

Assessing the Role of Observational Errors in Data Assimilation: Experiments with a Global Data Assimilation System

M.Tsyroulnikov, M.Tolstykh, R.Zaripov, and A.Bagrov

Russian Hydrometeorological research centre, Moscow, Russia

Introduction. The relative roles of different sources of errors (observational, model, and analysis-technique errors) in atmospheric data assimilation and forecasting are still unclear. The present research is intended to shed some light onto this problem. We propose an approach to experimental investigation of the role of observational errors in data assimilation. The approach is an extension of the OSE and OSSE methodologies.

Methodology. A simple theory is proposed for a stationary dynamical system in order to gain some insight into a more complicated realistic case and to help design numerical experiments with a realistic data assimilation system (DAS). For simplicity of presentation, we assume that the dynamical system is scalar.

Consider the standard *"analysis–forecast" suite*. At each discrete analysis time, t_n, the analysis, X^a, is

$$X_n^a = X_n^f + K_n(X_n^o - X_n^f), \tag{1}$$

where X_n^f is the "first guess" (the forecast started from the previous analysis, X_{n-1}^a), K_n denotes some pre-specified analysis gain matrix, and X_n^o are ("linear") observations:

$$X_n^o = X_n + \eta_n, \tag{2}$$

where X_n is the truth and η_n denotes the random observation error.

The forecast (analysis first guess) is accomplished using a forecast model, $M(X)$, so that

$$X_{n+1}^f = M(X_n^a). \tag{3}$$

This completes our description of the assimilation suite. Now, turn to *assimilation errors*.

Analysis error, δX^a, as it follows from Eqs. (1) and Eq. (2), comes from two sources: forecast error, δX^f, and observation error, η. Subtracting X_n from both sides of Eq. (1) and using Eq. (2) yields the following equation for the analysis error:

$$\delta X_n^a = (1 - K_n)\delta X_n^f + K_n\eta_n. \tag{4}$$

The forecast error also has two sources: an error in the analysis from which the forecast starts and the forecast-model imperfection. The model imperfection means that, being applied even to the true state, X_n, the forecast model produces a forecast at the next analysis time, $M(X_n)$, that *differs* from the true state, X_{n+1}, at that time: $M(X_n) = X_{n+1} + \xi$, where ξ is called the model error. Consequently, while the forecast is given by Eq. (3), the true state evolution is governed by the equation

$$X_{n+1} = M(X_n) - \xi. \tag{5}$$

Subtracting (5) from (3), expanding $M(X_n)$ in the Taylor series around X_n^a, and retaining only the first-order term in the series, yields the approximate forecast-error evolution equation:

$$\delta X_{n+1}^f = A_n \delta X_a^n + \xi, \tag{6}$$

where A_n is the Jacobian of M (the tangent linear model) evaluated at X_n^a. Thus, the error evolution in the DAS is governed by Eqs. (4) and (6).

Next, assume *stationarity* and analytically find the steady-state first-guess error variance as a function of the parameters of our simple DAS. We suppose that A_n, K_n, and all the error variances do not depend on n and ξ and η are not biased. If, furthermore, analysis, that is, K is not flow-dependent, then computing the variances of Eqs. (4) and (6) yields a system of two linear algebraic equations with respect to analysis and first-guess error variances. We easily solve this system, getting the stationary forecast-error variance:

$$\sigma_f^2 = \frac{Q}{1 - A^2(1-K)^2} + \frac{A^2 K^2}{1 - A^2(1-K)^2}\sigma_o^2. \tag{7}$$

Here σ_o stands for observation-error standard deviation and Q for model-error variance. We note that the stationary solution exists if and only if $|A(1-K)| < 1$. This latter condition is certainly satisfied for realistic atmospheric data assimilation, at least on average.

From Eq.(7), it follows that the first-guess error variance *linearly* depends on the observation-error variance. Therefore, to assess the potential benefit from nullifying the observation-error variance, it obviously suffices to plot a σ_f^2 versus σ_o^2 graph and simply extrapolate it to zero σ_o^2. That this graph is linear for the stationary system, suggests that the extrapolation will be well posed in the realistic (nonlinear and nonstationary) case, too.

We observe that with real observations, we cannot *reduce* their errors. Instead, we propose to *enhance* the observation errors (add artifical noise with the standard deviation σ_{added}), assimilate them in a DAS, then plot the above graph, σ_f^2 versus $\sigma_o^2 + \sigma_{added}^2$, for different noise variances, σ_{added}^2, and finally extrapolate the graph to zero total (real plus superimposed) observation-error variance. This is the main idea of our approach and the essence of our *experimental methodology*.

The DAS we used in the experiments is presented in (Tsyroulnikov et al. 2003) and is based on an optimum interpolation (OI) analysis and a semi-Lagrangian numerical weather prediction model. The numerical methods used in constructing the dynamical core of the forecast model are described in detail in (Tolstykh 2002 and Tolstykh 2001). The model resolution is 1.125° lat, 1.40625° lon, and 28 sigma levels. The time step is 36 min. The analysis step is based on the incremental approach (to assimilate upper-air observations). Also, we utilize a sequential assimilation: first, are assimilated the near-surface observations and, second, the upper-air observations. The assimilation step is 6 hours. Our DAS was tested for a period of several months and demonstrated an acceptable performance (see Tsyroulnikov et al. 2003 for some results).

Numerical experiments. In compliance with the above methodology, we perturb available observations. The noise variances are set to be proportional (with the proportionality coefficient α) to the estimates (known from the literature) of real observation-error variances. Thus, the total (real plus imposed) error variance is proportional to $1 + \alpha^2$.

Two experiments were conducted. In the first one, only radiosonde observations (TEMP) were perturbed. In the second experiment, perturbations were added to all used upper-air observations: TEMPs (radiosondes), PILOTs (wind balloons), AIREPs (aircraft winds), SATEMs (retrieved layer thicknesses from satellites), and SATOBs (cloud-motion winds).

We let α vary from 0 to 4 and plot the assimilation first-guess error total energy against $1 + \alpha^2$. On Fig.1, we display the resulting error curve (see figure caption) for perturbed radiosonde observations (the first experiment). The results for the second experiment, being qualitatively similar, are not shown.

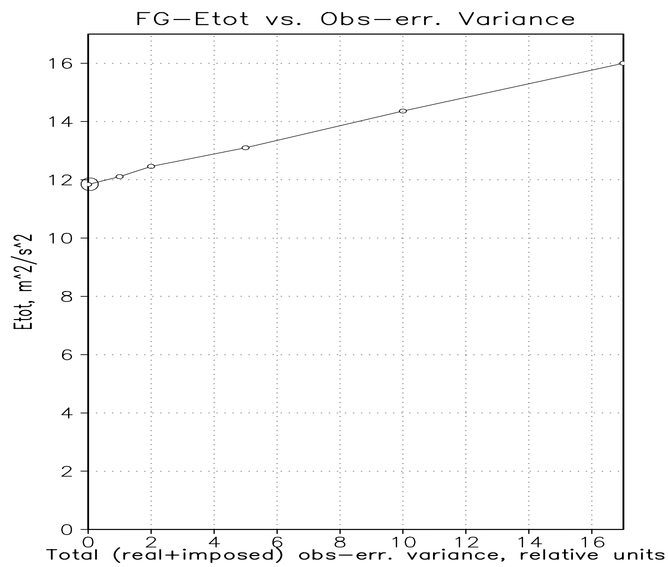

Figure 1: Assimilation error total energy (as computed against unperturbed radiosonde observations) vs. total (real plus added) observational (radiosonde) error variance. The extrapolated value is indicated by a big circle.

One can see that the resulting curve is surprisingly linear in accordance with the simple linear theory presented above. The main conclusion that can be drawn from Fig.1 is that decreasing the observation-error variance to zero would lead to a *very small decrease in the assimilation-error variance* (about 2 per cent). As a result, a very little effect is expected from improving the accuracy of the observational systems examined in this study.

Conclusions. We have proposed an experimental methodology to assess the role of observational errors in data assimilation: add pseudo-random errors to real observations, then run an assimilation cycle, assess the assimilation error with respect to the unperturbed observations, and plot an assimilation-error variance (total energy) against the variance of total (real + added) observational errors. Finally, extrapolate the resulting error curve to zero error variance. In this way, one can obtain an estimate of the potential benefit of improving the accuracy of observations in operational data assimilation.

The experimenatal results suggest that with the existing observational networks examined in this study, there is little sense to further improve their observational (measurement) accuracy. It would be more efficient to allocate resources in increasing the spatial and temporal resolutions of the observational systems. With the existing observational systems, almost all the data assimilation errors are due to model errors and the sub-optimality of the analysis scheme used. Because it is known that the change from OI to 3D-Var and even 4D-Var is not accompanied with immediate dramatic improvements in the quality of data assimilation (see Cohn et al. 1998, Courtier et al. 1998, Lindskog et al. 2001, Rabier et al. 2000, and others), we anticipate that the main conclusion of this work remains valid for more advanced assimilation techniques, at least for the observational types studied.

This work has been partially supported by the Russian Foundation for Basic Research (grants 01-05-64582 and 03-05-06054mas) and by the French-Russian A.M. Liapunov Centre (project 02-05).

References

Cohn S.E., Da Silva A., Sienkiewicz M., Lamich D. Assessing the effects of data selection with the DAO physical-space statistical analysis system. - Mon. Weather Rev., 1998, v. 126, 2913-2926.

Courtier P., Andersson E., Heckley W. Pailleux J., Vasiljević D., Hamrud M., Hollingsworth A., Rabier F. and Fisher M. The ECMWF implementation of three-dimensional variational assimilation (3D-Var). 1:Formulation. - Quart. J. Roy. Meteorol. Soc., 1998, v.124, 1783-1807.

Lindskog M., Gustafsson N., Navascués B., Mogensen K.S., Huang X.-Y., Yang X., AndræU., Berre L., Thorsteinsson S. and Rantakokko J. Three-dimensional variational data assimilation for a limited area model. - Tellus, 53A, 2001, N4, P. 447-468.

Rabier F., Järvinen H., Klinker E., Mahfouf J.-F. and Simmons A. The ECMWF operational implementation of four-dimensional variational assimilation. I: Experimental results with simplified physics. - Quart. J. Roy. Meteorol. Soc., 2000, v. 126, 1143-1171.

Tolstykh M. Semi-Lagrangian high resolution model for numerical weather prediction. - Russian Meteorology and Hydrology, 2001, N 4, 1-9 (Russian and English).

Tolstykh M. Vorticity-divergence semi-Lagrangian shallow-water model on the sphere based on compact finite differences. - J. Comput. Phys. 2002, v. 179, 180-200.

Tsyroulnikov M.D., M.A.Tolstykh, A.N.Bagrov and R.B.Zaripov. Development of a variable-resolution global data assimilation system. - Russian Meteorology and Hydrology, 2003, N 4 (Russian and English).

Variable resolution model of Russian Hydrometeorological Research Centre

Mikhail A. Tolstykh

Institute of Numerical Mathematics, Russian Academy of Sciences
and
Russian Hydrometeorological Research Centre
email: tolstykh@inm.ras.ru

1 Introduction

The increase of resolution of complete 3D atmospheric models is one of major ways to improve the forecast quality. It is expensive to increase the resolution over the whole globe. For example, doubling the horizontal resolution increases the wall-clock -time of model integration by a factor of 6-8, depending on numerical design of the model. If we are interested in relatively short range forecasts, one can consider an atmospheric model with high resolution in the region of interest only.

There are two ways of doing it: a regional limited-area model and a global variable-resolution model with locally high resolution. There are pros and contras in both approaches. In particular, a global variable-resolution model is free from the problems with posing lateral boundary conditions. It is also easier to implement data assimilation system with a global model.

Russian territory is stretched along longitude, and the most part is located north from 48 N. As the meridians of the spherical coordinate converge towards the poles, the longitudinal resolution increases while approaching the pole. There are only 3 NWP centres in Russia (Moscow, Novosibirsk, Khabarovsk), only two of them with research teams, and there are limited resources for simultaneous development of two or more new models. The strategy at Russian Hydrometeorological Research Centre (RHMC) in Moscow is to develop a model with constant resolution for medium-range weather forecasts, and to apply the same model with variable resolution in latitude for short range forecasts. A model on the latitude-longitude grid with variable resolution in latitude can provide the local increase of resolution in this area by a factor of 2.2 with respect to the constant resolution version without significant deformation of the horizontal grid. This increase can be achieved at virtually no cost.

The SL-AV is a global semi-Lagrangian NWP model described in [2]. This model uses the absolute vorticity as a prognostic variable and compact high-order finite differences on the unstaggered grid. A detailed description of the numerics for the 2D version of the model is given in [3]. The model includes the parameterization package of subgrid-scale processes from the French operational model ARPEGE/IFS [1]. Also, there is a possibility to use the spherical coordinate system with rotated poles which is not used here.

The article describes recent developments of the SL-AV model which consist in increase of the horizontal resolution and implementing and testing the variable resolution in latitude. The undergoing work on implementing the reduced latitude-longitude grid is briefly described.

2 Effect of the increase of resolution in the constant resolution version of the model

Recent istallation at RHMC of 16 processors (4x4) Itanium2-based Linux cluster with Myrinet2000 connections enabled an increase of the horizontal resolution in the constant resolution version of the SL-AV model from 1.40625x1.125 degrees in longitude and latitude respectievly to 0.9x0.72. Both versions with 28 vertical levels were tested with the set of twelve 5-day forecasts starting at 15th day of each month 1996, 0000 UTC. The initial data were uninitialized ECMWF analyses. Fig. 1 shows definite improvement of forecast quality. Currently, the constant resolution version of the model wiht the resolution 0.9x0.72 degrees is in quasioperational testing at RHMC.

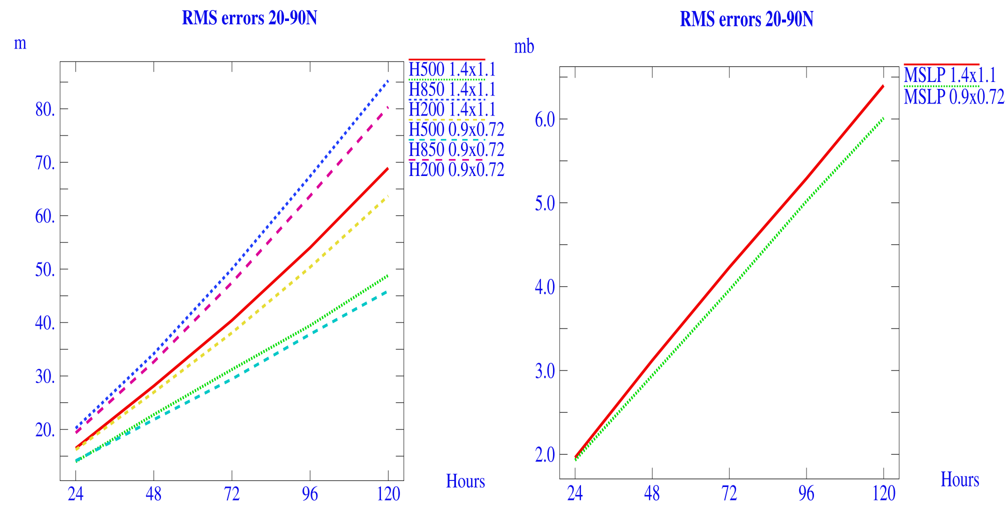

Figure 1: The averaged over 12 forecasts RMS errors in the region 20-90N for 200, 500, and 850 hPa geopotential (left) and mean sea-level pressure (right), different horizontal resolution of the model.

3 Forecasts with the variable resolution version of the model

The suggested approach for achieving locally high resolution in a global model, which is based on the SL-AV finite-difference model, allows to have an area of constant high resolution and at the same time use an efficient FFT-based algorithm for solving the systems of linear equations arising in the semi-implicit time stepping. The lack of variable resolution in longitude is partially compensated by the possibility to use a rotated spherical coordinate system. This possibility, though present in the model, is not used currently.

One can divide the task of implementing the variable resolution feature in the SL-AV model in two: implementation of the variable resolution in the semi-Lagrangian advection algorithm, and implementation of this feature for non-advective terms of the governing equations.

In the semi-Lagrangian advection part, it is necessary to implement changes related to the algorithm for search of the departure points of trajectories and interpolation on the variable resolution grid. The other parts of the model related to calculation of latitudinal derivatives (i.e. gradient, curl and divergence computations, reconstruction of velocity vector components) require more substantial modifications. The main goal here is to preserve high-order approximation along with minimization of the computational cost.

In this part, the variable resolution in latitude is implemented by introduction of an auxiliary coordinate (pseudolatitude) with constant step. The partial derivative in latitude φ of some function can be

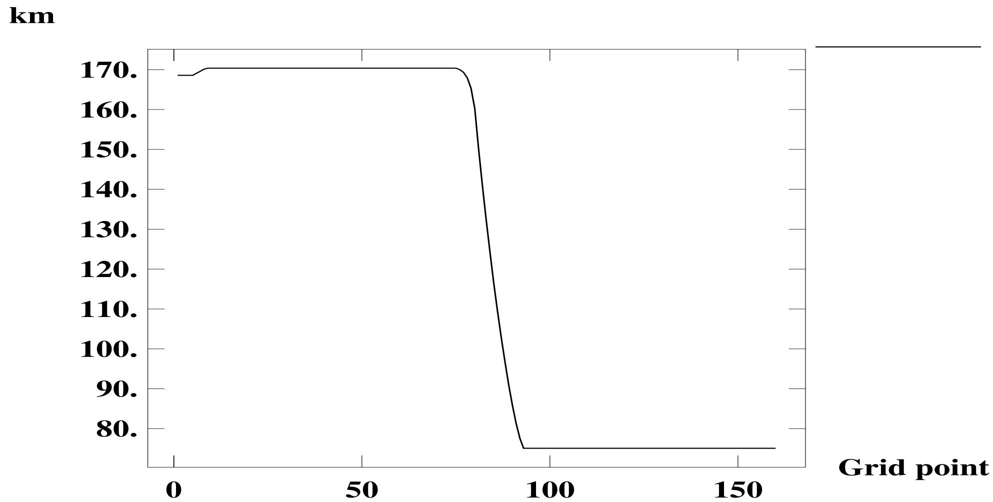

Figure 2: The latitudinal resolution as a function of gridpoint number. (from Southern pole to Northern pole)

written as

$$\frac{\partial f}{\partial \varphi} = \frac{\partial \varphi'}{\partial \varphi}\frac{\partial f}{\partial \varphi'},$$

where φ' is pseudolatitude, and $\frac{\partial f}{\partial \varphi'}$ is discretized as in the case of constant resolution. $\frac{\partial \varphi'}{\partial \varphi} = m$ is the map factor. All derivatives in this expression are discretized with the fourth order accuracy. Longitudinal derivatives are discretized as in the constant resolution case.

The way the latutidinal resolution is defined is a discrete coordinate transformation (given in the differential way, as a sequence of local map factors). This requires very moderate changes in the constant resolution code (introduction of map factors in computation of gradients, semi-implicit scheme etc) and also allows to preserve all compact differencing and its properties intact. The details of implementation of variable resolution in latitude are given in [5].

The variable resolution version of the 3D model was tested with the same set of twelve 5-day forecasts starting at 15th day of each month 1996, 0000 UTC. The initial data were uninitialized ECMWF analyses (truncated to T119 spectral resolution). Digital filter initialization was applied. The resolution was 1.40625 degrees in longitude, 28 irregularly spaced σ-levels and the time step was equal to 36 min, the same as for the constant resolution version. The resolution in latitude as a function of grid point number is depicted in Fig. 2. The high resolution ($\approx$ 75 km) zone is located between 30 and 90 N. The ratio between the adjacent mesh intervals does not exceed 1.065.

On Fig. 3 we present averaged over 12 cases root-mean squared (RMS) errors for 500, 850 hPa heights and mean sea-level pressure (MSLP) in the 50N-90N band for constant resolution (1.125 degrees) and variable resolution versions of the model.

It is known that the variable grid strategy is limited to the relatively short-range forecasts, since for medium-range forecasts, the high resolution region will come under influence of weather systems that at initial time are far away, and hence are poorly resolved in the analysis. Indeed, one can see that the variable resolution version is more accurate than constant resolution one up to approximately 84 hours range. At the same time, the RMS errors for ranges up to 72 hours are better by 1-2 m. The improvement is more visible in skill score (or gradient error) S1 (Fig. 4). In this case, the fields on variable resolution grid were interpolated to the constant resolution grid to enable the direct comparison.

Even beyond 84 hour range the errors of variable resolution forecasts do not grow too rapidly. The level of errors on the fifth day correspond to that of the model with constant resolution of 1.5 degrees in longitude and latitude [2].

It is important that the improvement of forecast quality is achieved virtually at no cost.

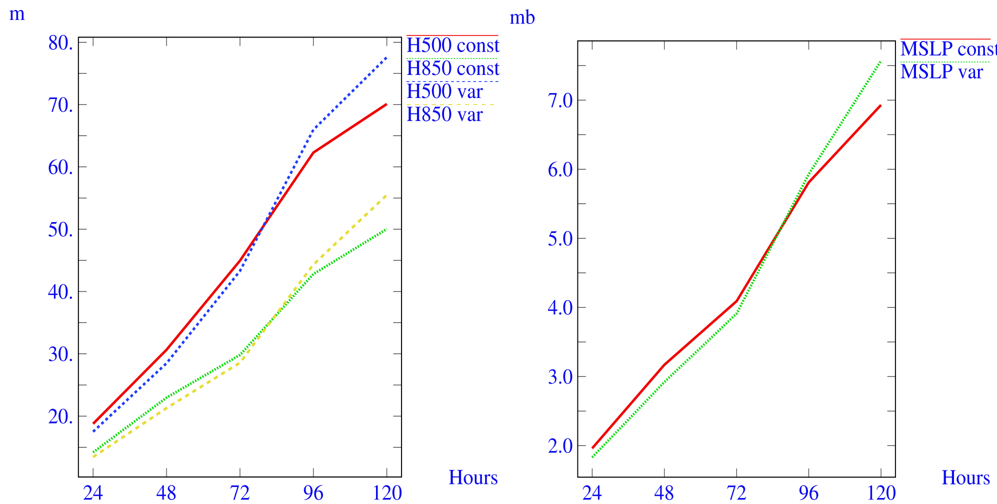

Figure 3: The averaged RMS errors for 500 and 850 hPa heights (left) and mean sea-level pressure (right) as functions of the forecast time.

4 Reduced latitude-longitude grid

A finite-difference atmospheric model formulated on a regular latitude-longitude grid has several drawbacks. Due to convergence of meridians, this grid has big nonuniformity of resolution in longitude and latitude near the poles (for the resolution 10 km in latitude, the mesh size in longitude near the pole would be about 150 m). This drawback leads to severe limitation on CFL number in Eulerian models, problems in use of parallel iterative solvers, and also to unapprovingly high expenses on calculation in ”wasted” grid points (about 25 % of total computation cost). The situation aggravates when one uses the variable resolution in latitude.

So for a high-resolution global finite-difference model it is necessary to implement a grid with the number of points along each latitudinal circle reducing while approaching the pole. The wide use of calculations in Fourier space in longitude inside the SL-AV model enables the application of such a grid. The implementation of the reduced grid in the SL-AV model can be split into four parts:

1. The implementation of the reduced grid in the blocks, which already use mixed Fourier-finite difference representation (semi-implicit integration time scheme, reconstruction of velocity field from vorticity and divergence, horizontal diffusion);

2. Calculation of the latitudinal derivatives arising in non-advective terms of atmospheric governing equations in space of longitudinal Fourier components;

3. The implementation of the reduced grid in grid-point semi-Lagrangian advection;

4. Rearrangement of computations for better load balancing in the parallel version of the model.

As a first step towards implementing the reduced grid, the filtering of high longitudinal wavenumbers was applied in the blocks, which already use mixed Fourier-finite difference representation (semi-implicit time integration scheme, reconstruction of velocity field from vorticity and divergence, horizontal diffusion). The number of retained waves in longitude gradually reduces while approaching the poles, subject to limitation caused by application of FFT. The calculation of these numbers for each latitudinal circle follows the methodology used in French spectral model ARPEGE. It turned out that some numerical noise can be seen if one uses the same numbers of waves (proportion vs. full number) as in ARPEGE. However, this noise disappears if one increases these numbers slightly. Thus we can conclude that the reduced grid on the sphere indeed can be used in a hybrid spectral-finite-difference model.

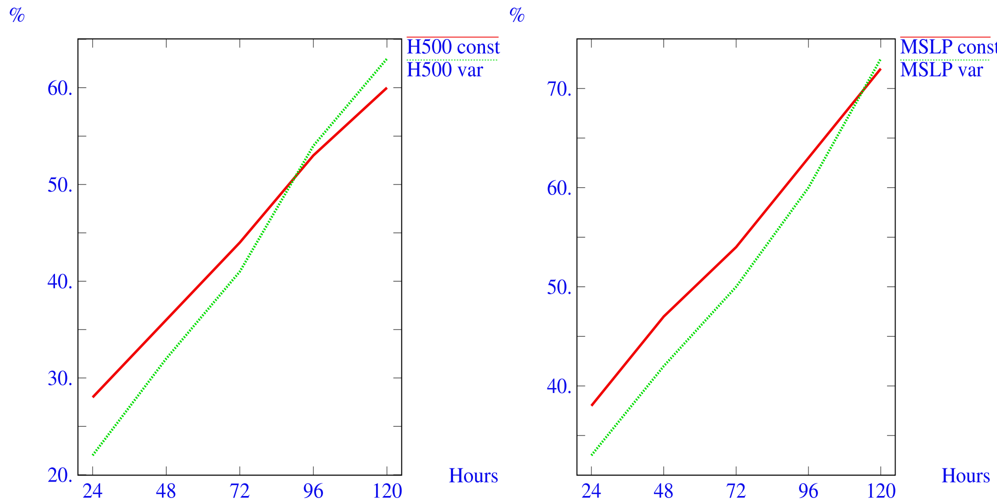

Figure 4: The averaged gradient errors S1 for 500 hPa height (left) and mean sea-level pressure (right) as functions of the forecast time.

5 Conclusions

Recent developments of the SL-AV model were presented. The variable resolution in latitude was implemented in the 3D global semi-Lagrangian finite-difference numerical weather prediction model SL-AV. The results from series of five-days forecasts with the 3D model show the benefit of using the variable resolution version of the model for three day forecasts over Russia. The work is underway to implement the reduced latitude-longitude grid in the model. The plans also include further increase in horizontal resolution and also testing a configuration with rotated poles and variable resolution for forecasts over European part of Russia.

This work was supported by the RFBR grant 01-05-64582 and French-Russian Lyapunov Institute grant 02-05.

References

[1] J.-F. Geleyn, E. Bazile, P. Bougeault *et al*, Atmospheric parameterization schemes in Meteo-France's ARPEGE N.W.P. model. In *Parameterization of subgrid-scale physical processes*, ECMWF Seminar proceedings (1994), 385-402.

[2] M.A. Tolstykh, Semi-Lagrangian high resolution model of the atmosphere for numerical weather prediction, *Russian Meteorology and Hydrology*, N4, 1-9 (2001). (Russian and English)

[3] M. Tolstykh, Vorticity-divergence semi-Lagrangian shallow-water model on the sphere based on compact finite differences, *J. Comput. Phys.* **179** (2002), 180-200.

[4] M.D. Tsyroulnikov, M.A. Tolstykh, A.N. Bagrov, R.B. Zaripov, Development of a global data assimilation system with variable resolution, *Russian Meteorology and Hydrology*, N4, 5-24 (2003). (Russian and English)

[5] M. Tolstykh, Variable resolution global semi-Lagrangian atmospheric model, *Russ. J. Numer. Anal. Math. Modelling*, **18** N4, 347-361.

Experiences from the pre-RCR runs at FMI

By Simo Järvenoja, Finnish Meteorological Institute

1 Introduction

In June 2003, the Hirlam Council approved a proposal made by FMI that FMI acts as the lead centre for maintaining a regular cycle of the HIRLAM Reference system (RCR), running the Reference system operationally under close surveillance by both scientists and duty forecasters.

Preparations for the RCR system at FMI started in summer 2003. Pre-operational runs have been carried out since August 2003, aiming at the operational status of the RCR system in early 2004. This write-up shortly describes the pre-RCR suites used and documents some preliminary results from these runs.

2 Parallel run set-up

The pre-RCR runs, based on the HIRLAM 6.1.2 version, have been run in parallel with the FMI operational HIRLAM 5.1.4 system since summer 2003. The runs have been conducted on the IBM at CSC. In the following, short descriptions for the FMI operational suite and the pre-RCR suites are given:

FMI operational suite, ATX (Hirlam 5.1.4) :

- 0.3° horizontal resolution, 40 levels in the vertical
- 256 × 186 grid points
- Semi-lagrangian advection, time step 450 s
- 3D-Var analysis (HL5.0.3)
- 6 h data assimilation cycle
- Cut-off time for observations : 2.5 h
- ISBA surface parameterization
- Lateral boundary conditions : ECMWF 0.4° frames, with 6 h temporal resolution
- Forecast length : 54 h
- Elapsed time 20 min with 1-hourly output

Pre-RCR suite, NAE (Hirlam 6.1.2) :

- 0.18° horizontal resolution, 40 levels in the vertical
- 406 × 306 grid points
- Semi-lagrangian advection, time step 360 s
- 3D-Var analysis (HL6.1.2), FGAT option

- 6 h data assimilation cycle
- Cut-off time for observations : 2.5 h
- ISBA surface parameterization
- Lateral boundary conditions : ECMWF 0.4° frames, with 6 h temporal resolution
- Physics changes compared to ATX : STRACO, ISBA
- Other changes compared to ATX : Filtered orography
- Forecast length : 54 h
- Elapsed time 45 min with 6-hourly output
- Run from late July until the end of September

Pre-RCR suite, V62 (Hirlam 6.1.2) :

- 0.2° horizontal resolution, 40 levels in the vertical
- 438 × 336 grid points
- Semi-lagrangian advection, time step 360 s
- 3D-Var analysis (HL6.1.2), FGAT option
- 3 h data assimilation cycle
- Cut-off time for observations : 2 h
- ISBA surface parameterization
- Lateral boundary conditions : ECMWF 0.2° frames, with 3 h temporal resolution
- Physics changes compared to ATX : STRACO, ISBA
- Other changes compared to ATX : Filtered orography, IDFI initialization
- Forecast length : 54 h for main synoptic times, else 6 h
- Elapsed time 65 min with 3-hourly output
- Run since late September

The pre-RCR runs started with the NAE experiment in late July 2003. The NAE area is just inside the ATX area thus enabling the use of the same ECMWF frames for lateral boundary conditions. In September it became possible to receive another set of boundary frames and the NAE experiment was replaced by the V62 run with a larger model domain. Figure 1 shows the operational ATX area as well as the planned RCR (V62) area. Both experiments are controlled by the SMS system. The NAE runs were scheduled to run after the operational runs. The V62 runs are scheduled to start before the operational runs, but are suspended during operations and are then completed after operations. The V62 runs receive the observational data via a different server and a shorter cut-off time (2 h instead 2.5 h in operations) is applied.

The idea of the RCR runs is to stick to the HIRLAM Reference system as closely as possible. However, some modifications to the Reference HIRLAM (6.1.2) were made in connection of the pre-RCR runs. These modifications affect surface analysis and file naming. The 'Finlake' option in surface analysis makes it possible to create pseudo observations for Nordic lakes from climatological data. Furthermore, additional SST and ice observations for the Baltic Sea are received from Finnish Institute of Marine

Research (FIMR). The surface analysis program has been parallelized with OpenMP, giving the speed-up of 8, which means about 10 min saving in the wall-clock time for the V62 suite. For initialization, incremental digital filter initialization (IDFI) is applied (in V62 suite). The file naming convention has been modified to be more user-friendly, i.e., the file names should be complete and self-explaining. Three modifications used in the pre-RCR runs, parallelized surface analysis, file naming and IDFI, have now been accepted into the present HIRLAM release 6.2.1.

3 Preliminary results

As mentioned in Section 2, pre-RCR systems have been run in parallel with the FMI operational HIRLAM since summer 2003. In the following, some preliminary results from these pre-RCR suites, NAE and V62, are presented, and the performance of these runs are compared to the FMI operational ATX runs.

3.1 Noise

When the FMI operational system was upgraded in 2002, it was found that the higher horizontal resolution makes the forecast fields noisier (Eerola, 2003; Järvenoja, 2003). Fields (T, u, v and q) in a 0.2° resolution include clearly more noise, i.e., waves of several grid lengths, than fields in a 0.4° resolution. This problem and the origin of it could not be understood and therefore the implementation of the 0.2° resolution system was abandoned and the 0.3° resolution suite was introduced into operations instead.

The same noise problem is seen in the pre-RCR runs, both in NAE and V62. The noise, the several grid length waves, can be seen in the lower troposphere as well as in the stratosphere. Closer examination has revealed that these waves are often associated with frontal systems and with convection. Spurious reflection from the top may also be involved - preliminary investigations have shown some sensitivity to the diffusion at the highest levels.

3.2 Validation of NAE

The pre-RCR NAE system was run during August and September. The month of August was a quiet month in terms of synoptic activity and the August verification scores for the operational ATX and the pre-RCR are very similar (not shown). Figures 2 and 3 demonstrate the two-metre temperature (T_{2m}) bias in 36 h forecasts valid at 12 UTC, as calculated against observations, for ATX nad NAE, respectively. The bias distributions are fairly similar. Positive bias can be seen over central Europe in both, but negative bias dominates large areas in northern Europe and Russia as well as in southern Europe. The pre-RCR NAE system seems to give slightly lower T_{2m} values than the operational ATX.

Figures 4 and 5 demonstrate the observation verification scores of mean-sea-level pressure (p_{msl}), two-metre temperature (T_{2m}), 10-metre wind (V_{10m}) and two-metre relative humidity (RH_{2m}) for September for ATX and NAE runs, respectively. Scores for all four parameters are rather similar. NAE has slightly smaller rms error in p_{msl} compared to ATX. The T_{2m} bias is small in both, but slightly more negative in NAE than in ATX. This verification, however, does not tell everything because statistics are calculated over all four daily cycles, which means that, eg. the diurnal cycle in bias is smoothed out. Both ATX and NAE show the typical problem of positive V_{10m} bias that has been a problem in HIRLAM for a couple of years. The RH_{2m} scores are similar in ATX and NAE as well. As a whole, it can be concluded that ATX and NAE perform equally well.

Observation verification statistics shown in Figs. 4 and 5 depict the model performance at EWGLAM stations, i.e. over Europe west of 30°E. These stations cover only a part of the whole model domain. Therefore field verification, covering the whole model area, can give more insight into the model behavior. Figures 6 and 7 demonstrate the geographical distribution of rms error of p_{msl} in 48 h forecasts for ATX and NAE, respectively. The error patterns are very similar, also outside Europe, which confirms equal performance of ATX and NAE systems.

Figures 8 and 9 show the systematic difference in T_{2m} between NAE and ATX systems (NAE-ATX) for 36 h (valid at 12 UTC) and 48 h (valid at 00 UTC) forecasts, respectively. The NAE values seem to be lower than those of ATX over land, especially at nighttime (Fig. 9). At coastal areas and over high orography differences can be of either sign. Over the Arctic, in the region of ice edge, NAE seems to give higher T_{2m} due to different ice fraction.

The two-month period of the pre-RCR parallel test showed that the NAE system performed equally well with the FMI operational ATX suite. The negatively biased T_{2m}, more negative than in ATX, is the only observable disadvantage for NAE.

3.3 Validation of V62

The RCR system in its planned horizontal domain was implemented as the V62 suite at the end of September. The verification scores for October are not fully representative due to some reasons mentioned in the following. The V62 configuration is more complicated as its uses a 3 h data assimilation cycle. The observations are received via a different server compared to ATX, and it was found that at least aircraft reports were missing for some time. Also the 3D-Var parameters were still tuned in late October. In addition, the observation data window was not correctly defined for the 3 h cycling, leading to possibility of using partly same observations in two consecutive cycles.

Figures 10 and 11 demonstrate the geographical distribution of p_{msl} rms error for 1-14 November for ATX and V62, respectively. The rms error values are of similar magnitude over most of Europe in ATX and V62. However, at high latitudes, over the Arctic Sea and over northern Russia, the values in V62 are clearly larger (8 hPa at most) than in ATX. The bias maps (not shown) indicate that bias contributes to a great deal in these high rms error values in V62. It seems that cyclones over the Arctic region are deeper in V62 than in ATX. This is supported by low level temperatures: V62 shows several degrees higher temperatures than ATX at the surface and in the lower tropospehere.

This problem has been traced back to a smaller fraction of ice in the polar region in the V62 suite. The problem has been identified only recently. The problem arises from the use of the ECMWF SST field for pseudo observation creation in the HIRLAM SST analysis and consequent diagnosis of the ice cover. The wrong limit for freezing temperature of the sea water was used, and this resulted in too large fraction of open sea over polar regions. The bug has been fixed now, but it has been in the pre-RCR runs all the time since summer. For this reason, the V62 runs for October and November have only limited value e.g., for model evaluation. The problem in NAE runs for August and September has not so large impact because the slightly different ice cover over polar regions in ATX and NAE did not matter in temperatures close to 0°C.

4 Summary and concluding remarks

The RCR system has been installed at FMI, and pre-operational test runs have been carried out since August 2003. Some results are reported in this write-up. The RCR system, based on the HIRLAM version 6.1.2 performed equally well with the FMI operational HIRLAM 5.1.4 system in August and September 2003. The performance of the RCR system was, however, affected in October and November due to a bug in creation of pseudo-observations for the SST analysis, resulting to a lesser ice cover over Arctic regions, and consequently to too deep cyclones.

The problem with creation of pseudo-observations was corrected in the beginning of December 2003, and at the same time the present HIRLAM Reference version 6.2.1 was installed as the RCR system. Development and implementation of an extensive tool package for monitoring and evaluating the RCR runs is going on at the moment, and the RCR system is expected to gain the operational status at FMI in early 2004.

References

Eerola, K., 2003: The operational HIRLAM at the Finnish Meteorological Institute. *HIRLAM Newsletter*, **43**, 1-8.

Järvenoja, S., 2003: Experiences from the pre-operational HIRLAM 5.1.4 tests at FMI. *HIRLAM Newsletter*, **43**, 154-167.

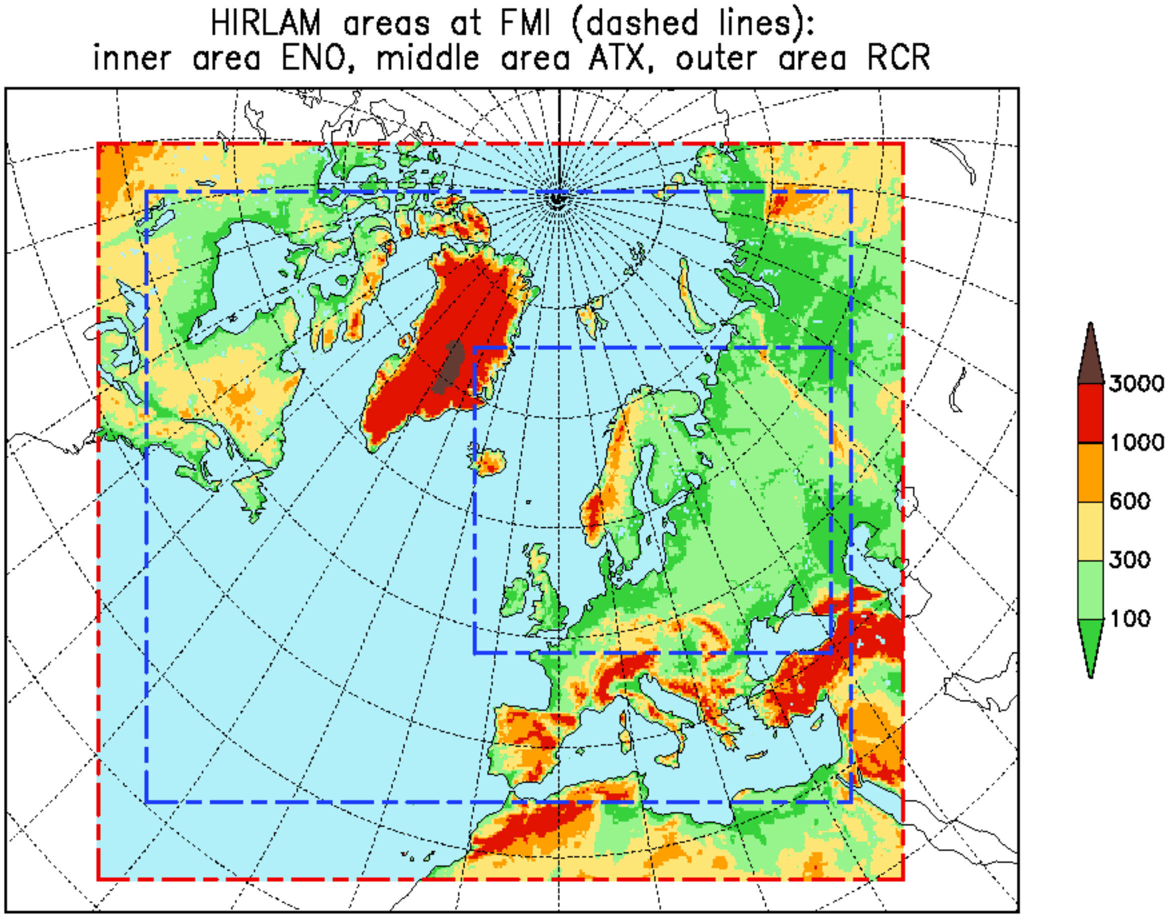

Figure 1: *HIRLAM areas at FMI. ATX: middle dashed line, V62: outer dashed line. The NAE area (not shown) is just inside the ATX area.*

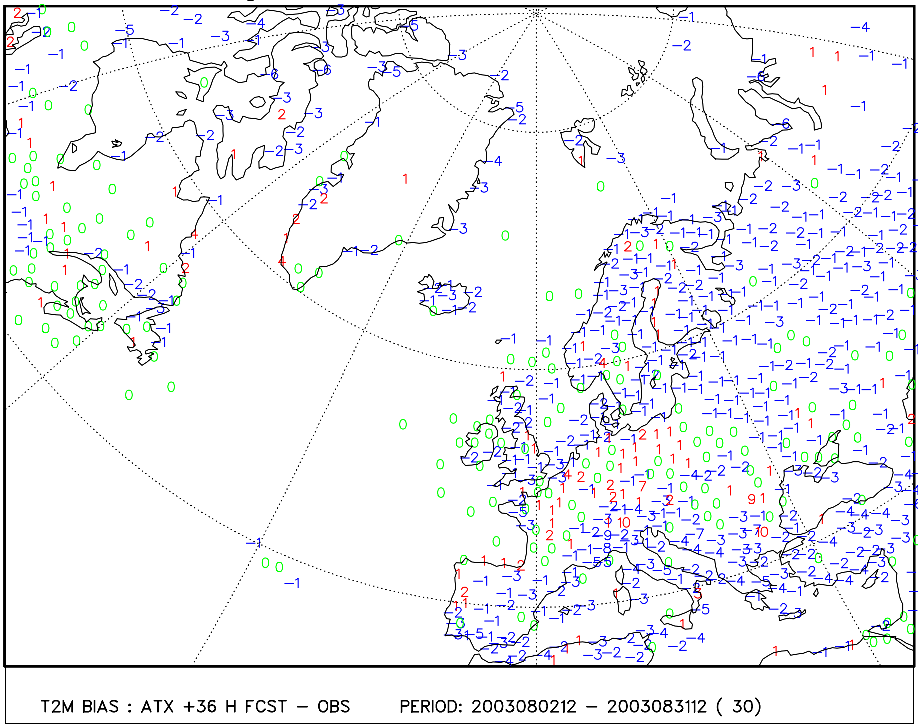

Figure 2: *T_{2m} bias (calculated against observations) in 36 h ATX forecasts valid at 12 UTC in August 2003.*

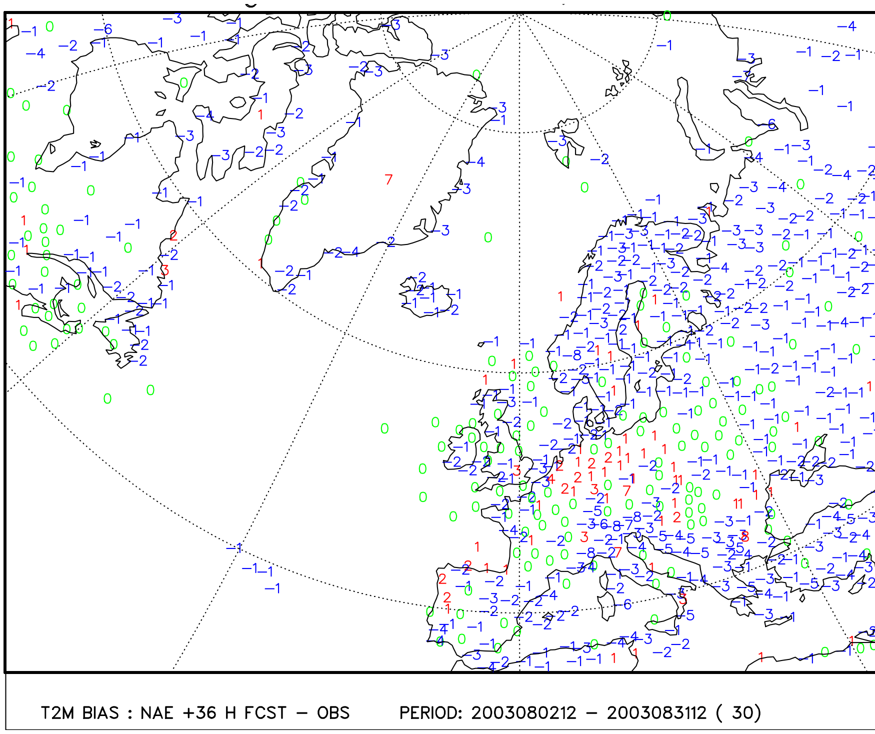

Figure 3: *T_{2m} bias (calculated against observations) in 36 h NAE forecasts valid at 12 UTC in August 2003.*

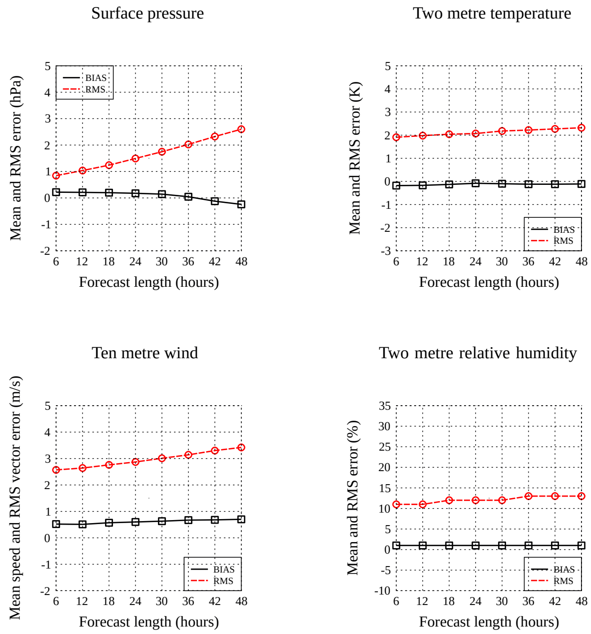

Figure 4: *Observation verification statistics for ATX forecasts in September 2003. Meteorological parameters:* p_{msl} *top left,* T_{2m} *top right,* V_{10m} *bottom left and* RH_{2m} *bottom right. Bias is indicated with squares, rms error with circles.*

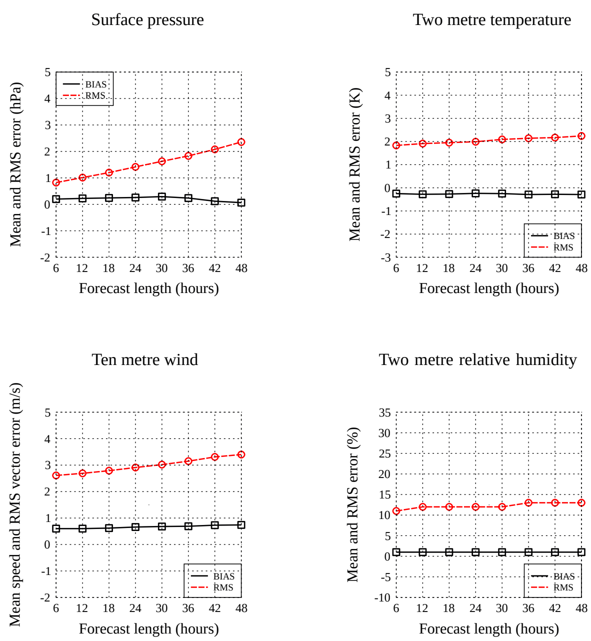

Figure 5: *Observation verification statistics for NAE forecasts in September 2003. Meteorological parameters:* p_{msl} *top left,* T_{2m} *top right,* V_{10m} *bottom left and* RH_{2m} *bottom right. Bias is indicated with squares, rms error with circles.*

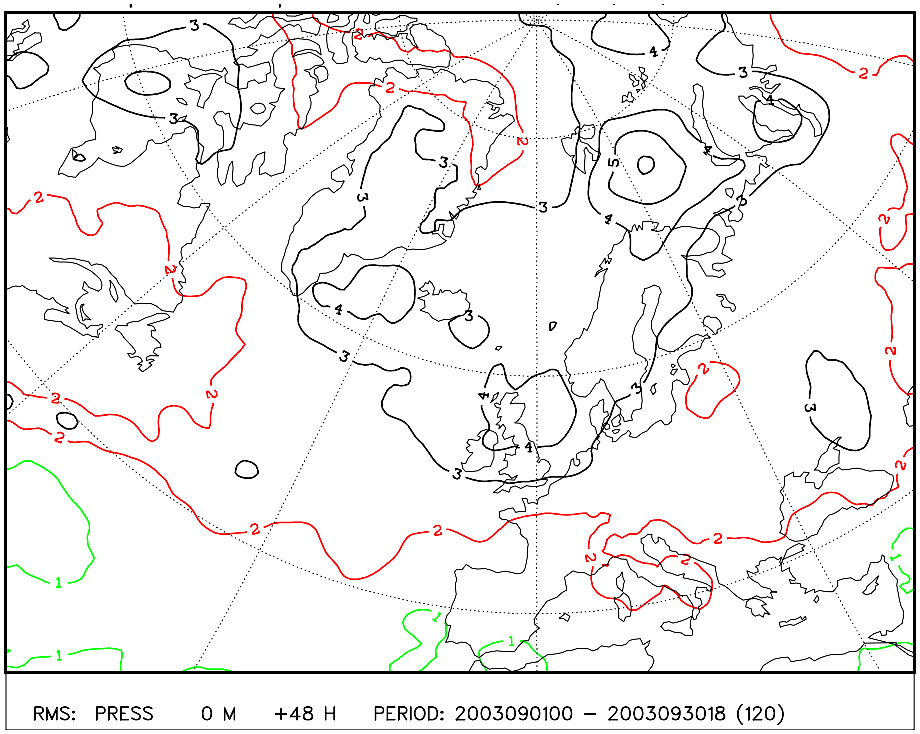

Figure 6: *Rms error in 48 h ATX p_{msl} forecasts in September 2003. Contour interval: 1 hPa.*

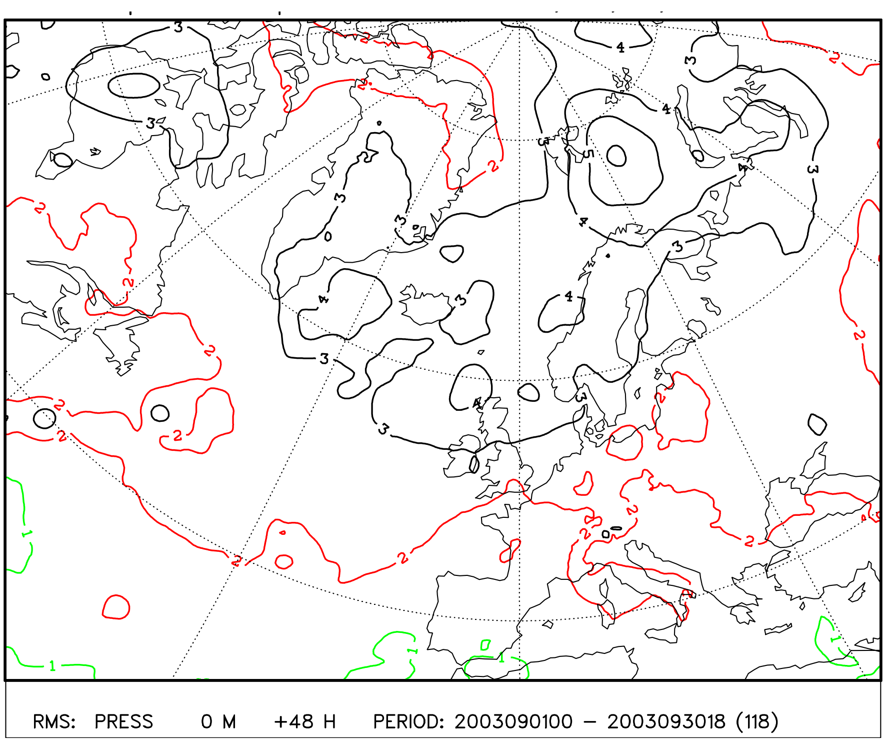

Figure 7: *Rms error in 48 h NAE p_{msl} forecasts in September 2003. Contour interval: 1 hPa.*

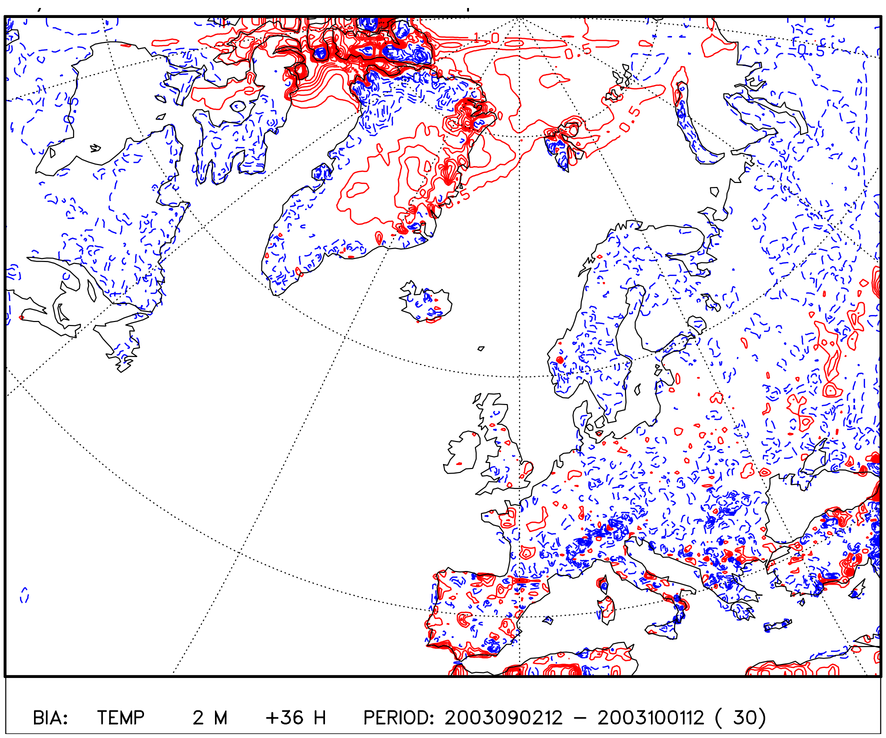

Figure 8: *Systematic difference in 36 h T_{2m} forecasts (valid at 12 UTC) between NAE and ATX (NAE - ATX). Contour interval: 0.5° C. The zero isoline not plotted, negative values indicated with dashed lines.*

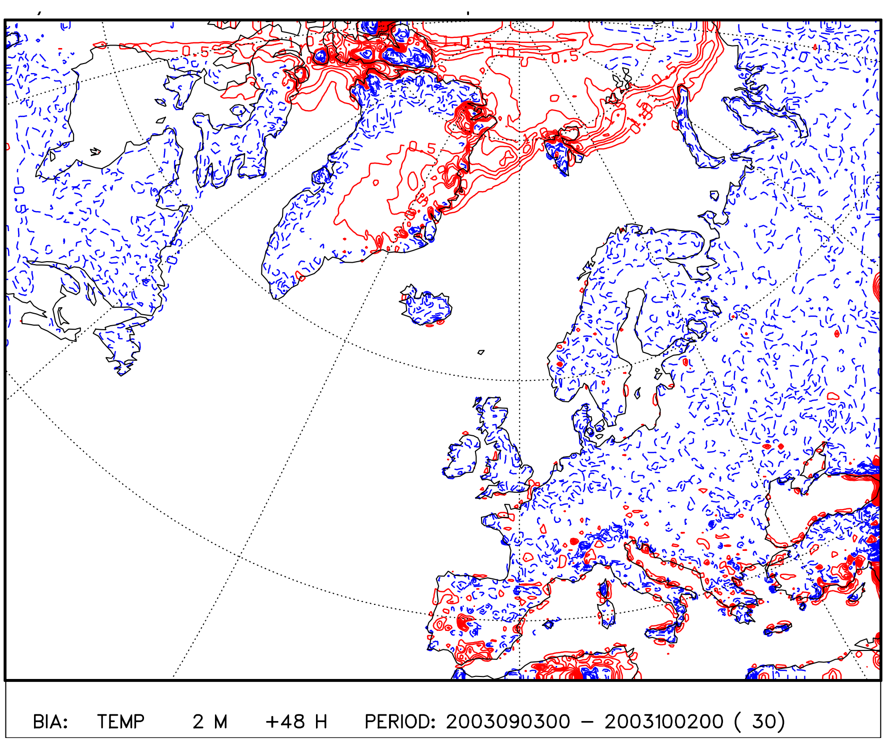

Figure 9: *Systematic difference in 48 h T_{2m} forecasts (valid at 00 UTC) between NAE and ATX (NAE - ATX). Contour interval: 0.5° C. The zero isoline not plotted, negative values indicated with dashed lines.*

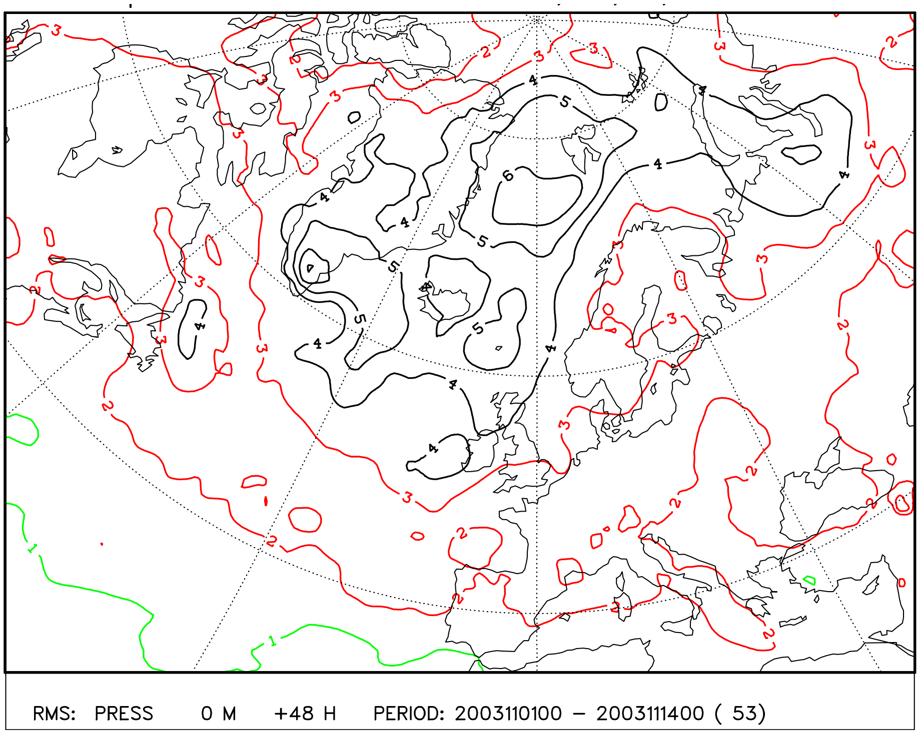

Figure 10: *Rms error in 48 h ATX p_{msl} forecasts for 1-14 November 2003. Contour interval: 1 hPa.*

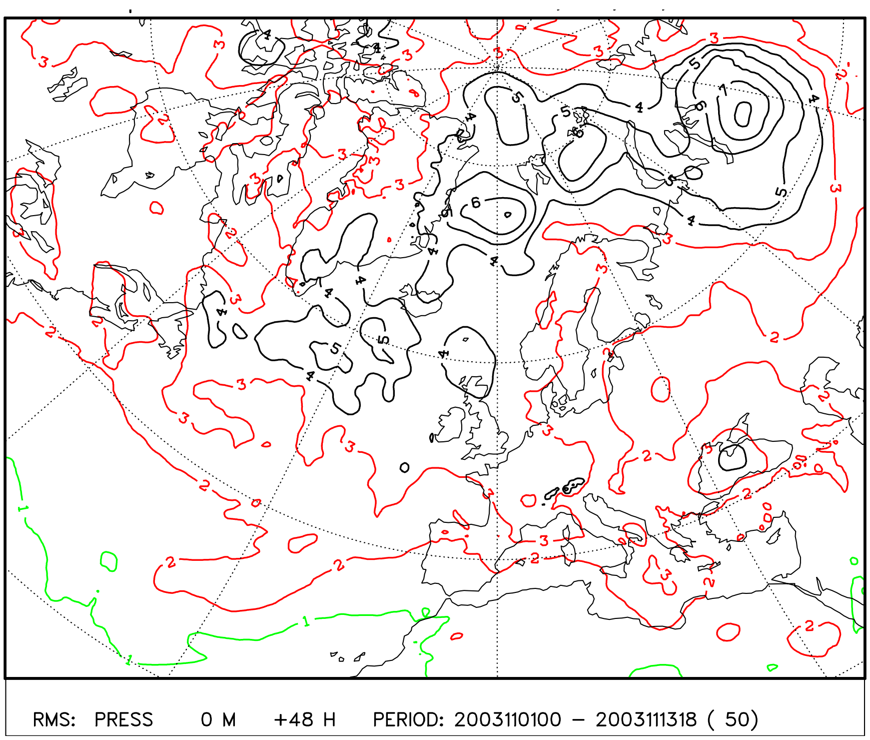

Figure 11: *Rms error in 48 h V62 p_{msl} forecasts for 1-14 November 2003. Contour interval: 1 hPa.*

Proceedings of Baltic HIRLAM Workshop, St.Petersburg, 17-20.11.2003

CONTENTS

LIST CONTINUES on the back side ...

http://hirlam.knmi.nl
http://hirlam.fmi.fi/Baltic